

# ELECTRICAL STIMULATION OF THE MEDIAL FOREBRAIN BUNDLE AS A POTENTIAL THERAPY FOR ALZHEIMER'S DISEASE: EFFECTS ON MOLECULAR MARKERS IN RODENT MODEL

**Irene Puig Parnau**

Per citar o enllaçar aquest document:

Para citar o enlazar este documento:

Use this url to cite or link to this publication:

<http://hdl.handle.net/10803/672300>

**ADVERTIMENT.** L'accés als continguts d'aquesta tesi doctoral i la seva utilització ha de respectar els drets de la persona autora. Pot ser utilitzada per a consulta o estudi personal, així com en activitats o materials d'investigació i docència en els termes establerts a l'art. 32 del Text Refós de la Llei de Propietat Intel·lectual (RDL 1/1996). Per altres utilitzacions es requereix l'autorització prèvia i expressa de la persona autora. En qualsevol cas, en la utilització dels seus continguts caldrà indicar de forma clara el nom i cognoms de la persona autora i el títol de la tesi doctoral. No s'autoritza la seva reproducció o altres formes d'explotació efectuades amb finalitats de lucre ni la seva comunicació pública des d'un lloc aliè al servei TDX. Tampoc s'autoritza la presentació del seu contingut en una finestra o marc aliè a TDX (framing). Aquesta reserva de drets afecta tant als continguts de la tesi com als seus resums i índexs.

**ADVERTENCIA.** El acceso a los contenidos de esta tesis doctoral y su utilización debe respetar los derechos de la persona autora. Puede ser utilizada para consulta o estudio personal, así como en actividades o materiales de investigación y docencia en los términos establecidos en el art. 32 del Texto Refundido de la Ley de Propiedad Intelectual (RDL 1/1996). Para otros usos se requiere la autorización previa y expresa de la persona autora. En cualquier caso, en la utilización de sus contenidos se deberá indicar de forma clara el nombre y apellidos de la persona autora y el título de la tesis doctoral. No se autoriza su reproducción u otras formas de explotación efectuadas con fines lucrativos ni su comunicación pública desde un sitio ajeno al servicio TDR. Tampoco se autoriza la presentación de su contenido en una ventana o marco ajeno a TDR (framing). Esta reserva de derechos afecta tanto al contenido de la tesis como a sus resúmenes e índices.

**WARNING.** Access to the contents of this doctoral thesis and its use must respect the rights of the author. It can be used for reference or private study, as well as research and learning activities or materials in the terms established by the 32nd article of the Spanish Consolidated Copyright Act (RDL 1/1996). Express and previous authorization of the author is required for any other uses. In any case, when using its content, full name of the author and title of the thesis must be clearly indicated. Reproduction or other forms of for profit use or public communication from outside TDX service is not allowed. Presentation of its content in a window or frame external to TDX (framing) is not authorized either. These rights affect both the content of the thesis and its abstracts and indexes.

DOCTORAL THESIS

**Electrical stimulation of the medial  
forebrain bundle as a potential therapy for  
Alzheimer's disease: effects on molecular  
markers in rodent model**



Irene Puig Parnau  
2021





DOCTORAL THESIS

**Electrical stimulation of the medial forebrain bundle as a potential therapy for Alzheimer's disease: effects on molecular markers in rodent model**

Irene Puig Parnau  
2021





DOCTORAL THESIS

**Electrical stimulation of the medial forebrain bundle as a potential therapy for Alzheimer's disease: effects on molecular markers in rodent model**

**Irene Puig Parnau**  
**2021**

Doctoral Programme in Molecular Biology, Biomedicine and Health

Co-directed by:

Dr. Gemma Huguet Blanco

Dr. Elisabet Kádár García

Dr. Pilar Segura Torres

PhD candidate:

Irene Puig Parnau

This thesis is submitted in fulfilment of the requirements to obtain the doctoral degree at the  
Universitat de Girona



*A la tia Ramona, la tia Lola, el tiu Palol, la iaia de la Laura,  
el pare d'en Karlos, la sogra de la Pilar i tanta altra gent.  
Perquè nosaltres sí que us recordem.*



## AGRAÏMENTS

Vaig començar aquesta tesi l'1 d'octubre de 2017. Abans no hauria imaginat que anades i vingudes de Bellaterra estarien marcades per la incertesa de múltiples dies de vaga general per la incapacitat de gestionar problemes polítics, per aiguats i temporals, i per un confinament amb dures restriccions per un nou coronavirus. Vull agrair sincerament a tothom que ha contribuït que, malgrat tot, pogués sortir-ne aquesta tesi tres anys i mig després.

Primer de tot, voldria donar les gràcies al grup i, especialment, a les directores de tesi, per haver-me permès participar en aquest projecte tan maco, amb el qual he après tant i que m'he pogut sentir tan meu estant alhora tan acompanyada. A la Gemma, pel seu seguiment, disponibilitat i interès total, i pel carisma constant imprescindible per tirar-ho tot endavant. A l'Elisabet, per l'excel·lent guiatge i capacitat de simplificar les dificultats, i per la seva energia i motivació característica, que, sense saber-ho, m'ha encomanat tan sovint quan n'anava faltada. I a la Pilar, perquè no se m'acut millor manera de ser-hi sense ser aquí.

I juntament amb la Pilar, a la Laura i a la resta de l'equip preciós de l'Autònoma. A la Laia i la Sol, que són tot voluntat, compromís, dedicació i harmonia: gràcies per fer tan lleugeres les hores amb olor de ciment. I a en Karlos i la Cristina, incansables: moltes gràcies per dedicar-vos tant, a això i així. Gràcies a tots per haver-me fet sentir integrada en el vostre equip.

Moltes gràcies també a tots els d'aquí, que d'alguna manera també han participat en el projecte des de Girona. A tots els estudiants de pràctiques, TFG o TFM amb qui he coincidit i que han participat en un punt o un altre en aquest projecte: la Xènia Puig, l'Andrea Riberas, la Irene Agustí, la Judit Fernández, la Laura Valls, la Laia Sala, la Gabriela Jarasunas, l'Adrián González, l'Aina Cardús, l'Anna Masó i l'Oriol Puig. And also thanks to Nasi for her work during those months. També volia donar les gràcies a la Carme, que a més d'obrir-me les portes a l'IdIBGi pel que ha calgut en aquest projecte, ja fa 7 anys em va ensenyar gran part del que sé al laboratori i des de llavors cada creuament ha sigut positiu i tranquil·litzador, contribuint sempre que tot vagi bé.

Moltíssimes gràcies també a qui ha marcat el dia a dia d'aquests anys. A tota la Granja. A en Pau, que em va rebre al grup ensenyant-me que es pot fer tot de manera serena. A la Carla, que també amb serenor, perspectiva i bona voluntat, des que vaig arribar la vaig poder sentir

molt al costat, i no només literalment. I amb ells, a les altres veteranes, la Sandra i l'Elena (i la Mireia al seu moment), que s'encarreguen que les arribades siguin fàcils, i que saben tant de què va això que pregunten abans que tu sàpigues que ho necessites. A tots ells: les vostres tesis m'han sigut molt útils! Però també moltes gràcies a tots els no tan veterans. Als suros que falten, l'Iker, la Carla i ara també en Javier, per estar sempre disposats a preguntar, a deixar i a no defallir intentant convidar a cafè. I a les súper micros, sempre allà, que acompanyen els dies que comencen més d'hora i acaben més tard: a l'Ellana per ser sempre positiva, a l'Eli per ser un recolzament discret però sempre present, i a la Paola i la Laura, que ho fan tot fàcil. A la Queralt (i l'Àlex) pels vespres de desconnexió a cal Mico, que ara ja queden molt llunyans. I a la Judit i a tots els genètics companys de planta. I també moltíssimes gràcies als millors veïns de dalt que pot tenir la Granja. Als bioquímics, l'Adrià, l'Àlex, l'Anna, la Laura i en Pedro, a tots un per un personalment, perquè feu molt més que fer-ho tot divertit i cuidar-vos que cada creuament pel passadís, hora de dinar o activitat social estigui plena de rialles.

I finalment, moltes gràcies a tota la família i amics. A en Marc Rabionet, perquè d'alguna manera ho vam començar i ho hem passat junts, ànims perquè aviat estaràs escrivint això. A la Laura, gràcies per seguir-me acompanyant en tots els moments d'aquestes vides paral·leles. I a la família, la més gran i la més petita. Als papas, per entendre tant sense entendre(-hi) res. A la Maria i en Miquel, per anar-hi siguent, al pati de casa seu i a la vida. I sobretot, a la Marta, per sentir-me i escoltar-me amb un full de paper plegat pel mig, per pensar en mi i amb mi i per donar una visió artística a tot plegat i regalar-me aquesta portada. I, a l'Arnau, per haver-ho viscut amb mi i haver sigut el millor suport des del principi fins, també, el final.

## PUBLICATION RESULTING FROM THIS THESIS

**Puig-Parnau I**, Garcia-Brito S, Faghihi N, Gubern C, Aldavert-Vera L, Segura-Torres P, Huguet G and Kádár E. (2020). Intracranial Self-Stimulation Modulates Levels of SIRT1 Protein and Neural Plasticity-Related microRNAs. *Mol Neurobiol.*, 57(6), 2551-2562. doi: 10.1007/s12035-020-01901-w

## ACKNOWLEDGEMENTS

This work has been funded by MINECO PSI2017-83202-C2-1-P and PSI2017-83202-C2-2-P (2018-2020) research projects.

Irene Puig Parnau was recipient of a pre-doctoral fellowship from Universitat de Girona (IFUdG2017/61).

## LIST OF ABBREVIATIONS

<b>Abbreviation</b>	<b>Description</b>
A $\beta$	Amyloid- $\beta$ peptide
ACh	Acetylcholine
AD	Alzheimer's disease
ADAM10	A disintegrin and metalloproteinase 10
ADAS-Cog	Alzheimer's disease assessment scale-cognitive subscale
AP	Anteroposterior coordinates
ApoE	Apolipoprotein E
APP	Amyloid precursor protein
ARC	Activity-regulated cytoskeleton-associated protein
ATN	Anterior thalamic nuclei
ATP	Adenosine triphosphate
BACE	$\beta$ -site APP cleaving enzyme
BBB	Blood brain barrier
BDNF	Brain-derived neurotrophic factor
CA	Cornu ammonis
CaMKII	Calmodulin kinase
cAMP	Cyclic adenosine monophosphate
CDK5	Cyclin-dependent kinase 5
cDNA	Complementary DNA
CREB	cAMP response element binding protein
CREM	cAMP responsive element modulator
CSF	Cerebrospinal fluid
Ct	Cycle threshold
DAB	3,3'-Diaminobenzidine
DBN	Drebrin
DBS	Deep brain stimulation
DEPC	Diethylpyrocarbonate
DG	Dentate gyrus
DMN	Default mode network
DNA	Deoxiribonucleic acid
DTT	Dorsal tenia tecta
DV	Dorsoventral coordinates
EC	Entorhinal cortex
Ect	Ectorhinal cortex
FC	Fold change
FDA	Food and drug administration
FDG-PET	Positron emission tomography with 18F-fluorodeoxyglucose
fMRI	Functional magnetic resonance imaging
FOXO3	Forkhead box O transcription factor 3
GABA	$\gamma$ -aminobutyric acid
GAPDH	Glyceraldehyde 3-phosphate dehydrogenase
GLUT	Glucose transporter
GSK-3 $\beta$	Glycogen synthase kinase 3 $\beta$
HFIP	Hexafluoroisopropanol
hil	Hilus region

<b>Abbreviation</b>	<b>Description</b>
HP	Hippocampus
ICER	Inducible cAMP early repressor
ICSS	Intracranial self-stimulation. In the context of this thesis, it refers to intracranial self-stimulation targeting the MFB.
icv	Intracerebroventricular
IGF	Insulin growth factor
IP	Infrapyramidale
IRBS	Insulin resistant brain state
L	Layer
LEnt	Lateral entorhinal cortex
LH	Lateral hypothalamus
LTM	Long-term memory
LTP	Long-term potentiation
MAPK/ERK	Mitogen activated protein kinase/extracellular-signal-regulated kinase pathway
MAPT	Microtubule-associated protein tau
MCI	Mild cognitive impairment
MEnt	Medial entorhinal cortex
MFB	Medial forebrain bundle
miRISC	miRNA-induced silencing complex
miRNA	MicroRNA
ML	Mediolateral coordinates
MMSE	Mini-mental state exam
mPFC	Medial prefrontal cortex
MRI	Magnetic resonance imaging
mRNA	Messenger RNA
MTL	Medial temporal lobe
MWM	Morris water maze
NAD <sup>+</sup> / NADH	Nicotinamide adenine dinucleotide (oxidized / reduced form)
NBM	Nucleus basalis of Meynert
NFT	Neurofibrillary tangles
NF- $\kappa$ B	Nuclear factor- $\kappa$ B
NGF	Nerve growth factor
NMDAR	N-methyl-D-aspartate receptor
NURR1	Nuclear receptor related 1 protein
OI	Optimum current intensity
PBS	Phosphate-buffered saline
PC	Posterior cingulate region
PCR	Polymerase chain reaction
PDD	Parkinson disease dementia
PET	Positron emission tomography
PFC	Prefrontal cortex
PGC1 $\alpha$	Peroxisome proliferator-activated receptor $\gamma$ co-activator-1 $\alpha$
PI3K	Phosphatidylinositol 3-kinase
PKA	Protein kinase A
PP	Protein phosphatase
PRh	Perirhinal cortex
PrL	Prelimbic cortex
PS	Presenilin

<b>Abbreviation</b>	<b>Description</b>
PSD-95	Postsynaptic density protein 95
p $\tau$	Phosphorylated tau
PVDF	Polyvinylidene difluoride
qRT-PCR	Quantitative reverse transcription PCR
RET	Receptor tyrosine-protein kinase
RNA	Ribonucleic acid
ROI	Region of interest
RSA	Agranular retrosplenial cortex
RSC	Retrosplenial cortex
RSG	Granular retrosplenial cortex
sAD	Sporadic Alzheimer's disease
SIRT1	Sirtuin1
SLM	Stratum lacunosum moleculare
SO	Stratum oriens
SP	Suprapyramidale
SR	Stratum radiatum
STM	Short-term memory
STZ	Streptozotocin
TBS	Tris-buffered saline
TBS-T	TBS containing Triton/Tween detergent
TWAA	Two-way active avoidance
UV	Ultraviolet
VDB	Vertical limb of the diagonal band
VEH	Vehicle-injected group
VTa	Ventral tegmental area

## LIST OF FIGURES

### INTRODUCTION

<b>Fig. 1</b> Prevalence of dementia by age-group in Western Europe.	2
<b>Fig. 2</b> Brain affectation in AD.	4
<b>Fig. 3</b> Plaques and tangles in AD.	7
<b>Fig. 4</b> Two possible proteolytic pathways of APP and the production of A $\beta$ 40/42.	8
<b>Fig. 5</b> Braak stages of neurofibrillary pathology in AD.	12
<b>Fig. 6</b> Causation cascade hypotheses in AD.	15
<b>Fig. 7</b> Interrelation of AD molecular hallmarks through different altered pathways.	17
<b>Fig. 8</b> MicroRNA biogenesis and function.	19
<b>Fig. 9</b> Major miRNAs in AD.	21
<b>Fig. 10</b> Neuroprotective pathways of SIRT1 in coordination with selected miRNAs.	24
<b>Fig. 11</b> Neuroanatomy of the Papez circuit.	33
<b>Fig. 12</b> Overview of memory circuits linked to AD.	38
<b>Fig. 13</b> Anatomy and connectivity of the human and rat medial forebrain bundle.	45

### MATERIALS AND METHODS

<b>Fig. 14</b> Experimental timeline for Study 1.	52
<b>Fig. 15</b> Experimental timeline for Study 2.	53
<b>Fig. 16</b> Experimental timeline for Study 3.	53
<b>Fig. 17</b> Target location of the ICSS electrode.	56
<b>Fig. 18</b> Target injection place for A $\beta$ and STZ toxics.	57
<b>Fig. 19</b> Images of stereotactic surgery procedure.	58
<b>Fig. 20</b> Image of a rat in the self-stimulation box.	59
<b>Fig. 21</b> Morris water maze configuration during the acquisition phase.	60
<b>Fig. 22</b> Representation of tissue distribution according to sample fate in each of the studies.	64
<b>Fig. 23</b> Images of hippocampal subdissection.	65
<b>Fig. 24</b> Total protein quantification for Western blot normalization.	71
<b>Fig. 25</b> Analysed photomicrographs in Nissl staining hippocampal sections.	74
<b>Fig. 26</b> Analysed photomicrographs in Nissl staining frontal sections.	75
<b>Fig. 27</b> Photomicrograph analysis for DBN and ptau immunostaining in parietal-temporal sections.	77
<b>Fig. 28</b> Photomicrograph analysis for DBN and ptau immunostaining in frontal sections.	79
<b>Fig. 29</b> Pipeline for ptau immunolabelling intensity measure.	80

## RESULTS I

<b>Fig. 30</b> Time-dependent changes of ICSS-regulated miRNA candidates after treatment, in CA1 and DG.	86
<b>Fig. 31</b> Differential miRNA expression in DG after ICSS treatment (volcano plot).	87
<b>Fig. 32</b> Relative expression of ICSS-regulated miRNA candidates in DG	89
<b>Fig. 33</b> Relative expression of ICSS-regulated miRNA candidates in CA1 and CA3	89
<b>Fig. 34</b> Relative expression of ICSS-regulated miRNA candidates in serum	90
<b>Fig. 35</b> Correlation between miR-132 levels in DG and in serum, after ICSS treatment.	91
<b>Fig. 36</b> Time-dependent changes after ICSS treatment on APP, ptau, tau and DBN levels in DG extracts.	92
<b>Fig. 37</b> Time-dependent changes after ICSS treatment on SIRT1 levels in hippocampal subfield extracts.	93
<b>Fig. 38</b> Levels of SIRT1 in serum and its relation with DG levels, after ICSS treatment.	94
<b>Fig. 39</b> Correlation between SIRT1 levels and miR-132 levels in serum after ICSS.	94
<b>Fig. 40</b> Levels of BDNF in serum and DG and their relation, after ICSS treatment.	95

## RESULTS II

<b>Fig. 41</b> Aggregation state of injected amyloid- $\beta$ peptide.	103
<b>Fig. 42</b> Effects of A $\beta$ injection on spatial task acquisition.	104
<b>Fig. 43</b> Effects of A $\beta$ injection on spatial probe test.	105
<b>Fig. 44</b> Effects of A $\beta$ injection on cognitive flexibility.	106
<b>Fig. 45</b> Effects of A $\beta$ injection on hippocampal neurodegeneration.	107
<b>Fig. 46</b> Effects of A $\beta$ injection on prelimbic cortex neurodegeneration.	108
<b>Fig. 47</b> Effects of A $\beta$ injection on DBN levels at day 22.	110
<b>Fig. 48</b> Correlation between DBN levels and percentage of neurodegeneration in superficial layers of prelimbic cortex, 22 days after A $\beta$ injection.	111
<b>Fig. 49</b> Correlation between DBN levels in layer Vb of lateral entorhinal cortex and behavioural variables, 22 days after A $\beta$ injection.	112
<b>Fig. 50</b> Correlation between DBN levels in layer V of prelimbic cortex and cognitive flexibility, 22 days after A $\beta$ injection.	113
<b>Fig. 51</b> Effects of A $\beta$ injection and ICSS treatment on DBN levels at day 33 (photomicrographs).	114
<b>Fig. 52</b> Effects of A $\beta$ injection and ICSS treatment on DBN levels at day 33 (graphs).	115
<b>Fig. 53</b> Correlation between DBN levels in superficial layers of lateral entorhinal cortex and spatial memory, 33 days after A $\beta$ injection.	116
<b>Fig. 54</b> Effects of A $\beta$ injection on ptau levels at day 22.	117



<b>Fig. 55</b> Correlation between ptau levels in hippocampus and neurodegeneration in prelimbic cortex, 22 days after A $\beta$ injection.	118
<b>Fig. 56</b> Correlation between ptau levels in rhinal cortices and DBN levels in prelimbic cortex, 22 days after A $\beta$ injection.	119
<b>Fig. 57</b> Effects of A $\beta$ injection and ICSS treatment on ptau levels at day 33 (photomicrographs).	120
<b>Fig. 58</b> Effects of A $\beta$ injection and ICSS treatment on ptau levels at day 33 (graphs).	121
<b>Fig. 59</b> Effects of ICSS treatment on spatial task acquisition and probe test in A $\beta$ -injected rats.	122
<b>Fig. 60</b> Relation between DBN levels in superficial layers of lateral entorhinal cortex and spatial memory in ICSS-treated AB rats.	123

### RESULTS III

<b>Fig. 61</b> Physiological affectations in STZ-injected rats.	132
<b>Fig. 62</b> Morphologic alterations in STZ-injected rat's brain.	133
<b>Fig. 63</b> Effects of STZ injection on spatial task acquisition.	134
<b>Fig. 64</b> Effects of STZ injection on spatial probe test.	135
<b>Fig. 65</b> Effects of ICSS treatment on STZ-induced disturbances on spatial learning and memory.	136
<b>Fig. 66</b> Effects of STZ injection and ICSS treatment on hippocampal neurodegeneration.	137
<b>Fig. 67</b> Effects of STZ injection and ICSS treatment on medial prefrontal cortex neurodegeneration.	139
<b>Fig. 68</b> Correlation between neurodegeneration in DTT and HP after STZ injection.	140
<b>Fig. 69</b> Effects of STZ injection and ICSS treatment on DBN levels (photomicrographs).	141
<b>Fig. 70</b> Effects of STZ injection and ICSS treatment on DBN levels (graphs).	142
<b>Fig. 71</b> Effects of STZ injection and ICSS treatment on ptau levels (photomicrographs).	144
<b>Fig. 72</b> Effects of STZ injection and ICSS treatment on ptau levels (graphs).	145
<b>Fig. 73</b> Effects of STZ injection and ICSS treatment on DBN, SIRT1, APP, ptau and tau levels in DG extracts.	147
<b>Fig. 74</b> Effects of STZ injection on DBN, SIRT1, APP, ptau and tau levels in mPFC extracts.	148
<b>Fig. 75</b> Correlation between APP levels in DG and behavioural variables, after STZ injection.	149
<b>Fig. 76</b> Effects of STZ injection and ICSS treatment on miRNAs in DG.	151
<b>Fig. 77</b> Effects of STZ injection and ICSS treatment on miRNAs in serum.	152
<b>Fig. 78</b> Effects of STZ injection and ICSS treatment on SIRT1 levels in serum.	153
<b>Fig. 79</b> Correlation between SIRT1 concentration in serum and neuronal density in DG after STZ injection.	153

## LIST OF TABLES

### INTRODUCTION

<b>Table 1</b> Methodological variation in A $\beta$ -injection rat model.	27
--	----

### MATERIALS AND METHODS

<b>Table 2</b> MicroRNAs analysed by qRT-PCR and used TaqMan Advanced Assays.	68
---	----

<b>Table 3</b> Conditions for Western blot analyses.	70
--	----

### RESULTS I

<b>Table 4</b> Summary of the groups composing Study 1.	84
---	----

<b>Table 5</b> Stability values for miRNA endogenous normalizer candidates at different times after ICSS treatment, in DG and CA1 samples.	85
--	----

<b>Table 6</b> Stability values for miRNA endogenous normalizer candidates 90 min post-treatment, in DG samples.	85
--	----

<b>Table 7</b> Stability values for miRNA endogenous normalizer candidates 90 min post-treatment, in serum samples.	85
---	----

<b>Table 8</b> Differentially expressed miRNAs in ICSS and sham conditions and their functional relations.	88
--	----

<b>Table 9</b> Detection frequencies of candidate miRNAs in serum samples.	90
--	----

### RESULTS II

<b>Table 10</b> Summary of the groups composing Study 2.	103
--	-----

<b>Table 11</b> Correlation analyses between DBN levels in parietal-temporal regions and neurodegeneration in prelimbic cortex, 22 days after A $\beta$ injection.	111
--	-----

<b>Table 12</b> Correlation analyses between DBN levels in layer Vb of LEnt and behavioural variables, 22 days after A $\beta$ injection.	112
---	-----

<b>Table 13</b> Summary of the main results in Study 2.	124
---	-----

### RESULTS III

<b>Table 14</b> Summary of the groups composing Study 3.	131
--	-----

<b>Table 15</b> Relationship between incidence of morphologic abnormalities and STZ administration.	133
---	-----

<b>Table 16</b> Correlation analyses between ptau Ser202/Thr205 levels in hippocampal regions and latency in 2 <sup>nd</sup> acquisition session in the MWM.	146
--	-----

<b>Table 17</b> Stability values for miRNA endogenous candidates in DG after STZ and ICSS.	150
--	-----

<b>Table 18</b> Stability values for miRNA endogenous candidates in serum after STZ and ICSS.	150
---	-----

<b>Table 19</b> Detection frequencies of candidate miRNAs in serum samples.	152
---	-----

<b>Table 20</b> Correlation analyses between SIRT1 serum levels and histopathological hallmarks.	154
--	-----

<b>Table 21</b> Summary of the main results in Study 3.	155
---	-----

# TABLE OF CONTENTS

<b>List of abbreviations</b>	<b>i</b>
<b>List of figures</b>	<b>iv</b>
<b>List of tables</b>	<b>vii</b>
<b>Table of contents</b>	<b>viii</b>
<b>Summary</b>	<b>xii</b>
<b>Resum</b>	<b>xiv</b>
<b>Resumen</b>	<b>xvii</b>
<b>INTRODUCTION</b>	<b>1</b>
<b>PART I. ALZHEIMER'S DISEASE: A MULTIFACTORIAL DISORDER WITHOUT TREATMENT</b>	<b>1</b>
1. EPIDEMIOLOGY AND CLINICAL PRESENTATION OF ALZHEIMER'S DISEASE	2
1.1. Epidemiology	2
1.2. Clinical affectations and neuroanatomical correlates	3
Memory function and memory dysfunction in AD	5
2. CELL AND MOLECULAR MARKERS OF AD PATHOGENESIS	7
2.1. Amyloid pathology	8
2.2. Tau pathology	11
2.3. Synaptic dysfunction	13
2.4. Glucose hypometabolism	14
3. GENE EXPRESSION REGULATORS OF AD PATHOLOGY: POTENTIAL NON INVASIVE BIOMARKERS	18
3.1. MicroRNAs in AD	18
3.2. SIRT1 in AD	22
<b>PART II. CONSIDERATIONS FOR THE DEVELOPMENT AND ASSESSMENT OF ALZHEIMER'S DISEASE TREATMENTS</b>	<b>25</b>
4. MODELLING AD IN RODENTS TO RELIABLY TEST AD TREATMENTS	26
4.1. Sporadic AD rat models	26
A $\beta$ -induced rat model	26
STZ-induced rat model	28
4.2. Evaluation of AD-related memory disturbances in rodent models through Morris water maze	29
5. VIEWING AD AS A NEURAL CIRCUIT DISORDER	31
5.1. Neuronal circuits supporting episodic memory disrupted in AD	31
The trisynaptic circuit: insight into the entorhinal cortex and the hippocampus	31
The complete Papez circuit: insight into the anterior nucleus of the thalamus and the retrosplenial cortex	34
The default mode network: insight into the medial prefrontal cortex	35
5.2. Modulatory systems of memory circuits disrupted in AD	36
Basal forebrain cholinergic circuit	37
Ascending monoaminergic systems: insight into mesocorticolimbic dopaminergic circuit	37
5.3. Implications of the circuit-disorder view of AD	39
<b>PART III. DEEP BRAIN STIMULATION AS A TREATMENT FOR ALZHEIMER'S DISEASE</b>	<b>40</b>
6. USE OF DBS FOR MEMORY IMPROVEMENT IN AD	41

6.1. Promising results and limitations of DBS trials in AD patients	41
6.2. Insights from laboratory animal studies	42
7. MFB AS A POTENTIAL DBS TARGET FOR AD TREATMENT: AN APPROACH FROM ICSS	44
7.1. Memory improving effects of MFB-ICSS	45
7.2. Cell and molecular mechanisms underlying MFB-ICSS that could mediate its behavioural effects	46
7.3. Consideration of DBS to the MFB as an AD treatment	47
<b>AIMS AND SCOPE</b>	<b>49</b>
<b>MATERIALS AND METHODS</b>	<b>51</b>
1. Animals and experimental design	51
1.1. Study 1	51
1.2. Study 2	52
1.3. Study 3	53
2. Chemicals	54
2.1. Preparation and assessment of amyloid- $\beta$ aggregates	54
2.2. Preparation of streptozotocin	55
3. Stereotactic surgery	55
3.1. Electrode implantation	55
3.2. Intracerebroventricular injection of amyloid- $\beta$	56
3.3. Intracerebroventricular injection of streptozotocin	57
4. Intracranial self-stimulation treatment	58
4.1. ICSS behaviour shaping	58
4.2. ICSS treatment	59
5. Behavioural analyses	60
5.1. Morris water maze acquisition phase	61
5.2. Morris water maze probe test	61
5.3. Morris water maze reversal test	62
6. Sample collection	62
6.1. Serum samples	62
6.2. Tissue samples	62
7. Molecular assays	65
7.1. Protein and RNA isolation and quantification	65
7.2. TaqMan OpenArray procedure	66
7.3. TaqMan miRNA qRT-PCR	67
7.4. Western blot	69
7.5. SIRT1 ELISA	71
7.6. BDNF ELISA	72
8. Histological analyses	73
8.1. Nissl staining	73
8.2. DBN and ptau immunostaining	76
8.3. Observation methodology	80
9. Statistical analyses	81
<b>RESULTS</b>	<b>83</b>
<b>STUDY I. MOLECULAR MECHANISMS LINKING ICSS EFFECTS WITH ALZHEIMER'S DISEASE PATHOLOGY</b>	<b>83</b>

1.1. ICSS-induced changes on miRNAs in specific hippocampal subfields and serum	84
miRNA endogenous normalizers in hippocampus and serum after ICSS treatment	84
Time of ICSS-induced changes on miRNAs	86
ICSS-regulated miRNA candidates	87
ICSS-induced miRNA changes in hippocampal subfields	89
ICSS-induced miRNA changes in serum	90
1.2. ICSS-induced changes on proteins associated to AD main hallmarks in DG hippocampal subfield	91
ICSS-induced changes on APP levels in DG	91
ICSS-induced changes on tau and ptau levels in DG	91
ICSS-induced changes on DBN levels in DG	91
1.3. ICSS-induced changes on other plasticity regulatory proteins related with early AD pathology in hippocampal subfields and serum	93
ICSS-induced changes on SIRT1 in hippocampal subfields and serum	93
ICSS-induced changes on BDNF in DG and serum	95
1.4. Discussion	96
Methodological considerations regarding miRNA analysis after ICSS treatment	96
ICSS-regulated miRNAs in physiological conditions link ICSS molecular mechanisms with AD	97
Serum ICSS-regulated miRNAs are potential treatment biomarkers	99
Overlapping molecular mechanisms between ICSS and AD were not demonstrated in physiological conditions in the levels of typical AD-associated proteins, but evidenced in SIRT1	99
Conclusions	101
<b>STUDY II. AMYLOID-<math>\beta</math> INJECTED MODEL TO EVALUATE ICSS TREATMENT IN EARLY ALZHEIMER'S DISEASE</b>	102
2.1. Amyloid- $\beta$ 1-42 oligomeric aggregates to be injected	103
2.2. Time-dependent alterations on behavioural and histopathological AD hallmarks in A $\beta$ -injected rats	104
Spatial learning and memory deficits in A $\beta$ -injected rats	104
Neurodegeneration in A $\beta$ -injected rats	106
Alteration of DBN levels in A $\beta$ -injected rats	109
Alteration of ptau levels in A $\beta$ -injected rats	116
2.3. Effects of ICSS on early AD-like hallmarks in A $\beta$ -injected rats	122
Evidence of ICSS effects on behavioural affectations in A $\beta$ -injected rats	122
Effect of ICSS on DBN levels in A $\beta$ -injected rats	123
Effect of ICSS on ptau levels in A $\beta$ -injected rats	123
2.4. Summary	124
2.5. Discussion	125
Methodological considerations regarding A $\beta$ injection to model AD	125
Behavioural and neurodegenerative AD-like affectations partially recover long after A $\beta$ injection	126
Molecular AD-like affectation presents a particular progression after A $\beta$ injection	126
ICSS treatment partially alleviates long-lasting molecular AD hallmarks in the A $\beta$ -injected model	128
Conclusions	128
<b>STUDY III. ICSS TREATMENT EFFECTS ON CELL AND MOLECULAR MARKERS OF EARLY ALZHEIMER'S DISEASE IN STZ-INJECTED MODEL</b>	130
3.1. Physiological, histomorphological and behavioural affectations in STZ-injected model	131
Physiological affectation in STZ-injected rats	131

Morphologic changes in lateral ventricles and periventricular structures in STZ-injected rats	132
Behavioural affectation in STZ-injected rats	134
3.2. ICSS effects on AD hallmarks in STZ-injected rats	135
Evidence of ICSS effect on behavioural affectations of STZ-injected rats	135
Effect of ICSS on neurodegeneration in STZ-injected rats	136
Effect of ICSS on DBN levels in STZ-injected rats	140
Effect of ICSS on tau and ptau levels in STZ-injected rats	143
Effect of ICSS APP evels in STZ-injected rats	149
3.3. STZ and ICSS effect on molecular regulators of AD hallmarks in DG hippocampal subfield and serum	150
miRNA endogenous normalizers in DG and serum after STZ injection and ICSS treatment	150
miRNA changes in DG after STZ injection and ICSS treatment	151
miRNA changes in serum after STZ injection and ICSS treatment	151
SIRT1 levels in DG and serum after STZ injection and ICSS treatment	152
3.4. Summary	155
3.5. Discussion	156
Methodological considerations regarding STZ injection to model AD	156
Long-lasting behavioural, histomorphological and molecular AD-like characteristics uphold the use of STZ-injected model for long-term treatment assessment in early AD	157
ICSS treatment affects AD-like molecular hallmarks in STZ-injected model	160
ICSS treatment affects molecular regulators of AD pathology in STZ-injected model: SIRT1 emerges as a promising biomarker for both AD-like pathology and ICSS treatment in STZ rat model	161
Conclusions	162
<b>GENERAL DISCUSSION</b>	<b>163</b>
About the suitability of animal AD models to study ICSS treatment effect	164
About the ability of ICSS to fight cell and molecular AD hallmarks	166
About the implication of AD-related gene expression regulators in ICSS facilitating effect: emergence of potential non-invasive treatment biomarkers	167
Concluding remarks and future directions	168
<b>CONCLUSIONS</b>	<b>169</b>
<b>REFERENCES</b>	<b>172</b>

## SUMMARY

Alzheimer's disease (AD) is the most common cause of dementia, mainly characterized by episodic memory disturbances among other disabling symptoms. Despite great efforts put in AD research, at present there is no treatment able to cure or stop the progression of the disease. In this situation, electrical stimulation of deep brain areas (deep brain stimulation, DBS) has been suggested as a novel neuromodulatory approach to restore memory circuits in AD. Although the biological mechanisms underlying this treatment are not completely understood, DBS aimed at different brain targets has shown promising results of cognitive efficacy in AD context, both in studies using experimental animals as well as in initial clinical trials. However, the election of the target region remains a critical controversial issue.

Our group has consistently demonstrated that stimulation of the medial forebrain bundle (MFB), an area part of the neural substrate of reward, by means of intracranial self-stimulation (ICSS), facilitates learning and memory in healthy adult rodents, as well as in rats with aged or lesion-related memory impairment. At a molecular level, MFB-ICSS has been found to regulate the expression of synaptic plasticity proteins in memory-related brain areas, such as the hippocampus. These previous results suggest that the MFB could be a promising stimulation target in AD treatment. Nevertheless, MFB-ICSS effects have never been evaluated in AD condition, not even in relation to the main molecular correlates of AD pathology. This thesis approaches for the first time this situation, aiming to assess the potential use of rewarding stimulation of the MFB (referred as "ICSS" in the context of this dissertation) as a treatment for AD in a rat model, focusing on its effects on molecular markers of AD pathology.

In a first study, the acute effect of three ICSS sessions on molecular correlates of AD was assessed in a physiological context. Despite no modulation in the levels of amyloid precursor protein (APP), phosphorylated tau (p $\tau$ ) and synaptic protein drebrin (DBN) has been demonstrated, the effect of ICSS on specific microRNAs and SIRT1 regulators is described for the first time. In particular, ICSS upregulated miR-132 in DG and CA1 hippocampal subfields, and miR-181c, miR-495 and SIRT1 in DG, 90 minutes after stimulation. ICSS modulation of these molecules, all of them related to synaptic plasticity and altered in AD, provide evidence of overlapping regulatory mechanisms with AD and, so, a mechanistic rationale to the use in this context. Moreover, serum miR-132, which was found upregulated after ICSS treatment, and serum SIRT1 arose as potential non-invasive DBS treatment biomarkers to further explore in AD condition.

Thus, subsequent studies aimed to assess the effects of ICSS treatment in an AD rat model, especially regarding the molecular markers of early pathology but also relating with memory improvement. To this end, two different sporadic onset models obtained by intracerebroventricular injection of amyloid- $\beta$  ( $A\beta$ ) and streptozotocin (STZ), respectively, have been characterized based on the evaluation of neurodegeneration, synaptopathology, tau pathology and amyloid pathology markers, together with spatial learning and memory in the Morris water maze. Both models showed cognitive and neuropathological alteration in different areas referable to AD. However,  $A\beta$  model failed in reproducing AD progression. Specifically, AD-like memory deficits were evident when evaluated at days 15-22 after  $A\beta$  injection, but marginal at days 26-33, suggesting a transient affectation. Moreover, localization of neuropathological alterations, consisting of neurodegeneration, decreased DBN levels and increased ptau levels, presented a regional transition from frontal regions (at day 22 after  $A\beta$  injection) to temporal-parietal structures (at day 33), inverting the expected progression for AD. For these reasons,  $A\beta$  model was considered inappropriate to assess long-term treatment effects in future studies. Instead, STZ model evaluated at days 33-40 after injection, evidenced long-lasting coexistence of behavioural and early neuropathological affectation. Administration of five ICSS sessions contingent with Morris water maze acquisition phase on days 33-37 after STZ injection results in alleviation of memory dysfunction and the underlying neuropathological alterations displayed at day 40. Remarkably, ICSS induced an increase in neuronal density and a decrease in APP and ptau levels in hippocampal subfields, recovering control levels. Moreover, levels of miR-146a in DG tend to be compensated by ICSS. ICSS treatment also increased SIRT1 serum levels, which were reduced in STZ model correlating with AD hallmarks. Therefore, the use of SIRT1 as a promising serum biomarker is further encouraged for DBS treatment in AD-like conditions.

Overall, MFB-ICSS mechanisms have shown to intercede with molecular markers of AD pathology. In this sense, ICSS has demonstrated to modulate the levels of plasticity and AD-related miRNAs and SIRT1, both in physiological and STZ-induced pathological context. Upregulation of serum miR-132 observed in physiological condition, and serum SIRT1 in pathological conditions boost the suggestion of their use as promising non-invasive biomarkers in DBS treatments for AD. Furthermore, ICSS treatment has demonstrated to mitigate neuropathological hallmarks of early AD and improve behavioural impairment in a well characterized sporadic AD rat model. Altogether, these results sustain the promising potential of electrical stimulation of the MFB for the treatment of AD and set interest in novel treatments for AD with rewarding approaches.



## RESUM

La malaltia d'Alzheimer (AD) és la causa més comuna de demència, caracteritzada, entre altres símptomes neuropsicològics, per la presència d'alteracions en la memòria episòdica. Malgrat els grans esforços destinats a la recerca de l'AD, en aquest moment no existeix cap tractament capaç de curar o aturar la progressió de la malaltia. En aquesta situació, s'ha proposat l'estimulació elèctrica d'àrees cerebrals profundes (DBS, de l'anglès "deep brain stimulation") com una estratègia neuromoduladora per restaurar els circuits de la memòria afectats en l'AD. Si bé és cert que els mecanismes biològics subjacents a aquest tractament no són del tot coneguts, la DBS dirigida a diferents regions cerebrals ha mostrat resultats prometedors en relació a la seva eficàcia cognitiva en un context d'AD, tant en estudis amb animals d'experimentació com en assajos clínics inicials. Tot i això, l'elecció de la regió a la qual dirigir l'estimulació continua generant controvèrsia.

El nostre grup ha demostrat consistentment que l'estimulació del feix prosencefàlic medial (MFB), una regió que forma part del substrat nerviós del reforç, mitjançant autoestimulació intracranial (ICSS), facilita l'aprenentatge i la memòria en rosegadors adults sans, així com també en rates envellides o amb dèficits de memòria causats per lesions. A nivell molecular, s'ha vist que la MFB-ICSS regula l'expressió de proteïnes associades amb la plasticitat sinàptica en àrees cerebrals relatives a la memòria, com ara l'hipocamp. Aquests resultats previs suggereixen que el MFB pot ser una diana d'estimulació prometedora per al tractament de l'AD. No obstant, els efectes de la MFB-ICSS no s'han avaluat mai en la condició d'AD o ni tan sols en relació als correlats moleculars de la patologia. Aquesta tesi aborda per primera vegada aquesta situació, amb l'objectiu d'avaluar la utilitat potencial de l'estimulació reforçant al MFB (designada com a "ICSS" en el context d'aquest treball) com a tractament per l'AD en un model en rata, atenent principalment als efectes sobre marcadors moleculars de la patologia.

En un primer estudi, els efectes aguts de tres sessions d'ICSS sobre els correlats moleculars de l'AD van ser valorats en un context fisiològic. Malgrat que els nivells de la proteïna precursora d'amiloide (APP), tau fosforilada (ptau) i la proteïna sinàptica drebrina (DBN) no es van mostrar modulats, es va demostrar per primera vegada l'efecte de l'ICSS en microRNAs específics i la proteïna SIRT1. En concret, l'ICSS va incrementar els nivells de miR-132 en les subregions hipocampals de DG i CA1, així com també els de miR-181c, miR-495 i SIRT1 en DG, 90 minuts després de l'estimulació. El fet que l'ICSS moduli aquestes molècules reguladores, totes elles relacionades amb plasticitat sinàptica i alterades en l'AD, evidencia l'existència de mecanismes reguladors convergents amb els de la patologia. Per tant, aquests resultats van esdevenir un fonament mecanístic per plantejar l'ICSS en context d'AD. A més a més, els nivells sèrics del miR-

132, que també es van trobar augmentats després del tractament d'ICSS, així com els de SIRT1 es van erigir com a biomarcadors no-invasius potencials per a tractaments DBS, que calia seguir explorant en condició d'AD.

Així doncs, els estudis consegüents pretenien avaluar els efectes del tractament d'ICSS en un model d'AD en rata, amb especial atenció als marcadors moleculars de patologia inicial però també en relació amb la millora de memòria. Dos models d'AD esporàdic obtinguts per injecció intracerebroventricular de  $\beta$ -amiloide ( $A\beta$ ) i estreptozotocina (STZ), respectivament, van ser caracteritzats en base a l'avaluació de marcadors de neurodegeneració, sinaptopatologia, taupatologia i amiloidpatologia, així com també de l'aprenentatge i la memòria en el laberint aquàtic de Morris. Ambdós models van mostrar alteracions assimilables a l'AD, tant a nivell cognitiu com neuropatològic en diferents àrees relacionades amb la memòria. Tanmateix, el model  $A\beta$  va mostrar limitacions pel que fa la seva similitud amb la progressió de l'AD. D'una banda, els dèficits de memòria assimilables a l'AD van resultar evidents en l'avaluació als 15-22 dies després de la injecció d' $A\beta$ , però eren molt reduïts als dies 26-33, suggerint una transitorietat dels efectes. D'altra banda, les alteracions neuropatològiques consistents en neurodegeneració, disminució de DBN i augment de ptau van presentar una evolució des de regions frontals (als 22 dies) cap a estructures parieto-temporals (als 33 dies), invertint la progressió descrita per a l'AD. Per aquests motius, el model  $A\beta$  es va considerar inapropiat per avaluar efectes a llarg termini en estudis futurs. En canvi, el model STZ va presentar alteracions conductuals i neuropatològiques concurrents 40 dies després de la injecció. L'administració de cinc sessions d'ICSS contingents amb la fase d'adquisició del laberint de Morris els dies 33-37 post-injecció va provocar una millora en les afeccions de la memòria així com en les alteracions neuropatològiques subjacents. Notablement, l'ICSS va induir un increment de la densitat neuronal i una disminució dels nivells d'APP i ptau en subregions hipocampals, recuperant els nivells propis de les rates control. A més, els nivells del miR-146a en DG van tendir a ser compensats per l'ICSS. El tractament ICSS també va provocar un increment en els nivells de SIRT1 a sèrum, que es trobaven reduïts en les rates STZ correlacionant amb els marcadors neuropatològics. Aquests resultats van reafirmar el potencial de SIRT1 en sèrum com a biomarcador prometedor en tractaments de DBS per a AD.

En general, doncs, en aquesta tesi s'ha evidenciat que els mecanismes d'ICSS al MFB intercedeixen amb els marcadors moleculars de l'AD. En aquest sentit, s'ha demostrat que l'ICSS modula els nivells de determinats miRNAs i de SIRT1, relacionats amb plasticitat i amb l'AD, tant en condicions fisiològiques com en condicions patològiques induïdes per l'STZ. L'augment del miR-132 sèric observat en un context fisiològic, com també del SIRT1 sèric en condicions patològiques

suscita el seu ús com a biomarcadors no-invasius de tractaments de DBS per l'AD. A més a més, s'ha comprovat com el tractament d'ICSS ha mitigat les alteracions neuropatològiques i cognitives en un model ben caracteritzat d'AD esporàdic, en rata. En conclusió, aquests resultats emparen el potencial prometedor de l'estimulació elèctrica al MFB com a tractament per a l'AD, i al·ludeixen a l'interès per possibles nous tractaments amb aproximacions reforçants.

## RESUMEN

La enfermedad de Alzheimer (AD) es la causa más frecuente de demencia, caracterizada, entre otros síntomas neuropsicológicos, por alteraciones en la memoria episódica. A pesar de los grandes esfuerzos destinados a la investigación del AD, actualmente no existe ningún tratamiento capaz de curar o detener la progresión de la enfermedad. En esta situación, la estimulación eléctrica de áreas cerebrales profundas (DBS, del inglés “deep brain stimulation”) se ha sugerido como estrategia neuromoduladora para restaurar los circuitos de la memoria afectados en el AD. Si bien es cierto que los mecanismos biológicos subyacentes a este tratamiento no son completamente conocidos, la DBS dirigida a diferentes regiones cerebrales ha mostrado resultados prometedores en relación a su eficacia cognitiva en un contexto de AD, tanto en estudios con animales de experimentación como en ensayos clínicos iniciales. Sin embargo, la elección de la región objeto de la estimulación continúa generando controversia.

Nuestro grupo ha demostrado consistentemente que la estimulación del haz prosencefálico medial (MFB), una región perteneciente al sustrato nervioso del refuerzo, mediante autoestimulación intracraneal (ICSS), facilita el aprendizaje y la memoria en roedores adultos sanos, así como también en ratas envejecidas o con déficits de memoria causados por lesiones. A nivel molecular, se ha observado que la MFB-ICSS regula la expresión de proteínas asociadas a la plasticidad sináptica en áreas relativas a la memoria, como el hipocampo. Estos resultados previos sugieren que el MFB puede ser una diana de estimulación prometedora para el tratamiento del AD. No obstante, los efectos de la MFB-ICSS nunca antes se han evaluado en la condición de AD, ni siquiera en relación a los correlatos moleculares de la patología. Esta tesis aborda por primera vez esta situación, con el objetivo de valorar la utilidad potencial de la estimulación reforzante en el MFB (designada como ICSS en el contexto de esta disertación) como tratamiento para el AD en un modelo en rata, atendiendo principalmente a los efectos sobre marcadores moleculares de la patología.

En un primer estudio, los efectos agudos de tres sesiones de ICSS sobre los correlatos moleculares del AD fueron evaluados en un contexto fisiológico. Pese a que los niveles de la proteína precursora de amiloide (APP), tau fosforilada (ptau) y la proteína sináptica drebrina (DBN) no se vieron modulados, se demostró por primera vez el efecto de la ICSS en microRNAs específicos y la proteína SIRT1. En concreto, la ICSS incrementó los niveles de miR-132 en la subregiones hipocampales de DG y CA1, así como también de miR-181c, miR-495 y SIRT1 en DG, 90 minutos tras la estimulación. El hecho que la ICSS module estas moléculas reguladoras, todas ellas relacionadas con plasticidad sináptica y alteradas en el AD, evidencia la existencia de mecanismos

reguladores convergentes con los de la patología. Por lo tanto, estos resultados proporcionaron un fundamento mecanístico para plantear la ICSS en contexto de AD. Además, los niveles séricos de miR-132, que también se vieron aumentados después del tratamiento de ICSS, así como los de SIRT1 se erigieron como potenciales biomarcadores no-invasivos para tratamientos de DBS, que cabía seguir explorando en la condición de AD.

Por lo tanto, estudios subsiguientes pretendían evaluar los efectos del tratamiento de ICSS en un modelo de AD en rata, con especial interés en los marcadores moleculares de patología temprana pero también en relación con la mejora de memoria. Dos modelos de AD esporádico generados por inyección intracerebroventricular de  $\beta$ -amiloide ( $A\beta$ ) y estreptozotocina (STZ), respectivamente, fueron caracterizados en base a la evaluación de marcadores de neurodegeneración, sinaptopatología, taupatología y amiloidopatología, así como también de aprendizaje y memoria en el laberinto acuático de Morris. Ambos modelos mostraron alteraciones asimilables al AD, tanto a nivel cognitivo como neuropatológico en diferentes áreas relacionadas con la memoria. Sin embargo, el modelo  $A\beta$  manifestó limitaciones referentes a su falta de semejanza con la progresión del AD. Por un lado, los déficits de memoria asimilables al AD resultaron evidentes en la evaluación a los 15-22 días tras la inyección de  $A\beta$ , pero se encontraban muy reducidos a los 26-33 días, sugiriendo una transitoriedad en los efectos. Por otro lado, las alteraciones neuropatológicas consistentes en neurodegeneración, disminución de DBN y aumento de ptau presentaron una evolución desde regiones frontales (a los 22 días) hacia estructuras parieto-temporales (a los 33 días), invirtiendo la progresión descrita en el AD. Por consiguiente, el modelo  $A\beta$  se consideró inapropiado para evaluar efectos a largo plazo en estudios futuros. Por el contrario, el modelo STZ presentó alteraciones conductuales y neuropatológicas concurrentes, 40 días después de la inyección. La administración de cinco sesiones de ICSS contingentes con la fase de adquisición del laberinto de Morris los días 33-37 post-inyección provocó una mejora en las afecciones en la memoria así como en las alteraciones neuropatológicas subyacentes. A destacar, la ICSS indujo un incremento de la densidad neuronal y una disminución de los niveles de APP y ptau en subregiones hipocampales, restableciendo los niveles propios de las ratas control. Además, los niveles del miR-146a en DG tendieron a ser compensados por la ICSS. El tratamiento ICSS también provocó un incremento de los niveles de SIRT1 séricos, que se encontraban reducidos en las ratas STZ correlacionando con los marcadores neuropatológicos. Estos resultados reafirmaron el potencial de SIRT1 en suero como biomarcador prometedor en tratamientos de DBS para AD.

En definitiva, en esta tesis se ha evidenciado que los mecanismos de la ICSS al MFB interceden con los marcadores moleculares de AD. En este sentido, se ha demostrado que la ICSS modula los niveles de determinados miRNAs y de SIRT1, relacionados con plasticidad y AD, tanto en condiciones fisiológicas como en condiciones patológicas inducidas por STZ. El aumento de miR-132 sérico observado en un contexto fisiológico, así como el de SIRT1 en condiciones patológicas suscita su aplicación como biomarcadores no-invasivos de tratamientos de DBS para AD. Asimismo, se ha comprobado que el tratamiento de ICSS mitigó las alteraciones neuropatológicas y cognitivas en un modelo bien caracterizado de AD esporádico, en rata. En conclusión, estos resultados avalan el potencial prometedor de la estimulación eléctrica al MFB como tratamiento para el AD, e inspiran el interés para posibles nuevos tratamientos con aproximaciones reforzantes.



# INTRODUCTION

## PART I. ALZHEIMER'S DISEASE: A MULTIFACTORIAL DISORDER WITHOUT TREATMENT

In November 1901, a 50-year-old woman entered the Frankfurt Psychiatric Hospital showing an unusual complex and progressive symptomatology including disturbances of memory, aggressiveness and confusion. Dr. Alois Alzheimer became interested in the course of this case up to her death 5 years later. Upon autopsy, he reported two kind of particular aggregates that characterise her brain: plaques between brain cells and tangles inside neurons. The resulting long-term study of the patient Auguste D. by Dr. Alzheimer transcended as the first described case of the subsequently named Alzheimer's disease (Stelzmann et al., 1995; Hippus and Neundörfer, 2003). Nowadays, Alzheimer's disease (AD) represents the most prevalent cause of dementia syndromes, constituting 60-80% of all cases.



# 1. EPIDEMIOLOGY AND CLINICAL PRESENTATION OF AD

## 1.1. Epidemiology

According to the latest available world report, dementia is estimated to affect 47 million people worldwide and 7.4 million people in Western Europe (Prince et al., 2015). Dementia prevalence in the world is estimated to be between 5 and 8% in people aged over 60, depending on the geographic area (Prince et al., 2013), showing an almost exponential increase with age doubling every 6.5 years in Western Europe (Prince et al., 2015)(Fig. 1). Spanish and Catalan estimations are in line with this general trend (Rodríguez-Sánchez et al., 2011; Tola-Arribas et al., 2013; Ponjoan et al., 2019).

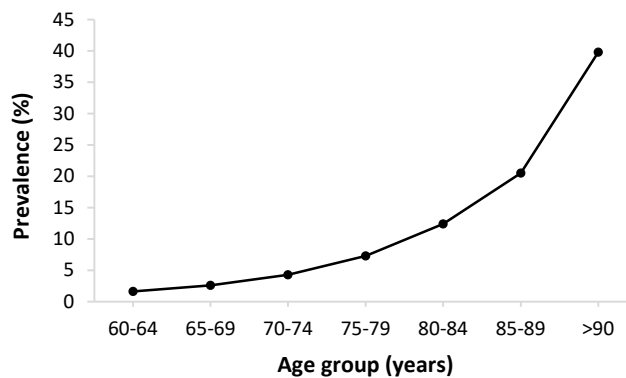


**Fig. 1 | Prevalence of dementia by age-group in Western Europe**, based on data from Prince et al., 2015.

Although dementia syndrome can arise from different causes, Alzheimer's disease (AD) is the most common type constituting 60-80% of all cases (Garre-Olmo, 2018). Two different forms of AD are described: familial and sporadic. The former, also known as early-onset AD, is diagnosed before the 65 years of age in individuals with inherited mutations. In contrast, sporadic AD (sAD), which accounts for 95% of the cases, presents different modifiable and non-modifiable risk factors associated, being the age the most significant (Amakiri et al., 2019). Thus, in the current ageing population, AD is predicted to achieve epidemic proportions, being already the third leading cause of death, only preceded by cerebrovascular diseases and cancers (Takizawa et al., 2014). Moreover, social impacts of the disease are especially considerable as AD patients become increasingly dependent of caregivers in emotional, psychological and physical terms (Brodsky and Donkin, 2009). Overall, estimated economic cost of the disease according to World Alzheimer Report 2015

is 818 billion dollars, with a marked increasing trend (Prince et al., 2015). The growing incidence of AD and its current lack of cure or effective treatment, together with its social and economic impacts, gives AD research a particular importance.

## 1.2. Clinical affectations and neuroanatomical correlates

Apart from the age of onset, familial and sporadic forms of AD cannot be distinguished by any clinical or neuropathological feature. Both show progressive and cumulative cognitive symptoms resulting from a selective and gradual neuronal loss in sequential brain areas (Fig. 2A). AD clinical progression can be classified in three stages: early, intermediate and later phase (dos Santos Picanço et al., 2018). It is also believed that a long presymptomatic stage precedes clinical outcomes. In this continuum progress, mild cognitive impairment (MCI) is thought to be a putative prodromal stage.

Brain pathology starts in areas located in the medial temporal lobe (MTL), especially the entorhinal/transentorhinal cortex and parts of the hippocampus (Braak and Braak, 1991a; Whitwell, 2010; Serrano-Pozo et al., 2011), being the latest a critical structure for specific types of memory. As the whole hippocampus is progressively affected, early symptoms arise. At the time of the diagnosis, hippocampal atrophy is estimated to be 23% (Shi et al., 2009), evolving at a rate of 4-5% per year (Barnes et al., 2009). In the intermediate stage, neuropathology spreads all through the structures traditionally classified in the limbic system, involving subcortical areas of the lateral temporal lobe, parietal and frontal lobe. Final stages include widespread areas in all the cerebral cortex, including association cortices. Additionally, damage to the brain stem also progresses over the course of the disease affecting, in final stages, the most vital functions (Rüb et al., 2016).

Overall, the whole brain results in a significant loss of matter, which is more pronounced in the hippocampus, and a resulting expansion of the ventricles (Whitwell, 2010; DeTure and Dickson, 2019) (Fig. 2B) visible by computed tomography and magnetic resonance imaging (MRI) (Blennow et al., 2006).

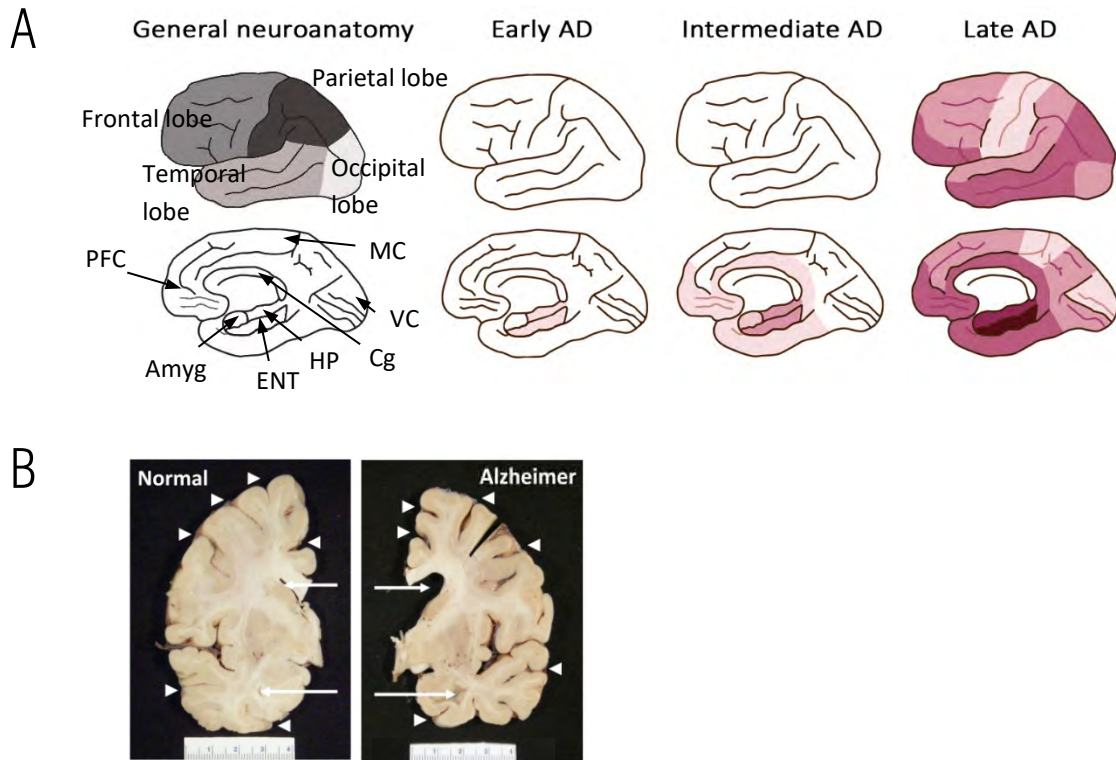


**Fig. 2 | Brain affection in AD.** **A.** Progression of neuropathology according to Braak & Braak stages (Braak and Braak, 1991a). First row of pictures show cortical views of the brain, while second row are sagittal sections. General neuroanatomic areas are depicted in the first column. Following pictures indicate progressive degenerating brain areas in each stage of AD, with darker shades representing higher affection. Abbreviations: Amyg: amygdala; Cg: cingulate; ENT: entorhinal cortex; HP: hippocampus; MC: motor cortices; PFC: prefrontal cortex; VC: visual cortices. Adapted from Serrano-Pozo et al., 2011. **B.** Coronal sections of an AD-affected brain compared to a normal brain, showing widening of sulcal spaces and narrowing of gyri (arrowheads), accompanied by enlargement of the frontal and temporal horns of the lateral ventricles (arrows). Adapted from DeTure and Dickson, 2019.

Thus, it is at later stages, usually 8-10 years after diagnose, that AD is a totally dementing illness and patients become fully dependent and unable to perform daily activities (Sweatt, 2010). Dementing symptoms consist on wide-ranging cognitive and perceptual effects, including impaired judgment, decision-making, aphasia (inability to comprehend or formulate language), apraxia (inability to plan or perform purposeful movements), agnosia (inability to recognize objects by use of the senses), impaired olfactory sensing and visuospatial processing and orientation. Neuropsychiatric symptoms, ranging from irritability and anxiety to apathy and depression, accompany the disease through all its time course (Robert et al., 2006; Lyketsos et al., 2011). However, consensus exists that, from the earliest phase, memory deficits are the main identity sign of AD, which worsen as the disease progresses.

## Memory function and memory dysfunction in AD

Memory is defined as the process of encoding, storage and retrieval of information (Stuchlik, 2014). Different categories of memory have been defined, which also rely on different neuroanatomical and neurophysiological systems within the brain (Brem et al., 2013; Gupta et al., 2018).

Depending on the duration of its accessibility, short-term memory (STM) and long-term memory (LTM) are distinguished. On the one hand, STM allows the retention of information from seconds to minutes. STM is closely related to the concept of working memory, which refers to the online maintenance and manipulation of information in an easily accessible state over brief periods of time, enabling the course of conscious everyday tasks, such as writing or computing. However, working memory also involves other processes like attention and retrieval of information stored in the LTM (Eriksson et al., 2015). In AD patients, deficits in attention and working memory associated to damage to the frontal lobe influence also executive functions, such as planning, problem solving, and goal-directed behaviour (Gold and Budson, 2009). On the other hand, in LTM, information is further consolidated persisting from minutes to years. The transition from STM to LTM depends on the occurrence of events to fix the neural representation of the memory through neuroplastic mechanisms including long-term potentiation (LTP), which results from the strengthening of synaptic connections, requiring gene expression changes and synthesis of new proteins. Memory representations formed in the hippocampus are thought to be reorganized for further permanent storage in neocortical areas in a process known as systems consolidation (Squire et al., 2015). Thus, because of early hippocampal affectation, impossibility to encode, store and retrieve new hippocampal-dependent memories is a main feature of the first stages of AD (Jahn, 2013). However, remote long-term memories, thought to be stored in the cortex, are vivid until latest phases of the disease, as their retrieval is hippocampal-independent.

Regarding the nature of the information, memory has been traditionally subdivided depending on whether it can be verbalized or not (Squire and Zola, 1996; Squire, 2004). On the one hand, non-declarative or implicit memory does not require conscious awareness and refers to procedural skills, such as perceptual and motor memory. This type of memory, that depends on different systems including associative cortices as well as diverse subcortical structures, is found relatively intact compared to other forms of memory in AD patients (Gold and Budson, 2009). On the other hand, declarative or explicit memory refers to the

knowledge that can be consciously recalled and verbalized (Squire and Zola, 1996). This memory can be further divided into episodic memory, for personal facts and events experienced at a specific time and space (and so including spatial memory), and semantic memory, referring to knowledge of the world, rules and concepts, independent of the spatio/temporal context (Squire, 2004). Semantic memory is disrupted in early to intermediate AD, attributed to pathology in the anterior and inferolateral temporal lobes, and the frontal lobes (Gold and Budson, 2009; Weintraub et al., 2012; Martínez-Nicolás et al., 2019). It is expressed through impaired language and verbal fluency together with difficulty in recognizing and naming people and objects (Bayles, 1982; Martin and Fedio, 1983; Becker and Overman, 2002; Aronoff et al., 2006). However, episodic memory, which is mainly supported by the MTL, especially by the hippocampus, is the most relevant memory type affected in AD and among its earliest symptoms (Gold and Budson, 2009; Weintraub et al., 2012). Spatial disorientation is pronounced, both in the sense of navigation and also in place recognition (Kalová et al., 2005; DeIpolyi et al., 2007; Kessels et al., 2010; Bird et al., 2010).

Thus, impairment in episodic memory has been the classical initial suggestion for early AD detection. Cognitive and neuropsychiatric tests are still the main tools for a probabilistic clinical diagnosis. Nevertheless, clinical observations are not unique and specific for AD (Dubois et al., 2007). Therefore, a definite diagnosis from initial phases, when disease-modifying therapies are likely to be more effective although behavioural affectations are limited to subjective memory complaints if any, should rely on distinctive markers of AD associated with specific characteristics of the disease. New criteria stipulate that clinical diagnosis should be complemented with imaging techniques, including structural MRI or positron emission tomography (PET), and analysis of specific molecular markers, examinable in cerebrospinal fluid (CSF) and in post-mortem tissue (Dubois et al., 2007; Lee et al., 2019), which will be addressed in the next section.

## 2. CELL AND MOLECULAR MARKERS OF AD PATHOGENESIS

Research following Dr. Alzheimer's observations identified the proteins that made up the peculiar aggregates observed in Auguste's brain, which became the two main hallmarks that define AD: extracellular senile plaques consisting on insoluble amyloid- $\beta$  ( $A\beta$ ) peptide (Glenner and Wong, 1984) and intracellular neurofibrillary tangles composed of hyperphosphorylated tau (ptau) protein (Grundke-Iqbal et al., 1986a, 1986b) (Fig. 3).

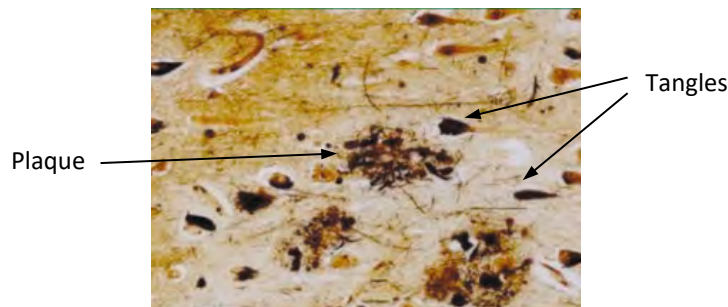


**Fig. 3 | Plaques and tangles in AD.** Extracellular senile plaques consisting of insoluble amyloid- $\beta$  ( $A\beta$ ) peptide and intracellular neurofibrillary tangles composed of hyperphosphorylated tau (ptau) protein in the cerebral cortex of a brain affected by AD. From Blennow et al., 2006.

Since their identification, a hypothetical causative role for the pathogenesis of AD has been imputed to these molecules. However, multiple additional cell and molecular changes co-occur in AD brains, including loss of neurons, synaptic damage, oxidative stress, mitochondrial dysfunction, neuroinflammation and glucose hypometabolism, among others (Serrano-Pozo et al., 2011; Sanabria-Castro et al., 2017; Tönnies and Trushina, 2017; Kinney et al., 2018). Some of these features, though not being specific for AD, correlate with cognitive decline and are suggested to play important roles in the pathology cascade. Still, their causality link and the underlying hierarchy is not fully understood. Some cell and molecular features of AD, their hypothetical contribution to disease process according to different theories, and their potential value as therapeutic and diagnostic targets will be reviewed in this section.

## 2.1. Amyloid pathology

Abnormal accumulation and deposition of amyloid- $\beta$  ( $A\beta$ ) in extracellular plates is the most evident hallmark of AD brains.  $A\beta$  is an aggregation-prone and toxic polypeptide, derived from the amyloid precursor protein (APP) proteolysis process.

APP is a transmembrane glycoprotein found in dimers at the cell membrane (Chen et al., 2017), which can undergo two different proteolytic pathways distinguished by whether it yields  $A\beta$  peptide formation or not (Qiu et al., 2015) (Fig. 4). In the amyloidogenic pathway, APP is cleaved in its extracellular N-terminus by  $\beta$ -secretase BACE1, causing the excision of sAPP $\beta$  fragment and leaving behind a C99 fragment. Then, the 4 kDa  $A\beta$  peptide is produced from the cleavage of C99 by  $\gamma$ -secretase, a protease complex including presenilin (PS) in the catalytic subunit. Excision at different positions leads to the release of  $A\beta$  peptide with varying number of residues between 37 and 49, being  $A\beta$ 40 and  $A\beta$ 42 the two prominent isoforms (Chen et al., 2017). While similar in structure,  $A\beta$ 42 is less abundant but more toxic, and it is the main  $A\beta$  variant that accumulates in the brain of AD patients (Qiu et al., 2015). In the non-amyloidogenic proteolytic pathway, APP is cleaved by the  $\alpha$ -secretase instead, leaving a C83 peptide unable to form a complete  $A\beta$ .

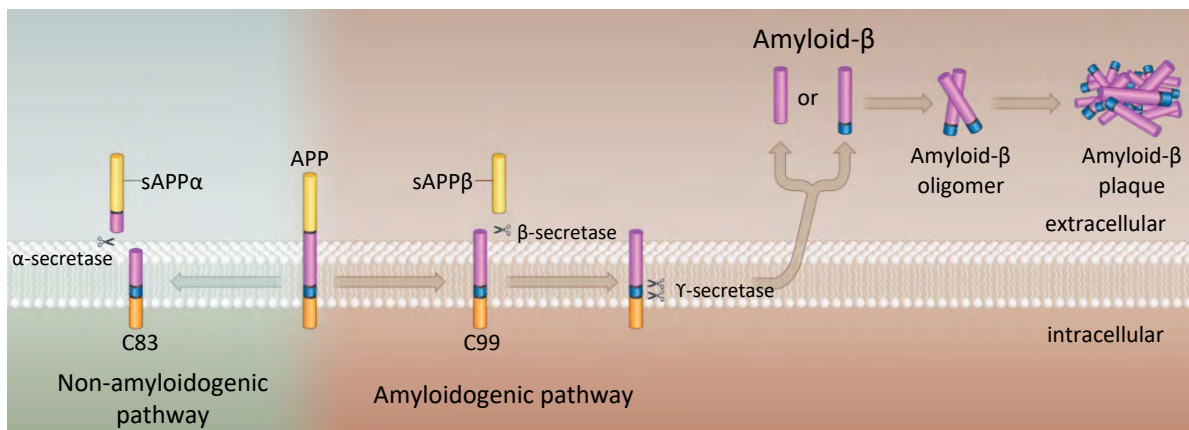


**Fig. 4 | Two possible proteolytic pathways of APP and the production of  $A\beta$ 40/42.** In the amyloidogenic pathway (red background in the right), APP is first cleaved by  $\beta$ -secretase and then by  $\gamma$ -secretase, leading to generation of  $A\beta$  peptide (mainly  $A\beta$ 40 and  $A\beta$ 42 forms) and its subsequent aggregation. In the non-amyloidogenic pathway (green background in the left) instead, APP is cleaved by  $\alpha$ -secretase and unable to form  $A\beta$ . Adapted from Makin, 2018.

Under physiological conditions, APP expression is enriched in the brain, where it is found in pyramidal neurons of the cortex and the hippocampus (Lorent et al., 1995), suggesting that it could have a role in neural plasticity. Different evidences insinuate the involvement of APP and their fragments in mediating synaptic contacts and increasing both presynaptic and postsynaptic plasticity (see Ludewig and Korte, 2017 for a review). Presynaptically, APP dimers were suggested to function as a G-protein coupled receptor activated by A $\beta$  monomer, which initiates calcium signalling contributing to glutamate release (Fogel et al., 2014). Thus, far from the view that A $\beta$  is an undesirable by-product of APP metabolism, some evidences support a positive role of A $\beta$  for plasticity and memory, when present at picomolar range concentration (Puzzo et al., 2008). This low concentration is maintained by an equilibrium between A $\beta$  peptide production and clearance.

However, in AD an increased production of A $\beta$  peptide is caused by an imbalance between amyloidogenic and non-amyloidogenic or A $\beta$  clearance pathways, resulting in the opposite effect on synaptic plasticity (Blennow et al., 2006). In familial AD, this imbalance is triggered by mutations on APP and PS genes, transmitted with an autosomal dominant pattern, which give rise to the overproduction of aggregation-prone forms of A $\beta$ . In sporadic forms, the cause of the imbalance is not known. Yet, apolipoprotein E (ApoE)  $\epsilon$ 4 allele, which is the main genetic risk factor known to increase predisposition to AD, is involved in A $\beta$  clearance and homeostasis (Chen et al., 2017).

High levels of A $\beta$  have shown to induce postsynaptic depression *in vitro* and *in vivo*, by altering glutamatergic transmission and causing loss of dendritic spines (Mucke and Selkoe, 2012). Moreover, the accumulation of A $\beta$  monomers is followed by its progressive aggregation into oligomers, which are believed to amplify this pathogenicity acting on both neurons and glial cells by inducing inflammatory cascades, oxidative stress, deregulation of calcium metabolism, synaptic dysfunction, tau phosphorylation and neuronal apoptosis (De-Paula et al., 2012; Mucke and Selkoe, 2012). These deleterious events to the neuronal cells lead to dysfunction of APP metabolism and further production of A $\beta$  peptides, in a positive feedback loop (De-Paula et al., 2012). A $\beta$  can also further aggregate into protofibrils and larger  $\beta$ -sheet fibrils, which are insoluble and finally deposit originating the characteristic amyloid plaques in the extracellular space (Chen et al., 2017) (Fig. 4).

Because of their visibility in AD brains, A $\beta$  plaques have focused the attention of A $\beta$  pathogenicity. However, plaques did not correlate with cognitive impairment, and they can be present in individuals with normal cognitive function (Amakiri et al., 2019). Low



molecular weight soluble oligomers (dimers, trimers and tetramers), which may spread throughout the brain, are believed to be the most toxic species. In this sense, plaques might act as relatively inactive reservoirs of these smaller aggregates delivering oligomers to the surroundings, as a result of an established equilibrium (Mucke and Selkoe, 2012). Still, the structure of A $\beta$  aggregate forms and the aggregation pathways, as well as their exact role in pathology, remain challenging research issues (see Chen et al., 2017 for a review).

Altogether, the high visibility of A $\beta$  plaques in AD brains and the proved toxicity of A $\beta$  oligomers, as well as the fact that familial AD is caused by mutations in the substrate or the key enzyme for A $\beta$  production, brought the believe that A $\beta$  is the main cause of AD. The amyloid hypothesis sets A $\beta$  accumulation as the initial event on a cascade leading to neuronal degeneration and dementia. This hypothesis has dominated AD neuropathology and treatment research for over 25 years (Hardy and Allsop, 1991; Hardy and Higgins, 1992; Hardy and Selkoe, 2002). However, lack of success of A $\beta$  therapeutic targeting and the low correlation of A $\beta$  burden with disease outcomes at least controvert this theory and admit an alternative view in which A $\beta$  overproduction in sporadic AD could be triggered as a compensatory mechanism in an attempt to palliate a pre-existing damage (Jankowsky et al., 2005; Makin, 2018).

Anyhow, imbalance of A $\beta$  levels is a distinctive feature of AD and so, it has been exploited for a diagnostic use. Decreased A $\beta$ 42 levels as well as A $\beta$ 42/A $\beta$ 40 ratio in CSF have been consistently reported from early stages of AD (Riemenschneider et al., 2002; Hampel et al., 2004; Lewczuk et al., 2004; Moonis et al., 2005). Moreover, with the introduction of amyloid-PET technique, which enables longitudinal imaging of aggregated A $\beta$  within the brain by utilizing amyloid tracers such as Pittsburgh Compound B (Klunk et al., 2004), it has been seen that A $\beta$  levels in CSF parallel its accumulation in the brain (Strozyk et al., 2003; Fagan et al., 2006; Grimmer et al., 2009). Thus, A $\beta$  levels in CSF have become a well-established biomarker useful for AD diagnosis, especially for research purpose (Lee et al., 2019).

## 2.2. Tau pathology

Together with A $\beta$  plaques, the presence of neurofibrillary tangles (NFT) inside neurons is considered the second neuropathological hallmark defining AD. These fibrous structures were shown to be composed of abnormally hyperphosphorylated tau protein (Grundke-Iqbal et al., 1986a, 1986b).

Tau is a normal microtubule-associated protein abundant in neurons and to a lesser extent in oligodendrocytes and astrocytes (Guo et al., 2017). Alternative splicing from a single gene (MAPT gene) gives rise to different isoforms that can be subject to a wide range of post-translational modifications, including acetylation and, more importantly, phosphorylation. Abundance in serine and threonine residues confer the potential to be phosphorylated in up to 20% of the protein (Stoothoff and Johnson, 2005). Different kinases (eg, GSK-3 $\beta$ , PKA and CDK5) and phosphatases (eg, PP-1 and PP-2A) target tau in a site-specific manner. Changeable phosphorylation state modulates tau affinity to microtubules, enabling its main function as a dynamic microtubule stability promoter (Shahani and Brandt, 2002). Temporal and spatial regulation of neuronal microtubule assembly is essential for controlling neuronal morphology, elongation and polarization needed both to maintain the intricate wiring and to promote structural plasticity.

In AD, hyperphosphorylation of tau causes microtubule disarrangement, resulting in impaired axonal transport and synaptic function and eventually leading to neurodegeneration (Shahani and Brandt, 2002). Besides, hyperphosphorylated tau (p $\tau$ ) is prone to self-aggregate into insoluble paired helical filaments which constitute the presumably cytotoxic NFT. In fact, whether it is NFT *per se* or tau species generated during the formation of NFT that are damaging to cells is still unknown (Guo et al., 2017). In any case, NFT become visible at early stages of the disease, and correlate with disease outcomes much better than A $\beta$  plaques (Shahani and Brandt, 2002), presenting a characteristic neuroanatomical distribution pattern that progresses through disease time course. Indeed, NFT progression has been used to define the six Braak stages of AD neuropathology: transentorhinal stages I-II, limbic stages III-IV and isocortical stages V-VI (Fig. 5) (Braak and Braak, 1991a; Braak et al., 2006a).

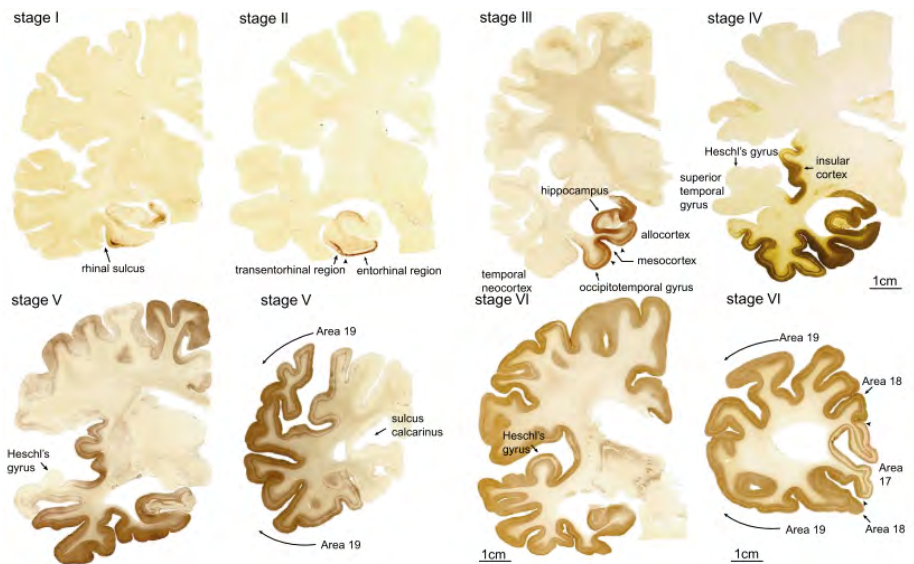


**Fig. 5 | Braak stages of neurofibrillary pathology in AD.** Human brain sections immunostained with antibody to phosphorylated tau. In stage I, labelling is limited to the transentorhinal region. Neurofibrillary pathology spreads to the entorhinal cortex in stage II. Stage III involves the hippocampus. Stage IV involves spread to the insula and inferior temporal neocortex. Finally, in stages V–VI even more neocortical areas are affected. Adapted from Braak et al., 2006b.

Correlating with NFT in the brain (Buerger et al., 2006; Tapiola et al., 2009), an increase in both ptau and total tau protein concentrations have been reported in CSF of AD patients (Blennow et al., 1995; Clark et al., 2003; Sunderland et al., 2003; de Souza et al., 2012). Thus, tau levels in CSF are used together with those of A $\beta$  resulting in integrative effective diagnostic tool, although tau proteins are not AD-specific biomarkers (Lee et al., 2019). In this sense, fluctuation of tau CSF levels also occur in both acute disorders and chronic neurodegenerative disorders. In fact, brain tau pathology is also found in other genetic and sporadic neurodegenerative diseases, termed tauopathies, where it appears unlinked from amyloid pathology. In AD, although it is likely downstream A $\beta$  alteration, tau role has also been suggested to be central to the disease process, leading to both neuronal death and synaptic dysfunction (Stoothoff and Johnson, 2005).

### 2.3. Synaptic dysfunction

Although neuronal death and resulting brain atrophy visible in MRI scans is an incontrovertible feature of AD, synaptic failure is considered to hold a preceding and more devastating role (Terry, 2000; Selkoe, 2002).

Synapses consist of presynaptic terminals containing vesicles of neurotransmitters and postsynaptic sites (dendritic spines) containing neurotransmitter receptors, postsynaptic density and actin cytoskeleton (Cohen, 2013). Number, structure and function of synapses change over time under a tight activity-dependent spatiotemporal regulation, conforming the most important type of plasticity in the brain. As exclusive points of contact between neurons, functional and plastic synapses are crucial for optimal connectivity and proper emerging cognitive functions and processes, including memory consolidation.

In AD, massive synaptic changes occur at different levels, both in structure and efficiency, which compromise cognitive performance from its earliest phase. Synaptic loss correlates more robustly with cognitive deficits than do numbers of plaques or tangles and degree of neuronal loss (Selkoe, 2002).

Imbalance in numerous neurotransmitters, especially of acetylcholine (ACh) and glutamate, is one important hallmark of early AD (Selkoe, 2002; Kandimalla and Reddy, 2017). In fact, the cholinergic hypothesis, which was one of the first postulated hypotheses to explain AD, considers that a deficit in the production of ACh contributes significantly to cognitive deterioration (see section 5.2 for further details) (Francis et al., 1999). But, in addition to neurotransmitter alterations, other indicators reveal the early synaptic failure.

Alteration in the levels of synaptic proteins involved in both synaptic vesicle trafficking as well as synaptic structure is observed from early AD (Counts et al., 2006). Among them, the postsynaptic protein drebrin (DBN) is found consistently decreased in the hippocampus and cortex of AD patients, becoming a sensitive and consistent early marker of synaptopathy (Harigaya et al., 1996; Counts et al., 2006, 2012; Ishizuka and Hanamura, 2017). DBN is an actin-binding protein involved in dendritic spine morphogenesis. One of the two major isoforms, drebrin A, is specifically found in neurons, where it accumulates in mature dendritic spines of excitatory synapses. DBN binding gives rise to a stable form of actin filaments (F-actin). Activity-regulated mobilization of DBN allows the remodelling and later restabilization of spines (see Shirao et al., 2017 for a complete review). In addition, DBN is also part of a large postsynaptic protein complex including N-methyl-D-aspartate receptor

for glutamate (NMDAR), CaMKII, cofilin, PSD-95, and actin, involved in synaptic transmission (Takahashi et al., 2003; Kojima and Shirao, 2007), and DBN seems to be involved in NMDAR regulation (Takahashi et al., 2006). Altogether, alteration of DBN levels in AD makes it impossible to fix the morphology and results in failure of enduring plasticity.

Although the precise cause of the DBN loss is not known, both A $\beta$  oligomers and tau are thought to directly and indirectly affect numerous signalling cascades that lead to pathological changes in synapse number, structure and function (Mucke and Selkoe, 2012; Forner et al., 2017; Chen et al., 2019). Thus, considering the downstream role of synaptic dysfunction in the pathology cascade, AD treatment strategies have mainly focused on A $\beta$  and tau.

However, precisely as an endpoint, which links protein pathology and disease symptoms, targeting synaptopathy becomes interesting for AD treatment (Jackson et al., 2019). In fact, the only drugs approved so far for AD intervene at this level, aiming to maintain activity in the remaining synapses (Jackson et al., 2019). Acetylcholinesterase inhibitors (e.g. Rivastigmine and Donepezil) act increasing the availability of ACh in the synaptic cleft (H. Ferreira-Vieira et al., 2016), while NMDAR antagonist (Memantine) aims to modulate the activity of glutamate (dos Santos Picanço et al., 2018). Nevertheless, as they are unable to compensate or recover dysfunctional or lost synapses or even stop ongoing synaptic loss, their efficacies are temporal and palliative, and limited in magnitude and by disease stage.

## 2.4. Glucose hypometabolism

Reduced glucose metabolism is another early and progressive well-established feature of AD (De Leon et al., 1983; Reiman et al., 1996; Small et al., 2000; Sperling et al., 2011). It was first believed that this sign was just a reflection of the neuronal loss. However, the decrease in glucose uptake is disproportionately more pronounced than that of oxygen, and appears decades prior clinical symptoms arise, even in the absence of structural brain atrophy (Costantini et al., 2008; Salkovic-Petrisic et al., 2009). Moreover, as it correlates with cognitive performance, detection of regional hypometabolism using PET with 18F-fluorodeoxyglucose (FDG-PET) has proved quite successful in diagnosing AD status (De Leon et al., 1983; Grady et al., 1986; Small et al., 2000; Mosconi, 2013). Furthermore, the increased risk of dementia found in individuals with insulin resistance, type 2 diabetes mellitus, hyperlipidemia or obesity evidence an association between metabolic disease and cognitive decline (Neth and Craft, 2017). It is for all these reasons that a stream of studies

have focused on the hypothesis that the brain loss of capacity to efficiently use glucose is an initial feature in AD cascade, implying a shift in the causation cascade proposed by the classical amyloid hypothesis (Fig. 6) (Grieb, 2016).

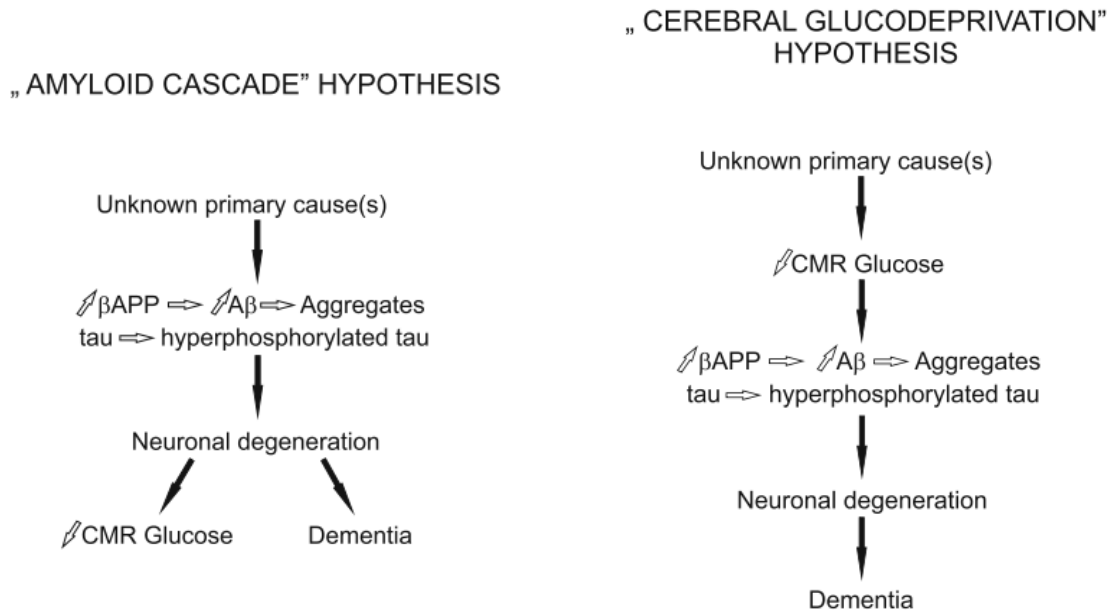


**Fig. 6 | Causation cascade hypotheses in AD.** Diagrams presenting the chain of causation of AD according to the “cerebral gluce deprivation” hypothesis (right), in contraposition to the classical “amyloid cascade” hypothesis (left). A suggested primary cause for the cerebral gluce deprivation hypothesis would be the insulin-resistant brain state. CMR: cerebral metabolic rate. From Grieb, 2016.

The brain is one of the most metabolically active organs, requiring great amounts of energy for proper function regarding neuronal survival, gene expression, neural plasticity and structural integrity. As neurons are quite dependent on the use of glucose as the main fuel, cognitive decline may arise if supply or ability to metabolize glucose is interrupted. In normal conditions, glucose enters cells from blood by glucose transporters in the blood brain barrier (mainly GLUT1) and distributed in the neuronal tissue (mainly GLUT 3, but also GLUT 2, 4 and others) (Koepsell, 2020). Inside the cell, glucose is then metabolized in the glycolysis taking place in the cytosol followed by the Krebs cycle and oxidative phosphorylation in the mitochondria. These processes yield ATP, essential for most of the cellular and molecular activities, reoxidized  $\text{NAD}^+$  and other by-products, such as Acetyl-CoA for the formation of acetylcholine neurotransmitter. As a rapid way to obtain only ATP, an alternative mechanism without complete oxidation, called aerobic glycolysis, is possible in highly metabolic regions, which are those related with cognitive function (Harris et al., 2014). Interestingly, these regions are the most vulnerable by AD pathology (Vlassenko et al., 2010; Mosconi, 2013).

The recognition of sporadic AD as an insulin resistant brain state (IRBS) offers a possible primary cause to the metabolic dysfunction. According to this model, AD could be considered a kind of diabetes mellitus restricted to the brain, in which reduced levels of insulin or insulin growth factor (IGF), as well as a failure of brain cells to respond to them as they normally would, result in the impairments in synaptic, metabolic and immune response characteristic of AD (see multiple reviews on this topic: Hoyer, 2002; Salkovic-Petrisic et al., 2009; Frisardi et al., 2010; Chen and Zhong, 2013; de la Monte, 2014; Neth and Craft, 2017). First, deficits in insulin would affect cerebral energy metabolism through insulin-dependent glucose transporters. In addition, decreased activity of insulin receptors would fail to activate PI3K/Akt and Ras/ERK pathways, responsible for metabolic effects, lipid/protein synthesis, cell growth, survival and gene expression. Through the mentioned pathways, insulin deficiency would affect expression of NMDARs, levels of neurotransmitters and also result in increased hyperphosphorylation of tau and production of A $\beta$ . Interestingly, the highest density of insulin producing cells and insulin receptors in the brain is found in the hippocampus, the cerebral cortex, the hypothalamus and the olfactory bulb, rendering them more vulnerable to insulin lack, which allows this theory to explain the regional selectivity in outburst of AD neurodegeneration. Moreover, this hypothesis matches the clinical efficacy shown in treatments targeting the insulin-glucose axis, although they are impractical for chronic use (Costantini et al., 2008). Finally, this model is reinforced by the use of the diabetogenic drug STZ to induce a metabolic model for AD, as will be presented in section 4.1. However, IRBS could be also explained by classical amyloid cascade by a desensitization and reduction of surface insulin receptors expression as a result of A $\beta$  toxicity (Ling et al., 2002; Xie et al., 2002).

Overall, AD causality cascade is still not clear and, indeed, it may be considered the result of a global molecular network dysregulation more than the result of a sequence of events. However, the study of the different hypotheses have provided evidence for multiple interrelated pathways in the onset of AD hallmarks, yielding clearly a multifactorial disease (Fig. 7).

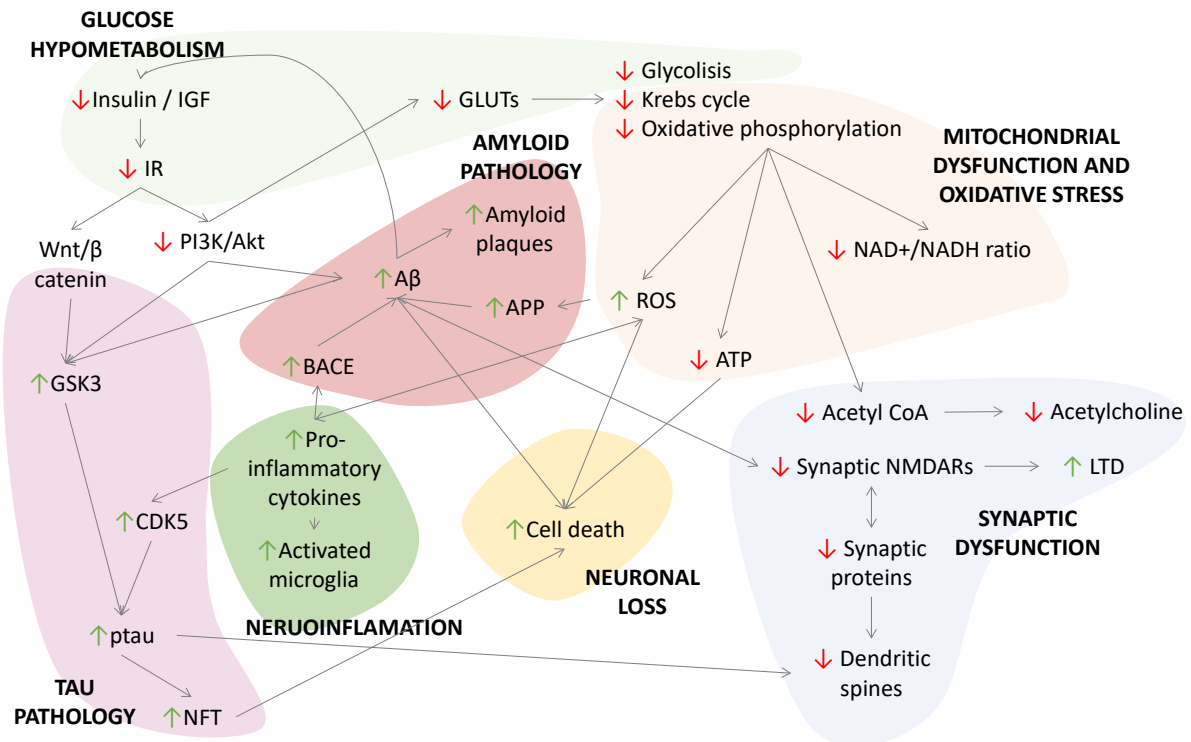


**Fig. 7 | Interrelation of AD molecular hallmarks through different altered pathways.** The diagram represents some, but not all, of the pathways altered in AD, with the aim of illustrate that, although the causality cascade is not clear, the different hypotheses provide evidence for interrelated pathways in the onset of amyloid pathology, tau pathology, neuroinflammation, neuronal loss, synaptic dysfunction and glucose hypometabolism, yielding a clear multifactorial disease (the different features are shaded in different colours). Abbreviations: A $\beta$ : amyloid- $\beta$ ; Akt: also known as protein kinase B (PKB); APP: amyloid precursor protein; ATP: adenosine triphosphate; BACE:  $\beta$ -site APP cleaving enzyme; CDK5: Cyclin-dependent kinase 5; GLUT: glucose transporter; GSK3: glycogen synthase kinase 3; IGF: insulin growth factor; IR: insulin receptor; LTD: long-term depression; NAD $^{+}$ : oxidized form nicotinamide adenine dinucleotide; NADH: reduced form nicotinamide adenine dinucleotide; NFT: neurofibrillary tangles; NMDAR: N-methyl-D-aspartate receptor; PI3K: phosphoinositide 3-kinase; ptau: phosphorylated tau protein; ROS: reactive oxygen species; Wnt: wingless-related integration site. Construction of the diagram was based on information in Frisardi et al., 2010; Mucke and Selkoe, 2012; Tönnies and Trushina, 2017; Kinney et al., 2018.



### 3. GENE EXPRESSION REGULATORS OF AD PATHOLOGY: POTENTIAL NON-INVASIVE BIOMARKERS

AD diagnosis using neuroimaging- and CSF-derived biomarkers relies on the main hallmarks of AD pathology presented in the previous section. Unfortunately, these biomarkers have a very limited use in routine clinical screening due to their intrusiveness and economic limitations, restricting early AD diagnosis. In contrast, the accessibility and inexpensiveness of blood collection makes it an attractive candidate source of novel biomarkers for early AD diagnosis and treatment prognosis. However, classical pathological hallmarks have not yet been accepted as reliable indicators in blood analyses due to inconsistent research results (Lee et al., 2019).

As concluded in the last section, AD complex pathogeny relies on the dysregulation of many biological pathways at multiple levels, yielding an intricate picture without a clear causation chain. Regulatory elements that control these pathways at a molecular level could have a major role in orchestrating the global dysregulation in AD and constitute potential biomarkers. Different molecules have been studied to this purpose (Altuna-Azkargorta and Mendioroz-Iriarte, 2020), including neurotrophic factors like BDNF (Ventriglia et al., 2013; Gezen-Ak et al., 2013), different protein kinases (Janel et al., 2011; Hugon et al., 2018), inflammatory mediators (Gezen-Ak et al., 2013) and gene expression regulators. In this latest category, microRNAs and SIRT1 are emerging as promising early and reliable AD biomarkers present in blood.

#### 3.1. MicroRNAs in AD

MicroRNAs (miRNAs) are a large family of small RNAs, approximately 18–25 nucleotides in length, with integral function in gene expression regulation. They are generated as pri-miRNAs from transcription of non-coding miRNA genes by RNA polymerase II or III, and cleaved to pre-miRNAs in the nucleus. After being exported to the cytoplasm, hairpin shaped pre-miRNA is cleaved to produce a double-stranded miRNA duplex. Unwinding of the duplex produces two single strand RNAs of ~22 nucleotides, coming from the 5' and the 3' arm of pre-miRNA respectively (named -5p and -3p). Usually one of these strands degenerate, while the other becomes a mature miRNA, often with multiple isoforms differing by few nucleotides (denoted by the addition of the letter a, b, c to the miRNA name). Rarely, both strands can serve as mature functional miRNA. Mature miRNAs form a multiprotein

complex named miRNA-induced silencing complex (miRISC), which bind to complementary sequences on their target messenger RNAs (usually 3' UTRs), and cause their degradation or translation blocking (Fig. 8) (Shaik et al., 2018). Thus, miRNAs negatively regulate gene expression by somehow inhibiting mRNA translation to functional proteins.

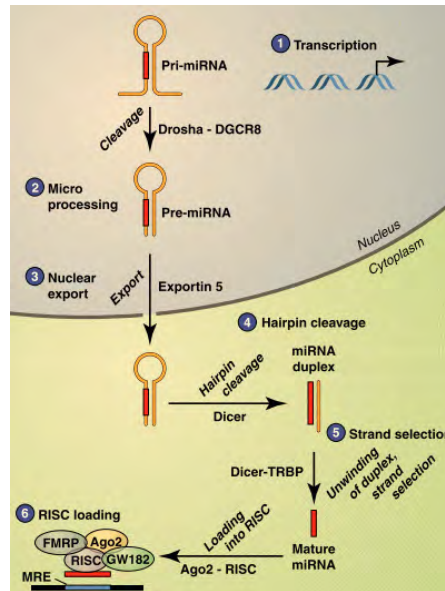


**Fig. 8 | MicroRNA biogenesis and function.** (1) pri-miRNAs (50–120 nt) are transcribed by RNA polymerase II or III, and form a hairpin secondary structure. (2) Pri-miRNAs are cleaved by the Drosha-DCRC8 complex, yields the pre-miRNA, which is exported from the nucleus to the cytoplasm by Exportin-5. (3) In the cytoplasm, Dicer cleaves the hairpin loop to generate a miRNA duplex. (4) Unwinding results in a ~22 nt single-stranded mature miRNA, from one arm of the pre-miRNA. (5) The mature miRNA is incorporated into the RNA-induced silencing complex (RISC), and targets specific mRNA transcripts through complementary base-pairing interactions. From Im and Kenny, 2012.

Post-transcriptional regulation by miRNAs plays a role in almost all biological processes, such as proliferation, development, apoptosis and inflammation. In the brain, some specifically expressed miRNAs regulate neuronal differentiation, synaptic plasticity, neurotransmitter release and neurite outgrowth (Kuss and Chen, 2008; Im and Kenny, 2012). Tissue-specific expression, together with regional and temporal distribution, evidence a tight regulation of miRNA function. Dysregulation of miRNA expression has been associated with several pathologies, with AD not being an exception. Thus, miRNA-targeting therapies could reduce AD pathology (Shaik et al., 2018). But what makes miRNAs even more interesting is that they are abundantly and stably present in circulatory biofluids, where they can be released by diffusion, inside exosomes or associated to lipoproteins (Kumar and Reddy, 2016). Thus, blood levels of specific miRNAs have been suggested as accessible and non-invasive biomarkers for AD diagnosis and prognosis.

A wealth of studies report altered expression of many different miRNAs in AD brain and blood (Geekiyana and Chan, 2011; Wang et al., 2011; Kumar et al., 2013a; Hadar et al., 2018) and several reviews intend to compile the reported roles of selected miRNAs in the regulation of each of the cellular changes of AD described in the previous section (Tan et al., 2013; Femminella et al., 2015; Reddy et al., 2017; Shaik et al., 2018; Amakiri et al., 2019), in order to identify potential AD biomarkers. Fig. 9 summarizes these data for major microRNAs in AD.

MiR-132, probably the best-studied miRNA in the field of learning and memory, is one of the suggested blood biomarkers of early AD pathology (Sheinerman et al., 2012; Xie et al., 2018). In the brain of AD patients, miR-132 is found consistently downregulated in different areas (Pichler et al., 2017; Shaik et al., 2018). Indeed, miR-132 expression has been associated with neuroprotective effects against AD hallmarks, acting both on amyloid and tau pathology (Smith et al., 2015; Salta et al., 2016) as well as prevention of neuronal death (Wong et al., 2013). However, its main roles are related to neural plasticity (Qian et al., 2017). Expression of miR-132 is regulated by cAMP response element binding (CREB) protein (Aksoy-Aksel et al., 2014), an important transcription factor in memory function which is also downregulated in the cortex of AD patients (Bartolotti et al., 2016). In memory-related pathways, miR-132 closely interacts with miR-134, BDNF and the longevity associated protein SIRT1 (Miller and Wahlestedt, 2010; Im and Kenny, 2012; Earls et al., 2014; Hadar et al., 2018). Interestingly, miR-134 family has also been suggested as a potential plasma biomarker that differentiate MCI from normal control population (Sheinerman et al., 2012) and miR-134 was revealed upregulated in AD patient brain samples in a recent miRNA profiling meta-analysis (Moradifard et al., 2018).

MiR-181c is another suggested AD blood biomarker (Tan et al., 2014a; Siedlecki-Wullich et al., 2019). It is found especially reduced in the cortex of AD patients negatively correlating with A $\beta$  levels (Femminella et al., 2015). MiR-181c targets serine palmitoyltransferase, which, if disinhibited, leads to enhanced BACE activity and increased A $\beta$  production (Geekiyana and Chan, 2011). A $\beta$  peptide, in turn, has shown to cause downregulation of miR-181c *in vitro* (Schonrock et al., 2012).

In addition to A $\beta$ - and plasticity-associated miRNAs, other miRNAs related to other hallmarks of AD have also been suggested as peripheral biomarkers. This is the case of miR-146a, which shows a selective upregulation in brain regions affected by AD pathology (namely hippocampus and neocortex) (Lukiw et al., 2008; Sethi and Lukiw, 2009).

Transcription of miR-146a is controlled by NF- $\kappa$ B, a nuclear factor with an important role in inflammatory response. MiR-146a suppresses translation of complement factor H and, thus, miR-146a overexpression contributes to neuroinflammatory spreading and subsequent increased neurodegeneration (Lukiw et al., 2008).

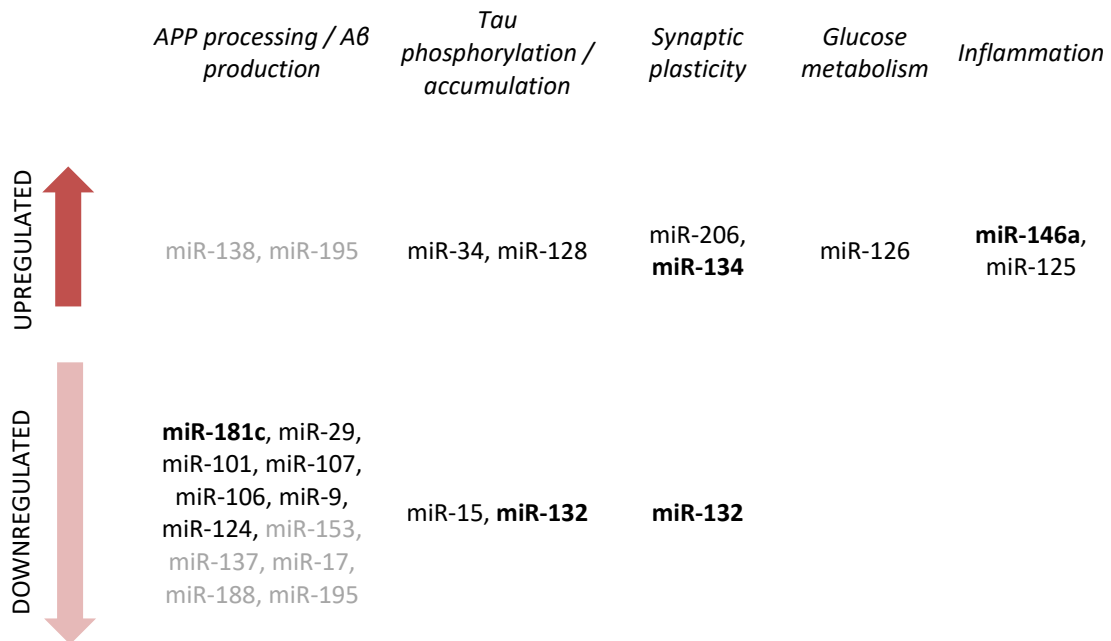


**Fig. 9 | Major miRNAs in AD.** Up arrow indicates reported increased levels of the miRNAs in AD patients' brain with respect to normal brain, while down arrow indicates downregulated ones. Columns refer to the main AD neuropathological trait to which miRNAs are associated, although they may be also interrelated with others. Black miRNAs are more consistently reported to be related with AD pathology than grey ones. Highlighted miRNAs refer to those mentioned in the text. From data on Tan et al., 2013; Femminella et al., 2015; Reddy et al., 2017; Shaik et al., 2018; Amakiri et al., 2019.

Overall, miRNAs establish extremely complex regulatory pathways interacting among them and with other regulatory molecules that contribute to AD pathogenesis, such as SIRT1 (Fig. 10). Although difficult to elucidate, persistent study of miRNA alteration seems a crucial step to identify the converging mechanisms involved in AD and its potential therapeutic and diagnostic targets.

### 3.2. SIRT1 in AD

Sirtuins (silent information regulators or SIRT) are a family of nicotinamide adenine dinucleotide (NAD<sup>+</sup>)-dependent deacylases that can deacetylate histones, causing chromatin remodelling often associated with transcription repression. They can also act on numerous non-histone protein targets (Martínez-Redondo and Vaquero, 2013). As a result, they exert regulation on a wide range of cellular processes (Herskovits and Guarente, 2014). Especially, sirtuins have been traditionally linked with beneficial effects of calorie restriction in aging and longevity. Because of the strong correlation between AD and age, investigating the role of sirtuins in relation to AD had taken interest.

SIRT1 is the most extensively studied sirtuin in AD. In this context, SIRT1 was not only found reduced in brain areas such as parietal cortex, correlating with markers of disease severity (Julien et al., 2009), but also in serum, being proposed as an early biomarker for early detection of AD (Kumar et al., 2013b).

According to different cell culture and genetic mouse models works, overexpression of SIRT1 exerts a neuroprotective role in AD (Lalla and Donmez, 2013). Although the exact pathway is not known, SIRT1 has been seen involved in different routes that may contribute to prevent AD features (Bonda et al., 2011)(Fig. 10).

It acts on the already mentioned CREB/BDNF axis, promoting synaptic plasticity through different routes (Gao et al., 2010; Ng et al., 2015). Moreover, SIRT1 promotes axonogenesis by activating Akt, which inhibits GSK3 (Li et al., 2013). In relation to that, SIRT1 can interfere on tau aggregation state, not only preventing its phosphorylation by inhibiting GSK3, but also directly deacetylating tau, which also prevent aggregation (Futch and Croft, 2018).

SIRT1 is also known to promote non-amyloidogenic processing of APP by activating ADAM10 (Lalla and Donmez, 2013), a protein with  $\alpha$ -secretase activity (Tippmann et al., 2009). In this regard, and based on its NAD<sup>+</sup>-dependent activity, SIRT1 has been suggested to have a key role linking selective vulnerability to amyloid deposition and glucose metabolism in AD (Bonda et al., 2011). As already mentioned, in a healthy state, high-energy demanding regions, most notably the MTL structures related with memory formation, rely on aerobic glycolysis as a rapid source of ATP (Bauernfeind et al., 2014; Harris et al., 2014) alternative to complete oxidative metabolism. Aerobic glycolysis may eventually lead to a gradual depletion of NAD<sup>+</sup> reserves, through increased NADH production and decreased

NAD<sup>+</sup> regeneration through oxidative phosphorylation. According to this hypothesis, SIRT1 inhibition due to lack of NAD<sup>+</sup> could lead to increased amyloidogenic processing in regions more dependent on aerobic glycolysis (Bonda et al., 2011).

Moreover, regarding glucose metabolism, SIRT1 holds a reciprocal regulatory relation with different elements in the insulin signalling (Liang et al., 2009; Wang et al., 2010). Furthermore, SIRT1 also acts on other pathways promoting antioxidant (FOXO3, PGC1 $\alpha$ ) (Brunet et al., 2004; Wang et al., 2010), antiinflammatory (NF- $\kappa$ B) (Yeung et al., 2004) and antiapoptotic response (p53) (Langley et al., 2002), as well as neurogenesis (Notch) (Bonda et al., 2011).

On the basis of SIRT1 situation at the intersection of these multiple pathways (Fig. 10), therapeutic upregulation of SIRT1 has been proposed for AD. Activation of SIRT1 mediated by NAD<sup>+</sup>, by resveratrol (a natural polyphenolic compound found in foods such as grapes or berries) or by the resveratrol-analogous pterostilbene have provided promising *in vitro* and *in vivo* evidences of SIRT1 therapeutic potential (Kim et al., 2007; Albani et al., 2009; Wang et al., 2010; Bonda et al., 2011).

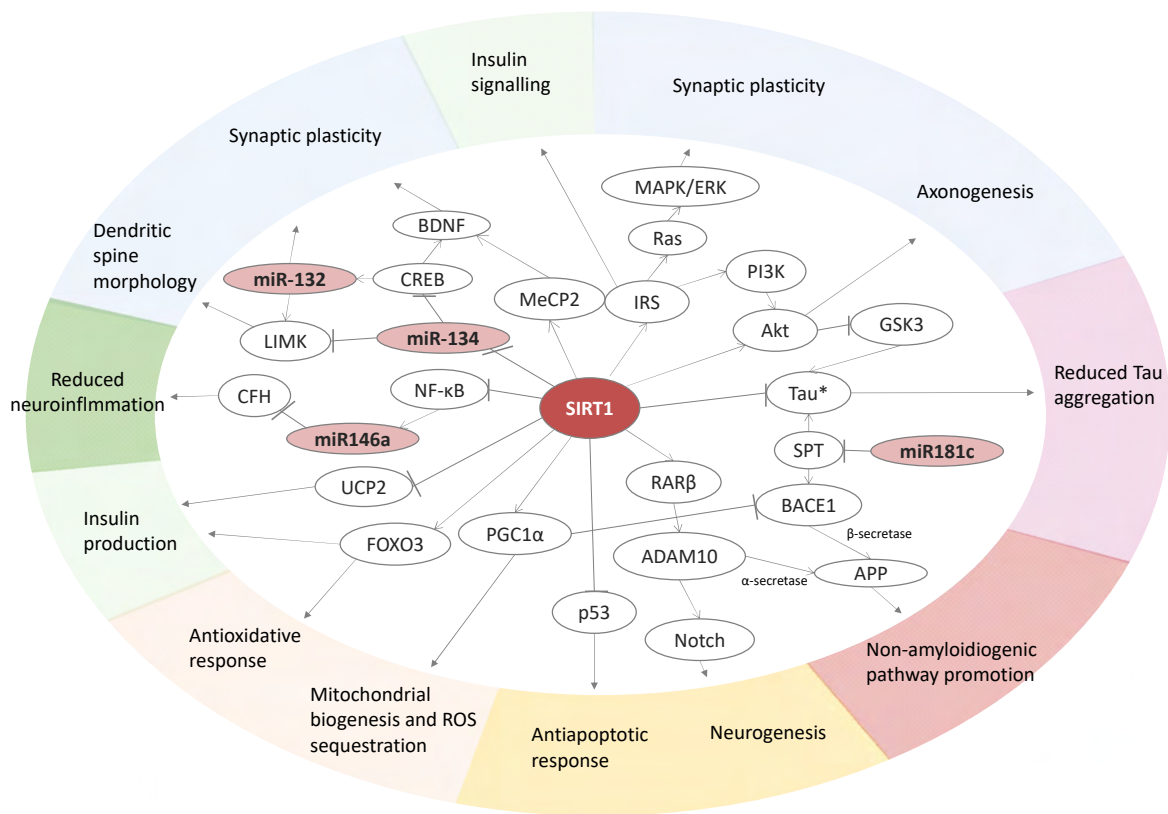


**Fig. 10 | Neuroprotective pathways of SIRT1 in coordination with selected miRNAs.** While activation of these pathways is associated with longevity, their deregulation may be central to AD features. Pathways contributing to each AD feature are shaded in different colours, in correspondence with Fig. 7. Additional interrelations between these pathways, such as complex interactions between specific miRNAs and SIRT1, have been also reported but are not depicted. Abbreviations: ADAM10: A disintegrin and metalloproteinase 10; Akt: also known as protein kinase B (PKB); APP: amyloid precursor protein; BACE1:  $\beta$ -site APP cleaving enzyme; BDNF: brain-derived neurotrophic factor; CFH: complement factor H; CREB: cAMP-response element binding protein; FOXO3: Forkhead box O transcription factor 3; GSK3: glycogen synthase kinase 3; IRS: insulin receptors substrates; LIMK: LIM domain kinase; MAPK/ERK: mitogen activated protein kinase/extracellular-signal-regulated kinase pathway; MeCP2: Methyl CpG binding protein 2; NF- $\kappa$ B: nuclear factor kappa B; PGC1 $\alpha$ : peroxisome proliferator-activated receptor  $\gamma$  co-activator-1 $\alpha$ ; PI3K: phosphoinositide 3-kinase; RAR $\beta$ : Retinoic acid receptor  $\beta$ ; SPT: serine palmitoyltransferase; Tau\*: aggregation-prone forms of tau protein (hyperphosphorylated or acetylated). Diagram construction is mainly based on information on Im and Kenny, 2012; Herskovits and Guarente, 2014; Jeřko et al., 2017; Xu et al., 2018, in addition to references in the text.



## PART II. CONSIDERATIONS FOR THE DEVELOPMENT AND ASSESSMENT OF ALZHEIMER'S DISEASE TREATMENTS

Overall, the previous part gives the idea that the physiopathology of AD is complex and results from several simultaneous assaults. Each individual feature is a potential target for specific therapeutic strategies. Despite the efforts put in AD treatment research, no anti-AD drug has been approved by the Food and Drug Administration (FDA) since 2003 (Bachurin et al., 2017). To date only five drugs are approved for the disease, consisting on cholinesterase inhibitors and/or NMDAR antagonist, and none is able to cure or stop the progression of the disease, or even to consistently fight symptoms (Alzheimer's Association, 2019). The substantial failure rate of experimental treatments in the clinical phase may be attributed to the lack of translationality of preclinical tests (Zhang et al., 2020). In this sense, animal models used in treatment assessment need to be reviewed in order to reliably recapitulate targeted AD features. On the other hand, most of the failed therapies are related to a single AD causative hypothesis (see Du et al., 2018 for a review), suggesting that new therapeutic approaches should consider a holistic vision of the disease, resulting in a multiscale intervention.

This part will look into these different considerations, giving an insight into the available models for AD preclinical testing, and presenting an alternative view of AD that opens the door to new treatment strategies.



## 4. MODELLING AD IN RODENTS TO RELIABLY TEST AD TREATMENTS

Rodents, and especially rats, are considered a good model for human neurological diseases, because of their similar brain connectivity and rich behavioural phenotype, together with their physiological, morphological and genetic characteristics. However, rats do not naturally develop AD, a condition that is considered to be unique to humans (Fincha and Austad, 2015) or at least primates (Toledano et al., 2012). Strategies to recapitulate the disease have basically relied on transgenic models including human genetic mutations associated with familial AD, such as APP or PS1 (see Benedikz et al., 2009 for a review). Nevertheless, these models dismiss the majority group of sporadic onset AD. In this regard, literature gathers different strategies to induce memory-associated cognitive impairment in adult rodents coupled with the cell and molecular hallmarks that define AD, mainly based on the delivery of neurotoxic chemicals into the brain (Lecanu and Papadopoulos, 2013; Malekzadeh et al., 2017; Zhang et al., 2020). Although no single model fully reproduces all aspects of AD, it is essential to have knowledge of the exact neuropathology displayed by each particular model and be aware of its limitations, so that it can be useful for reliable treatment testing and the likelihood of translation to human studies can increase.

### 4.1. Sporadic AD rat models

#### A $\beta$ -induced rat model

Relying on the popular amyloid hypothesis, the delivery of toxic A $\beta$  aggregates into the brain through stereotactic surgery has become one of the most extended strategies to model sAD. Regardless of the fact that A $\beta$  peptide of human type is often used to obtain the highest toxicity and aggregation propensity, there is a widespread disparity in each and every step of the procedure. This variability relates to the species of peptide infused (e.g., A $\beta$ 1-40, A $\beta$ 1-42 or A $\beta$ 25-35), solvent used, state of aggregation (monomeric, oligomeric or fibrillary forms), site (mainly ventricles or hippocampus), dose, volume and manner of introduction (single injection, repeated acute injections or chronic infusion through osmotic pumps), age of the animals and time frame when behavioural and molecular effects are assessed. This variability is evidenced in the selection of studies included in Table 1. Likewise, disparate results are noted regarding tau hyperphosphorylation, synaptic deficits, neurodegeneration and spatial memory deficits triggered by amyloid infusion. Still, A $\beta$  injection is one of the most used models to study preclinical effects of drugs proposed for AD treatment.

**Table 1 | Methodological variation in A $\beta$ -injection rat model.** Methodological variables are presented for a selection of woks using A $\beta$ -induced model.

Reference	Rats		A $\beta$ preparation			Injection			Model assessment		
	Strain	Age at start (weeks)	Peptide specie	Solvent	Aggregation procedure and state	Injection site	Repetition	Final dose (nmol/rat)	Assessment time	Affected behaviour	Affected cell/molecular variables
Asadbegi et al., 2017	Wistar	12-13	A $\beta$ 1-42	PBS	fibrillary: 221.5 $\mu$ M, 37°C for 7 days	DG bilateral	1	0.88	4 weeks	spatial memory in MWM	lipid profile and A $\beta$ plaques in HP
Farbood et al., 2017	Wistar	24	A $\beta$ 1-42	PBS	fibrillary: 200 ng/ $\mu$ L, 37°C, 5 days and finally diluted to 10 ng/ $\mu$ L	DG bilateral	1	0.014	17-23 days	spatial learning and memory in MWM and memory retention in passive avoidance task	diffused plaques in DG, number of spikes/bin in DG
Hui et al., 2017	Spragey-Dawley	not specified	A $\beta$ 25-35	H2O	not specified: incubated at 37°C for 1 week	icv bilateral	1	4.4	25-31 days	spatial learning and memory in MWM	dendritic density and levels of synaptic plasticity-associated proteins in HP
Kasza et al., 2017	Charles River-Harlan rats	not specified	A $\beta$ 1-42	PBS	oligomeric (37 °C for 24h/168 h at 25/75/200 $\mu$ M)	icv bilateral	1	0.15	7 days	spatial learning in MWM	LTP, number of viable neurons, tau levels and number of dendritic spines in the HP
Patnaik et al., 2018	Sprague-Dawley	20-25	A $\beta$ 1-40	saline	not specified	icv (left)	once daily for 4 weeks	1.13 / day	30 days	-	blood-brain barrier (BBB) breakdown, oedema formation, neuronal, glial injuries and A $\beta$ deposits
Yamashita et al., 2017	Wistar	12	A $\beta$ 1-40	35% acetonitrile + 0.1% trifluoroacetic acid (pH 2.0)	monomeric	icv bilateral	osmotic pump, continuous 2 weeks	4.9-5.5	2 weeks	learning in radial maze	-

### STZ-induced rat model

The intracerebroventricular (icv) injection of streptozotocin (STZ), a glucosamine-nitrosurea compound isolated from the soil bacteria *Streptomyces achromogenes*, has recently gained popularity to reproduce sAD (Grieb, 2016).

Initially developed as an antibiotic and as an anticancer agent, in 1963 STZ was reported to present a diabetogenic action (Rakieten et al., 1963). Since then, systemic administration of high dose STZ ( $\geq 40$  mg/kg) has been used to model type 1 diabetes in rats (Junod et al., 1969; Grieb, 2016). Further exploration of the mechanisms revealed that STZ presents selective cytotoxicity to beta pancreatic cells expressing high levels of glucose transporter GLUT2, which is required for STZ internalization across the cell membrane (Schnedl et al., 1994; Lenzen, 2008). Once inside the cell, STZ causes DNA alkylation, which triggers activation of poly(ADP-ribose) polymerase in an attempt to repair DNA, leading to depletion of cellular NAD<sup>+</sup> and ATP and subsequent cell necrosis (Lenzen, 2008). As blood-brain barrier lacks GLUT2 transporter, the brain is not directly affected by intravenous or intraperitoneal injection of STZ (Grieb, 2016). Nevertheless, the injection of a subdiabetogenic dose directly into the brain was suggested to damage cerebral glucose and energy metabolism (Hoyer et al., 1994).

Thus, based on the hypothesis that glucose hypometabolism is an upstream event in the AD cascade, Lannert and Hoyer proposed in 1998 the use of icv injection of STZ to decrease glucose uptake and trigger sporadic AD-like pathology (Lannert and Hoyer, 1998). Since then, an increasing number of works have used a fairly consistent methodology, consisting in single or double icv injection of STZ at a dose of 1-3 mg/kg, to assess pathological alteration induced by the drug. They reported progressive time- and dose-dependent alterations analogous to sAD features, including increase in A $\beta$  protein (Park et al., 2015; Knezovic et al., 2015; Bao et al., 2017; De La Monte et al., 2017; Wang et al., 2017), APP (De La Monte et al., 2017; Wang et al., 2017; Mishra et al., 2018), ptau (Chen et al., 2013; Knezovic et al., 2015; Dehghan-Shasaltaneh et al., 2016; Bao et al., 2017; De La Monte et al., 2017; Mishra et al., 2018; Moreira-Silva et al., 2018), neurodegeneration (Santos et al., 2012; Dehghan-Shasaltaneh et al., 2016; Mishra et al., 2018; Voronkov et al., 2019) and altered synaptic protein levels (Chen et al., 2013; Bao et al., 2017; De La Monte et al., 2017; Moreira-Silva et al., 2018) in different brain areas, expansion of the brain ventricles (Moreira-Silva et al., 2018; Voronkov et al., 2019), increased oxidative stress and prominent neuroinflammation (Kraska et al., 2012; Chen et al., 2013; De La Monte et al., 2017; Mishra

et al., 2018; Amani et al., 2019), spatial and recognition memory deficits (Santos et al., 2012; Chen et al., 2013; Mehla et al., 2013; Knezovic et al., 2015; Dehghan-Shasaltaneh et al., 2016; Mishra et al., 2018; Moreira-Silva et al., 2018; Zappa Villar et al., 2018) and anxiety- and depression-like behaviours (Chen et al., 2013; Amani et al., 2019), among others.

Hypothetical molecular mechanisms underlying these alterations were compiled in different reviews (Kostrzewa, 2014; Kamat, 2015; Grieb, 2016). Selective cytotoxicity to GLUT2-expressing neuronal and glial cells, mainly found in the hypothalamus but also in the hippocampus (Jurcovicova, 2014), is among the possible explanations, by analogy to peripheral cytotoxicity. However, insulin desensitizing via insulin receptor damage and subsequent impaired PI3K/Akt/GSK-3 signalling transmission, as well as free radical generation and inflammatory cytokine release are also contemplated as triggers of STZ effects in the brain. Although none of these mechanisms is confirmed, icv injection of STZ seems to alter multiple metabolic and cell signalling pathways conferring a general picture reminiscent of human sAD, legitimating this model as one of the most useful approaches to test therapeutic strategies (Salkovic-Petrisic et al., 2013).

#### 4.2. Evaluation of AD-related memory disturbances in rodent models through Morris water maze

In order to study the episodic memory disruption characteristic of AD in rodent models, the assessment of hippocampal-dependent spatial memory is especially valuable. The Morris water maze (MWM), described by Richard Morris in 1984 (Morris, 1984), provides a consolidated framework in which spatial learning and memory can be assessed in rodents. Different configurations of the MWM have been extensively used to evaluate effects of aging, lesions, drugs and treatments, as well as to characterize different neurocognitive models, regarding learning and memory (see D'Hooge and De Deyn, 2001 for a review).

MWM is a navigation task in which the animal, placed in a large circular pool, is expected to find an invisible platform based on the principle that water is a natural aversive stimulus to rodents that would motivate them to escape. In order to do so, the animal must benefit from the presence of a configuration of visual cues, which it must learn to identify, associate with and locate in reference to the escape platform, and remember in successive learning sessions (acquisition phase). These cognitive processes involve the integration of different brain regions but, as hippocampus is the primary substrate of the spatial memory, it is typically

considered a hippocampal-dependent task with particular sensitivity to effects of lesions in this structure (D'Hooge and De Deyn, 2001). Retention of this hippocampal-dependent memory is further assessed in a probe test session, in which the platform is no longer in the pool.

In this sense, the measure of escape latencies (the amount of time that it takes the animal to find the platform) across the acquisition phase estimates the level of learning the animals achieve. Moreover, the time spent in the target area during the probe test provides a measure of spatial memory. However, apart from these most salient variables, the MWM provide additional valuable information for further behavioural characterization related with subtle emotional and cognitive disturbances, such as the thigmotaxis during the acquisition sessions, the mean distance to target area in the probe test or the time used to find the platform in a reversal test (Vorhees and Williams, 2006; Gallagher et al., 2015).

Increased escape latencies in the acquisition phase and mean percentages of time in the target quadrant during the probe test in the MWM were repeatedly reported in different studies after single icv injection of A $\beta$ 1-42 (Zhang et al., 2015a; Kalra et al., 2016; Akbarnejad et al., 2017; Kasza et al., 2017; Jiang et al., 2019; Liu et al., 2019) as well as icv injection of STZ (Santos et al., 2012; Xu et al., 2014; Bao et al., 2017; Adeli et al., 2017; Pilipenko et al., 2019; Sharma and Garabadu, 2020).

## 5. VIEWING AD AS A NEURAL CIRCUIT DISORDER

AD is traditionally categorized as a neurodegenerative disease referring to progressive loss of neurons and resulting structural damage. However, understanding that neurons are not isolated entities but nodes in a functional network linked by synapses, and that anatomical brain regions do not act as independent unities, leads to the view of AD as a neural circuit disorder, in which the most affected circuits are those subserving episodic memory (i.e. the Papez circuit and the default mode network) (Sperling et al., 2010; Fletcher et al., 2014; Ferguson et al., 2019).

### 5.1. Neuronal circuits supporting episodic memory disrupted in AD

#### The trisynaptic circuit: insight into the entorhinal cortex and the hippocampus

The hippocampus (HP) is a curved cortical structure folded onto the medial surface of the temporal lobe. Adjacent to the HP lies the parahippocampal gyrus (Van Strien et al., 2009)(Fig. 11A-B), including strongly interconnected areas named entorhinal, perirhinal and ectorhinal cortices (Brodmann areas 28 and 34, 35 and 36, respectively). The parahippocampal gyrus represents the major input to the hippocampal circuit (Fig. 11D), a glutamatergic circuit especially involved in episodic memory processing. As introduced in section 1, hippocampal formation and parahippocampal gyrus are the first structures to degenerate in AD.

The entorhinal cortex (EC) acts as a polymodal sensory association area where both non-spatial sensory information (from the lateral entorhinal cortex [LEnt]) and spatial information (from the medial entorhinal cortex [MEnt]) is conveyed (Basu and Siegelbaum, 2015). The EC receives most of its cortical inputs from the perirhinal/ectorhinal area and, in turn, gives rise to most of the cortical input to the HP (Witter et al., 2000, 2006). The HP then acts as a further processing and associative hub to encode cohesive memories of individual events within the context in which they occurred. The hippocampal formation is composed of different subfields that are involved in different processing steps, including cornu ammonis (CA) region, comprising mainly CA1 and CA3 regions, the dentate gyrus (DG) and the subiculum (Llorens-Martín et al., 2014) (Fig. 11D).

DG granule cells receive excitatory (glutamatergic) input from EC layer II through the perforant path. DG is assumed to reduce interference between similar memories, exerting a

pattern differentiation (Sahay et al., 2011; Nakashiba et al., 2012). Internal hippocampal circuit follows with DG Mossy fibre projections to CA3 pyramidal neurons. Within CA3, recurrent collaterals are thought to contribute in memory completion (Nakazawa et al., 2002). Moreover, CA3 projects to CA1 in the proximal regions of apical and basal dendrites (*stratum radiatum* and *oriens*) through Schaffer collateral path, resulting in a sparse pattern output in CA1 that becomes a unique representation of the memory. In this sense, information arrives HP through DG and, after being processed in the so-called trisynaptic pathway, reaches CA1, which constitute the major output. Hippocampal circuit has also several inhibitory GABAergic interneurons to locally modulate its activity, contributing to the processed output. In addition to the trisynaptic pathway, there is also an alternative direct route (monosynaptic pathway) from EC layer III to distal regions of CA1 apical dendrites (*stratum lacunosum-moleculare*), through the temporoammonic path (Basu and Siegelbaum, 2015) (Fig. 11D). While the trisynaptic circuit seems to be related to the detection and acquisition of new memories, the monosynaptic pathway is thought to contribute to the strength of previously established memories (Llorens-Martín et al., 2014). Axons of CA1 pyramidal neurons project, directly or indirectly via subiculum, back to EC layer V, which connects to layer II/III, completing the EC-HP-EC loop. These feedback pathways are the basis of information retrieval in front of experienced cues.

Initial neuronal damage in AD is thought to occur in upper layers of the EC, especially layer II in LEnt (van Hoesen et al., 1991; Gómez-Isla et al., 1996; Khan et al., 2014), where the first signs of neurofibrillary pathology appear according to Braak stages (Braak and Braak, 1991a; Braak et al., 2006a). Thus, neurons in the perforant path are the first to be pathologically concerned (Bonda et al., 2011). In this sense, the trisynaptic pathway is thought to be the most affected pathway (Llorens-Martín et al., 2014), impairing the formation of new episodic memories. CA1 region is subsequently damaged and becomes the most atrophied subfield (West et al., 1994).

Disruption of the major input (perforant path) and output (CA1 pyramidal efferents) disconnect the HP from the rest of the brain. According to the hippocampal dissociation hypothesis, the HP is a crucial node in the entire neural network whose breakdown in connectivity spreads the activity failure to functionally connected areas.

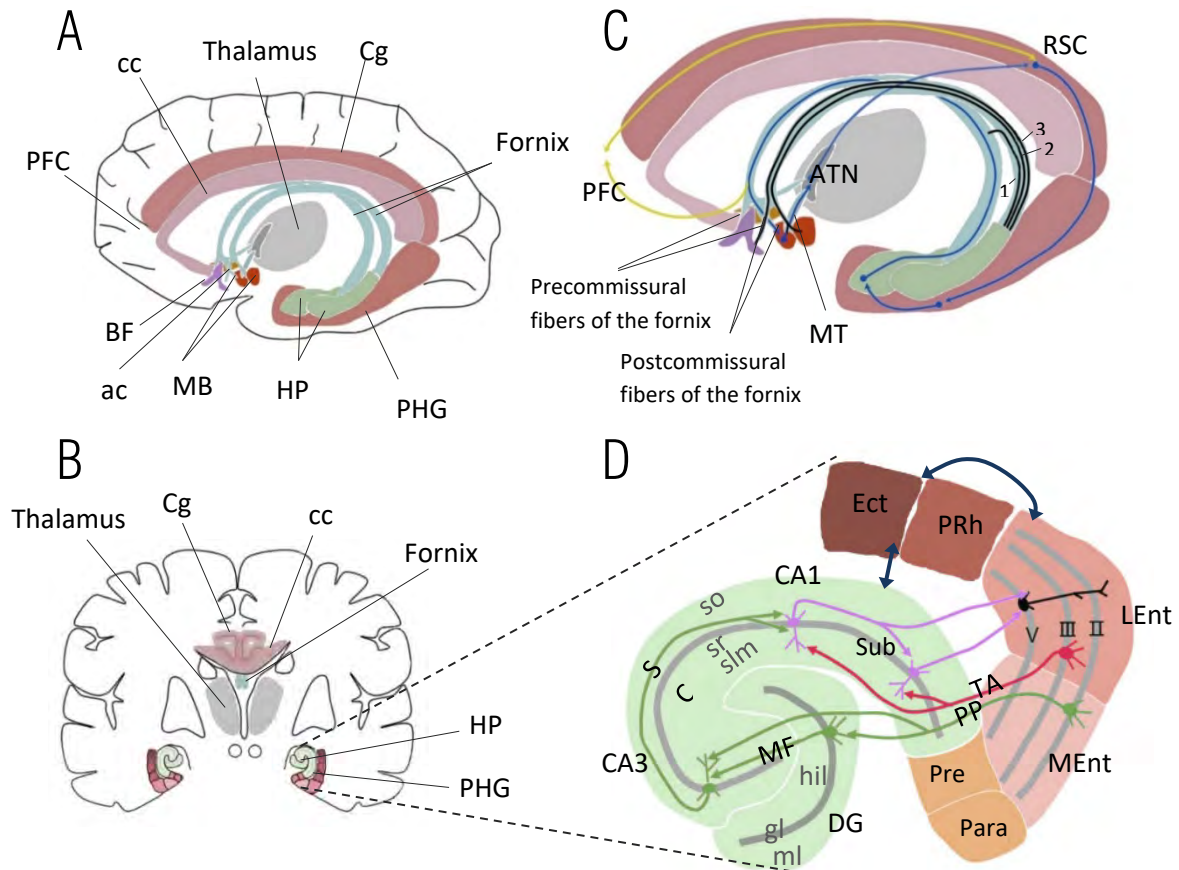


**Fig. 11 | Neuroanatomy of the Papez circuit. A-B.** Lateral-medial (A) and coronal (B) views of a human brain showing location of the hippocampus and parahippocampus gyrus in the medial temporal lobe, as well as other components of the Papez circuit. **C.** Magnification of A detailing anatomy of the fornix and Papez circuit. Blue lines indicate path of the classical Papez circuit (HP-fornix-MB-MTT-ATN-Cin-EC-HP). Black lines show columns of the fornix: 1. fibres crossing the hippocampal commissure to join the contralateral fornical body; 2. postcommissural fibres of the fornix that arise primarily from the subiculum and project to the mammillary body and 3. precommissural fibres of the fornix that arise from the pyramidal cell layer of the HP and project to the BF. Yellow lines represent interconnections with PFC. **D.** Partial magnification of B, with a 90° counter clockwise rotation, showing anatomy of the traditional EC-hippocampus circuit. EC projects mainly to the DG through PP, following internal hippocampal circuit to CA3 through MF and then to CA1 through SC, constituting the classical trisynaptic pathway (green lines). EC also projects to CA1 via TA (red lines). CA1 sends the main HP output (pink lines) back to the EC, completing the EC-HP-EC loop. Interconnections with the PRh/Ect area within the hippocampal/parahippocampal gyrus have been also represented in dark blue. Abbreviations: ac: anterior commissure; ATN: anterior thalamic nuclei; BF: basal forebrain; cc, corpus callosum; Cg: cingulate gyrus; DG: dentate gyrus; EC: entorhinal cortex; Ect: entorhinal cortex; gl: granular layer; hil: hilus; LEnt: lateral entorhinal cortex; MB: mammillary body; MEnt: medial entorhinal cortex; MF: Mossy fibers; ml: molecular layer; MTT: mammillothalamic tract; Para: parasubiculum; PFC: prefrontal cortex; PHG: parahippocampal gyrus; PP: perforant path; Pre: presubiculum; RSC: retrosplenial cortex; Sub: subiculum; SC: Schaffer collateral; slm: *stratum lacunosum-moleculare*; so: *stratum oriens*; sr: *stratum radiatum*; TA: temporoammonic path. Adapted from Yu et al., 2019, including information on Van Strien et al., 2009; Kealy and Commins, 2011; Aggleton et al., 2016.



## The complete Papez circuit: insight into the anterior nuclei of the thalamus and the retrosplenial cortex

The hippocampal formation is part of an extended circuit, called Papez circuit, which connects different structures of the limbic system (Fig. 11A-B). Although it was initially described as an emotion circuit, its implication in episodic memory and navigation was later noticed (Valenstein et al., 1987; Ferguson et al., 2019).

In addition to the direct output from CA1 or subiculum back to EC, efferent fibres from HP (mainly subiculum) travel to more anterior areas along the so-called fornix, a large axonal bundle running through the medial brain that atrophies in AD prodromal stage (Hooper and Vogel, 1976; Metzler-Baddeley et al., 2012). Some of these fibres constituting the postcommissural column of the fornix target the mammillary bodies of the hypothalamus. The mammillothalamic tract connects these structures to the anterior nuclei of the thalamus (ATN), which are connected to the posterior cingulate region (PC), especially to the retrosplenial cortex (RSC). The PC then connects to EC, which is coupled with HP, completing the classical Papez loop. Additionally to this traditional unidirectional loop, limbic structures are multiply interconnected via reciprocal interactions (see Bubb et al., 2017 for review). Early degeneration in these connections is found in AD (Aggleton et al., 2016), involving not only the HP, but other structures within the circuit that may be also associated with AD memory impairment, especially the ATN and the RSC.

The thalamus is a large diencephalic structure composed of a group of functionally diverse nuclei that act as relay station from different subcortical areas and cerebral cortex. Among them, the anterior thalamic nucleus stands out for its role in cognition (Aggleton and Brown, 1999). ATN is affected by structural atrophy during normal aging (Fama and Sullivan, 2015) and by neurofibrillary pathology in AD (Braak and Braak, 1991b). ATN holds direct reciprocal connections with HP via fornix and an interdependent relation with RSC that support spatial learning (Jankowski et al., 2013; Aggleton et al., 2016; Mitchell et al., 2018). Moreover, a role in attention regulation has been suggested for ATN, reflecting its dense connection with prefrontal and parietal cortices (Aggleton et al., 2016). Thus, its dysfunction in AD may contribute to the lack of orientation during spatial navigation and attentional deficits.

The RSC, composed of Brodmann areas 29 (granular) and 30 (agranular) and 6 cortical layers, is included in the PC region. In humans, but not in rodents, the PC also contains the posterior

cingulate cortex (areas 23 and 31), but RSC holds the more pronounced connections with both ATN and HP (Todd et al., 2015; Bubb et al., 2017). RSC hypoactivity, detected from FDG-PET and functional MRI (fMRI) studies, is often the first metabolic change detected in AD (Minoshima et al., 1997; Nestor et al., 2003), and especially decreased connectivity is found between the PC and the HP (Sperling et al., 2010). The main functions of RSC, and so the consequences of its dysfunction, arise from the situation of this area at the crossroads between HP and other areas. Further its role in-between ATN and HP, RSC acts also as a hub for HP connection with parietal cortex (which integrates sensory information), enabling visuospatial orientation and translation between egocentric and allocentric spatial information, a capacity impaired in AD patients (Tu et al., 2015). It also connects the HP to prefrontal cortex (PFC), which is consistent with RSC activation detected during retrieval of contextual information and autobiographical memory (Katche et al., 2013; Aggleton et al., 2016). In contrast, during memory formation a deactivation of RSC coordinated with HP activation is required (Sperling et al., 2010). This distinctive firing during encoding and retrieval evidence the inclusion of RSC (and PC in general) also to the default mode network.

#### The default mode network: insight into the medial prefrontal cortex

The default mode network (DMN) comprises a set of distributed cortical regions that conform a large-scale neural network, characterised for showing greater activity during resting state than during cognitive tasks. It is involved in memory encoding and retrieval, among other cognitive functions, such as passive thinking and planning.

Multiple fMRI studies have revealed alterations in these networks in early AD patients (Greicius et al., 2004; Sperling et al., 2010), as well as at-risk individuals, such as ApoE  $\epsilon$ 4 carriers (Sorg et al., 2007; Persson et al., 2008; Pihlajamaki et al., 2010; Sheline et al., 2010; Petrella et al., 2011; Jahn, 2013). Indeed, DMN regions widely overlap with hypometabolic areas detected through FDG-PET and areas with early A $\beta$  plaque deposition (Zott et al., 2018). Aberrant DMN activity, both during resting state and task related state, may impair the ability to switch from different brain function modes and, therefore, have consequences on encoding and retrieval.

Together with PC, the medial prefrontal cortex (mPFC) forms the core of DMN (Fig. 12) and exhibits the strongest functional connections with the MTL structures (Buckner et al., 2008; Kaboodvand et al., 2018). The mPFC comprises a set of areas that lie along the frontal midline, which in rodents are reduced to three: the anterior cingulate, prelimbic and

infralimbic regions. In this sense, the greatest area in human (area 32) is homologous to prelimbic (PrL) region in rodents (Bicks et al., 2015). mPFC establishes bidirectional connections with HP, both directly and indirectly (Jin et al., 2015). Indirect pathways connect posterior HP (dorsal in rodents) with mPFC, including a subcortical diencephalic route through thalamus, that contribute to attention, and a cortical cingulate route through RSC (Fig. 11C), being both importantly involved in contextual learning (Bubb et al., 2017; Sampath et al., 2017). Moreover, indirect connections from anterior HP (ventral in rodents), concerning the amygdala, nucleus accumbens and ventral tegmental area, are more related to emotional- and anxiety-related behaviours (Sampath et al., 2017). Direct contact between HP and PFC also exists through precommissural fibres of the fornix. Pathways from HP to mPFC support the transition of memory formed in HP to consolidated memory in neocortical schemas. mPFC then accumulates information about the context of related memories, and helps to develop updated schemas. Outputs from the mPFC to parahippocampal gyrus may control the retrieval of selected memories in the HP, relevant to the current context (Preston and Eichenbaum, 2013). Therefore, high amyloid- $\beta$  accumulation in PFC and PFC-HP disconnection found in severe AD patients (Grady et al., 2001; Allen et al., 2007), may contribute to deficits in systems consolidation, disrupted cognitive flexibility and attention, and emotional disturbances (Sampath et al., 2017).

## 5.2. Modulatory systems of memory circuits disrupted in AD

Mnemonic processes, including consolidation of memory, are also assisted by systems that somehow tag events in relation to their worthiness to be remembered. Saliency of an event is given by aspects such as the risks, novelty, effort or reward related to it. Neuromodulatory systems, which rely on several different neurotransmitters (e.g. acetylcholine, dopamine, serotonin, noradrenaline, etc.), track these signals and interact with multiple brain regions, strongly influencing their activity (see Avery and Krichmar, 2017 for a review). Deprivation of hippocampal and cortical neurons from the critical influence of neuromodulatory systems contributes to AD cognitive symptoms.

### Basal forebrain cholinergic circuit

Cholinergic neurons, characterized for realising acetylcholine as a neurotransmitter, are found in distinct connected subcortical regions of the brain and extend as a diffuse network through almost all the brain, affecting cognitive processes such as attention and learning and memory (Klinkenberg et al., 2011; Okada et al., 2015). Cholinergic system failure was the first evidence for selective network-level dysfunction in AD, giving rise to the cholinergic hypothesis (Whitehouse et al., 1981; Francis et al., 1999).

A group of nuclei located in the basal forebrain is one of the major cholinergic sources. These nuclei, especially the nucleus basalis of Meynert (NBM), are selectively degenerated in AD (Whitehouse et al., 1982; Mesulam et al., 2004). The NBM constitutes the main cholinergic innervation to the entire cortical surface (Fig. 12). The vertical limb of the diagonal band (VDB), another basal forebrain region, is the major source of cholinergic innervation to HP (Yu et al., 2019), and is also severely affected in AD (Vogels et al., 1989). In physiological conditions, cholinergic release to cortex and HP mediated through pre- and postsynaptic receptors influences its neuronal excitability and synaptic transmission and induces synaptic plasticity (Picciotto et al., 2012). Thus, disruption of cholinergic inputs to the cortex and HP can impair attention and decision-making, as well as memory encoding (Muir et al., 1992; Rogers and Kesner, 2004).

Three of the approved drugs to treat AD aim to maintain the cholinergic tone by inhibiting its ACh inactivation by cholinesterase enzyme. Their efficacy, albeit limited and insufficient to reverse the progression of AD, suggest that the loss of ACh regulatory tone exacerbates dysfunction and accelerates memory loss (Ferreira-Vieira et al., 2016).

### Ascending monoaminergic systems: insight into mesocorticolimbic dopaminergic circuits

Besides the cholinergic system, monoaminergic systems originated in subcortical nuclei (relying on dopamine, serotonin, norepinephrine and histamine neurotransmitters) also diffusely synapse onto hippocampal and neocortical neurons with several modulatory effects. All four principal nuclei of the ascending monoaminergic systems (i.e. ventral tegmental area, locus coeruleus, medial septal nucleus and raphe complex) undergo early degeneration in AD, taking part in both cognitive and non-cognitive symptoms (see Trillo et al., 2013 for a review).

In particular, dopamine neurons in the ventral tegmental area (VTA) have been found to be compromised very early in sporadic AD patients, correlating to both cognitive and neuropsychiatric symptoms (De Marco and Venneri, 2018; Serra et al., 2018). VTA neurons project, mainly via the medial forebrain bundle (MFB), to cortical and subcortical regions, including the nucleus accumbens, the prefrontal cortex, the hippocampus and the amygdala, constituting the mesocorticolimbic dopaminergic pathways (Morales and Margolis, 2017) (Fig. 12). These connections are at the basis of the role of this system in reward, motivated behaviours, emotional processing and learning and memory (Lisman and Grace, 2005; Cha et al., 2014; Bariselli et al., 2016). Thus, degeneration of dopamine neurons at pre-A $\beta$  plaque stage, coupled with decreased levels of dopamine and dopamine receptors found in AD condition (Gibb et al., 1989; Pan et al., 2019), has been suggested to largely contribute to hippocampal synaptic plasticity deficits and consequent impairment in hippocampus-dependent memory encoding, as well as to neuropsychiatric symptoms such as apathy and anhedonia (Nobili et al., 2017; Cordella et al., 2018; Krashia et al., 2019). For this reason, increase in dopaminergic tone has been also proposed as a possible therapeutic strategy for AD (Martorana and Koch, 2014).

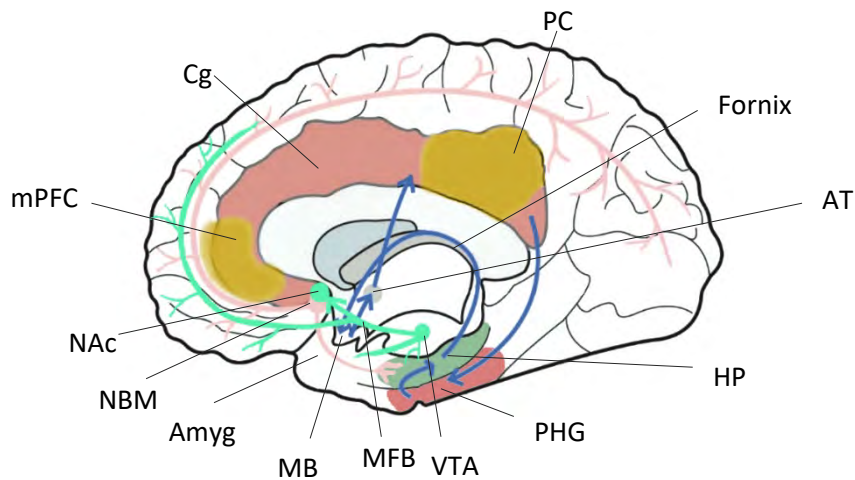


**Fig. 12 | Overview of memory circuits linked to AD.** 1. The Papez circuit (blue lines) is viewed in more detail in Fig. 10. 2. The default-mode network (yellow patches) includes the medial prefrontal cortex (mPFC) and posterior cingulate region (PC), with strong connections to the hippocampus and amygdala. 3. The basal forebrain circuit (pink lines), based on nucleus basalis of Meynert (NBM) cholinergic projections, innervates the neocortex and hippocampus. 4. The mesocorticolimbic dopaminergic circuits (turquoise lines), based on projections from ventral tegmental area (VTA) to nucleus accumbens (NAc) through the medial forebrain bundle (MFB), also innervates the HP and PFC. Abbreviations: Amyg: amygdala; ATN: anterior thalamic nuclei; Cg: cingulate gyrus; HP: hippocampus; MB: mammillary body; MFB: medial forebrain bundle; mPFC: medial prefrontal cortex; NAc: nucleus accumbens; NBM: nucleus basalis of Meynert; PC: posterior cingulate region; PHG: parahippocampal gyrus; VTA: ventral tegmental area. Adapted from Lv et al., 2018 and Krashia et al., 2019.

### 5.3. Implications of the circuit-disorder view of AD

Most of the failed therapeutic approaches to AD are drugs that aimed to chemically modulate a single specific feature affected in the disease. The view of the disease as a circuit disorder opens the door to circuit-level neuromodulatory interventions (Mirzadeh et al., 2015). These treatments aim to maximize the function of interrelated circuits whose failure contributes to behavioural deficits, in order to prevent structure isolation and restore the functional network. This is the case of deep brain stimulation (DBS), whose suggested applicability for AD (Lv et al., 2018) will be approached in the next part of introduction.



## PART III. DEEP BRAIN STIMULATION AS A TREATMENT FOR ALZHEIMER'S DISEASE

Deep brain stimulation (DBS) is a procedure that involves the surgical implantation of an electrode to deep brain areas to deliver electric pulses, thereby intervening in the electrical dimension of brain connection. The use of DBS to modulate the activity of dysfunctional circuits relevant to particular disease has been proposed to treat many circuit disorders. It has been initially investigated for Parkinson's disease, in which it is currently successfully used for treating motor dysfunction in patients refractory to pharmacological treatments (Benabid et al., 1987; Groiss et al., 2009). DBS efficacy in this disease has encouraged the consideration brain stimulation aimed at new neuroanatomical targets to treat other disorders, such as epilepsy, depression, dystonia, obsessive-compulsive disorders, substance-related addiction and, interestingly, also Alzheimer's disease (Lyons, 2011).

## 6. USE OF DBS FOR MEMORY IMPROVEMENT IN AD

DBS aimed to improve human memory in AD context has been directed at different critical nodes on memory circuits. To date, only two primary DBS targets have been tested in clinical trials involving AD patients: the nucleus basalis of Meynert (NBM) and the fornix.

On the one hand, the NBM was first targeted in 1984 when Turnbull et al. implanted an electrode to a 74-year-old man with probable AD, in an attempt to excite the remaining cholinergic ascending inputs to the cortex (Turnbull et al., 1985). Although no clinically significant improvement was reported after 8 months stimulation, the purpose of stimulating the NBM for dementia was retaken in 2009, in a case-report of a Parkinson disease dementia (PDD) patient showing improvement in global cognitive functions (Freund et al., 2009).

On the other hand, the idea of stimulating the fornix arises from a serendipitous finding. In 2002, a patient suffering from morbid obesity and refractory to other treatments was referred to hypothalamic stimulation to modulate his appetite (Hamani et al., 2008). The patient reported vivid autobiographical memory retrievals when testing the electrode contacts. From postoperative images, electrode coordinates were estimated to be adjacent to the columns of the fornix. As a core white matter in Papez circuit and default-mode network, being the main input and output of MTL, stimulation of the fornix was then considered as a possible treatment for AD.

### 6.1. Promising results and limitations of DBS trials in AD patients

The described case-studies led to multiple DBS clinical trials targeting either the NBM or the fornix in AD patients, some of which are still ongoing (see Aldehri et al., 2018; Lv et al., 2018; Yu et al., 2019 for recent reviews on this topic, and check recruiting and completed trials in [clinicaltrials.gov](https://clinicaltrials.gov) registry (U. S. National Institutes of Health, 2021)).

Overall, phase I trials demonstrated that 1 year of DBS is safe and well tolerated in AD patients. Moreover, promising early data on its clinical effectiveness are reported in both phase I and few phase II trials. In this regard, stable or even improved cognitive abilities, assessed by neuropsychological tests such as Alzheimer's disease assessment scale-cognitive subscale (ADAS-Cog) or Mini-Mental State Exam (MMSE), were reported for some patients (Laxton et al., 2010; Kuhn et al., 2015). Additionally, an increase in glucose metabolism in parietal, temporal and frontal lobes was detected in FDG-PET scans (Laxton et al., 2010; Smith et al., 2012; Fontaine et al., 2013; Kuhn et al., 2015; Lozano et al., 2016). Furthermore,



Sankar et al. describe a sustained significant increase in hippocampal volume detected by structural MRI (Sankar et al., 2015).

However, these results still present some limitations. To begin with, some of the studies did not report any effect on cognition (Gratwicke et al., 2018) or point that deficit is alleviated only temporarily or exclusively in a specific group of patients (Kuhn et al., 2015; Lozano et al., 2016; Hardenacke et al., 2016; Baldermann et al., 2018). Moreover, with the exception of the ADvance trial comprising 42 patients (Lozano et al., 2016), the great majority of studies present a small sample size, consisting of less than 10 patients, limiting the statistical power and possibly leading to over-interpretation of data. Finally, although some studies have referred that possible mechanisms underlying the therapeutic effect could include synaptic plasticity, neurogenesis and gliogenesis induction or even increased vascularization in the hippocampal region, all the studies conclude that knowledge on the implied neurobiological mechanisms and evidence of neuroprotective effect is still lacking.

To overcome these limitations, contribution from studies in laboratory animals carried out in parallel to the ongoing phase I/II and nascent phase III clinical trials may be considered to guide future clinical studies.

## 6.2. Insights from laboratory animal studies

Increasing amount of experimental studies using laboratory animals provide evidence on the effectiveness of DBS of the NBM or the fornix to improve memory function in rodents, both in physiological and, although lesser in number, in AD-mimicking conditions (McLin et al., 2002; Montero-Pastor et al., 2004; Boix-Trelis et al., 2006; Hescham et al., 2013, 2017; Zhang et al., 2015b; Lee et al., 2016; Huang et al., 2019). These type of studies have started to yield important insights into the underlying mechanisms of action, including increased neurotransmitter release, release of growth factors, neurogenesis, enhanced synaptic plasticity and long-term potentiation, as well as regulation of AD-related molecular hallmarks.

Electrical stimulation of the NBM has been shown to cause acetylcholine (Rasmusson et al., 1992) and nerve growth factor (NGF) (Hotta et al., 2009) release, as well as to induce neuroplastic changes (Kilgard and Merzenich, 1998), in the cortex of wild-type rats. In a comprehensive study using AD transgenic mice, NBM-DBS was shown to down-regulate A $\beta$ , increase neuron survival, reduce apoptosis, mitigate oxidative stress and regulate ACh

levels in the hippocampus and cortex (Huang et al., 2019). Forniceal DBS was suggested to act by generally activating the Papez circuit (McKinnon et al., 2019), as it showed rapid activation of the hippocampus (Hescham et al., 2016), together with increased hippocampal acetylcholine and synaptic proteins (Gondard et al., 2015; Hescham et al., 2016), in wild-type rats. In TgF344-AD rat model, chronic forniceal DBS decreased amyloidosis, inflammatory responses and neuronal loss in both cortex and hippocampus (Leplus et al., 2019).

In addition to the great contribution in deciphering the molecular mechanisms, animal experimentation is also helpful to explore conditions that could lead to enhanced effective DBS treatment. On the one hand, some studies have been devoted to investigate the effect of NBM or fornix stimulation parameters in the resulting cognitive improvement in AD rat models (Hescham et al., 2013; Koulousakis et al., 2020). On the other hand, the choice of the target region, which is directly associated with the outcome, remains a critical controversial issue. Beyond the serendipitous revelation of NBM and fornix, progressive understanding of the neural circuitry underlying learning and memory has broaden the range of potential DBS targets for AD. Thus, a multiplicity of new targets, including structures in the proper Papez memory circuit as well as elements in the modulatory circuits, are being interrogated for memory function enhancing (see Bick and Eskandar, 2016; Khan et al., 2019 for review).

## 7. MFB AS A POTENTIAL DBS TARGET FOR AD TREATMENT: AN APPROACH FROM ICSS

The medial forebrain bundle (MFB) is a tract of ascending and descending axons that connects midbrain and forebrain areas passing through the lateral hypothalamus (LH) in a rostral-caudal direction (Coenen et al., 2018; Döbrössy et al., 2020) (see Fig. 13 for MFB anatomy and connectivity in both human and rat). Among the heterogeneous monoaminergic modulatory pathways contained in it, the MFB accommodate the dopaminergic fibres of the mesocorticolimbic circuits (reviewed in section 5.2). Thus, the MFB is considered part of the neural substrate of reward. Attending to the implication of the reward system in reinforcing learning and memory by strengthening the associations created by an immediate memory (Huston et al., 1977), electrical stimulation of the reward substrate, and the MFB in particular, had been suggested to facilitate memory consolidation (Routtenberg, 1974; Huston and Mueller, 1978).

In animals, administration of DBS by means of intracranial self-stimulation (ICSS) ensures a physiological activation of this substrate. ICSS, discovered in rats in the early 1950s by Olds and Milner (Olds and Milner, 1954), is an operant response resulting from the stimulation of the reward system. In this sense, rats will maintain the motivated behaviour of pressing a lever in a Skinner box in order to receive the rewarding stimulation through an electrode chronically implanted in these areas. ICSS behaviour was also shown in mice (Cazala et al., 1974; Stoker and Markou, 2011), dogs (Stark et al., 1962), cats (Roberts, 1958; Angyán, 1975), pigeons (Goodman and Brown, 1966), goldfish (Boyd and Gardner, 1962), nonhuman primates (Rolls et al., 1980) and humans (Bishop et al., 1963; Heath, 1963), and was immediately appreciated to resemble response to natural reinforcers such as food and sex. ICSS seems to be highly rewarding, or even pleasurable (Heath, 1963), as reported by different studies in which animals and humans would choose stimulation over food, water or heat, or even endure foot shocks to reach ICSS lever (Olds, 1958; Falk, 1961; Bishop et al., 1963; Routtenberg and Lindy, 1965; Carlisle and Snyder, 1970; McMurray et al., 2017).

Many studies, in which our partner group did a great contribution, demonstrate that ICSS of the MFB administered after training sessions facilitate different forms of learning and memory in both healthy and memory impaired rodents.

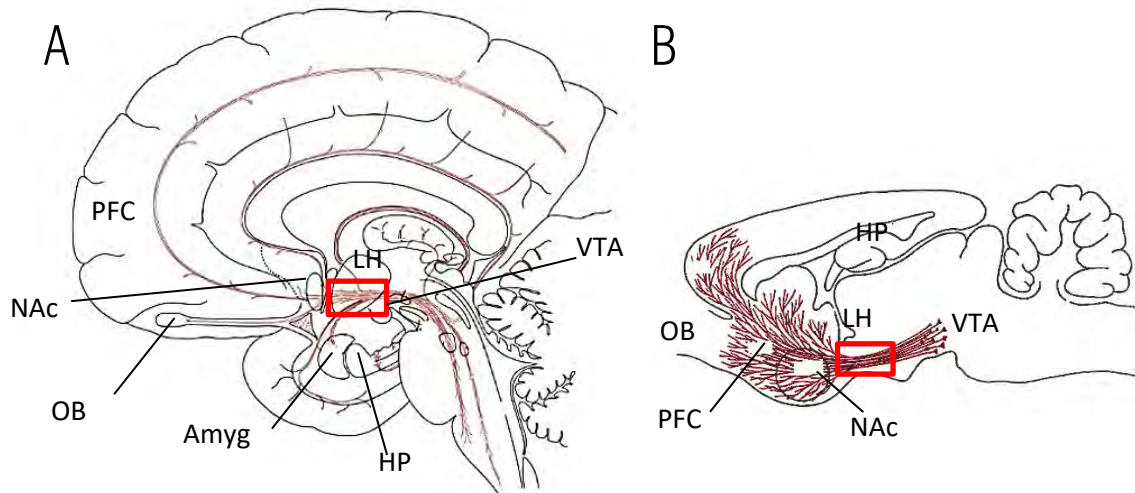


**Fig. 13 | Anatomy and connectivity of the human and rat medial forebrain bundle.** Magenta lines represent the main projections passing by the medial forebrain bundle (MFB, bounded in a red box) in a schematic drawing of a sagittal view in **A.** human and **B.** rat brain. The MFB is a tract of ascending and descending axons that connects midbrain and forebrain areas passing through the lateral hypothalamus (LH) in a rostral-caudal direction. Among the heterogeneous pathways contained in it, the MFB accommodate the dopaminergic fibres of the mesocorticolimbic circuits. Main anatomical structures of the mesocorticolimbic circuits are indicated. Abbreviations: Amyg: amygdala; HP: hippocampus; LH: lateral hypothalamus; NAc: nucleus accumbens; OB: olfactory bulbs; PFC: prefrontal cortex; VTA: ventral tegmental area. Adapted from Panther et al., 2019 and Wright and Panksepp, 2012.

### 7.1. Memory improving effects of MFB-ICSS

MFB-ICSS has demonstrated facilitative effects on both implicit and explicit types of memory in healthy adult rats. On the one hand, MFB-ICSS has shown to improve implicit memory when administered after learning a task, evaluated in passive avoidance (Mondadori et al., 1976; Huston and Mueller, 1978) and two-way active avoidance (TWAA) (Segura-Torres et al., 1988; Redolar-Ripoll et al., 2002; Aldavert-vera et al., 2013) paradigms, as well as in a visual discrimination task (García-Brito et al., 2017). In addition, a recent study from our group demonstrates that MFB-ICSS effects are not restricted to learning-concurrent facilitation, but can also prevent forgetting of remote memories, evaluated in the TWAA (Huguet et al., 2020). On the other hand, regarding AD clinical affectations, the outcome that has MFB-ICSS in hippocampal-dependent explicit memory has turned out to be particularly relevant. Consolidation of flexible spatial memory was facilitated by MFB-ICSS, evaluated mainly in the MWM (Soriano-Mas et al., 2005; Ruiz-Medina et al., 2008; Chamorro-López et al., 2015).

Moreover, MFB-ICSS has been able to recover memory impairment observed for TWAA in aged rats (Aldavert-Vera et al., 1997), as well as in brain-injured rats with lesions in the parafascicular nucleus (Redolar-Ripoll et al., 2003) and the basolateral (Segura-Torres et al., 2009) and lateral amygdala (Kádár et al., 2014). MFB-ICSS was also found to compensate for spatial and visual discrimination memory impairment caused by orexin-1 receptor blockade (García-Brito et al., 2020).

## 7.2. Cell and molecular mechanisms underlying MFB-ICSS that could mediate its behavioural effects

As for any type of DBS, molecular mechanisms underlying MFB-ICSS effects are not completely understood. However, recent works including research in our group have contributed to identify several cell and molecular changes accompanying behavioural improvements induced by MFB-ICSS.

In the first place, MFB-ICSS has shown to trigger activation of different distributed brain areas, revealed by increased cFos expression (Waraczynski, 2006). Some of these areas, such as the VTA, might be merely associated with its rewarding effect, while others demonstrate the activation of different memory systems. In this sense, MFB-ICSS bilaterally activates lateral and basolateral amygdala (Kádár et al., 2011), as well as CA3 and DG hippocampal subfields (Huguet et al., 2009) and granular and agranular retrosplenial cortex (Kádár et al., 2016). Activation found in different areas is also present or even reinforced when combined with learning tasks (Aldavert-Vera et al., 2013; Kádár et al., 2016).

Secondly, it has also been shown that MFB-ICSS resulted in increased plasticity in memory-related regions. Long-lasting structural changes, including extended dendritic arborisation of pyramidal CA1 hippocampal subfield neurons, were found in MFB-ICSS treated rats (Chamorro-López et al., 2015). Similarly, Rao et al. reported that ICSS aimed at proximal substrates of the reward circuit increased number of dendritic branches, intersections, dendritic spines and synaptic contacts in CA3 hippocampal subfield (Rao et al., 1993, 1994, 1999a, 1999b). Moreover, the same group reported increased neurotransmitter levels in the hippocampus after ICSS, both in normal and stress-induced rats, suggesting the involvement of the systems depending on noradrenaline, dopamine, glutamate and acetylcholine in ICSS effects (Rao et al., 1998; Ramkumar et al., 2008). Recently, our group also reported different

levels of involvement of the orexinergic system in the facilitation of memory by MFB-ICSS (García-Brito et al., 2020).

Additionally, increased neurogenesis is also induced after MFB-ICSS. Takahashi et al. described that increased new-born neurons in the hippocampal DG endure into maturity in MFB-ICSS treated rats and mice (Takahashi et al., 2009). Our group also demonstrated increased neurogenesis and migration of DG new-born cells in older rats, related with the maintenance of MFB-ICSS facilitating effect on remote memory retention (Huguet et al., 2020).

Neuroplastic events induced by MFB-ICSS in memory-related areas have been also observed at a molecular level. Expression of dozens of genes related with antiapoptosis, neurogenesis and neuroprotection as well as learning and memory functions was found regulated in the hippocampus after MFB-ICSS (Huguet et al., 2009). In more detail, expression of Bdnf, Arc, Crem, Icer, Fos or Ret, among other plasticity-related genes, revealed a time-dependent increase in both hippocampus and amygdala (Kádár et al., 2011, 2013). Consistently, expression of learning-associated protein NURR1 is also regulated in these areas (Aldavert-Vera et al., 2013), and structural plasticity-related protein ARC was found increased in specific subregions of hippocampus, amygdala, granular retrosplenial cortex and thalamic nucleus (Kádár et al., 2013, 2016, 2018).

Thus, the means by which MFB-ICSS is able to facilitate different types of learning and memory are becoming clear thanks to the latest cell and molecular studies. However, despite these precious cues, much information still lacks in order to unravel the mechanism by which all these cell and molecular changes are coordinated with such a time and region specificity.

### 7.3. Consideration of DBS to the MFB as an AD treatment

The observed effects of MFB-ICSS on cognitive dimension in rodents, including episodic memory facilitation, support the idea that stimulation targeting of MFB could be a suitable candidate treatment for AD. The fact that MFB-ICSS has been found capable of recovering memory disturbances of different nature, including those of natural aging and lesion-induced, further upholds this hypothesis. And so do the induction of different types of neural plasticity observed after MFB-ICSS in the hippocampus, one of the earliest and most affected areas in AD.

In humans, DBS of the MFB has been already tested to treat major depression, showing both safeness in the procedure as well as promising results on the alleviation of depressive symptoms (Fenoy et al., 2018; Dandekar et al., 2018; Coenen et al., 2019), suggesting a potential added value mitigating neuropsychiatric symptoms in AD. A recent study debuts in the administration of MFB-DBS to AD patients, although cognitive effects have not been included in the publication (Panther et al., 2019).

Indeed, much more preclinical evidence is needed before challenging the MFB as a DBS target for AD therapeutic use. First of all, information regarding mechanism of MFB-ICSS reported effects, as for any other type of DBS, should be further elucidated, especially in relation to molecular regulators implied in AD pathology. Secondly, and more important, effects of MFB-ICSS should be assessed in a reliable experimental AD model. In this context, and with the intention of making an approach to overcome these limitations, arises this thesis.

## AIMS AND SCOPE

As described in the last section of introduction, MFB-ICSS has demonstrated to facilitate learning and memory as well as trigger molecular plasticity events. Based on these evidences, it is suggested that rewarding DBS aimed at the MFB could be effective to treat memory deficits associated with AD pathology. However, its effects had never been assessed in AD context nor in relation to the molecular correlates of the pathology. This thesis approaches for the first time this situation by assessing the potential of MFB-ICSS (from now on, simply ICSS) as a treatment for AD in a rodent model, focusing on the molecular dimension, hypothesizing that: “ICSS will modulate molecular markers related to AD pathology progression contributing to mitigate neuropathological signs of AD and, thus, to improve behavioural impairment in this pathological context”. In order to challenge this hypothesis, three studies were defined, each addressing one of the following aims including specific sub-objectives:

1. Assess the effects of ICSS administered in physiological conditions on molecular markers of AD pathology (addressed in **Study 1**):
  - 1.1. Analyse ICSS effects on the hippocampal levels of protein markers related to the main hallmarks of AD: amyloid pathology (APP), tau pathology (ptau) and synaptopathology (DBN), as well as miRNAs and SIRT1, in physiological conditions.
  - 1.2. Analyse ICSS effect on the serum levels of miRNAs, SIRT1 and BDNF and assess their potential use as non-invasive treatment biomarkers in physiological conditions.
  - 1.3. Derived from aims 1.1. and 1.2., establish a methodological framework to assess miRNA changes in hippocampal tissue and serum after ICSS treatment.



2. Assess the molecular effects of ICSS treatment on early AD neuropathological hallmarks in a sporadic AD rat model obtained by A $\beta$  icv injection (addressed in **Study 2**):
  - 2.1. Characterize the main histopathological affectations of the A $\beta$  model, including neurodegeneration, taupathology (ptau levels) and synaptopathology (DBN levels) in the brain regions affected in AD and relate them with behavioural impairments.
  - 2.2. Analyse the effects of ICSS on markers of early AD pathology (ptau and DBN levels) in the main brain regions affected in AD in relation to behavioural outcome in the A $\beta$  model.
  
3. Assess the molecular effects of ICSS treatment on early AD neuropathological hallmarks in a sporadic AD rat model obtained by STZ icv injection (addressed in **Study 3**):
  - 3.1. Characterize the main histopathological affectations of the STZ model, including neurodegeneration, taupathology (ptau levels), synaptopathology (DBN levels) and amyloid pathology (APP levels) in the main brain regions affected in AD and relate them with behavioural impairment.
  - 3.2. Analyse the effects of ICSS on AD markers, including neurodegeneration, ptau levels, DBN levels and APP levels in the main brain regions affected in AD in relation to behavioural outcome in the STZ model.
  - 3.3. Analyse the effects of ICSS on miRNAs and SIRT1, both in hippocampus and serum, as potential treatment biomarkers in a sAD model obtained by STZ injection.

# MATERIALS AND METHODS

In this chapter, a common methodology with particular specifications for each study is presented.

## 1. Animals and experimental design

A total of 148 adult male Wistar rats from the breeding of the Psychobiology Laboratory of the Autonomous University in Barcelona (UAB) (B99-00029) were used for the studies in this thesis, which were approved by the University Animal Welfare committee (CEEAH, protocol numbers 2023R and 4848 P1). Rats were individually housed in a controlled environment (20-24 °C temperature, 40-70% humidity, 12-h light/dark cycle) and were allowed free access to water and rodent chow. All experiments were carried out in compliance with the ethical and legal requirements from the European Community Council Directive (86/609/CEE, 92/65/CEE, 2010/63/UE), Royal Decree 53/201, and the Generalitat de Catalunya (5/1995, 214/1997) for care and use of laboratory animals.

### 1.1. Study 1

A total of 58 adult male Wistar rats, with a mean age of 14.97 weeks ( $SD \pm 1.66$ ) and a mean weight of 465.35 g ( $SD \pm 51.87$ ) at the time of the surgery, were used in this study.

Animals were randomly distributed into two main experimental conditions: electrode-implanted rats that received intracranial self-stimulation treatment (ICSS groups) and electrode-implanted rats that did not receive ICSS, but sham treatment instead (sham group,  $n=22$ ). Most of the ICSS animals were sacrificed 90 min after the last ICSS session (ICSS90 group,  $n=22$ ). For simplification, ICSS90 group is also designated as ICSS group in results chapter 1, when compared only to sham. Additional ICSS animals were used for time-course

studies, being sacrificed at 30 min and 180 min after last ICSS session, constituting ICSS30 (n=7) and ICSS180 (n=7) groups, respectively (Fig. 14). For OpenArray analysis, samples from 12 sham and 12 ICSS90 rats were pooled to generate 4 pools/group of 3 rats each. For other analyses, samples from individual rats were used.

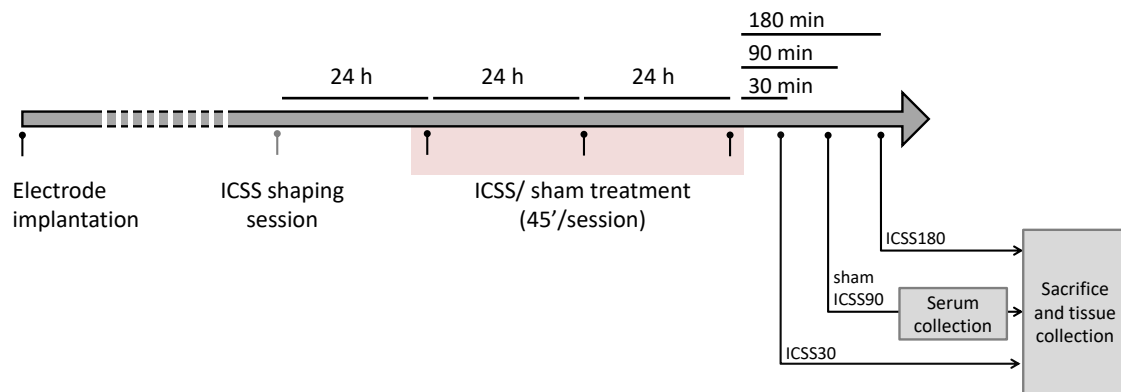


**Fig. 14 | Experimental timeline for Study 1.** Rats in the ICSS group were treated with three ICSS sessions (45'/session/day), with a previous ICSS establishment session. Rats in the sham group were exposed to sham sessions. Ninety min after last ICSS/sham session, serum samples were obtained and rats were sacrificed in order to obtain hippocampal subfield samples to perform molecular analyses. For ICSS30 and ICSS180 groups, rats were sacrificed 30 and 180 min after last ICSS session, respectively. n= 22, 7, 22 and 7 rats/group (sham, ICSS30, ICSS90 and ICSS180, respectively).

## 1.2. Study 2

A total of 52 adult male Wistar rats, with a mean age of 11.78 weeks ( $SD \pm 0.92$ ) and a mean weight of 363.50 g ( $SD \pm 27.89$ ) at the time of surgery, were used in this study.

At day 0, rats were icv injected with an oligomerized amyloid- $\beta$  preparation (AB and AB+ICSS groups) or PBS as the vehicle (VEH and ICSS groups). A subgroup of AB and VEH rats, designed as AB22 (n=8) and VEH22 (n=8), were trained on MWM task between day 15 and 19 and tested and sacrificed at day 22 post injection. Another subgroup, termed AB33 (n=10) and VEH33 (n=8), together with ICSS33 (n=8) and AB+ICSS33 (n=10) groups, were trained between day 26 and 30 and tested and sacrificed at day 33 (Fig. 15). ICSS and AB+ICSS rats were electrode-implanted animals that received intracranial self-stimulation treatment, while VEH and AB were electrode-implanted rats that received sham treatment.

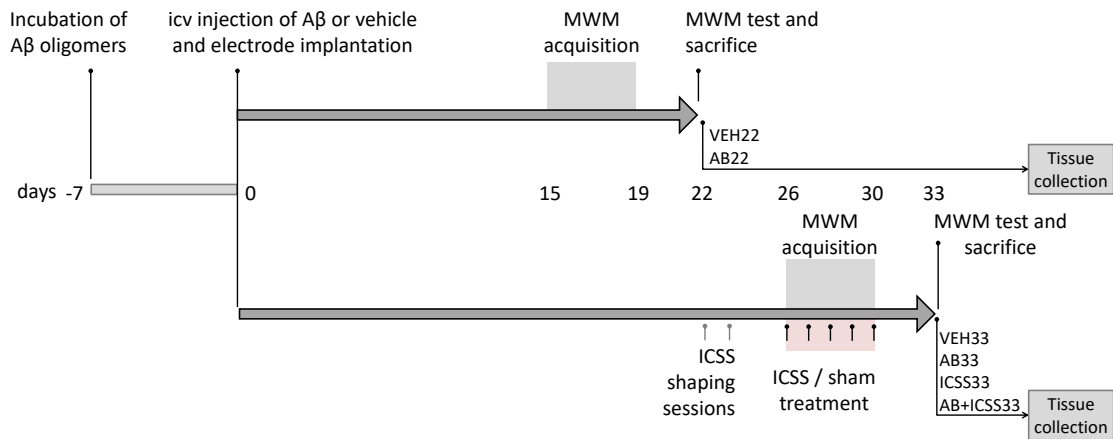


**Fig. 15 | Experimental timeline for Study 2.** Oligomeric A $\beta$ - and vehicle-injected rats trained on MWM task between day 15 and 19 and tested and sacrificed at day 22 post injection conform the AB22 and VEH22 groups. AB33 and VEH33 were trained on MWM task between day 26 and 30 and tested and sacrificed at day 33 post injection. Rats in the AB+ICSS33 and ICSS33 groups were analogous to AB33 and VEH33 rats, respectively, but treated with five ICSS sessions contingent with MWM training sessions. n=8, 8, 8, 10, 8 and 10 rats/group (VEH22, AB22, VEH33, AB33, ICSS33 and AB+ICSS33, respectively).

### 1.3. Study 3

A total of 38 adult male Wistar rats, with a mean age of 13.62 weeks (SD $\pm$ 1.10) and a mean weight of 395.74 g (SD $\pm$ 16.57) at the time of surgery, were used in this study.

Animals were distributed into four experimental groups. Rats in STZ (n=13) and STZ+ICSS (n=6) were icv injected with STZ, while VEH (n=13) and ICSS (n=6) rats were injected with vehicle (citrate buffer). ICSS and STZ+ICSS were electrode-implanted rats that received intracranial self-stimulation treatment, while VEH and STZ were electrode-implanted rats that received sham treatment (Fig. 16).

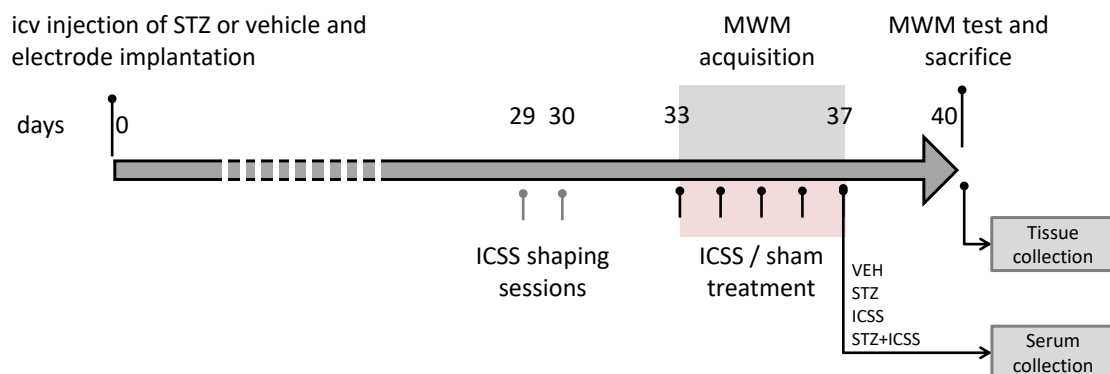


**Fig. 16 | Experimental timeline for Study 3** (see figure on the previous page). STZ and vehicle injected rats were trained on MWM task between day 33 and 37 and tested and sacrificed at day 40 post injection. Rats in the STZ+ICSS and ICSS groups were analogous to STZ and VEH rats, respectively, but treated with five ICSS sessions contingent with MWM training sessions. n=13, 13, 6 and 6 rats/group (VEH, STZ, ICSS and STZ+ICSS, respectively).

## 2. Chemicals

### 2.1. Preparation and assessment of amyloid- $\beta$ oligomeric aggregates

Amyloid- $\beta$  for icv injection was prepared based on Kasza and colleagues' study to obtain well-characterized toxic oligomers (Kasza et al., 2017). Briefly, amyloid- $\beta$  protein fragment 1-42 (Sigma A9810) was pre-treated with HFIP (Sigma 105228-5G) in order to solubilize it and separate it into aliquots. After that, HFIP is removed by overnight evaporation followed by 1.5 h in an exsiccator attached to a vacuum inlet. Aliquots containing 3.75 nmol of dried peptide film were stored at  $-80^{\circ}\text{C}$  until use. At day -7, A $\beta$ 1-42 soluble peptide aliquots were freshly prepared by dissolving the dried peptide in PBS pH 7.4 (DPBS Lonza Biowhitaker (BE17-512F, pH 7.0-7.6; 136.893 mM NaCl, 2.683 mM KCl, 8.058 mM  $\text{Na}_2\text{HPO}_4 \cdot 7 \text{H}_2\text{O}$ , 1.47 mM  $\text{KH}_2\text{PO}_4$ ) at a concentration of 25  $\mu\text{M}$ . Aliquots were sonicated in normal bath sonicator for 5 min and, after that, were incubated at  $37^{\circ}\text{C}$  for 168 h. Before use at day 0, each aliquot was subsequently diluted to the final injection concentration of 15  $\mu\text{M}$ .

Presence of oligomeric aggregates into the injected sample was assessed by Western blot. Twenty-eight (28)  $\mu\text{L}$  of amyloid- $\beta$  peptide prepared equally to the ones to be injected (15  $\mu\text{M}$ ) were loaded onto a Criterion TGX Stain-Free PreCast Gels 4-15% polyacrylamide (Bio-Rad) lane and electrotransferred to PVDF membrane. A lane containing 3.5  $\mu\text{L}$  of protein molecular weight standards (Thermo Scientific PageRuler Prestained Protein Ladder) was also included. After 1 h of blocking with 5% Bovine Serum Albumin (Sigma) in TBS-T (tris-buffered saline [100 mM NaCl, 10 mM Tris-HCl, pH 7.5] containing 0.1% Tween-20), membrane was incubated with rabbit anti-amyloid- $\beta$  H31L21 primary antibody (1:1,000, #700254 Thermofisher) at  $4^{\circ}\text{C}$ , overnight. Goat anti-rabbit peroxidase-conjugated secondary antibody was used for 1h at room temperature (1:20,000, no. 31460, ThermoScientific). Antibody reactive bands were detected using Immobilon Western Chemiluminescent HRP Substrate (EMD Millipore) in a FluorChem luminometer.

## 2.2. Preparation of streptozotocin

Streptozotocin (S0130, Sigma-Aldrich) was stored until use at -20°C in aliquots containing 5 mg of undiluted powder. In order to prevent decomposition of the drug, STZ was not diluted until day 0, immediately before the injection of each individual subject. Freshly prepared citrate buffer (0.05 M, pH 4.4-4.5) was used to dissolve STZ powder in each aliquot to the required concentration for each rat according to its weight, in order to inject a total of 2 mg/kg in 8  $\mu$ L, as detailed in stereotactic surgery section.

## 3. Stereotactic surgery

Animals were general anesthetized and set on a stereotactic apparatus for electrode implantation and/or intracerebroventricular (icv) injection of toxics. For Study 1 and 2, intraperitoneal injection of ketamine and xylazine (110 mg/kg Ketolar® ketamine chlorhydrate (Parke-Davis S.L. Pfizer, Madrid, Spain) and 0.08 ml/100 g Rompun® xylazine 23 mg/ml; i.p. (Bayer, Barcelona, Spain)) was used as anaesthesia. For Study 3, a mixture of 5% isoflurane with oxygen was used as induction anaesthesia, and 2.5% isoflurane mixed with oxygen as maintenance anaesthesia. With the animal set on a stereotactic apparatus, a midline incision was made using a bistoury, from the frontal cranial bones to the back of the parietal cranial bones, to expose the dorsal surface of the skull. The intersection point between the coronal suture and the sagittal suture, known as Bregma, was used as the reference point for the stereotactic coordinates used in electrode implantation and icv injections of chemicals (Fig. 19A).

### 3.1. Electrode implantation

Both ICSS and sham rats were chronically implanted with an ICSS electrode aimed at the MFB in the LH. A little hole was drilled in the skull, at AP=-2.3 mm and ML=2.0 mm from Bregma, in the right hemisphere (ipsi hemisphere), according to stereotaxic atlas (Paxinos and Watson, 2006) (Fig. 17). A monopolar stainless steel electrode (150  $\mu$ m in diameter) was implanted at DV=-8.8 mm. Electrodes were anchored to the skull with jeweller's screws and dental cement, and the incision site was stitched up, leaving the connector protruding outside. Different phases of stereotactic surgery corresponding to electrode implantation are illustrated in Fig. 19C-E. In the post-surgery recovery period (7 days), the animals were weighted and handled daily.

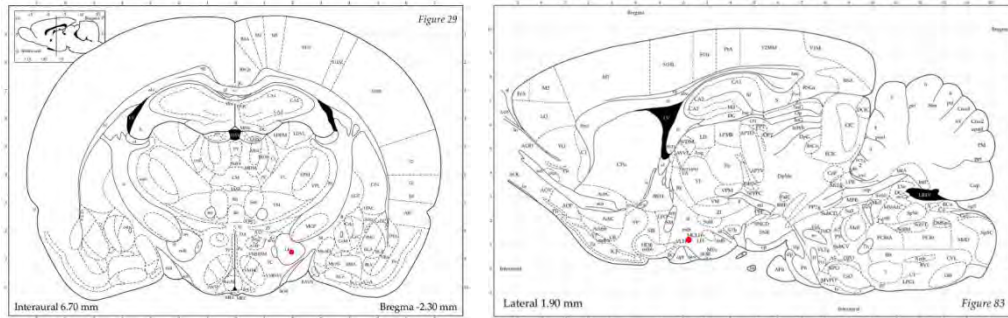


**Fig. 17 | Target location of the ICSS electrode.** ICSS electrode was aimed at the MFB (in the LH), in the right hemisphere. A red dot represents the target location of the electrode tip overprinted in coronal (left) and sagittal (right) sections of the rat brain stereotaxic atlas (Paxinos and Watson, 2006).

### 3.2. Intracerebroventricular injection of amyloid- $\beta$

Rats in Study 2 were injected with amyloid- $\beta$  oligomeric solution or vehicle to the brain ventricles right before the electrode implantation. Two incisions were made at skull, AP=-0.7 mm and ML=-1.6/+1.6 mm from Bregma, according to stereotaxic atlas (Paxinos and Watson, 2006) (Fig. 18). For rats in AB and AB+ICSS groups, 10  $\mu$ L of A $\beta$ 1-42 oligomeric preparation at 15  $\mu$ M was bilaterally icv injected (2x5  $\mu$ L) with a 10  $\mu$ L Hamilton syringe penetrating at DV=-4.00 mm, with the cranium surface as the dorsal reference (illustrated in Fig. 19B). The infusion was made over about 7 min (rate of 0.7  $\mu$ L/min) and retained 3 min to allow for complete diffusion of drug (total of 10 min per hemisphere). The needle was slowly withdrawn after injection. The amount of A $\beta$ 1-42 injected at the concentration of 15  $\mu$ M in each case equalled 0.15 nmol or 0.677  $\mu$ g of A $\beta$  peptide per rat. Rats in VEH and ICSS groups underwent the same procedures except that only vehicle (PBS solution) was injected. Stereotactic protocol for Study 2 was followed with electrode implantation, as described in previous section.

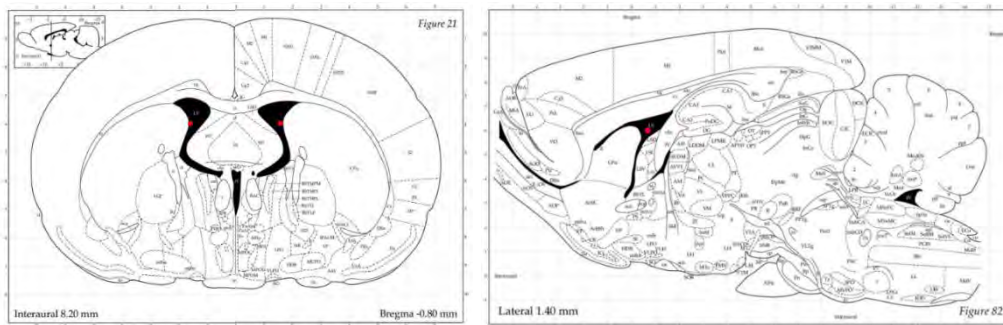


**Fig. 18 | Target injection place for A $\beta$  and STZ toxics.** Bilateral injections of A $\beta$  or STZ preparations were aimed at the lateral ventricles. Two red dots represents the target injection place overprinted in coronal (left) and sagittal (right) sections of the rat brain stereotaxic atlas (Paxinos and Watson, 2006).

### 3.3. Intracerebroventricular injection of streptozotocin

Rats in Study 3 were injected with STZ solution or vehicle into the brain ventricles right before the electrode implantation. The procedure and coordinates for icv injection were the same as described in the previous 3.2 section (Fig. 18). For rats in STZ and STZ+ICSS groups, 8  $\mu$ L solution of STZ dilution were bilaterally injected icv (2x4  $\mu$ L). The amount of STZ injected equalled 2 mg per kg of body weight. Rats in control groups underwent the same procedures except that only vehicle (citrate buffer) was injected. Surgery protocol for Study 3 follows with electrode implantation, as described above.

Post-surgery cares were intensified for STZ-injected animals, which receive wet pellets and wet corn flakes inside the cage for 9 days after the surgery. Physiological variables, including reactivity to handling (classified in 4 levels from “non-sensitive to manipulation” to “very reactive to manipulation”) and body weight were monitored during this period. Those rats exhibiting body weight lose above 10% after surgery were supplied with 0.2 mL dose of condensed milk until weight recovery. In order not to bias glucose intake, all animals received one dose of condensed milk at post-surgery day 10.



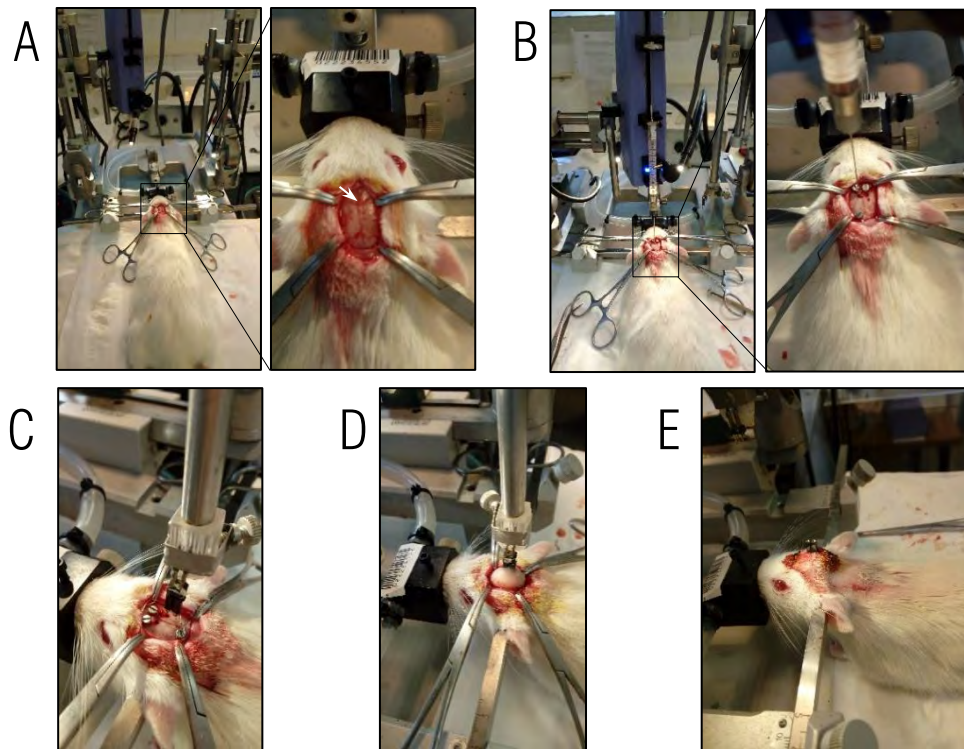


**Fig. 19 | Images of stereotaxic surgery procedure.** **A.** Rat placed on the stereotaxic apparatus, hold by the ear bars and with the top incisors attached to the bite plate of the stereotaxic frame. The dorsal surface of the skull was exposed and Bregma can be distinguished at the intersection point between the coronal suture and the sagittal suture (white arrow). **B.** Bilateral injection of toxins to the cerebral ventricles was done through the incisions made at the specific coordinates (AP=-0.7 mm and L=-1.6/+1.6 mm from Bregma) in the skull, using a Hamilton microsyringe. **C.** Monopolar electrode aimed at the MFB was implanted through the incisions made at the specific coordinates (AP=-2.3 mm; L=-1.8 mm) in the skull. **D.** Electrode was anchored to the skull with jeweller's screws and dental cement. **E.** The incision site was stitched up, leaving the connector protruding outside.

#### 4. Intracranial self-stimulation treatment

##### 4.1. ICSS behaviour shaping

At the day marked as ICSS shaping session in experimental timelines (Fig. 14-16), animals were randomly assigned into one of the two experimental groups according to the independent variable “stimulation treatment” (ICSS or sham). Rats in the ICSS group were taught to self-stimulate by pressing a lever in a conventional Skinner box (25x20x20 cm<sup>3</sup>). Electrical brain stimulation consisted of 0.3 sec trains of 50 Hz sinusoidal waves at intensities ranging from 30 to 175  $\mu$ A. The self-stimulating behaviour was shaped (on one or two consecutive days) to establish optimum current intensity (OI) for each rat. OI was calculated

from the mean of the two current intensities producing the highest response rate (responses/min).

#### 4.2. ICSS treatment

During the ICSS treatment, ICSS rats were placed in a self-stimulation box and were free to press the lever in order to self-administer electrical stimulation at the OI established during the shaping phase for each subject (Fig. 20). Sham rats were handled and allowed to explore the ICSS box for an equivalent amount of time (45 min in Study 1 and 30 min for Study 2-3) but did not receive any electrical stimulation.

For Study 1, ICSS treatment consisted of 3 sessions of 45 min each (1 session/day for the 3 consecutive days after the ICSS establishment session (Fig. 14)).

For Studies 2 and 3, ICSS treatment consisted of 5 sessions (1 session/day for 5 consecutive days), administered immediately after each Morris water maze acquisition session. Each session consists of 2500 trains of stimulation.



**Fig. 20 | Image of a rat in the self-stimulation box.** Rats were placed in the ICSS box and the protruding electrode is connected to stimulation apparatus through a cable. During the ICSS session, rats were free to press the lever in order to self-administer electrical stimulation at the OI established during the shaping phase for each subject.

## 5. Behavioural analyses

In Studies 2 and 3, spatial learning and memory were assessed in the Morris water maze (MWM). MWM apparatus consisted of an elevated circular pool (2 m diameter), which was virtually divided into four equal quadrants using the four cardinal points (Fig. 21). A clear Plexiglas platform (11 cm diameter) was placed 2 cm below the surface of the water in the middle of the SE quadrant, becoming the escape target. Spatial cues are generally distinctive objects (lights, boxes, toys, balls, etc.) that provide distal visual aid for the animals to locate themselves within the tank and in reference to the platform, regardless of the entry point.

The standard training procedure consists of three phases: the habituation phase, the acquisition phase and the probe trial. In the habituation phase, which is performed without cues or platforms present in the tank and took place 72 h before the acquisition phase, animals were introduced into the pool and allowed to freely swim for 60 sec in order to reduce emotional reactivity. During the acquisition phase, both the cues and the platform are placed in the pool (configuration in Fig. 21). The animals were repeatedly introduced into the tank from a different entry point (pseudorandomized) in each of the trials and expected to learn to locate the platform by using the distal cues as spatial guides as the trials progress. To assess spatial memory at the end of the learning phase, a probe trial is given, which consists of removing the platform but not the cues before introducing the animal into the tank. If the animal has learned to locate the platform based on the spatial cues, it will be reflected in a more accurate trajectory of the navigation as well as in more time spent in the quadrant where the platform used to be during the acquisition phase. During the MWM tasks, all swim paths were recorded using a closed-circuit video camera (Smart Video Tracking System, Version 2.5, Panlab).

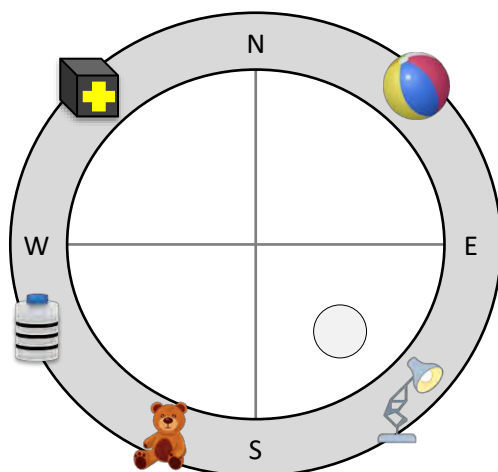


**Fig. 21 | Morris water maze configuration during the acquisition phase.** The pool is divided into four equal quadrants, named as the cardinal points. Salient objects are placed around the pool for spatial orientation. The escape platform is depicted in the SE quadrant.

### 5.1. Morris water maze acquisition phase

Rats were given 5 acquisition sessions, one per day on consecutive days (see Experimental timelines: Fig. 15 and 16). Each acquisition session consisted of 4 trials for Study 2, or 2 trials for Study 3, with a mean intertrial interval of 120 sec. Each trial consisted of one swim from the edge of the pool to the platform, starting from one of the four different cardinal points in a semi-random schedule. If a rat failed to find the platform within 90 sec, it was manually guided to the platform, let there for 15 sec and removed from the pool. Otherwise, when animals found the platform before the completion of the trial, they were left on it for 15-30 sec and then were removed by the experimenter. The following variables were extracted from the video recorded during the MWM acquisition sessions, in order to be used for behavioural characterization of AD models (Study 2 and 3) as well as for correlation analyses with molecular variables:

- Latency: time spent to reach the platform for each rat.
- Thigmotaxis: percentage of time spent in the peripheral zone, in contact with the walls of the swimming arena, with respect to the whole trial duration. This measure has been taken as a measure of anxiety in rodents (Treit and Fundytus, 1988; Song et al., 2012).

All variables were calculated for each session as the mean of the different acquisition trials.

### 5.2. Morris water maze probe test

The probe test was performed 72 h after the last acquisition session. The animal was introduced to the pool from the E entry and let swim for 60 sec. The following variables were extracted from the video recorded during the probe test, in order to be used for behavioural characterization of AD models (Study 2 and 3) as well as for correlation analyses with molecular variables:

- Mean distance to target area: mean distance between the rat body centre and the place where the platform used to be in the acquisition phase, during the whole test or during the first 30 sec.
- Percentage of time in the target quadrant: percentage of time spent in the quadrant where the platform used to be during the acquisition phase, with respect to the whole duration of the test or during the first 30 sec.

- Percentage of time in the annulus: percentage of time spent in the target annulus with respect to the whole duration of the test.

### 5.3. Morris water maze reversal test

To assess cognitive flexibility in animals from Study 2, immediately after the probe test, the reversal test was performed. The escape platform was introduced again to the pool, but changed to the NW quadrant. Reversal session consist of 3 trials, which were performed similarly to acquisition session trials. The following variables were extracted from the video recorded during the reversal session:

- Latency: time spent to find the platform for each rat.
- Percentage of time in error quadrant: percentage of time spent in the quadrant where the platform used to be during the acquisition phase (SE quadrant).

## 6. Sample collection

### 6.1. Serum samples

Blood samples were obtained immediately before sacrifice at the indicated time after last ICSS/sham session for Study 1, and right after the last ICSS/sham session for Study 3. A small cut was made in the lateral tail vein and a total of 600  $\mu$ L of blood were collected using Microvette tubes (Microvette® CB 300, SARSTEDT Sau). Tubes were maintained 45 min at room temperature and centrifuged for 10 min at 1,670 x g to collect serum. Serum samples were stored at -80°C until use for molecular assays.

### 6.2. Tissue samples

Animals were sacrificed by decapitation at the indicated time after last ICSS/sham session for Study 1 and immediately after the MWM test for studies 2 and 3. Brain was extracted and the two hemispheres were separated, using a blade. Tissue samples were collected according to their fate (see Fig. 22 for tissue distribution in the different studies). A brain matrix was

used to cut in the indicated coordinates, according to Paxinos & Watson stereotaxic atlas (Paxinos and Watson, 2006).

To use in molecular assays, tissue was dissected and the regions of interest were isolated. On the one hand, whole hippocampus (for Study 1) or the anterior (dorsal) part of the hippocampus (Bregma anterior to -4.00, for Study 3) was extracted (Fig. 22A,C). Regions enriched in the different hippocampal subfields CA1, CA3 and DG were isolated dissecting along the visible boundaries, using a Vannas scissors and a curved tip forceps (Fig. 23) as previously described (Lein, 2004). On the other hand, a 2 mm-coronal slice of the frontal lobe was obtained by cutting on Bregma 1.70-2.00 and on Bregma 3.70-4.00. Medial prefrontal cortex (mPFC) containing prelimbic and infralimbic regions, was dissected in this slice, following corpus callosum edge as illustrated in Fig. 22C. Tissue samples corresponding to CA1, CA3, DG or mPFC dissected pieces were collected individually in eppendorfs containing Allprotect Tissue Reagent (Qiagen) and stored at -80°C until use.

To use in histological analyses, whole hemispheres were fixed in 4% formaldehyde in 0.01 M PBS for 24 h at 4°C. Post-fixed entire hemispheres were cryopreserved 48 h in sucrose 15% 0.01 M PBS at 4°C followed by 48 h in sucrose 30% 0.01 M PBS at 4°C, frozen using freeze aerosol and stored at -80 °C until cryotomy. Serial coronal sections were obtained in a cryostat (Reichert-Jung Cryocut 1800, with 2020 microtome) at -25 °C at the coordinates between Bregma -2.50 and -3.80 (for parietal-temporal lobe sections) and 2.00 to 3.50 (for frontal lobe sections). Sections of 12 µm thick were mounted onto microscope slides and stored at -80°C to use for Nissl staining. Sections of 35 µm thick were collected into Eppendorf tubes and stored at -80°C until their use for free-floating immunohistochemistry.

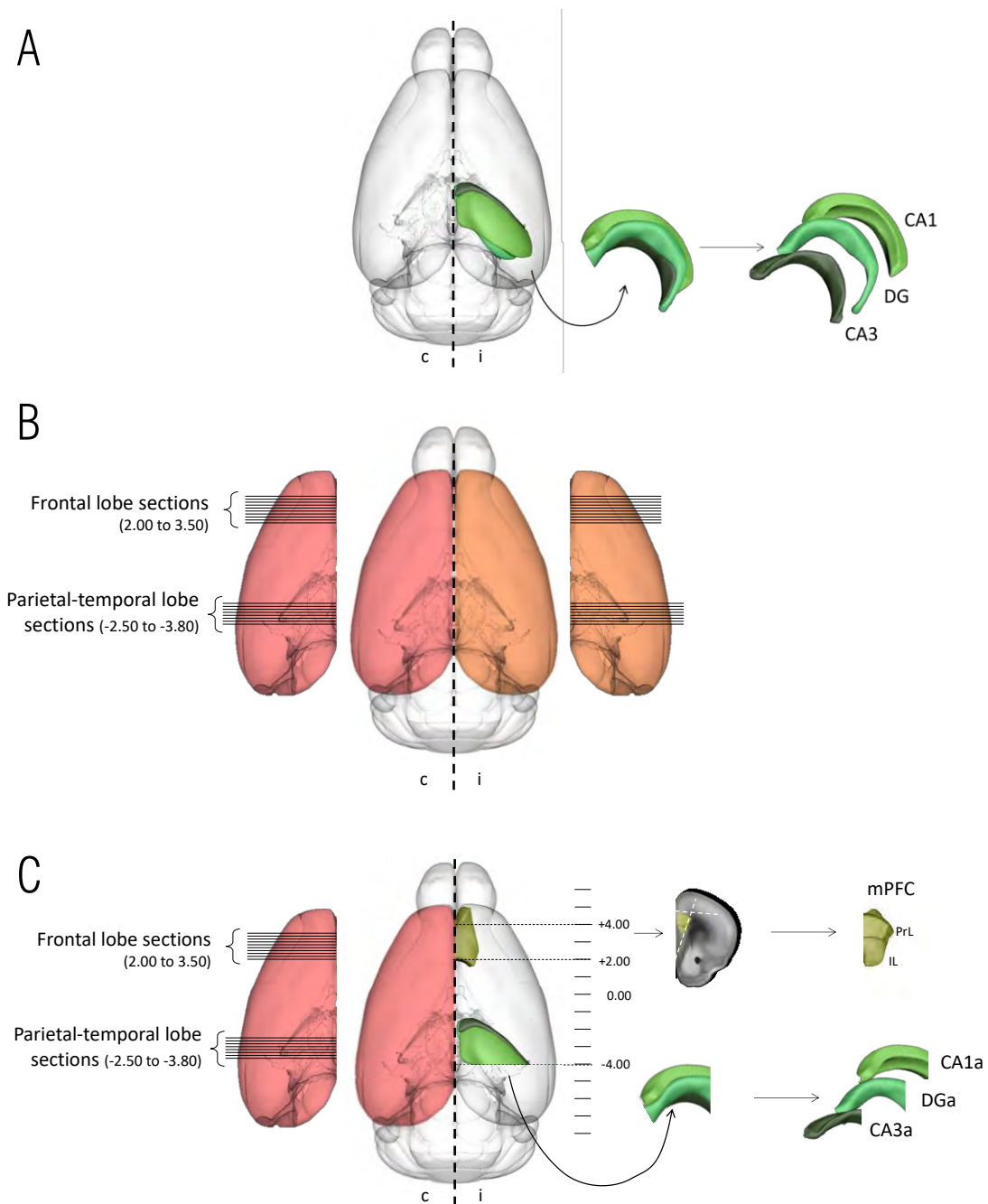


**Fig. 22 | Representation of tissue distribution according to sample fate in each of the studies. A.** Study 1. **B.** Study 2. **C.** Study 3. Pieces of tissue to be used in molecular assays are highlighted in shades of green, while pieces for histological analyses are shaded in red/orange. Rodent brain figures were obtained with the aid of Scalable Brain Atlas (Bakker et al., 2015) using data from Allen Brain Atlas (Lein et al., 2007). Numbers refer to coordinates with respect to Bregma, which were adapted to rat brain according to Rat Brain atlas (Paxinos and Watson, 2006). Abbreviations: c: contra hemisphere; CA1a/CA3a/DGa: anterior part of the CA1/CA3/DG; DG: dentate gyrus; i: ipsi hemisphere; IL: infralimbic cortex; mPFC: medial prefrontal cortex; PrL: prelimbic cortex.

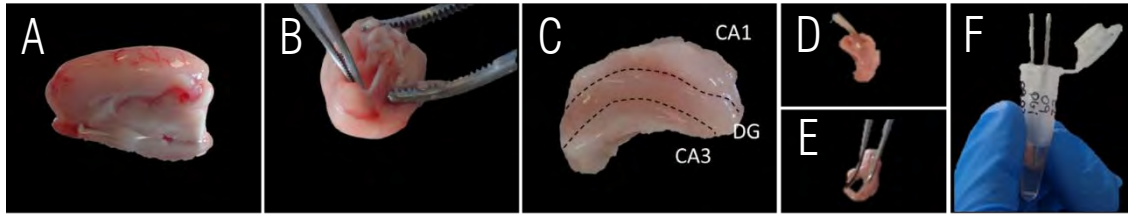


**Fig. 23 | Images of hippocampal subdissection.** **A.** Right hemisphere (ipsi) was separated. **B.** Hippocampus was detached from the overlying neocortex and **C.** removed as an intact structure, where the boundaries of the subregions can be seen (indicated by black dashed lines). **D-E.** CA1, DG and CA3 subregions were dissected. **F.** isolated subregions were individually stored in Allprotect containing Eppendorf tubes and stored at  $-80^{\circ}\text{C}$ .

## 7. Molecular assays

### 7.1. Protein and RNA isolation and quantification

Both total RNA and protein were extracted from pieces of tissue to be used in molecular assays (hippocampal or mPFC tissue samples for Studies 1 and 3), using mirVana PARIS Kit (Ambion). Samples, which weighted between 5 and 15 mg, were homogenized in 200  $\mu\text{L}$  of Cell Disruption Buffer, containing a phosphatase inhibitor (250  $\mu\text{g}/\text{mL}$  of sodium orthovanadate), using a Heidolph DIAX900 mechanic homogenizer. Exceptionally, whole DG samples, which weighted above 20 mg, were homogenized in 400  $\mu\text{L}$  of Cell Disruption Buffer.

Half of the homogenate (100  $\mu\text{L}$ , or 200  $\mu\text{L}$  for whole DG samples) was used for RNA extraction, using mirVana PARIS Kit (Ambion), following kit instructions. For serum samples, 100  $\mu\text{L}$  were used to obtain RNA extracts employing the same instructions. Briefly, the homogenate was mixed with 100  $\mu\text{L}$  of 2 X Denaturing Solution provided in the kit, and incubated in ice for at least 5 min. 200  $\mu\text{L}$  of acid phenol:chloroform was added, mixing thoroughly for 50 sec, and centrifuged for 5 min at 16,100 x g to separate the mixture into aqueous and organic phases. The aqueous phase (120  $\mu\text{L}$ ) was retrieved and mixed with 150  $\mu\text{L}$  of absolute ethanol and pipetted onto the filter cartridges supplied in the kit. All the volumes used until this point were doubled for whole DG samples. Filter cartridge was centrifuged three times 30 sec at 10,000 x g and the flow-through was discarded. The filter was washed with three consecutive steps using kit wash solutions (700  $\mu\text{L}$  of Wash Solution1, 500  $\mu\text{L}$  Wash Solution 2/3 and 500  $\mu\text{L}$  Wash Solution 2/3), centrifuging 15 sec at 10,000 x g in each step and discarding the flow-through, and at last it was spun for 1 min



at 10,000 x g to remove residual fluid. Finally, RNA was recovered into a fresh collection tube, eluting with 100 µL of preheated (95°C) DEPC water centrifuging 30 sec at 10,000 x g. The concentration of RNA was determined using a NanoDrop 1000 Spectrophotometer (ThermoFisher) and quality was assessed using Agilent Bioanalyzer 2100, showing RNA integrity ranking between RIN 7.0 and RIN 8.6.

The other half of the homogenate (100 µL, or 200 µL for whole DG samples) was further processed for protein analyses by two rounds of centrifugation to get rid of cell and tissue debris (5 min at 16,100 x g followed by 25 min at 16,100 x g, at 4°C). Protein quantification was performed using Pierce BCA Protein Assay kit (ThermoScientific), following kit instructions. Briefly, 10 µL of sample dilution or albumin standards were pipetted in duplicate in a 96-well plate, using a 1:15 dilution for hippocampal samples and 1:5 dilution for mPFC samples. 200 µL of the working reagent supplied in the kit was added to each well and the plate was mixed for 30 sec. After 30 min incubation at 37°C in the dark, the absorbance was measured at 562 nm and the concentration of each sample was determined by interpolating the standard curve fitting a four-parameter logistic regression.

After the extraction process, RNA and protein extracts were stored at -80°C until use.

## 7.2. TaqMan OpenArray procedure

For Study 1, four sham samples and four ICSS90 samples were used for miRNA expression comparison using OpenArray panels containing 750 well-characterized rodent miRNA sequences from the Sanger miRBase v15. Each sample consisted of pooled RNA from DG extracts from three rats. In this way, biological variability can be reduced while minimizing the number of required panels, as demonstrated by Kendzioriski and colleagues (Kendzioriski et al., 2005). cDNA was synthesized from 100 ng total RNA, using Megaplex Primer pools A and B and the MicroRNA Reverse Transcription kit (Life Technologies). Pre-amplified samples (1:40 dilution) were loaded onto TaqMan® OpenArray® Rodent MicroRNA Panel (ThermoFisher), using the AccuFill System, to be run on QuantStudio™ 12K Flex Real-time PCR system (Applied Biosystems).

miRNA profiling data were analysed using Expression Suite Analysis Software v1.1 (ThermoFisher). Wells that presented an AmpScore below 1.24 were inspected and, if the shape of the amplification curve was atypical, they were omitted from analysis. Maximum

allowed Ct was fixed to 28.0 to avoid false positive results. Relative quantification value for each miRNA was obtained by the algorithms implemented in the software for the comparative  $\Delta\Delta\text{Ct}$  method, using sham group as the reference biological group and a global normalization method. The global normalization method uses the global mean Ct value of targets common to all samples as the normalization value, and is the recommended and most robust strategy for normalization in large scale ( $> 384$ ) miRNA expression profiling studies (Mestdagh et al., 2009). A list of differentially expressed miRNAs between sham and ICSS pools was obtained using a FoldChange Boundary of 1.3 and p-value Boundary of .05. No Benjamini-Hochberg false discovery rate was used to adjust p-values in order to avoid false negative results, because it would unnecessarily limit the set of candidate list for further validation. The differentially expressed miRNAs were functionally investigated using prediction tools accessible from DIANA mirPath v.3 and TargetScan v7.2, together with bibliographic research.

### 7.3. TaqMan miRNA qRT-PCR

A subset of 6 miRBase-annotated miRNAs, which were also interesting on a functional basis, were selected for further qRT-PCR validation from among the OpenArray differential expressed miRNA list. Additionally, miR-132-3p, miR-134-5p, miR-146a-5p and miR-181c-5p were also selected as potential ICSS-regulated miRNA candidates for their role in neural plasticity and relation with AD, according to literature presented in the introduction chapter. Moreover, miR-16-5p, miR-103a-3p, miR-124-3p, let-7a-5p and let-7b-5p were included as endogenous normalizer candidates. Expression levels of all the ICSS-regulated miRNA candidates and endogenous normalizer candidates (listed in Table 2) were determined in DG and serum samples from Study 1. In addition, miR-495-3p, miR-132-3p and miR-181c-5p were further analysed in CA1 and CA3 subregions in this study. A subset of miRNAs, including miR-495-3p, miR-196a-5p, miR-132-3p, miR-134-5p, miR-146a-5p and miR-181c-5p as ICSS-regulated candidates and miR-16-5p, miR-124-3p, let-7a-5p and let-7b-5p as endogenous normalizer candidates, were analysed in DG and serum samples from Study 3.

cDNA was synthesized and preamplified from 10 ng total tissue RNA from individual subjects, using TaqMan® Advanced miRNA cDNA Synthesis Kit (Applied Biosystems), in an AB vecti 96 well thermocycler (Applied Biosystems), following kit instructions. Briefly, 2  $\mu\text{L}$  of extracted RNA, diluted in DEPC water to a concentration of 5 ng/ $\mu\text{L}$  was mixed with 3  $\mu\text{L}$  of poly(A) reaction mix in a 96-well reaction plate, and it was incubated into the thermal

cycler following the polyadenylation settings detailed in kit instructions (45 min at 37°C, 10 min at 65°C). After that, 10 µL of Ligation reaction mix were added to each well in order to ligate the adaptor, and incubated into the thermal cycler (16°C, 60 min). Reverse transcription was performed by adding 15 µL of RT reaction mix and incubating into the thermal cycles (15 min at 42°C, 5 min at 85°C). Finally, for the miRNA preamplification (miR-Amp), 45 µL of miR-Amp reaction mix were mixed with 5 µL of RT reaction product and incubated into the thermal cycles (5 min at 95°C, 14 cycles of denaturing at 95°C for 3 sec and annealing-extending at 60°C for 30 sec, and 10 min at 99°C). Slight modifications were included for serum samples regarding the initial RNA extract volume (3 µL of undiluted RNA extract was used) and the number of cycles of the miR-Amp reaction (16 cycles).

PCRs were run on an AB QuantStudio 7, using the TaqMan Advanced miRNA qPCR assays (Applied Biosystems) listed in Table 2. To do so, 2.5 µL of diluted miR-Amp reaction product were added to each well of a 384-reaction plate, containing 7.5 µL of PCR Reaction mix including a specific assay from the list. PCR conditions consist on 20 sec at 95°C for enzyme activation, followed by 40 cycles of denaturing (95°C for 1 sec) and annealing-extending (60°C for 20 sec).

**Table 2 |** MicroRNAs analysed by qRT-PCR and used TaqMan Advanced Assays.

<i>Selection criteria</i>	<i>Type</i>	<i>miRNA symbol</i>	<i>TaqMan Advanced miRNA assay name</i>	<i>TaqMan Advanced miRNA assay ID</i>
<i>OpenArray-based</i>	ICSS-regulated candidate	miR-196a-5p	hsa-miR-196a-5p	478230_mir
		miR-485-3p	mmu-miR-485-3p	mmu481854_mir
		miR-495-3p	mmu-miR-495-3p	mmu482634_mir
		miR-185-5p	hsa-miR-185-5p	477939_mir
		miR-154-5p	hsa-miR-154-5p	477925_mir
		miR-197-3p	hsa-miR-197-3p	477959_mir
<i>Literature-based</i>	ICSS-regulated candidate	miR-132-3p	rno-miR-132-3p	rno480919_mir
		miR-134-5p	rno-miR-134-5p	rno480922_mir
		miR-146a-5p	rno-miR-146a-5p	rno481451_mir
		miR-181c-5p	rno-miR-181c-5p	rno481295_mir
		miR-16-5p	hsa-miR-16-5p	rno481312_mir
		miR-103a-3p	rno-miR-103a-3p	rno478253_mir
	Endogenous normalizer candidate	miR-124-3p	rno-miR-124-3p	rno480901_mir
		let-7a-5p	hsa-let-7a-5p	478575_mir
		let-7b-5p	hsa-let-7b-5p	478576_mir

Relative expression of each target miRNA was determined as  $2^{-\Delta\Delta C_t}$  ( $\Delta\Delta C_t = \Delta C_t \text{ sample} - \Delta C_t \text{ reference sample}$ ;  $\Delta C_t = C_t \text{ target} - C_t \text{ normalizer}$ ), using the mean in the sham group as the reference sample and an endogenous normalizer specific for each sample type.

To define the most suitable miRNA endogenous normalizer among the candidates in hippocampal tissue and serum samples under our specific experimental conditions, both NormFinder (Andersen et al., 2004) algorithm and the version of GeNorm implemented in ThermoFisher Cloud (Vandesompele et al., 2002) were used. These different algorithms rank the set of candidates according to their expression stability in a given sample set, assigning lower values to most optimal candidates for a specific experimental design. NormFinder takes into account the biological group of each sample and estimates both intra-group and inter-group gene variation to evaluate its stability. GeNorm determines the pairwise standard deviation of Ct values of all genes, and then excludes the one with the lowest stability, repeating the process until only two genes remain, which are then considered the most stable ones.

#### 7.4. Western blot

Samples containing 30  $\mu\text{g}$  of total protein extracted from DG, CA1 or CA3 subfields (Study 1) or 20  $\mu\text{g}$  of total protein from DG or mPFC (Study 3) were loaded onto a Criterion TGX Stain-Free PreCast Gels 18 well comb (Bio-Rad) under reducing conditions, and electrotransferred to PVDF membranes. A lane containing 3.5  $\mu\text{L}$  of protein molecular weight standards from 10 to 180 kDa (Thermo Scientific PageRuler Prestained Protein Ladder) was also included. Images of the protein bands transferred to the membrane were obtained by exposing the membranes to 30 sec trans-UV in a FluorChem luminometer, taking advantage of the trihalo compounds present in the Stain-Free gels that react with tryptophan residues in a UV-induced reaction to produce fluorescence. These images serve both for quality control of protein separation and transference, as well as for total protein quantification, as described below.

After 1 h of blocking with 5% Bovine Serum Albumin (Sigma) in TBS-T (tris-buffered saline [100 mM NaCl, 10 mM Tris-HCl pH 7.5] containing 0.1% Tween-20), membranes were incubated with DBN, SIRT1, APP, ptau S202/T205, ptau S396 or GAPDH primary antibodies, using conditions shown in Table 3. Peroxidase-conjugated secondary antibodies were used for 1h at room temperature: goat anti-rabbit (1:20,000, no. 31460,

ThermoScientific; exceptionally at 1:40,000 for ptau S396) or goat anti-mouse (1:20,000, no. 115-035-044, Jackson ImmunoResearch), according to Table 3. Intensities of antibody reactive bands were detected using Immobilon Western Chemiluminescent HRP Substrate (EMD Millipore) in a FluorChem luminometer, and quantified by densitometry using FluorChem SP software (AlphaEaseFC™). After that, membranes used for ptau determination were stripped and reblotted with tau 46 antibody for total tau using the conditions specified in Table 3. Stripping consisted on a 30 min incubation at 50°C and 180 rpm in a solution containing 2% SDS and 100 mM  $\beta$ -mercaptoethanol in order to remove antibodies previously attached to the membrane.

**Table 3 | Conditions for Western blot analyses.** Primary antibodies and incubation conditions used for Western blot determination of protein expression levels. The “Molecular weight” column shows the approximate molecular weight of the band/s corresponding to the analysed protein.

<i>Protein</i>	<i>Antibody</i>	<i>Dilution</i>	<i>Incubation time</i>	<i>Secondary antibody</i>	<i>Molecular weight</i>
<i>DBN</i>	Sc-374269, Santacruz	1:5,000	ON, 4°C	mouse	130 kDa
<i>SIRT1</i>	07-131, Millipore	1:2,000	ON, 4°C	rabbit	110 kDa
<i>APP</i>	803001, Biolegend	1:2,000	ON, 4°C	mouse	135 kDa
<i>ptau Ser202/Thr205</i>	AT8 (ser202, thr205). MN1020, ThermoFisher	1:1,000	ON, 4°C	mouse	50-70 kDa
<i>ptau Ser396</i>	phospho S396, [EPR2731] ab109390, Abcam	1:70,000	ON, 4°C	rabbit (exceptionally at 1:40,000 dilution)	50-70 kDa
<i>Total tau</i>	Tau46, sc-32274, Santacruz	1:2,000, post- stripping	1 h, room temperature	mouse	50-70 kDa
<i>GAPDH</i>	MAB374, Millipore	1:800,000	ON, 4°C	mouse	38 kDa

Protein relative intensities were obtained by normalization using GAPDH band quantification, as a common used housekeeping protein in physiological conditions, or total amount of protein, as an alternative reliable loading control (Aldridge et al., 2008). Total protein was quantified in membrane Stain-Free images, as described by Aldridge et al. (Aldridge et al., 2008) and as shown in Fig. 24. In the case of ptau band intensities, they were normalized by total tau band intensities to obtain phosphorylation ratio. Moreover, in all cases, protein relative intensities were normalized by mean protein relative intensity in control group, which was used as reference.

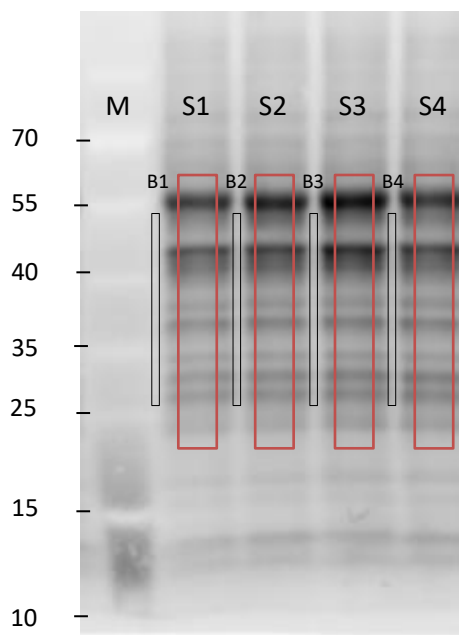


**Fig. 24 | Total protein quantification for Western blot normalization.** Representative image of total protein quantification using membranes transferred from Stain-Free gels. Larger red rectangles represent quantified area, while narrow black adjacent rectangles represent subtracted background between the lanes. Numbers represent the molecular weight (kDa) of protein markers. Abbreviations: M: marker lane; S1, 2, 3 and 4: samples in four different lanes; B1, 2, 3 and 4: background for each lane.

## 7.5. SIRT1 ELISA

Concentration of SIRT1 protein in serum samples was determined by ELISA (LifeSpan BioSciences, LS-F21634), according to manufacturer's instructions. Briefly, 100  $\mu$ L of diluted samples (1:15), standards or blank were pipetted in duplicate into the coated 96-well plate provided in the kit. After 90 min of incubation (all the incubations at 37°C and 60 rpm), the liquid was aspirated and 100  $\mu$ L of the biotinylated detection antibody supplied in the kit was added to each well, the plate was mixed and incubated for 1 h. Then it was washed for 3

times with 300  $\mu\text{L}$  of the wash buffer supplied in the kit and 100  $\mu\text{L}$  HRP conjugate working solution was added to each well. After 30 min of incubation and 5 washes, 90  $\mu\text{L}$  of TMB substrate solution was added to each well and the plate was incubated for 15 min, protected from light. Finally, 50  $\mu\text{l}$  of stop solution was added to each well and the absorbance was measured at 450 nm. The concentration of each sample was determined by interpolating the standard curve fitting a four-parameter logistic regression.

## 7.6. BDNF ELISA

Concentration of BDNF protein in serum and DG samples for Study 1 was determined by ELISA (Biosensis®, BEK-2211-1P/2P), according to manufacturer's instructions. Briefly, 100  $\mu\text{L}$  of diluted samples (1:60 for serum and 1:8 for DG), standards or blank were pipetted in duplicate into the coated 96-well plate supplied in the kit, and incubated for 45 min on a plate shaker (140 rpm) at room temperature. After that, wells were washed 5 times with 200  $\mu\text{L}$  of the wash buffer supplied in the kit, and 100  $\mu\text{L}$  of detection antibody was added to each well. After 30 min of incubation and 5 washes, 100  $\mu\text{L}$  of streptavidin-HRP conjugate was added to each well. The plate was incubated for 30 min, washed and 100  $\mu\text{L}$  of TMB was added. After 4.5 min of incubation protected from light, the reaction was stopped with 100  $\mu\text{L}$  of stop solution. The absorbance was measured at 450 nm and the concentration of each sample was determined by interpolating the standard curve fitting a four-parameter logistic regression.

For DG samples, the concentration of BDNF was normalized by the total amount of protein resulting from the BCA quantification of these samples (described in section 7.1.).

## 8. Histological analyses

### 8.1. Nissl staining

Nissl staining was used to assess neurodegeneration induced by toxic injection in Studies 2 and 3. Slides containing 3 parietal-temporal sections and 3 frontal sections of left hemisphere for each rat were transferred from -80°C to a 37°C plate. When warm, preparations were stained with filtered 0.5% cresyl violet solution [2.5 g cresyl violet (Sigma C5042), 300 ml H<sub>2</sub>O, 30 ml sodium acetate (1.0 M), 170 ml acetic acid (1.0 M)] for 2.7 min, rinsed in water for 5 min and subsequently dehydrated in 70%, 95% and twice in 100% ethanol for 3-5 min each. Slides were finally placed in HistoClear twice for 5 min each and coverslipped in Pertex medium.

Photomicrographs for 4 hippocampal subregions (CA1, CA3, CA3hil and DG) and for prelimbic cortex layers II-III and dorsal tenia tecta were obtained from parietal-temporal and frontal stained sections, respectively (Fig. 25A,26), using an Olympus Vanox-T AH-2 microscope attached to an Olympus DP73 digital camera, using a 6.3x objective.

ImageJ was used to count the number of neurons. For layer-shaped regions (CA1, CA3, CA3hil and DG), total counts were normalized by 250  $\mu\text{m}$  length (see Fig. 25B). Neuronal density was also estimated in these regions by measuring layer thickness. For prelimbic cortex (PrL) and dorsal tenia tecta (DTT), normal and degenerating neurons were separately counted in defined regions of interest (ROIs). An area of 0.1 mm<sup>2</sup> (350x260  $\mu\text{m}$ ), corresponding to layer II-III, was defined for PrL, while in DTT, results from 3 circular ROIs of 0.03 mm<sup>2</sup> were averaged (Fig. 26). Normal neurons were identified by their rounded shape with purple-stained cytoplasm, pale nuclei and visible nucleoli, whereas shrunken, deformed, indistinct borders between the nucleus and cytoplasm, pyknotic and hyperchromatic neurons were counted as degenerating neurons. Percentage of neurodegeneration was obtained as the percentage of degenerating neurons with respect to the total number of neurons (normal plus degenerating neurons). Values for each subject were obtained by averaging the results for the 3 sections.



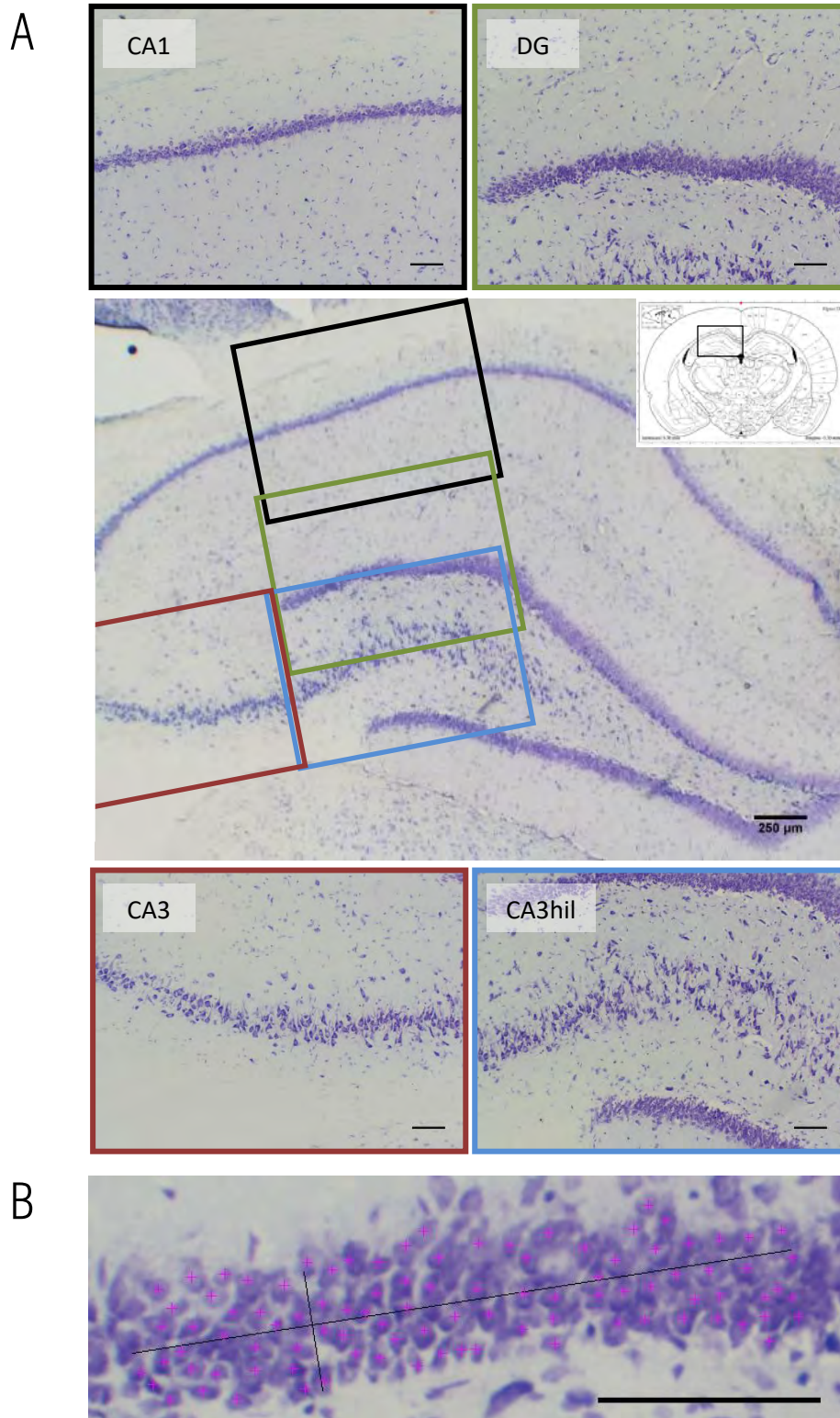


**Fig. 25** | Analysed photomicrographs in Nissl staining hippocampal sections. **A.** Location of photomicrographs for each analysed subregion in the hippocampus of a Nissl-stained parietal-temporal section (-3.30 mm from Bregma, according to Paxinos and Watson's atlas (Paxinos and Watson, 2006). Scale bar=100 μm when not specified. **B.** Representation of cell count in layer-shaped hippocampal subregions. Black segments show the length and width in which neurons, labelled with a pink marker, are counted. Abbreviations: DG: dentate gyrus; hil: hilus.

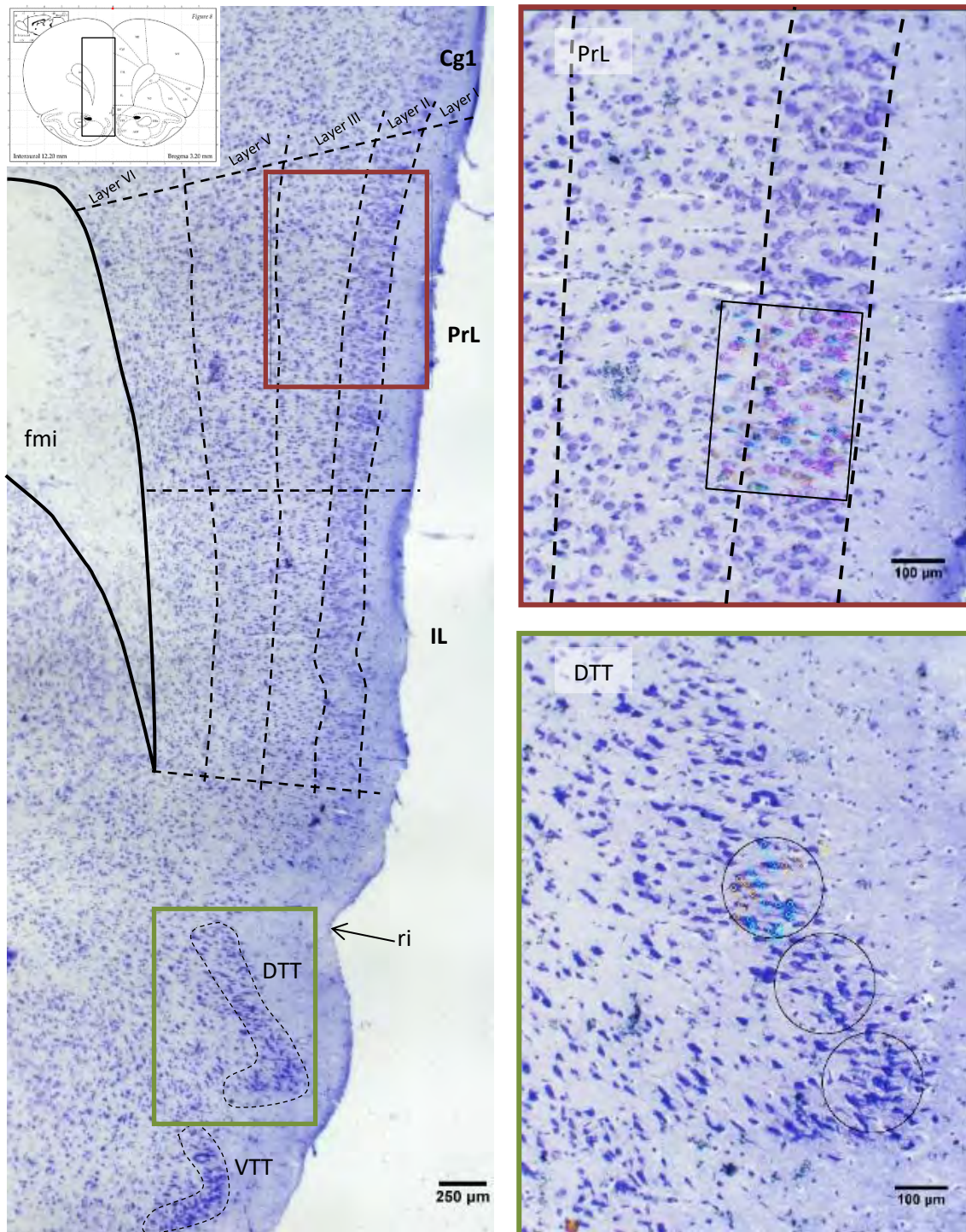


**Fig. 26** | Analysed photomicrographs in Nissl staining prefrontal sections. Location of photomicrographs for PrL layer II-III and DTT (right) in the medial prefrontal cortex (left) of a Nissl-stained frontal section (+3.00 mm from Bregma) with superimposed regions adapted from Paxinos and Watson's atlas (Paxinos and Watson, 2006). In PrL and DTT photomicrographs (right), rectangular or circular regions of interest (ROIs), respectively, are shown superimposed. Neurons are counted in each ROI, classifying according to their shape in normal or degenerating neurons, as can be seen with markers of different colour. Abbreviations: Cg1: cingulate cortex area 1; DTT: dorsal tenia tecta; fmi: forceps minor of the corpus callosum; IL: infralimbic cortex; PrL: prelimbic cortex; ri: rhinal incisure; VTT: ventral tenia tecta.

## 8.2. DBN and ptau immunostaining

Free-floating immunohistochemistry was used to assess DBN and ptau levels in Studies 2 and 3. Free-floating sections were set in 24-well plates in TBS [50 mM Tris; 150 mM NaCl; pH 7,6] and incubated in 0.3% H<sub>2</sub>O<sub>2</sub> in TBS-T [0.5% triton TBS] for 40 min to block endogenous peroxidase. Previously, sections to be used in DBN immunostaining were fixed in 2% formaldehyde in TBS for 20 min. They were then washed (TBS-T 3x15 min) and incubated in blocking solution (7% normal goat serum, Vector S-1000, in TBS-T) for 1 h at room temperature, followed by incubation with primary antibody. Rabbit anti-DBN1 (ABN207, EMD Millipore) was diluted 1:3,000 and incubated for 4 h at room temperature followed by 1 overnight 4°C. Mouse anti-ptau (AT8, MN1020, ThermoScientific), which recognizes phosphorylation site Ser202/Thr205 from tau protein, was applied in a 1:200 dilution in immunobuffer (TBS-T containing 1% BSA) for 4 h at room temperature followed by overnight 4°C, 1 h at room temperature and another overnight at 4°C. Sections were washed as previously detailed and incubated in a 1:600 dilution of the biotinylated secondary anti-rabbit or anti-mouse antibody (goat anti-rabbit IgG Biotin, 111-066-144 and goat anti-mouse IgG Biotin, 115-065-166; Jackson Immunoresearch), respectively, for 1.5 h at room temperature. After washing, sections were incubated in ABC (diluted 1/3 after a preincubation) in TBS-T (Vectastain Elite ABC-Peroxidase kit, PK-6100, Vector) for 35 min. Then they were washed in TBS and in tris-HCl and incubated in DAB (40 sec for DBN sections, and 3.7 min for ptau sections), prepared as manufacture indications, without nickel. Sections were mounted onto gelatinized slides and let dried overnight. Finally, sections were subsequently dehydrated in ethanol 50% (2x3 min), 70% (2x3 min), 96% (3x3 min) and 100% (2x5 min), placed in HistoClear (2x5 min) and cover-slipped in Pertex medium (Sigma, Aldrich). To prevent the effect of differences between immunostaining batches, all the samples from each specific experiment were immunostained in a single batch.

Photomicrographs for hippocampal region, rhinal cortices and retrosplenial cortex, as well as for prelimbic cortex were obtained from parietal-temporal and frontal sections, respectively (Fig. 27A, 28A), using an Olympus Vanox-T AH-2 microscope attached to an Olympus DP73 digital camera, using a 2x objective.

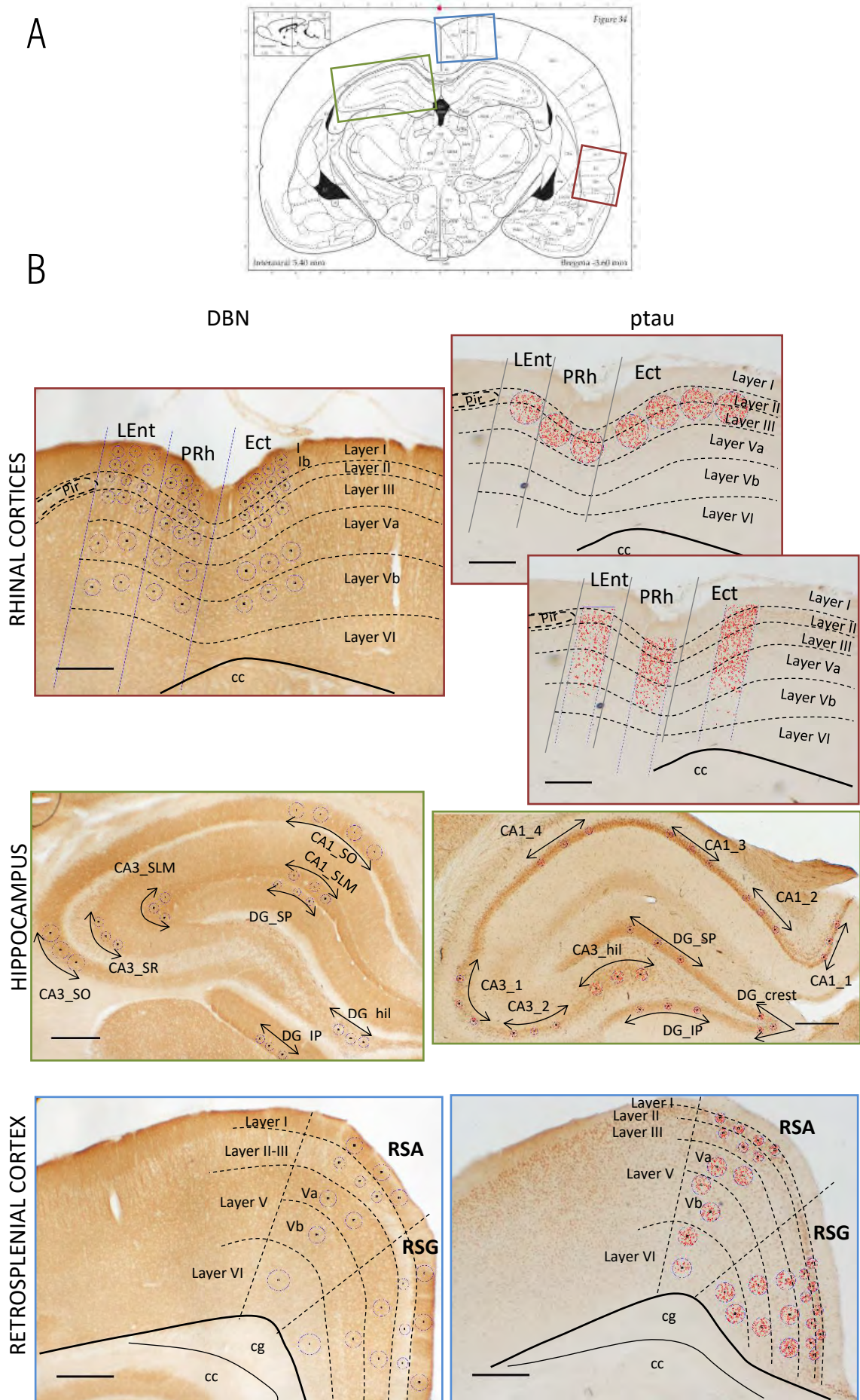


**Fig. 27 | Photomicrograph analysis for DBN and ptau immunostaining in parietal-temporal sections** (see figure on the previous page). **A.** Location of photomicrographs for analysed regions in a parietal-temporal section (-3.60 mm from Bregma). Areas covered by photomicrographs are shown with rectangular frames of different colors, which correspond to the border color of photomicrographs in B. Areas are indistinctly shown in the two hemispheres, only for a reason of a better understanding. **B.** Location of regions of interest (ROIs) employed to quantify labelling intensity levels in each of the analysed regions, shown superimposed in blue in a DBN (left) and ptau (right) stained parietal-temporal section. Area selected for the thresholded measure, imposed for ptau analysis, is shown in red. In black, the different regionalization of each area is shown, according to Paxinos and Watson's atlas (Paxinos and Watson, 2006). Scale bar=500  $\mu$ m. Abbreviations: cc: corpus callosum; cg: cingulum; DG: dentate gyrus; Ect: ectorhinal cortex; hil: hilus; IP: infrapyramidale; Lent: lateral entorhinal cortex; Pir; piriform cortex; PRh: perirhinal cortex; RSA: retrosplenial agranular cortex; RSG: retrosplenial granular cortex; SLM: *stratum lacunosum moleculare*; SO: *stratum oriens*; SP: suprapyramidale; SR: *stratum radiatum*.

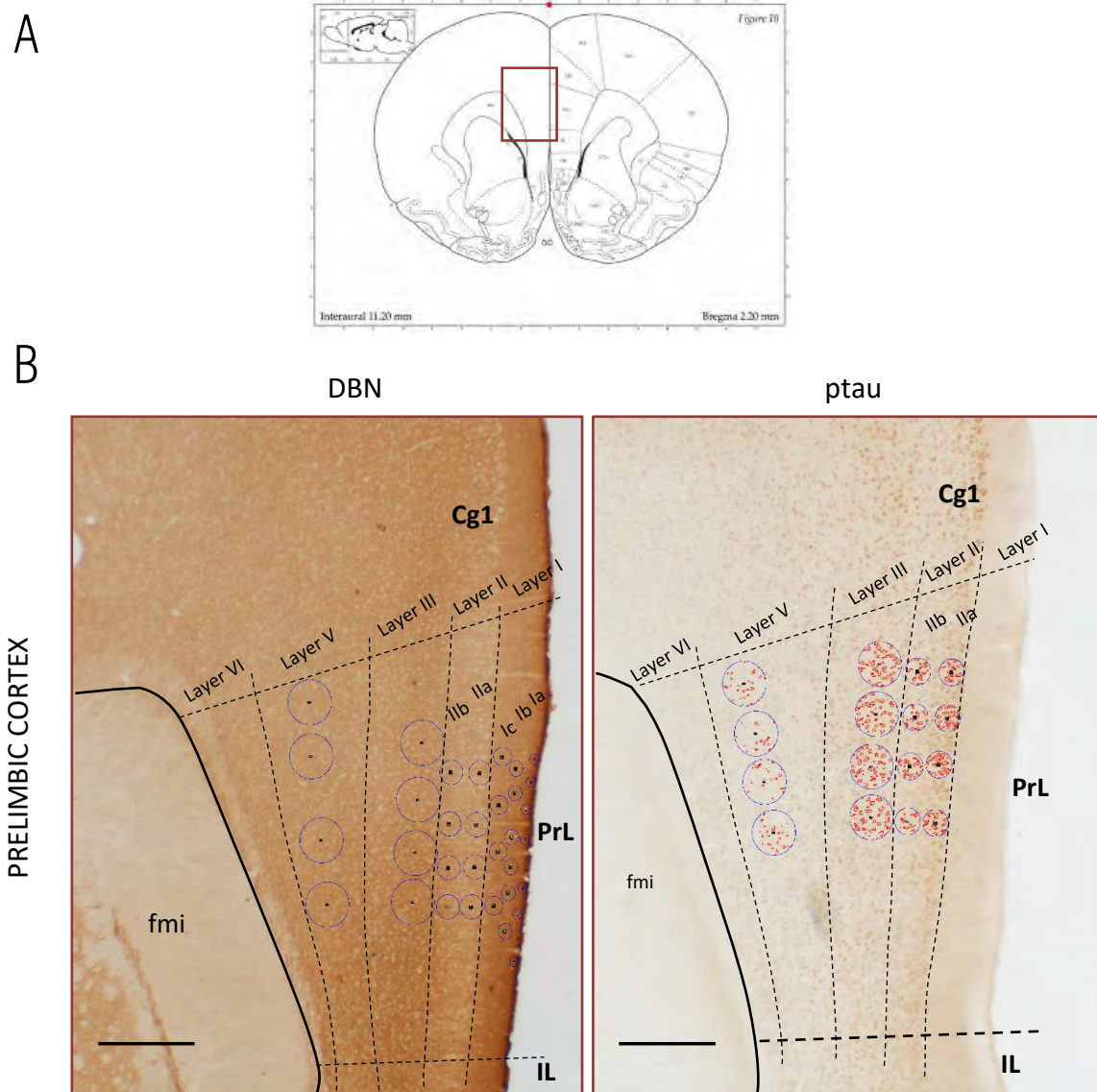


**Fig. 28 | Photomicrograph analysis for DBN and ptau immunostaining in frontal sections. A.** Location of photomicrographs for prelimbic cortex analysis in a frontal section (+2.20 mm from Bregma). **B.** Location of regions of interest (ROIs) employed to quantify labelling intensity levels in each of the analysed layers, shown superimposed in blue, in a DBN (left) and ptau (right) stained frontal section. Area selected for the thresholded measure, imposed for ptau analysis, is shown in red. In black, the different regionalization of medial prefrontal cortex is shown, according to Paxinos and Watson's atlas (Paxinos and Watson, 2006). Scale bar=500  $\mu$ m. Abbreviations: Cg1:cingulate cortex area1; fmi: forceps minor of the corpus callosum; IL: infralimbic cortex; PrL: prelimbic cortex.

ImageJ was used to quantify immunolabelling intensity. Mean intensity values were measured in circular regions of interest (ROIs) set at the different layers and subregions for each specific region (Fig. 27B, 28B). For ptau in rhinal cortices, rectangular ROIs were also used to measure intensity in the whole set of layers. In order to get rid of background noise and quantify intracellular labelling, ptau images were colour thresholded to measure intensity inside a masked ROI (Fig. 29). The analysed area inside ROIs is traced in red in photomicrographs in Fig. 27 and 28. Labelling intensity values were obtained by subtracting mean intensity in the ROI from 255 as the maximum intensity value corresponding to white. Mean value for different sections, obtained by averaging different ROIs for one layer in the same section, was used to obtain labelling intensity value for each rat.

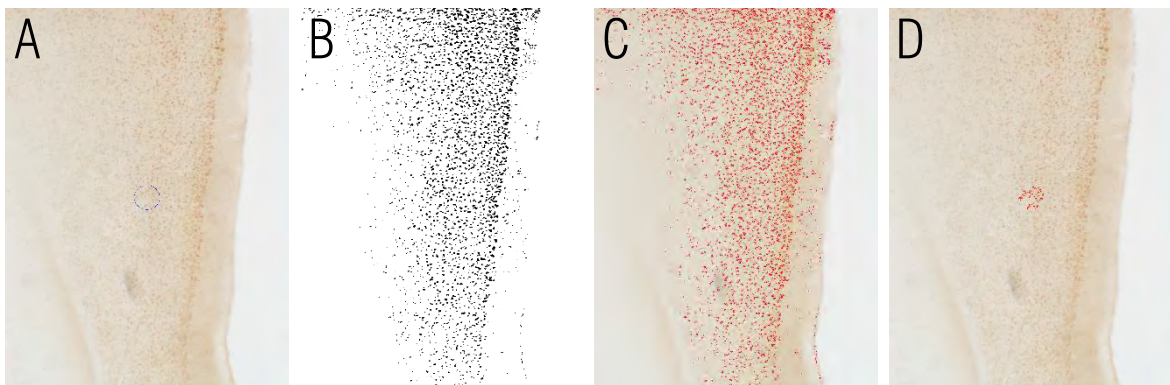


**Fig. 29 | Pipeline for ptau immunolabelling intensity measure.** In order to get rid of background noise and quantify intracellular labelling, ptau photomicrographs (A) were color thresholded to obtain a mask (B) and select intracellular labelling specifically (C). Intensity was measured inside the masked ROI (traced in red in D), based on the intracellular labelling in the initial circular ROI (traced in blue in A).

### 8.3. Observation methodology

During the histological processes, including cryosectioning, Nissl staining and immunohistochemical analyses, presence of different morphologic alterations in the lateral ventricles and periventricular structures were recorded by observation, in samples from Study 3. On the one hand, lateral ventricle enlargement was considered when the intraventricular space surrounding the hippocampus was evident, and compression of the hippocampus was considered when the CA region was notably deformed. On the other hand, reduction in corpus callosum thickness was considered when a clear breakage in its medial region is observed during cryosectioning, making it impossible to collect it. Observation analyses were performed without group identification, to avoid manual bias.

## 9. Statistical analyses

All statistical analyses were performed using IBM SPSS Statistics 25. Normality analyses were performed for data of each group using the Shapiro-Wilk normality test. Statistical differences between paired groups were assessed using independent samples t-test, for parametric comparisons, or Mann–Whitney U test, for nonparametric comparisons. Additionally, a  $2 \times 5$  ANOVA for repeated measures was conducted to study the mean latency in the MWM acquisition phase using GROUP, SESSION and GROUP  $\times$  SESSION as main factors. Correlations between variables were estimated using the Spearman's correlation test. Differences between groups in the incidence of morphological alterations, resulting from observation methodology, were assessed using chi-square test. Statistical significant results were considered when  $p < .05$  using 95% confidence interval. Statistical tendencies were also highlighted in graphs when  $p \leq .07$ .





# RESULTS

## STUDY I. MOLECULAR MECHANISMS LINKING ICSS EFFECTS WITH ALZHEIMER'S DISEASE PATHOLOGY

This section presents the results from Study 1, which addressed the first aim of this thesis. According to it, effects of ICSS on molecular markers of AD pathology were assessed in a physiological context, in order to establish a mechanistic rationale to the hypothesis that ICSS would be also effective in an AD-like context. A special focus was devoted to inspect ICSS regulation on miRNAs, both in specific hippocampal subfields and in serum, because of their potential use as non-invasive biomarkers and involvement on AD dysregulation. For the same reason, SIRT1 and BDNF were also evaluated. Moreover, regulation by ICSS in physiological conditions was also assessed for other proteins associated to the main hallmarks of AD pathogeny, including APP, tau and DBN.

From the total of 58 rats intended for this study, six subjects were excluded from the analysis. Three subjects lost the electrode in the middle of the treatment, two did not continue to respond to the ICSS treatment and one showed stereotypies and convulsions derived from ICSS treatment. The final sample consisted of 52 subjects. Final sample size in each group is shown in Table 4, which summarizes the experimental conditions of the groups analysed in this study. There was no statistical difference between groups in weight change. ICSS groups present no differences in the number of received reinforcements per session nor in the current intensity of stimulation treatment ( $2697 \pm 891$  reinforcements at  $106 \pm 40 \mu\text{A}$  for ICSS30;  $2667 \pm 626$  reinforcements at  $88 \pm 24 \mu\text{A}$  for ICSS90, and  $2520 \pm 583$  reinforcements at  $82 \pm 23 \mu\text{A}$  for ICSS180).

**Table 4 | Summary of the groups composing Study 1** is presented as a brief recap of the experimental design in Study 1, including final sample size for each group.

<i>Group</i>	<i>Treatment</i>	<i>Sacrifice after last treatment session</i>	<i>Final sample size</i>
<i>sham</i>	3 sham sessions	90 min	21
<i>ICSS30</i>	3 ICSS sessions	30 min	6
<i>ICSS90 (ICSS)</i>	(1 session of 45	90 min	19
<i>ICSS180</i>	min/day)	180 min	6

### 1.1. ICSS-induced changes on miRNAs in specific hippocampal subfields and serum

#### miRNA endogenous normalizers in hippocampus and serum after ICSS treatment

In order to define a suitable endogenous normalizer to be used in miRNA analyses, the stability of selected endogenous normalizer candidates was tested in ICSS context. Table 5 shows the stability values for miR-16, miR-103a, miR-124 and let-7a calculated using NormFinder and GeNorm algorithms in a first subset of samples from DG and CA1 hippocampal subfields, obtained at different times after ICSS treatment (30, 90 and 180 min) and after sham treatment. According to both algorithms, miR-16 presents the lowest scores and so it was determined to be the most stable miRNA in both CA1 and DG subfields.

In order to confirm these results, the stability of miR-16, miR-124, let-7a and let-7b was further assessed in a second larger subset of samples obtained 90 minutes after ICSS, from DG (Table 6) and serum (Table 7). miR-124 was not included for serum as it was not detected in most of the samples. GeNorm results for DG samples slightly dissent from NormFinder

ranking. In this case, NormFinder ranking, pointing at miR-16 as the most stable gene, was taken as the decisive because, unlike GeNorm, it takes into account intergroup measures of variability in addition to intragroup variation. In the case of serum samples, both algorithms converged to let-7a as the most stable candidate.

Altogether, miR-16 was selected as the endogenous normalizer to be used for miRNA analyses in hippocampal tissue, whereas let-7a was determined for serum samples.

**Table 5 | Stability values for miRNA endogenous normalizer candidates at different times after ICSS treatment, in DG and CA1 samples.** NormFinder and GeNorm stability values were calculated from the Ct values resulting from qRT-PCR of four endogenous normalizer candidates, selected from literature. DG and CA1 samples from sham and ICSS30, ICSS90 and ICSS180 rats. n=6 samples/group.

	DG		CA1	
	NormFinder stability value	GeNorm score	NormFinder stability value	GeNorm score
<i>miR-16-5p</i>	0.104	0.456	0.037	0.385
<i>let-7a-5p</i>	0.104	0.474	0.110	0.493
<i>miR-124-3p</i>	0.176	0.550	0.114	0.494
<i>miR-103a-3p</i>	0.146	0.565	0.134	0.534

**Table 6 | Stability values for miRNA endogenous normalizer candidates 90 min post-treatment, in DG samples.** NormFinder and GeNorm stability values were calculated from the Ct values resulting from qRT-PCR of four endogenous normalizer candidates. DG samples from sham and ICSS90 rats were used. n=12 samples/group.

	NormFinder stability value	GeNorm score
<i>miR-16-5p</i>	0.024	0.264
<i>let-7a-5p</i>	0.027	0.251
<i>let-7b-5p</i>	0.047	0.286
<i>miR-124-3p</i>	0.059	0.336

**Table 7 | Stability values for miRNA endogenous normalizer candidates 90 min post-treatment, in serum samples.** NormFinder and GeNorm stability values were calculated from the Ct values resulting from qRT-PCR of three endogenous normalizer candidates. Serum samples from sham and ICSS90 rats were used. n=11 and 12 samples/group (sham and ICSS, respectively).

	NormFinder stability value	GeNorm score
<i>let-7a-5p</i>	0.029	0.724
<i>let-7b-5p</i>	0.117	0.868
<i>miR-16-5p</i>	0.235	1.272

Time of ICSS-induced changes on miRNAs

In order to approach time-dependent changes induced by ICSS on miRNAs in the hippocampus, the levels of four neural plasticity and AD-related miRNAs, including miR-132, miR-134, miR-146a and miR-181c, were assessed in a subset of samples from CA1 and DG hippocampal subfields at different times after ICSS treatment (Fig. 30).

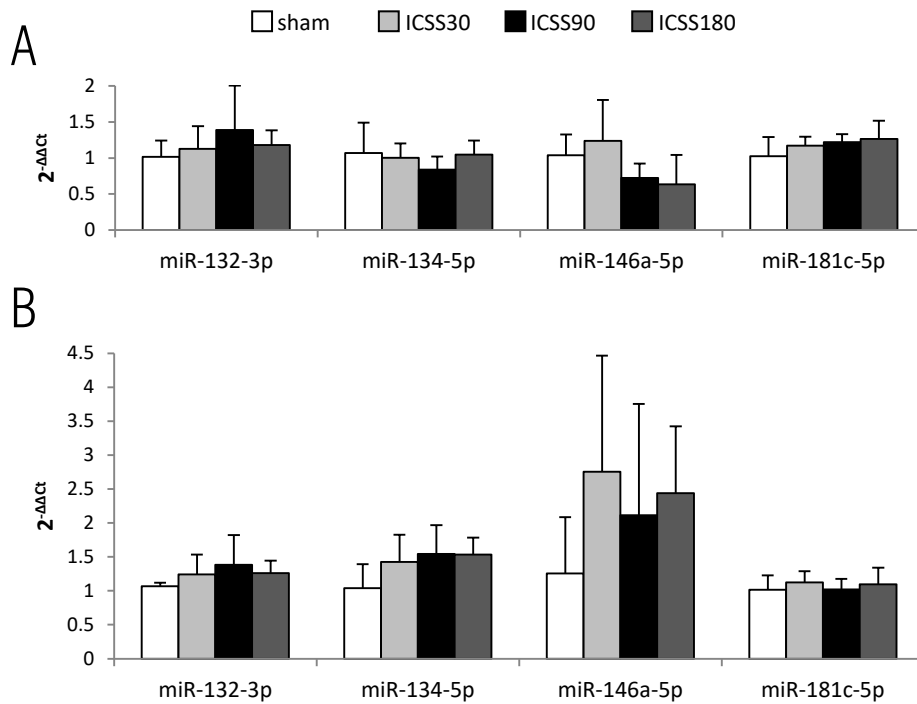


**Fig. 30 | Time-dependent changes of ICSS-regulated miRNA candidates after treatment, in CA1 and DG.** Relative expression of miR-132, miR-134, miR-146a and miR-181c for sham and ICSS condition (samples obtained 30, 90 and 180 min after ICSS), detected by qRT-PCR, calculated as  $2^{-\Delta\Delta C_t}$  using miR-16 as endogenous normalizer and sham group mean as the reference, in **A.** DG and **B.** CA1 samples. Data are presented as mean  $\pm$  SD; n=5-6 rats/group. No statistical significant differences or tendencies were found between groups.

No significant results were obtained for none of the regions. However, one-way ANOVA revealed a slight tendency of the GROUP factor influencing miR-146a levels in DG ( $p=.071$ ), suggesting a trend of reduction in this miRNA at 90 minutes (t-test  $p=.080$ ).

### ICSS-regulated miRNA candidates

From TaqMan Openarray expression data, 14 miRNAs were identified as differentially expressed between sham and ICSS condition ( $FC \geq 1.3$ ;  $p < .05$ ), in DG subfield 90 minutes after treatment, as shown in Fig. 31.

Functional analyses and bibliographic research on these targets revealed that some of the miRNAs are associated with neuroplasticity pathways and target synaptic plasticity-related proteins, such as DBN, BDNF and SIRT1. They also appeared to be altered in AD pathology or related with AD main molecular hallmarks, such as APP or tau tubulin kinase (Table 8). Based on these relations, six miRNAs (four upregulated and two downregulated, highlighted in Table 8) were selected among the 14. These six miRNAs, together with miR-132, miR-134, miR-146a and miR-181c, selected according to their reported role in neural plasticity and relation with AD (described in the introduction section), were defined as the 10 ICSS-regulated candidate miRNAs to be further evaluated (see Table 2 in the materials and methods section).

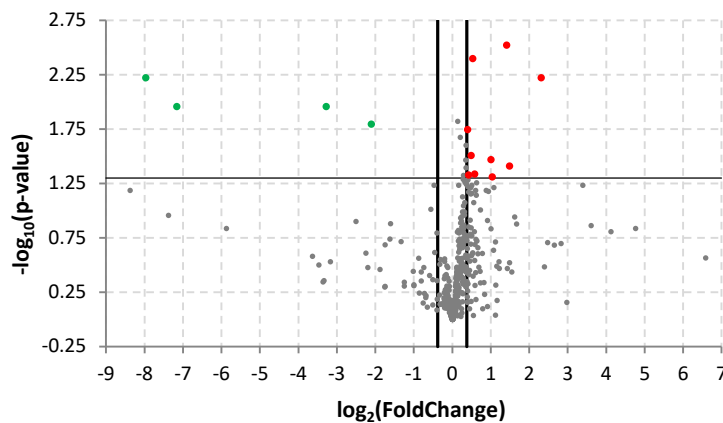


**Fig. 31 | Differential miRNA expression in DG after ICSS treatment.** Volcano plot representing comparative miRNA expression of ICSS versus sham group in DG subfield, 90 minutes after ICSS treatment, using TaqMan OpenArray MicroRNA Rodent Panel. X-axis represents difference in expression level on a  $\log_2$  scale, whereas y-axis corresponds to the p-values on a negative  $\log_{10}$  scale. Green dots depict miRNAs significantly downregulated in ICSS group relative to sham, while red ones depict miRNAs upregulated in ICSS group. Grey dots represent miRNAs with no significant differential expression between the two groups.  $n=4$  pools of 3 rats per group. Fold-Change Boundary=1.3; p-value Boundary=.05

**Table 8 | Differentially expressed miRNAs in ICSS and sham conditions and their functional relations.**

List of assays showing differential expression between ICSS and sham pools in DG subfield, using TaqMan OpenArray MicroRNA Rodent Panel, and their functional relations according to literature and data base research. miRNAs in bold indicate those selected as MFB-ICSS-regulated candidates for further qRT-PCR analysis.

TaqMan OpenArray Assay	miRNA	FC	Up- or down-regulated	Interesting pathways / putative pathways	Interesting putative targets	Alteration in AD
<b>hsa-miR-196A</b>	<b>miR-196a</b>	<b>4.964</b>	<b>UP</b>	$\beta$ -tubulin polymerization [1] cytoskeleton remodelling [1,2], ABC transporters [2]	APPB, BACE	-
<i>mmu-miR-1959</i>	miR-1959	2.805	UP	-	-	-
<i>rno-miR-24-1#</i>	miR-24-1	2.665	UP	-	BACE	-
<i>mmu-miR-300</i>	miR-300	2.055	UP	axon guidance, glutamatergic synapse	APP, APPB, BDNF, TTBK	-
<i>mmu-miR-196a#</i>	miR-196a	2.007	UP	$\beta$ -tubulin polymerization [1] cytoskeleton remodelling [1,2], ABC transporters [2], LTD	APP, APPB, BACE, BDNF, TTBK	-
<i>rno-miR-345</i>	miR-345	1.499	UP	-	APPB, BACE, DBN	↑ in CSF [3]
<i>mmu-miR-485</i>	<b>miR-485</b>	<b>1.447</b>	<b>UP</b>	dendritic spine development [4], axon guidance	APPB, SIRT1	↓ in cortical grey matter [5]
<i>mmu-miR-495</i>	<b>miR-495</b>	<b>1.404</b>	<b>UP</b>	axon guidance, dopaminergic, cholinergic and GABAergic synapses, prion diseases, LTP	APPB, ARC, BDNF, SIRT1	↓ in cortical grey matter [5]
<b>hsa-miR-185</b>	<b>miR-185</b>	<b>1.337</b>	<b>UP</b>	axon guidance, BDNF pathway	APP	↓ in cortical white matter [5]
<i>mmu-miR-187</i>	miR-187	1.319	UP	synaptic vesicle cycle, axon guidance	-	-
<b>hsa-miR-197</b>	<b>miR-197</b>	<b>0.233</b>	<b>DOWN</b>	synaptic vesicle cycle	APP, BACE, DBN, SYN	↑ in temporal cortex [6], CSF [3]; ↓ white matter middle temporal cortex [5]
<i>rno-miR-333</i>	miR-333	0.103	DOWN	-	-	-
<b>hsa-miR-154</b>	<b>miR-154</b>	<b>0.007</b>	<b>DOWN</b>	GABAergic synapses, BDNF pathway	APPB	↑ in Blood Derived Monocytes [7]; ↓ in CSF [3]
<i>mmu-miR-2182</i>	miR-2182	0.004	DOWN	-	-	-

n=4 pools of 3 rats per group. Fold-Change Boundary=1.3; p-value Boundary=.05. Abbreviations: APP: amyloid beta precursor protein; APPB: APP binding family; ARC: activity-regulated cytoskeleton-associated protein; BACE: beta-site APP-cleaving enzyme; BDNF: brain derived neurotrophic factor; CSF: cerebrospinal fluid; DBN: drebrin family; FC: Fold-Change; LTD: long-term depression; LTP: long-term potentiation; SIRT1: sirtuin1; SYN: synapsin; TTBK: tau tubulin kinase. References: [1] Her et al., 2017; [2] Fu et al., 2015; [3] Cogswell et al., 2008; [4] Cohen et al., 2011; [5] Wang et al., 2011; [6] Hébert et al., 2008; [7] Guedes et al., 2016.

### ICSS-induced miRNA changes in hippocampal subfields

ICSS-regulated candidate miRNAs were analysed by qRT-PCR in individual hippocampal subfield samples obtained 90 minutes post-treatment. Initially, levels of the 10 miRNA candidates were assessed in DG subfield (Fig. 32), revealing an increased expression of miR-495, miR-132 and miR-181c in ICSS group relative to sham ( $p=.041$ ,  $p=.005$  and  $p=.020$ , respectively). miR-196a, miR-485, miR-185, miR-154, miR-197, miR-134 and miR-146a did not appear to be significantly different between ICSS and sham groups in this subfield.

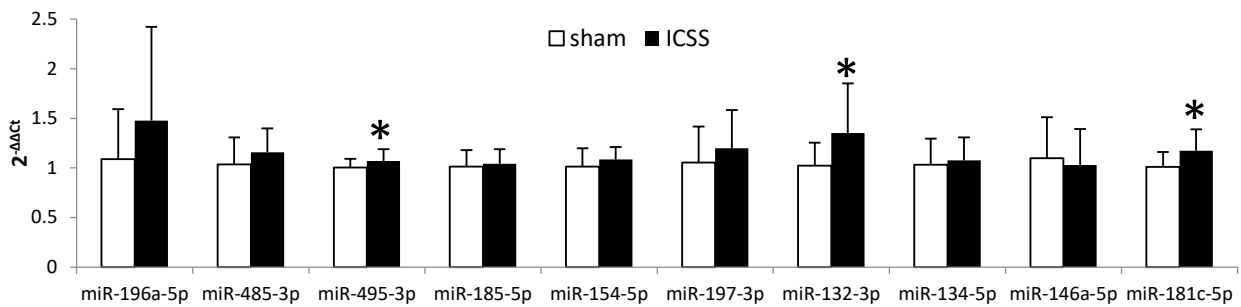


**Fig. 32 | Relative expression of ICSS-regulated miRNA candidates in DG.** Levels of the ten ICSS-regulated candidate miRNAs were detected by qRT-PCR in DG samples from sham and ICSS90 groups, calculated as  $2^{-\Delta\Delta C_t}$ , using miR-16 as endogenous normalizer, and sham group mean as the reference sample. Data are presented as mean $\pm$ SD; n=12-17 rats/group. \* $p<.05$ .

In order to assess the hippocampal region-specificity of the changes found in DG, levels of miR-495, miR-132 and miR-181c were further evaluated in CA1 and CA3 subfields. Only miR-132 showed a significant increase in CA1 ( $p=.011$ ) (Fig. 33B). No statistically significant changes were found in CA3, for any of the three miRNAs (Fig. 33A-C).

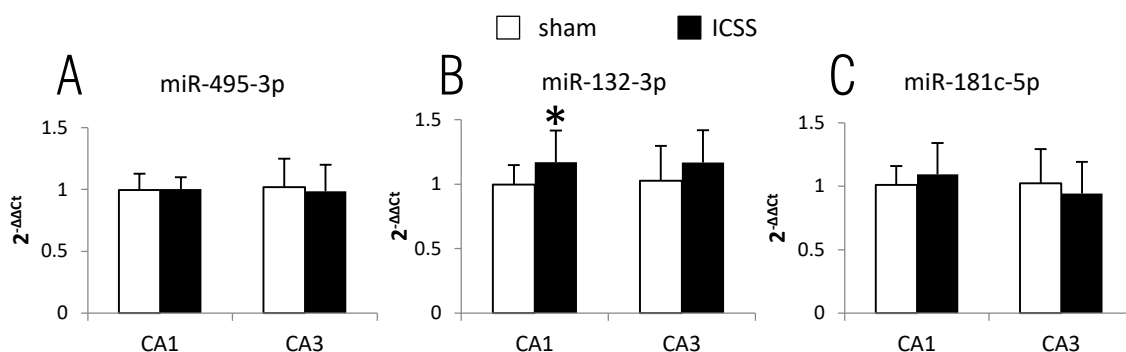


**Fig. 33 | Relative expression of ICSS-regulated miRNA candidates in CA1 and CA3, including A. miR-495, B. miR-132 and C. miR-181c.** Levels of miRNAs were detected by qRT-PCR in sham and ICSS90 samples, and calculated as  $2^{-\Delta\Delta C_t}$ , using miR-16 as endogenous normalizer, and sham group mean as the reference sample. Data are presented as mean $\pm$ SD, n=12-17 rats/group for CA1 subfield and 6 rats/group for CA3 subfield. \* $p<.05$ .



ICSS-induced miRNA changes in serum

Changes on the 10 ICSS-regulated candidate miRNAs were also assessed in serum samples obtained 90 minutes post-treatment. Levels of miR-485, miR-495, miR-154 and miR-134 were under the detection limit for many serum samples, belonging to both sham and ICSS group (Table 9), so comparative analysis between groups could not be performed. Regarding other miRNAs, while no differences were found between the two conditions in miR-196a, miR-185, miR-197, miR-146a and miR-181c (Fig. 34A), miR-132 was found to be significantly upregulated ( $p=.048$ ) in ICSS compared to sham rats' serum (Fig. 34B).

Moreover, miR-132 levels in serum presented a significant negative correlation with their levels in DG, specifically for ICSS group (Fig. 35). No correlations were observed in CA1 and in CA3.

**Table 9 | Detection frequencies of candidate miRNAs in serum samples.** Percentage of samples that presented a detectable Ct is shown for each target miRNA in each group and in the whole sample set.  $n=11$  and 12 rats/group (sham and ICSS, respectively).

	miR-196a-5p	miR-485-3p	miR-495-3p	miR-185-5p	miR-154-5p	miR-197-3p	miR-132-3p	miR-134-5p	miR-146a-5p	miR-181c-5p
Sham	100	54.55	45.45	100	36.36	100	100	27.27	100	100
ICSS	100	16.67	41.67	100	50.00	100	100	16.67	100	100
TOGETHER	100	34.78	43.48	100	43.48	100	100	21.74	100	100

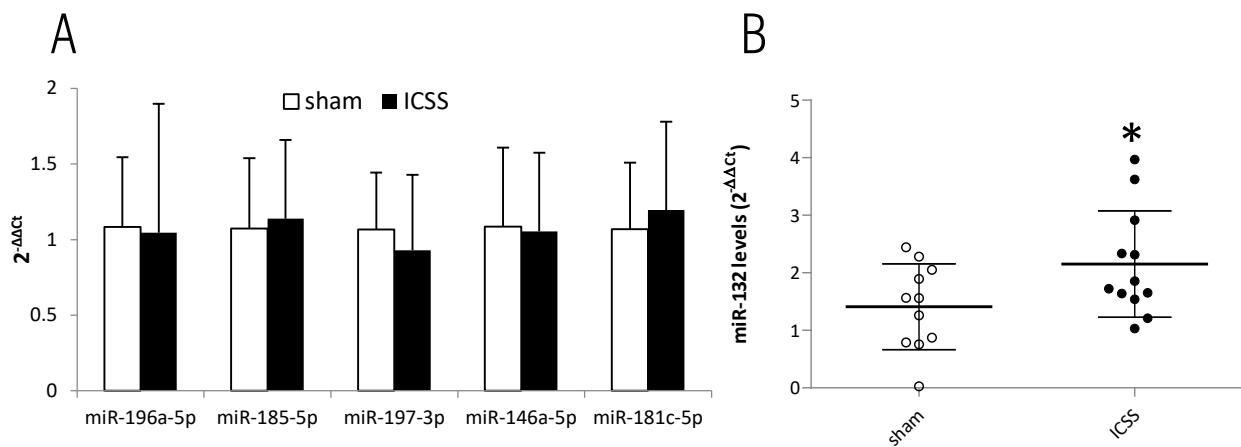


**Fig. 34 | Relative expression of ICSS-regulated miRNA candidates in serum, 90 min after treatment, including A. detected candidates non-differentially expressed, and B. miR-132, which was upregulated in ICSS condition.** Levels of miRNAs were detected by qRT-PCR in sham and ICSS90 samples, and calculated as  $2^{-\Delta\Delta Ct}$ , using let-7a as endogenous normalizer, and sham group mean as the reference sample. In A. data are presented as mean $\pm$ SD, while in B. each dot represents a single rat, and group mean $\pm$ SD is depicted.,  $n=11$  and 12 rats/group (sham and ICSS, respectively). \* $p<.05$ .

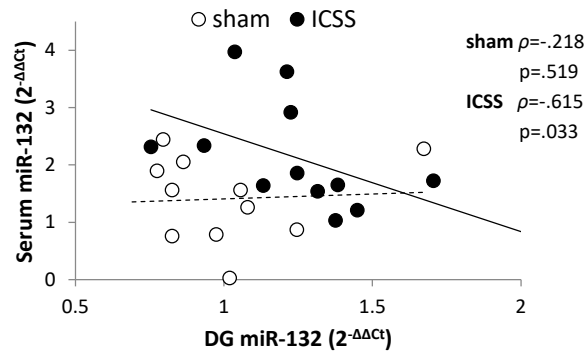


**Fig. 35 | Correlation between miR-132 levels in DG and in serum, after ICSS treatment.** Scatter plot for both sham and ICSS groups. Each dot represents a single rat. Spearman's correlation test was used to determine significance ( $p < .05$ ).  $\rho$  = Spearman's correlation coefficient;  $n = 11$  and  $12$  rats/group (sham and ICSS, respectively).

## 1.2. ICSS-induced changes on proteins associated to AD main hallmarks in DG hippocampal subfield

### ICSS-induced changes on APP levels in DG

Western blot analysis revealed that ICSS did not cause any change in full-length APP levels in any of the analysed time points (30, 90 and 180 minutes after last treatment session) (Fig. 36). Any band corresponding to A $\beta$  monomer could be detected at 4 kDa in the resulting blots.

### ICSS-induced changes on tau and ptau levels in DG

Levels of tau protein were not found to be significantly changed after ICSS treatment in the analysed time points (Fig. 36). However, phosphorylation at the site Ser202/Thr205 was found significantly increased 180 min after ICSS ( $p = .011$ ), but neither at 30 nor at 90 min, regarding its normalized ratio to total tau (Fig. 36).

### ICSS-induced changes on DBN levels in DG

Levels of the postsynaptic protein DBN were also analysed in DG at the different time points after ICSS treatment. No significant differences were revealed between sham and ICSS groups at any of the analysed times (Fig. 36).

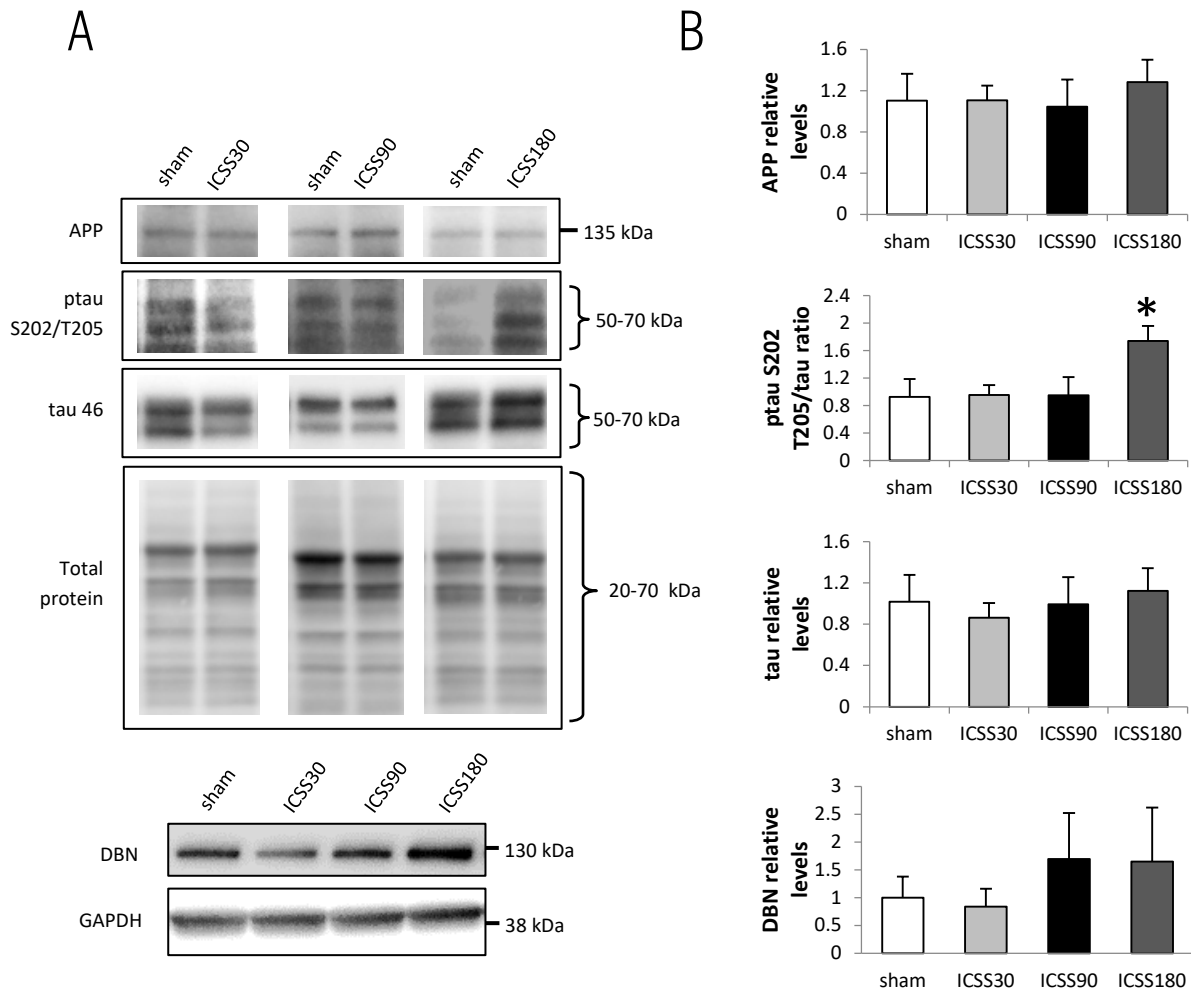


**Fig. 36 | Time-dependent changes after ICSS treatment on APP, ptau, tau and DBN levels in DG extracts.** **A.** Representative Western blots for APP, ptau S202/T205 and tau proteins, together with total protein band patterns, as well as for DBN and GAPDH, for sham and ICSS conditions (samples obtained 30, 90 and 180 min after ICSS). **B.** Resulting relative protein quantification using total protein or GAPDH as endogenous normalizers and sham group as reference, in sham, ICSS30, ICSS90 and ICSS180 group. Data are presented as mean ± SD; n=8, 6, 8 and 6 rats/group (sham, ICSS30, ICSS90 and ICSS180, respectively). \*p < .05 vs sham.

### 1.3. ICSS-induced changes on other plasticity regulatory proteins related with early AD pathology in hippocampal subfields and serum

#### ICSS-induced changes on SIRT1 in hippocampal subfields and serum

Levels of the deacetylase SIRT1 were studied in DG subfield at the different time points after ICSS treatment. A significant increase was found 90 minutes after ICSS treatment compared with sham ( $p=.039$ ), but not at 30 or 180 minutes (Fig. 37A). In order to assess the subfield specificity of this effect, SIRT1 levels were also analysed in CA1 and CA3 subfields, where no significant differences were perceived (Fig. 37B-C).

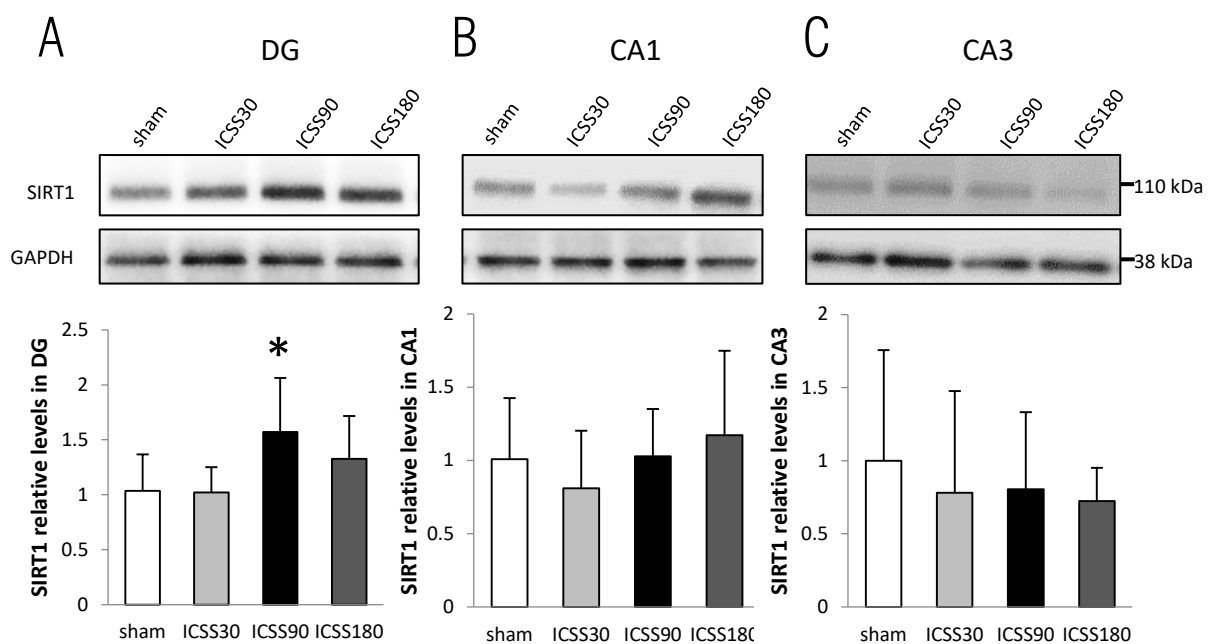


**Fig. 37 | Time-dependent changes after ICSS treatment on SIRT1 levels in hippocampal subfield extracts.** Representative Western blots and resulting relative protein quantification using GAPDH as endogenous normalizer and sham group as reference, in sham, ICSS30, ICSS90 and ICSS180 groups in **A.** DG **B.** CA1 and **C.** CA3 hippocampal subfields. Data are presented as mean $\pm$ SD; n=7, 6, 6 and 6 rats/group (sham, ICSS30, ICSS90 and ICSS180, respectively). \* $p<.05$  vs sham.

To test the potential use of SIRT1 as a treatment biomarker, its levels were also assessed in the serum obtained 90 minutes after ICSS treatment. SIRT1 was detected in all the samples, but no differences in its levels were perceived between the two groups (Fig. 38A). Significant correlations between SIRT1 levels in serum and in DG were not found (Fig. 38B). However, a positive correlation between SIRT1 serum levels and miR-132 levels in serum was revealed, specifically in the ICSS-treated group (Fig. 39).

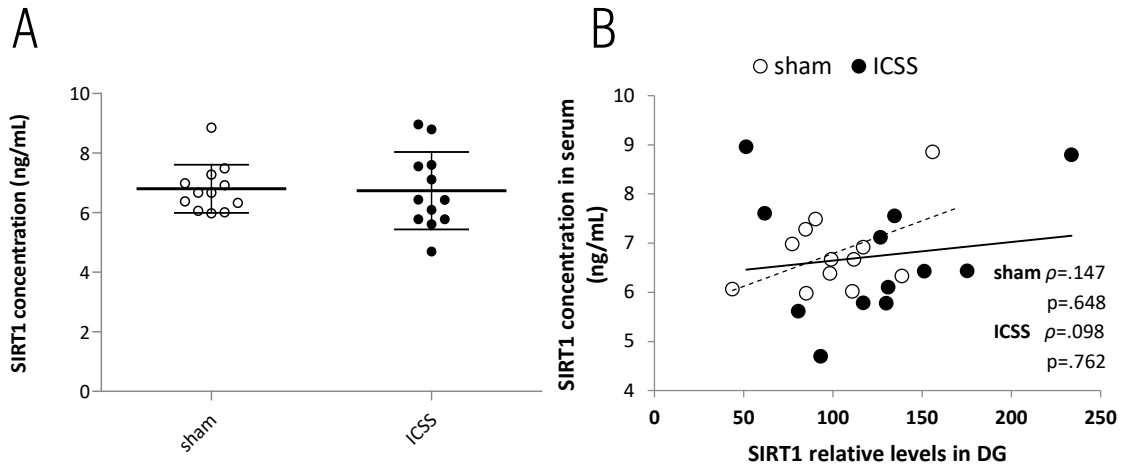


**Fig. 38 | Levels of SIRT1 in serum and its relation with DG levels, after ICSS treatment. A.** Concentration of SIRT1 in the serum obtained 90 minutes after treatment in sham and ICSS-treated rats, assessed by ELISA. Each dot represents a single rat, and group mean $\pm$ SD is depicted. **B.** Scatter plot showing lack of correlation between SIRT1 levels in serum and its levels in DG, both in sham and ICSS-treated groups. Each dot represents a single rat. Spearman’s correlation test was used to determine significance ( $p < .05$ ).  $\rho$  = Spearman’s correlation coefficient;  $n = 12$  rats/group.

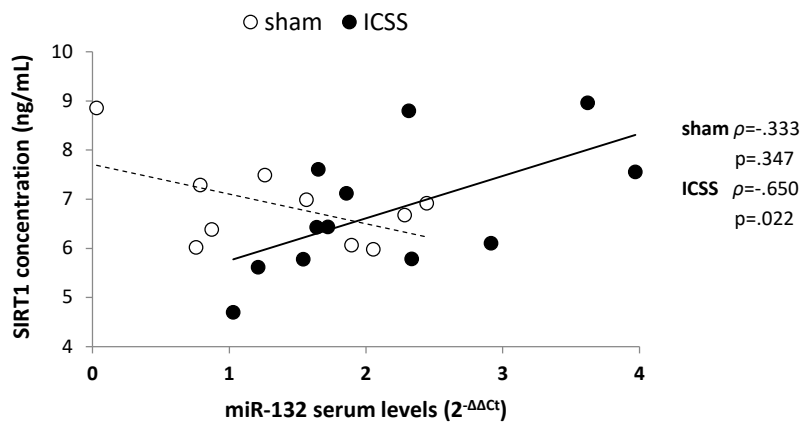


**Fig. 39 | Correlation between SIRT1 levels and miR-132 levels in serum after ICSS.** Scatter plot showing the correlation between SIRT1 levels and miR-132 levels in the serum obtained 90 minutes after treatment in sham and ICSS-treated rats. Each dot represents a single rat. Spearman’s correlation test was used to determine significance ( $p < .05$ ).  $\rho$  = Spearman’s correlation coefficient;  $n = 10$  and  $12$  rats/group (sham and ICSS, respectively).

### ICSS-induced changes on BDNF in DG and serum

Levels of BDNF were also studied in the serum obtained 90 minutes after ICSS. No differences were revealed between sham and ICSS-treated animals (Fig. 40A). Moreover, any correlation was found between BDNF levels in serum and in DG (Fig. 40B), where differences between groups were also not found (Fig. 40C), and neither with any of the other studied molecules.

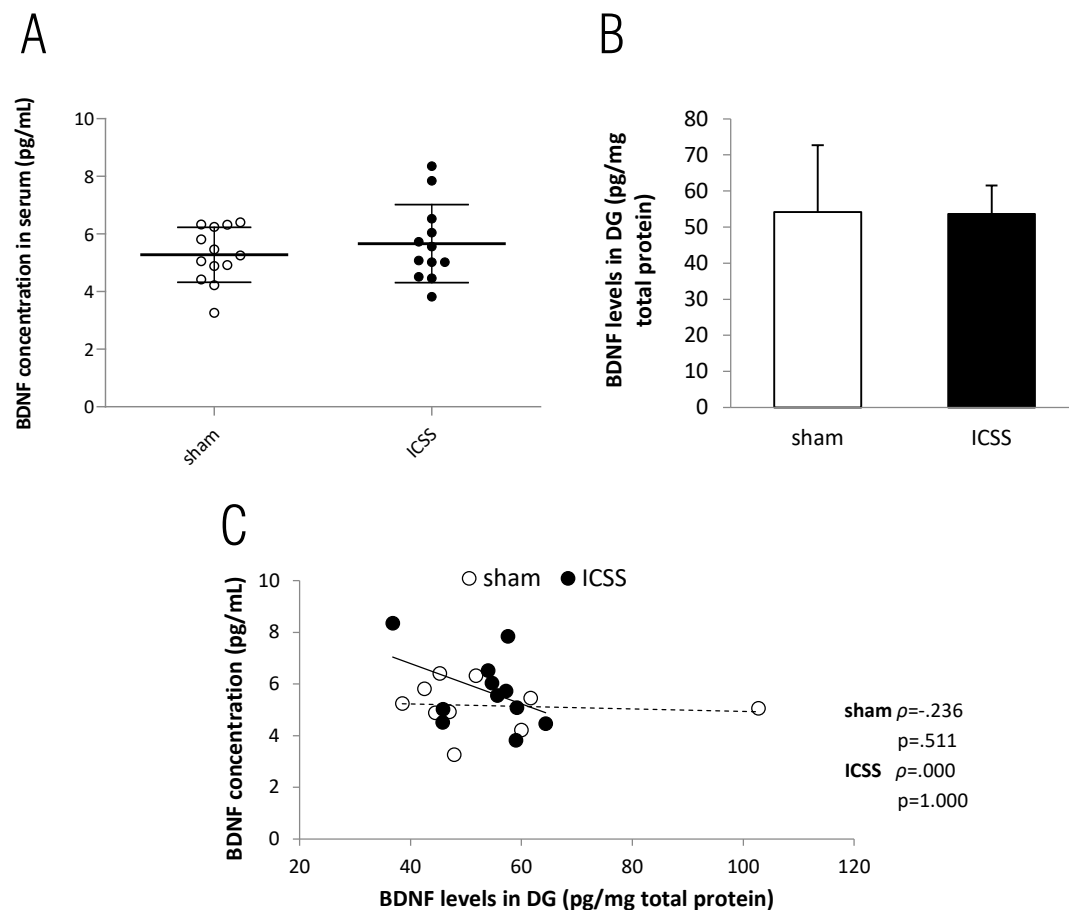


**Fig. 40 | Levels of BDNF in serum and DG and their relation, after ICSS treatment. A.** Concentration of BDNF in the serum obtained 90 minutes after treatment in sham and ICSS-treated rats, assessed by ELISA. Each dot represents a single rat, and group mean  $\pm$ SD is depicted;  $n=13$  and  $12$  rats/group (sham and ICSS, respectively). **B.** Levels of BDNF normalized by total amount of protein in DG extracts of sham and ICSS-treated rats sacrificed 90 minutes after treatment, assessed by ELISA. Data presented as mean  $\pm$ SD;  $n=10$  and  $11$  rats/group (sham and ICSS, respectively). **C.** Scatter plot showing lack of correlation between BDNF levels in serum and its levels in DG, both in sham and ICSS-treated groups. Each dot represents a single rat. Spearman's correlation test was used to determine significance ( $p < .05$ ).  $\rho$  = Spearman's correlation coefficient;  $n=10$  and  $11$  rats/group (sham and ICSS, respectively).

## 1.4. Discussion

The main contribution of this study was the finding that ICSS effects in physiological conditions rely on regulatory molecules common with those altered in AD pathology, supporting a potential applicability of DBS to the MFB in AD context. In particular, it has been seen that specific miRNAs and SIRT1 protein are affected by ICSS in hippocampal tissue, and a potential use for them as treatment biomarkers in serum is suggested.

Different studies, including the latest research in our lab, have established that memory-enhancing DBS to different brain targets induces increased hippocampal expression of synaptic plasticity protein markers, which are prominent molecular correlates of memory consolidation (Kádár et al., 2013; Gondard et al., 2015). However, molecular mechanisms leading to DBS memory improving effect are not yet clearly understood. In this work, the main focus was set, for the first time, on the effects of ICSS procedure on miRNAs regulating plasticity processes and/or altered in AD pathology. Moreover, the potential use of miRNAs as predictive treatment biomarkers was also a main aim of this study, taking into consideration a potential applicability of DBS for AD treatment.

### Methodological considerations regarding miRNA analysis after ICSS treatment

The first contribution of this work was the establishment of a specific framework to evaluate miRNA changes in samples from different nature obtained after ICSS. Precise measurements of miRNA expression are critically important, since modest changes can end up in profound cellular outcomes (Latham, 2010).

Thus, on the one hand, it is essential to overcome the lack of a standardised protocol for normalization in miRNA analyses. The use of an endogenous stable miRNA, rather than the use of total RNA or snRNA/rRNA, is considered the best normalization strategy (Peltier and Latham, 2008; Schwarzenbach et al., 2015). In this work, four miRNAs, including miR-16, miR-103a, miR-124 and let-7a were considered endogenous normalizer candidates for their reported use in literature using different types of brain and serum samples from both rat and AD patients (Peltier and Latham, 2008; Kroh et al., 2010; Nelson and Wang, 2010; Visani et al., 2013; Bhatnagar et al., 2014; Mao et al., 2016; Schwarzenbach et al., 2016). Let-7b was later included attending its low stability score in an OpenArray screening (data not shown). According to stability analysis using the five candidates, miR-16 was determined to be the most suitable endogenous normalizer to be used in hippocampal samples after ICSS conditions, while let-7a was determined to be the best for serum samples.

On the other hand, as expression of many miRNAs has been found to have a high temporal and spatial specificity (Kosik and Krichevsky, 2005), a concrete space-time context was established. Induction time described for different miRNAs after various learning or plasticity-related stimuli (Nudelman et al., 2010; Pai et al., 2014), together with subtle results obtained in a pilot time course, suggested that 90 min after stimulation would be an appropriate time to assess ICSS-regulated changes on miRNAs. Besides, miRNA changes were separately evaluated in DG, CA1 and CA3 hippocampal subfields, since these regions are known to differ in terms of neural plasticity mechanisms (Hussain and Carpenter, 2005; Mcbain, 2008). DG subfield is one of the few regions that preserve neurogenesis in the adult life, which is crucial for maintaining synaptic connectivity (Taupin and Gage, 2002). Due to this singularity, and since DG has shown to respond to ICSS by enhancing neurogenesis in our previous works (Huguet et al., 2009, 2020), this region was used for a first screening of ICSS-induced changes.

#### ICSS-regulated miRNAs in physiological conditions link ICSS molecular mechanisms with AD

An initial OpenArray screening using DG pooled samples showed differential expression of 14 miRNAs in ICSS condition. Interestingly, functional search revealed relations of these miRNAs with main AD hallmarks (Table 8), suggesting for the first time that ICSS could be interacting with molecular pathways altered in AD.

Based on its functional interest, 6 of the 14 OpenArray-suggested miRNAs were selected as candidates for further validation. Out of them, only miR-495 was found to be significantly upregulated in ICSS-treated rats, revealing the need of validating array results with a complementary technique and increased sample size. The specific role of miR-495 in the brain and learning and memory function has not yet been well characterized. However, it may be involved in activity-dependent remodelling of synaptic plasticity (Wang et al., 2012) and Bdnf and Arc mRNAs have been identified among its putative targets (Prins et al., 2014; Bastle et al., 2018). Interestingly, previous studies of our lab reported changes in the levels of these mRNAs after ICSS in extracts of total hippocampus (Kádár et al., 2013). Moreover, miR-495 is reported to be downregulated in AD cortical grey matter (Wang et al., 2011). Here, the increase of miR-495 expression was found to be specific for DG, but not for CA1 and CA3.

In accordance with the idea that ICSS could be affecting molecular regulators of AD, other miRNAs known to be altered in AD pathology, including miR-132, miR-134, miR-146a and miR-181c (see section 3.1 in the introduction chapter), were also analysed in individual



samples. An upregulation of hippocampal miR-132 and miR-181c, which has been related to enhanced learning and memory (Hansen et al., 2013; Wang et al., 2013; Fang et al., 2016), was found 90 minutes after ICSS.

MiR-132 is found to be strongly and reproducibly reduced in different brain regions including the hippocampus in AD patients from early stages of the disease (Lau et al., 2013; Wong et al., 2013; Qian et al., 2017; Hadar et al., 2018), correlating with better cognition scores (Hadar et al., 2018). Mechanistically, miR-132 has been suggested to play a rather upstream role in the pathogenic cascade of AD (Lau et al., 2013), being related to both amyloid pathology and tau phosphorylation (Smith et al., 2015; Hernandez-Rapp et al., 2016; Salta et al., 2016; Fatimy et al., 2018). Moreover, alteration of miR-132 has recently been suggested as a mediator of impaired hippocampal neurogenesis in AD (Salta et al., 2020).

In this work, ICSS-induced increase of miR-132 was found in both DG and CA1, but not in CA3 hippocampal subfield. Firstly, regarding the adult DG, miR-132 has been reported to coordinate the proliferation, differentiation and integration of new neurons in the hippocampus (Luikart et al., 2011; Salta et al., 2020). This evidence together with our results suggest that miR-132 could be participating in the increase of neurogenesis after ICSS (Huguet et al., 2009, 2020; Takahashi et al., 2009). And, what is more, this miR-132-mediated pathway seem to be sufficient to restore relevant memory deficits in AD mouse models (Salta et al., 2020). Secondly, it has been reported that miR-132 is linked to spinogenesis, spine enlargement and dendritic growth in cultured neurons (Vo et al., 2005; Impey et al., 2010), and our group has previously demonstrated that ICSS induces an increase in dendritic arborisation and synaptic density in CA1 (Chamorro-López et al., 2015). Moreover, it has been reported that LTP can produce simultaneous induction of the cytoskeleton regulator Arc mRNA and miR-132 (Wibrand et al., 2012). Interestingly, in agreement with this study, the ICSS-induced regional regulation of miR-132 matches results from our previous studies reporting hippocampal Arc mRNA increase at 90 min and increased ARC protein at 4.5 hours after ICSS in DG and CA1, but not in CA3 (Kádár et al., 2013).

Regarding miR-181c, it has also been mechanistically related with AD main hallmarks. miR-181c was found to be downregulated in hippocampal neurons treated with amyloid beta peptides, as well as in the hippocampus of APP23 transgenic mice (Schonrock et al., 2010), and negative correlations between amyloid beta and miR-181c were observed in AD patients' brains (Geekiyana and Chan, 2011). miR-181c has also been related to tau phosphorylation (Tan et al., 2014b). Present results show that miR-181c upregulation after ICSS only reaches

statistical significance in DG subfield. Although its specific role in this regions is not completely clear, it has been suggested that miR-181c can modulate dendritic branching and synaptogenesis in vitro (Olde Loohuis et al., 2015; Fang et al., 2016; Kos et al., 2016).

Thus, our results suggest that miR-132, together with miR-181c and miR-495, could be essential miRNAs for orchestrating the regional mechanisms of ICSS memory improvements, by which AD pathology could result alleviated.

#### Serum ICSS-regulated miRNAs are potential treatment biomarkers

In line with the idea that DBS could be an effective treatment for AD, the potential of miRNAs as treatment biomarkers is worth to study, specially taking into account that both miR-132 and miR-181c have been proposed as AD biomarkers (Kumar et al., 2013a; Xie et al., 2018; Siedlecki-Wullich et al., 2019). Burgos et al. report that miR-132 is downregulated in cerebrospinal fluid of AD patients (Burgos et al., 2014), even though some studies seem to report contrary results (Sheinerman et al., 2012). In this study, ICSS-treated rats showed increased miR-132 serum levels, consistent with miR-132 DG changes but resulting in a negative correlation, specifically for the ICSS group. This negative correlation could be explained by a gradual clearance of miR-132 from brain tissue to blood, which would result in a progressive decrease of its peak levels in the tissue coupled with an increase in its serum levels. In the case of miR-181c circulatory levels, contradictory results regarding the sense of alteration in AD were also reported (Geekiyana et al., 2012; Siedlecki-Wullich et al., 2019). In our study, miR-181c was not found to be altered in serum 90 min after ICSS in physiological conditions. Still, it remains an interesting potential target of ICSS to be analysed in serum after ICSS administered to AD-like pathological conditions.

#### Overlapping molecular mechanisms between ICSS and AD were not demonstrated in physiological conditions in the levels of typical AD-associated proteins, but evidenced in SIRT1

Altogether, both functional analyses and putative targets imputation on OpenArray-suggested candidates (Table 8) as well as reported information for miR-132 and miR-181c indicate that ICSS-regulated miRNAs are strongly interrelated with APP and tau pathological cascades. Thus, it was hypothesized that ICSS will be also regulating the levels of these proteins. A first approach to tackle this hypothesis is presented in this study, by assessing the expression levels of APP as well as tau and ptau proteins in DG at different time points after ICSS. In a physiological environment, any significant effect of ICSS neither in APP nor in tau expression levels is reported. Our results agree with the ones presented by Gondard et

al., which assessed the amount of the same proteins in hippocampus at different time points after a single session of bilateral forniceal DBS and found no change (Gondard et al., 2015). However, we found a significant increase on tau phosphorylation ratio at site Ser202/Thr205 180 min (3 h) after ICSS session, but not before. This increase could also match the non-significant peak reported by Gondard et al., 5 h after DBS session, which had disappeared at 25 h (Gondard et al., 2015). As a hypothesis, this ICSS-induced increment could be understood as a transient and reversible hyperphosphorylation of tau to promote dendritic remodelling in a physiological environment. Actually, it has already been suggested that, despite its association with disease, tau phosphorylation also plays an important role in neuroplasticity to trigger network modulation, given the propensity of ptau to dissociate from microtubules (Rissman, 2009).

In addition to APP and tau, OpenArray results also suggested that ICSS could be regulating other plasticity-related proteins that are also altered in early phases of AD, including DBN, SIRT1 and BDNF. While levels of the three are found decreased in AD-affected brain areas (Harigaya et al., 1996; Julien et al., 2010; Ishizuka and Hanamura, 2017; Ng et al., 2019), SIRT1 and BDNF are especially interesting for their presence in blood and their potential use as AD peripheral biomarkers (Kumar et al., 2013b; Ventriglia et al., 2013).

In the present work, any significant change in the levels of DBN was found in the DG at any of the analysed time points after ICSS (30, 90 and 180 min) in physiological conditions. Still, its possible regulations in pathological conditions needs to be further assessed. In contrast, SIRT1 levels were found significantly increased after ICSS treatment administered in physiological conditions. Taking into account that SIRT1 deficiency has been associated with both amyloid production (Bonda et al., 2011) and tau pathology (Julien et al., 2010; Sang-Won Min et al., 2018), SIRT1 regulation by ICSS revealed once more the interaction of ICSS mechanisms with AD-regulatory pathways.


Specifically, SIRT1 levels were found increased in DG hippocampal subfield 90 minutes after stimulation in this work. In hippocampal neurons, SIRT1 has been reported to regulate dendritic development and axonal elongation (Michán et al., 2010; Codocedo et al., 2012; Herskovits and Guarente, 2014). Specifically in DG, Ma et al. reported an increase of SIRT1 expression during neural stem cell differentiation, suggesting that SIRT1 is an important regulator of the differentiating/self-renewal balance of adult neural stem cells (Ma et al., 2014). Mechanistically, Sirt1 mRNA has been suggested to be targeted by all miR-132, miR-181c and miR-495 (Schonrock et al., 2012; Prins et al., 2014; Hadar et al., 2018). In

accordance with our results, parallel changes of SIRT1 and miR-132 (Hadar et al., 2018) and even positive correlations between them in brain tissue (Hernandez-Rapp et al., 2016) have been described in AD patients. Salta et al. present a bimodal regulatory network by which an increase in miR-132 results in increased SIRT1 expression in glial progenitors during development (Salta et al., 2014). Thus, taking these observations into account, once induced by ICSS, SIRT1 and regulated miRNAs could work together to improve neurogenesis and synaptic plasticity in DG.

Moreover, ICSS-regulation of SIRT1 in DG further motivates its assessment as a potential treatment biomarker. In this work, SIRT1, as well as BDNF, were successfully detected in serum obtained 90 minutes after treatment. Neither SIRT1 nor BDNF serum levels were able to distinguish between sham and ICSS-treated rats and none of them showed significant correlations between serum and DG levels, which are unaltered for BDNF. However, a positive correlation between SIRT1 levels in serum and those of miR-132 and SIRT1 was observed in the ICSS-treated rats, contributing once more to the idea that these two molecules work together improving neural plasticity. Instead, BDNF levels did not correlate with any ICSS-regulated molecule, and some have reported controversies regarding its use as AD biomarker (Baliatti et al., 2018). In this sense, SIRT1 is suggested as a more promising biomarker to be further studied in AD-like condition.

### Conclusions

In conclusion, the main findings of this study showed that ICSS administered in physiological conditions induces miRNA changes, including miR-132, miR-181c and miR-495, with a specific hippocampal subfield pattern, 90 min after treatment. This study also reports DG upregulation after ICSS of SIRT1 protein. The functional pathways reported for these molecules not only provide insight to molecular signalling underlying ICSS memory-improving effects, but also link ICSS mechanisms with regulatory routes of AD molecular pathology. Thus, the study of DBS to the MFB as a treatment for AD is encouraged. In this direction, changes in miR-132 levels in serum after ICSS serve as preliminary evidence to suggest its future potential use as a DBS treatment biomarker, while assessment of other miRNAs and SIRT1 for this use should not be discontinued in an AD-like context. Overall, future studies assessing ICSS effects on the ICSS-regulated candidates revealed in this study, which include specific miRNAs, SIRT1, DBN, APP and tau, would be of great interest in AD-like pathology condition.



## STUDY II. AMYLOID- $\beta$ INJECTED MODEL TO EVALUATE ICSS TREATMENT IN EARLY ALZHEIMER'S DISEASE

Evidences from Study 1 suggest that molecular mechanisms regulated by ICSS overlap molecular regulators of AD pathology. Thus, assessment of ICSS treatment in AD condition become especially interesting. This section presents the results from Study 2, which aimed to approach this situation, according to the second aim of this thesis. Thus, effects of ICSS treatment on molecular markers of early AD pathology were intended to be assessed in a sAD rat model obtained by A $\beta$  icv injection. First, neuropathological cell and molecular signs related to the behavioural presentation of the model were characterized at two different time points after A $\beta$  injection, to meet the conditions leading to molecular affectation resembling early pathology. Then, the main effects of ICSS were assessed on early AD-like molecular affectations.

From the total of 52 animals intended for this study, three subjects were excluded from the analysis. One subject had a leg ulcer non-related with the treatment, one broke the teeth with the ICSS lever and one was revealed to be an outlier according to statistical analyses on behavioural variables. Thus, the final sample consisted of 49 subjects. Final sample size in each group is shown in Table 10, which summarizes the experimental conditions of the groups analysed in this study.

**Table 10** | Summary of the groups composing Study 2 is presented as a brief recap of the experimental design in Study 2, including final sample size for each group.

Group	Icv injection	Treatment	MWM acquisition	MWM probe test	Sacrifice	Final sample size
VEH22	Vehicle	-	On days	Day 22	Day 22	8
AB22	A $\beta$	-	15-19			7
VEH33	Vehicle	5 sham sessions				8
AB33	A $\beta$	on days 26-30	On days	Day 33	Day 33	10
ICSS33	Vehicle	5 ICSS sessions	26-30			7
AB+ICSS33	A $\beta$	on days 26-30				9

## 2.1. Amyloid- $\beta$ 1-42 oligomeric aggregates to be injected

The presence and aggregation state of amyloid- $\beta$  1-42 (A $\beta$ ) peptide in the solution to be injected was confirmed by Western blot. Different bands, corresponding to different oligomeric species of A $\beta$  (dimers, trimers and tetramers), were revealed between 8-20 kDa, indicating the presence of soluble toxic A $\beta$ 1-42 species in the injected solution (Fig. 41).

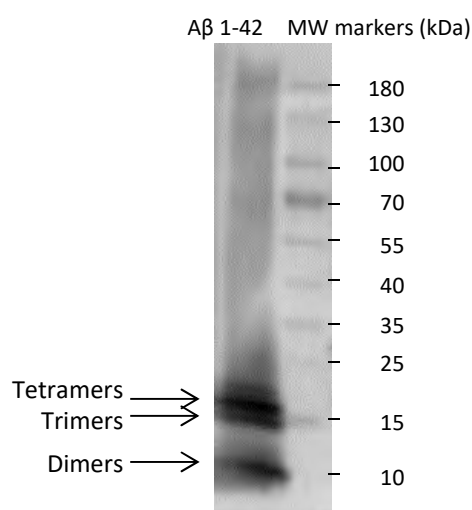


**Fig. 41** | Aggregation state of injected amyloid- $\beta$  peptide. Western blot of A $\beta$  solution to be injected: sonicated A $\beta$  1-42 peptide dilution (25  $\mu$ M in PBS) was incubated for 168 h at 37°C and diluted to 15  $\mu$ M before loading the sample on PAGE and transfer it on a PVDF membrane, probed with amyloid- $\beta$  monoclonal antibody H31L21, revealing the presence of A $\beta$  aggregates of 8-20 kDa (dimers, trimers and tetramers). Molecular weight standards are indicated in the lane on the right.

## 2.2. Time-dependent alterations on behavioural and histopathological AD hallmarks in A $\beta$ -injected rats

Effects of A $\beta$  injection on behavioural and histopathological hallmarks are presented in this section, regarding comparisons between VEH22/AB22 and VEH33/AB33 groups.

### Spatial learning and memory deficits in A $\beta$ -injected rats

Spatial learning curves for VEH and AB rats are presented in Fig. 42, which depicts the evolution in mean escape latencies across the different acquisition sessions in the MWM. Fig. 42A refers to rats trained on days 15-19 after A $\beta$  injection (groups named VEH22 and AB22), while Fig. 42B shows results for rats trained on days 26-30 (groups named VEH33 and AB33). A 2 $\times$ 5 ANOVA for repeated measures revealed that main effect of the SESSION factor was statistically significant, showing learning in both VEH and AB groups, both trained at 15-19 days and at 26-30 days ( $F_{4,52}=81.473$ ,  $p<.001$  and  $F_{4,64}=18.814$ ,  $p<.001$ , respectively). Analysis of the GROUP effect and GROUP  $\times$  SESSION interaction did not reach statistical significance at any assessed time ( $F_{1,13}=2.952$ ,  $p=.109$  and  $F_{4,52}=.771$ ,  $p=.549$ , respectively for days 15-19, and  $F_{1,16}=.012$ ,  $p=.913$  and  $F_{4,64}=.819$ ,  $p=.518$ , respectively for days 26-30). However, further simple effect analysis revealed significant differences between VEH22 and AB22 groups trained between day 15-19, in the 4<sup>th</sup> and 5<sup>th</sup> acquisition sessions ( $p=.007$  and  $p=.050$ , respectively), while no differences were found for any acquisition session between VEH33 and AB33 rats, trained at days 26-30 after injection.

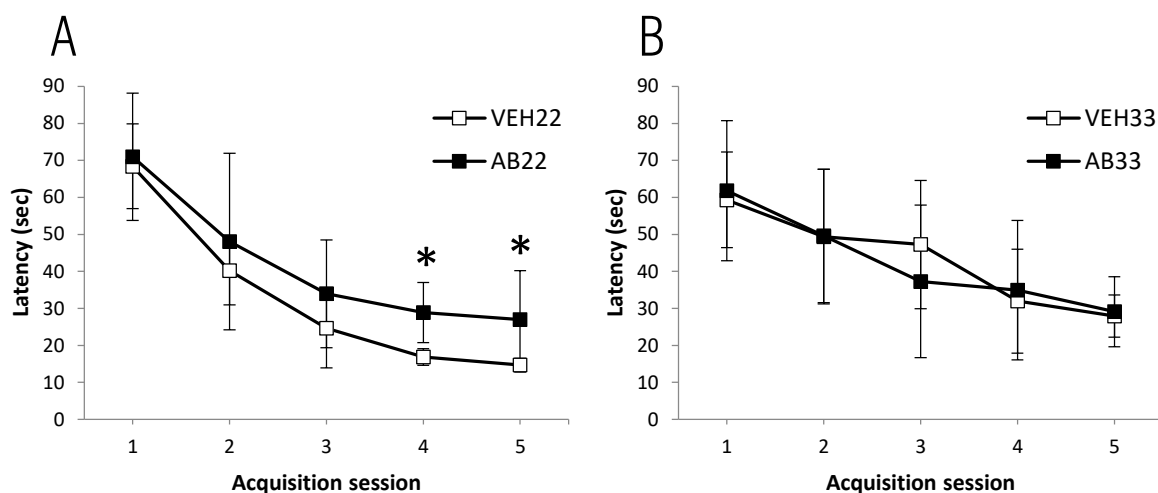


**Fig. 42 | Effects of A $\beta$  injection on spatial task acquisition.** Mean escape latencies ( $\pm$ SD) for the five acquisition sessions in the MWM, for AB and VEH rats trained between **A.** days 15-19 and **B.** days 26-30 after A $\beta$  or PBS injection.  $n=8, 7, 8$  and  $10$  rats/group (VEH22, AB22, VEH33 and AB33, respectively). \* $p<.05$ .

In the probe test, AB22 group (trained between days 15-19 and tested on day 22) presented a significant decrease in the percentage of time in the target quadrant ( $p=.004$ ) (Fig. 43A) and in the annulus area ( $p=.004$ ) (Fig. 43B) together with an increase in mean distance to target area ( $p<.001$ ) (Fig. 43C). No significant differences were found in any of these variables between AB33 and VEH33 groups, which were trained between days 26-30 and tested on day 33, although differences between these groups become perceptible in mean distance to target area evaluated during the first 30 sec of test ( $p=.040$ ) (Fig. 43D).

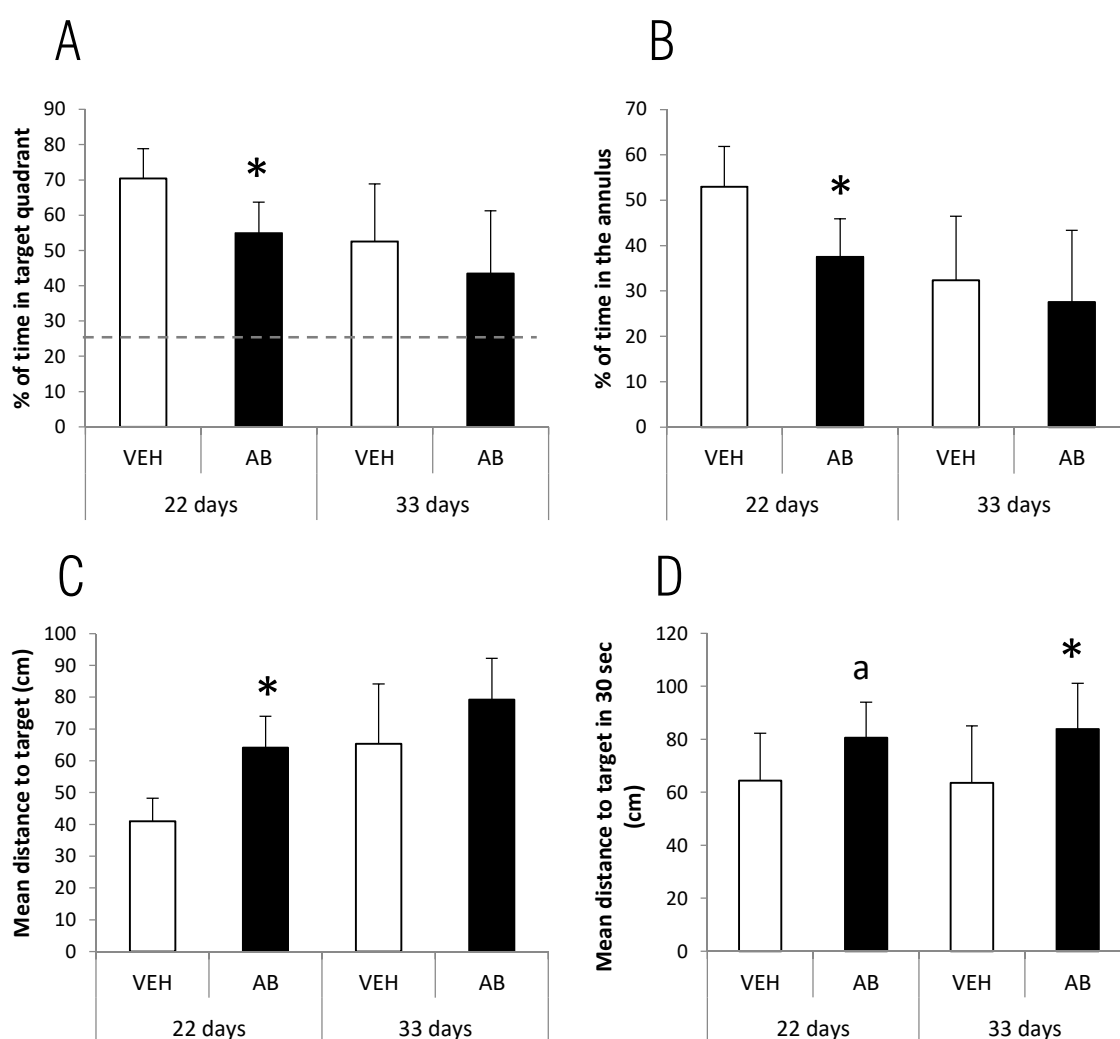


**Fig. 43 | Effects of A $\beta$  injection on spatial probe test.** Results of the MWM probe test for rats tested at 22 days and 33 days after injection. **A.** Percentage of time spent in the target quadrant. The dashed line represents chance level. **B.** Percentage of time spent in the annulus area. **C-D.** Mean distance to target area during the whole test (C) and during the first 30 seconds of test (D). Data are presented as mean $\pm$ SD;  $n=8, 7, 8$  and  $10$  rats/group (VEH22, AB22, VEH33 and AB33, respectively). \* $p<.05$  vs corresponding VEH; <sup>a</sup> $p\leq.07$  vs corresponding VEH.



In the reversal test, AB22 group presented a significant increase in the mean escape latency considering the average of the 3 trials with respect to control ( $p=.017$ ) (Fig. 44A). For AB33, significant increased mean escape latency was found only in the first reversal trial ( $p=.013$ ) (Fig. 44B), but not in the others neither in the average.

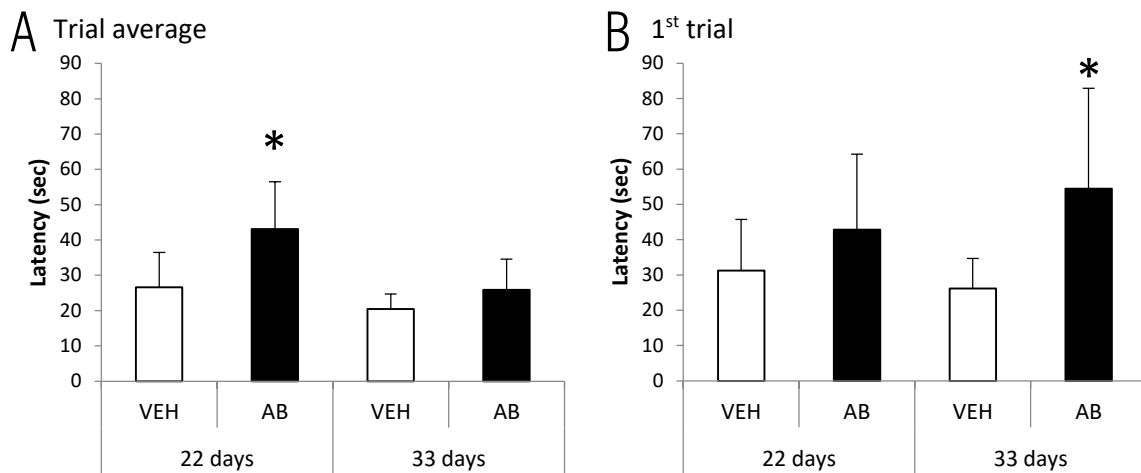


**Fig. 44 | Effects of A $\beta$  injection on cognitive flexibility.** Mean escape latencies ( $\pm$ SD) in the MWM reversal test, for rats tested at 22 days and 33 days after injection. **A.** Average of 3 reversal trials. **B.** First reversal trial.  $n=8, 7, 8$  and  $10$  rats/group (VEH22, AB22, VEH33 and AB33, respectively). \* $p<.05$  vs corresponding VEH.

### Neurodegeneration in A $\beta$ -injected rats

Nissl staining was used to assess the effects of A $\beta$  on neurodegeneration in rats sacrificed both at 22 days and 33 days. In the hippocampus, no differences were found between AB22 and VEH22 groups in the number of neurons in any hippocampal subfield (Fig. 45A,B). In contrast, AB33 rats showed a reduced number of neurons in both distal ( $p=.011$ ) and proximal (hilus region) ( $p=.037$ ) CA3 compared with control (Fig. 45A,C).

In prelimbic cortex, AB22 rats presented a reduced number of neurons in layer II-III ( $p=.025$  for normal neurons and  $p=.026$  for total neurons) (Fig. 46A,D). Among present cells in AB22 group, both necrotic, pyknotic, apoptotic and vacuolated morphologies were found (Fig. 46B), leading to a marked increasing tendency in the percentage of neurodegeneration ( $p=.052$ ) (Fig. 46C). However, 33 days after injection, no significant differences were found between groups regarding neurodegeneration in layer II-III of prelimbic cortex (Fig. 46A,C,E).

No significant correlations were found between neurodegeneration in these areas and behavioural impairment, neither in AB22 nor in AB33 groups.

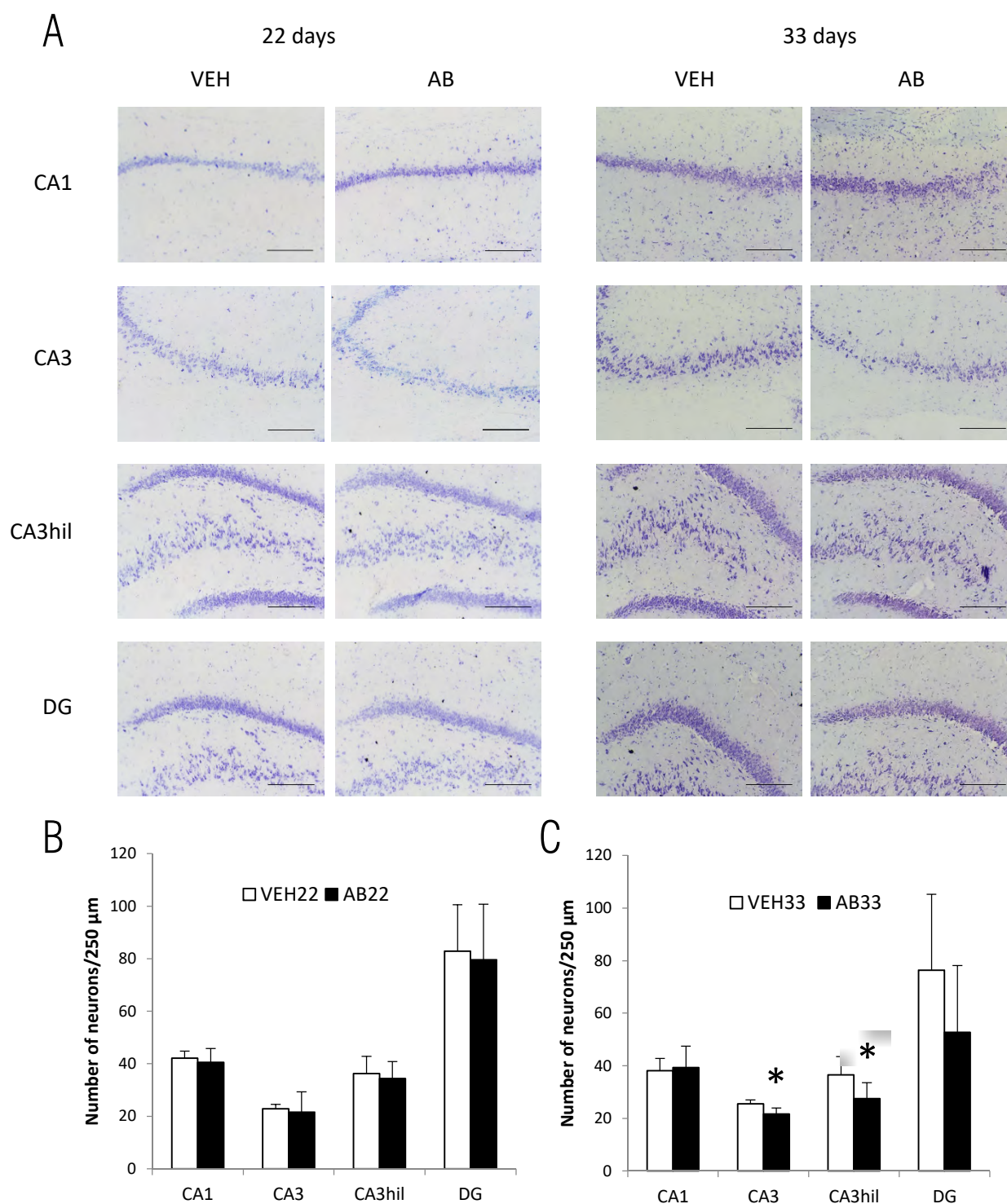


**Fig. 45 | Effects of A $\beta$  injection on hippocampal neurodegeneration.** Results of Nissl staining analysis in hippocampal subregions, for AB and VEH groups 22 and 33 days after A $\beta$  injection. **A.** Representative photomicrographs for Nissl staining in each hippocampal subregion for each group (scale bar=250  $\mu\text{m}$ ). **B-C.** Neuronal count in 250  $\mu\text{m}$  layer length in CA1, CA3 (distal part), CA3hil (proximal part, at the region of hilus) and dentate gyrus (DG) hippocampal subregions in AB and VEH rats 22 days (B) and 33 days (C) after injection. Data are presented as mean $\pm$ SD: n=7, 7, 6 and 6 rats/group (VEH22, AB22, VEH33 and AB33, respectively). \*p<.05 vs VEH.

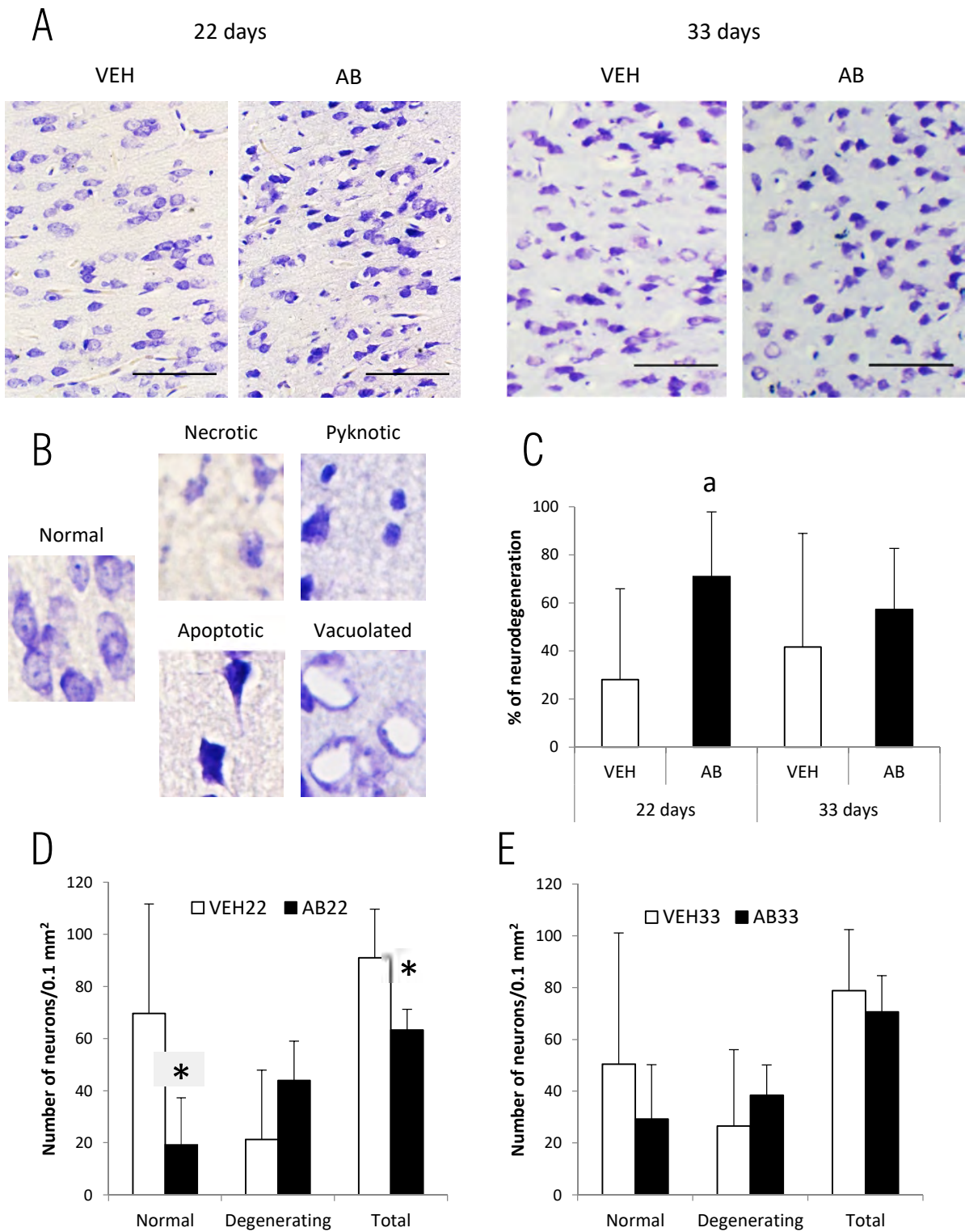


**Fig. 46 | Effects of A $\beta$  injection on prelimbic cortex neurodegeneration.** Neurodegeneration in prelimbic cortex layer II-III, for AB and VEH groups, 22 and 33 days after A $\beta$  injection. **A.** Representative photomicrographs of Nissl staining for each group. **B.** Examples of normal and neurodegenerating morphologies found in Nissl stained sections. **C.** Percentage of neurodegeneration and **D-E.** categorized neuronal count. Data are presented as mean $\pm$ SD: n=5, 6, 4 and 6 rats/group (VEH22, AB22, VEH33 and AB33, respectively). \*p<.05 vs VEH; **a** p $\leq$ .07 vs corresponding VEH.

### Alteration of DBN levels in A $\beta$ -injected rats

Effects of A $\beta$  injection on DBN levels were assessed by immunohistochemistry both in rats sacrificed 22 days after injection as well as rats sacrificed 33 days.

Focusing first in the results found 22 days after injection:

AB22 group did not present any significant decrease in DBN levels in any of the analysed regions in parietal-temporal lobe, but rather an increase which was found significant in layer Va agranular retrosplenial cortex ( $p=.044$ ). In frontal lobe, a decrease in DBN levels was found in layers IIb and III of prelimbic cortex ( $p=.021$  and  $p=.017$ , respectively), while an increase was detected in layer V ( $p=.005$ ) (Fig. 47).

Interestingly, DBN levels in different parietal-temporal regions (LEnt layers I and II, CA1 at SLM, DG at SP and both RSG and RSA at layers II-III and VI) (Table 11) and in prelimbic cortex layer Ib (Fig. 48) positively correlate with percentage of neurodegeneration in prelimbic cortex, specifically for the AB22 group.

In other layers of rhinal cortices, DBN levels correlate with certain acquisition and probe test behavioural variables (Table 12 and Fig. 49), being the subjects with higher DBN levels the ones with better performance, especially for the AB22 group.

In prelimbic cortex, no significant correlations were found between DBN levels and acquisition and probe test parameters. However, DBN levels in layer V of prelimbic cortex negatively correlate with time spent in the error quadrant during the third trial of the reversal test, for AB22 group (Fig. 50C). In the case of VEH22 group, there was a statistical tendency for this correlation in the second trial of reversal test (Fig. 50B). In fact, a tendency to a gradual reversion in the direction of correlation was noted along the three reversal sessions, which was found delayed for AB22 group respect to VEH22 group (Fig. 50A-C).

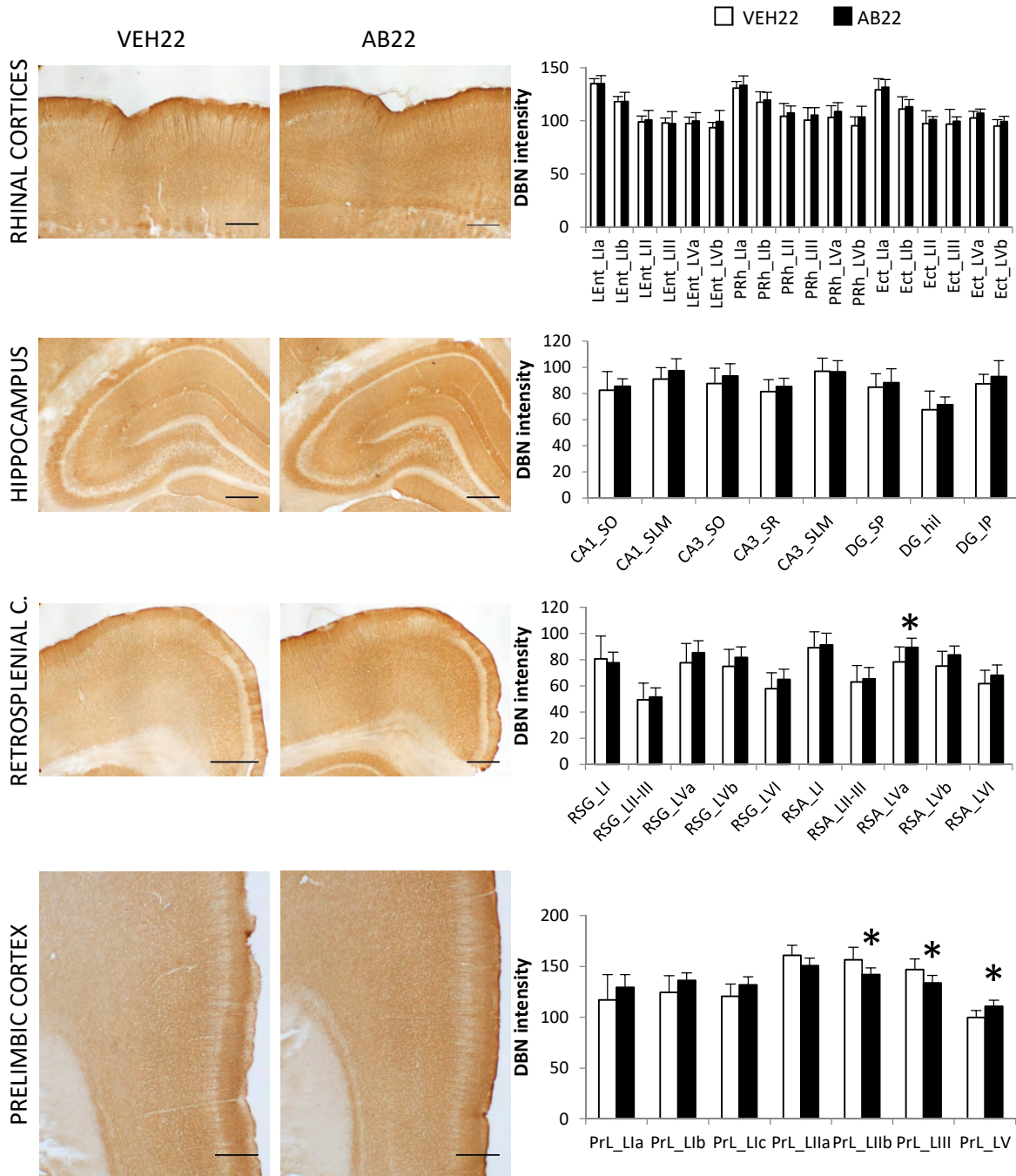


**Fig. 47 | Effects of A $\beta$  injection on DBN levels at day 22.** DBN levels in rhinal cortices, hippocampus, retrosplenial cortex and prefrontal cortex, in VEH22 and AB22 rats, sacrificed 22 days after A $\beta$  injection. In the left, representative photomicrographs showing DBN immunolabelling for each group in each region (scale bar=500  $\mu$ m). In the right, results of labelling intensity quantification. Data are presented as mean $\pm$ SD; n=8 and 7 rats/group (VEH22 and AB22, respectively). \*p<.05 vs VEH22. Abbreviations: DG: dentate gyrus; Ect: ectorhinal cortex; hil: hilus; IP: infrapyramidale; L: layer; LEnt: lateral entorhinal cortex; PRh: perirhinal cortex; PrL: prefrontal cortex; RSA: retrosplenial agranular cortex; RSG: retrosplenial granular cortex; SLM: *stratum lacunosum moleculare*; SO: *stratum oriens*; SP: suprapyramidale; SR: *stratum radiatum*.

**Table 11** | Correlation analyses between DBN levels in parietal-temporal regions and neurodegeneration in prelimbic cortex, 22 days after A $\beta$  injection. Table includes the correlations found significant for AB22 group, according to Spearman's correlation test ( $p < .05$ , in bold in the table).

		% of neurodegeneration in PrL_LII-III	
		AB22	VEH22
DBN intensity levels	LEnt_LIa	$\rho = .829$ <b><math>p = .042</math></b>	$\rho = .100$ $p = .873$
	LEnt_LIb	$\rho = .829$ <b><math>p = .042</math></b>	$\rho = .000$ $p = 1.000$
	LEnt_LII	$\rho = .829$ <b><math>p = .042</math></b>	$\rho = .000$ $p = 1.000$
	CA1_SLM	$\rho = .829$ <b><math>p = .042</math></b>	$\rho = -.100$ $p = .873$
	DG_SP	$\rho = .829$ <b><math>p = .042</math></b>	$\rho = -.100$ $p = .873$
	RSG_LII-III	$\rho = .829$ <b><math>p = .042</math></b>	$\rho = -.100$ $p = .873$
	RSG_LVI	$\rho = .886$ <b><math>p = .019</math></b>	$\rho = -.200$ $p = .747$
	RSA_LII-III	$\rho = .829$ <b><math>p = .042</math></b>	$\rho = -.600$ $p = .285$
	RSA_LVI	$\rho = .886$ <b><math>p = .019</math></b>	$\rho = -.100$ $p = .873$

$\rho$  = Spearman's correlation coefficient;  $n = 5$  and  $6$  rats/group (VEH and AB, respectively); Abbreviations: DG: dentate gyrus; L: layer; LEnt: lateral entorhinal cortex; PrL: prelimbic cortex; RSA: retrosplenial agranular cortex; RSG: retrosplenial granular cortex; SLM: *stratum lacunosum moleculare*; SP: suprapyramidale.

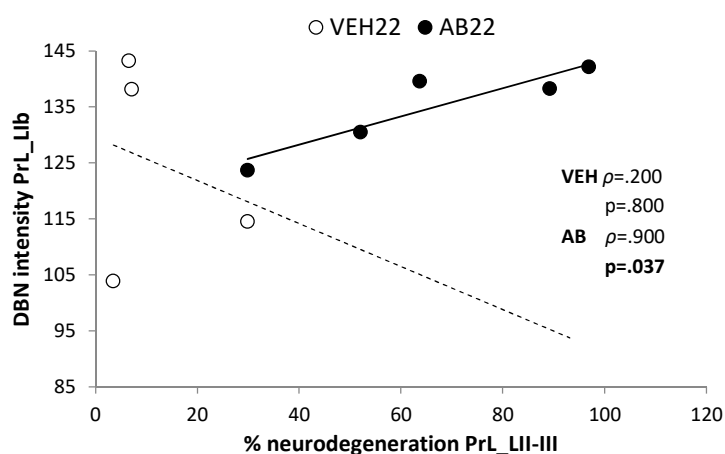


**Fig. 48** | Correlation between DBN levels and percentage of neurodegeneration in superficial layers of prelimbic cortex, 22 days after A $\beta$  injection. Scatter plot showing the relation between DBN immunolabelling intensity in layer Ib of prelimbic cortex and percentage of degenerating neurons distinguished by Nissl staining in layer II-III of prelimbic cortex, in VEH22 and AB22 groups, sacrificed 22 days after A $\beta$  injection. Each dot represents a single rat. Spearman's correlation test was used to determine significance ( $p < .05$ ).  $\rho$  = Spearman's correlation coefficient;  $n = 4$  and  $5$  rats/group (VEH22 and AB22, respectively). Abbreviations: L: layer; PrL: prelimbic cortex.

**Table 12** | Correlation analyses between DBN levels in layer Vb of LEnt and behavioural variables, 22 days after A $\beta$  injection. Table includes the correlations found significant for AB22 group, according to Spearman’s correlation test ( $p < .05$ , in bold in the table). Correlation with A4 and Mdt is depicted as example in Fig. 49.

	DBN intensity levels in LEnt_LVb	
	AB22	VEH22
A2	$\rho = -.929$ <b><math>p = .003</math></b>	$\rho = -.143$ $p = .736$
A4	$\rho = -.893$ <b><math>p = .007</math></b>	$\rho = -.310$ $p = .456$
A5	$\rho = -.857$ <b><math>p = .014</math></b>	$\rho = -.429$ $P = 0.289$
Mdt	$\rho = -.821$ <b><math>p = .023</math></b>	$\rho = -.810$ <b><math>p = .015</math></b>
% of time in quadrant	$\rho = .786$ <b><math>p = .036</math></b>	$\rho = .286$ $p = .439$

$\rho$  = Spearman’s correlation coefficient;  $n = 8$  and  $7$  rats/group (VEH and AB, respectively); Abbreviations: A: mean latency for a specific acquisition session; Mdt: mean distance to target area; L: layer; LEnt: lateral entorhinal cortex.

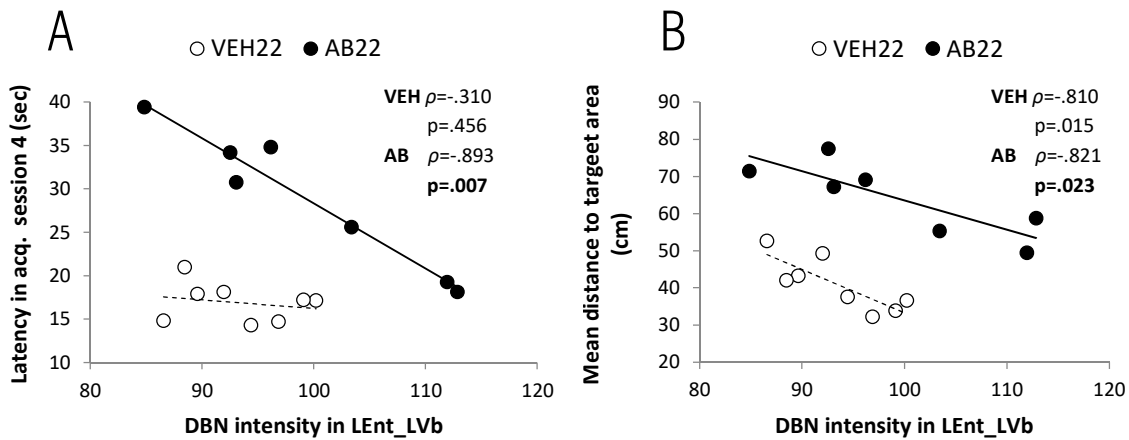


**Fig. 49** | Correlation between DBN levels in layer Vb of lateral entorhinal cortex and behavioural variables, 22 days after A $\beta$  injection. Scatter plot showing the relation between DBN immunolabelling intensity in layer Vb of lateral entorhinal cortex and **A.** latency in the 4<sup>th</sup> MWM acquisition session and **B.** mean distance to target area during the MWM probe test, in VEH22 and AB22 groups sacrificed 22 days after A $\beta$  injection. Each dot represents a single rat. Spearman’s correlation test was used to determine significance ( $p < .05$ ).  $\rho$  = Spearman’s correlation coefficient;  $n = 8$  and  $7$  rats/group (VEH22 and AB22, respectively). Abbreviations: L: layer; LEnt: lateral entorhinal cortex.

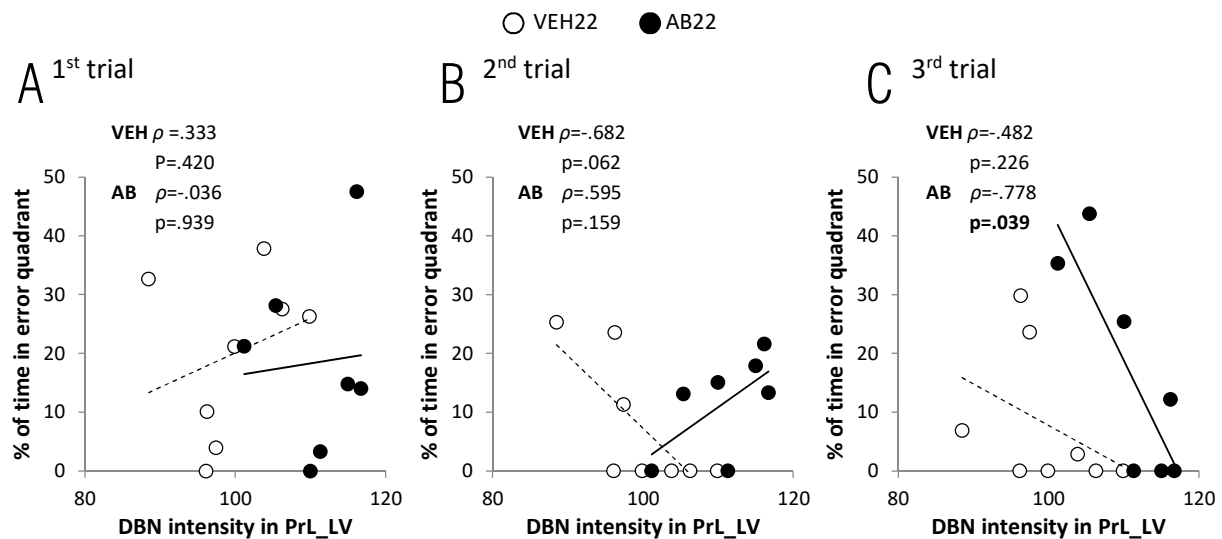


**Fig. 50 | Correlation between DBN levels in layer V of prelimbic cortex and cognitive flexibility, 22 days after A $\beta$  injection.** Scatter plot showing the relation between DBN immunolabelling intensity in layer V of prelimbic cortex and percentage of time spent in the error quadrant during the **A.** first, **B.** second and **C.** third reversal trials, in VEH22 and AB22 groups, sacrificed 22 days after A $\beta$  injection. Each dot represents a single rat. Spearman's correlation test was used to determine significance ( $p < .05$ ).  $\rho$  = Spearman's correlation coefficient;  $n = 8$  and  $7$  rats/group (VEH22 and AB22, respectively). Abbreviations: L: layer; PrL: prelimbic cortex.

Regarding now the effects of A $\beta$  injection on DBN levels after 33 days:

AB33 rats presented significant decreased DBN levels in layers Ib and II ( $p = .040$  and  $p = .021$ , respectively), and a tendency ( $p = .062$ ) of reduction in layer III of lateral entorhinal cortex, but not in perirhinal nor in entorhinal cortices (see Fig. 51, 52 minding to focus only on groups not receiving ICSS treatment; others will be reviewed in next section). DBN levels in these regions presented a significant correlation with affected behavioural variables in AB rats, being again the rats with higher DBN levels the ones with better performance (Fig. 53). In hippocampus, a significant reduction was found in outer molecular layer of suprapyramidal branch in DG ( $p = .009$ ), and a tendency ( $p = .056$ ) was detected in CA1 *stratum oriens*. Significant decrease was also found in layer I of granular retrosplenial cortex ( $p = .043$ ). In prelimbic cortex, DBN levels were found reduced in layer III ( $p = .016$ ) (see Fig. 51, 52 minding to focus only on groups not receiving ICSS treatment; others will be reviewed in next section). DBN levels in any of these regions significantly correlate with neurodegeneration found at 33 days in hippocampus.



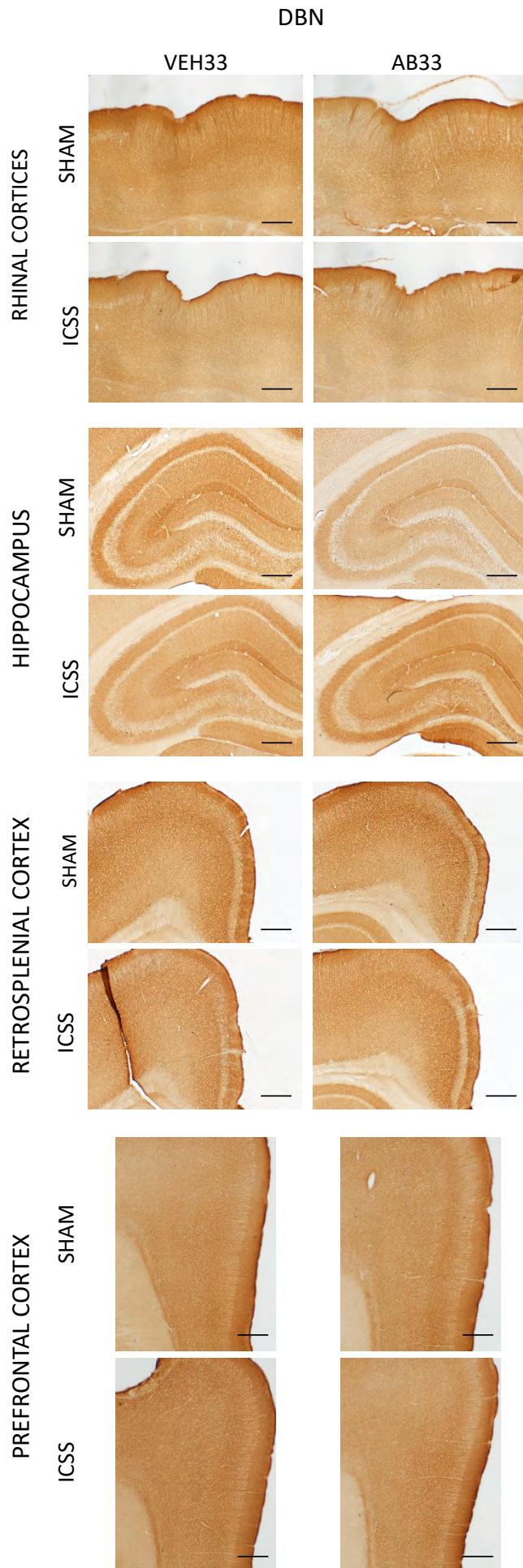


**Fig. 51** | Effects of A $\beta$  injection and ICSS treatment on D $\beta$ N levels at day 33. Representative photomicrographs of D $\beta$ N immunolabelling in rhinal cortices, hippocampus, retrosplenial cortex and prefrontal cortex, for VEH33, AB33, ICSS33 and AB+ICSS33 rats, sacrificed 33 days after A $\beta$  injection (scale bar=500  $\mu$ m).

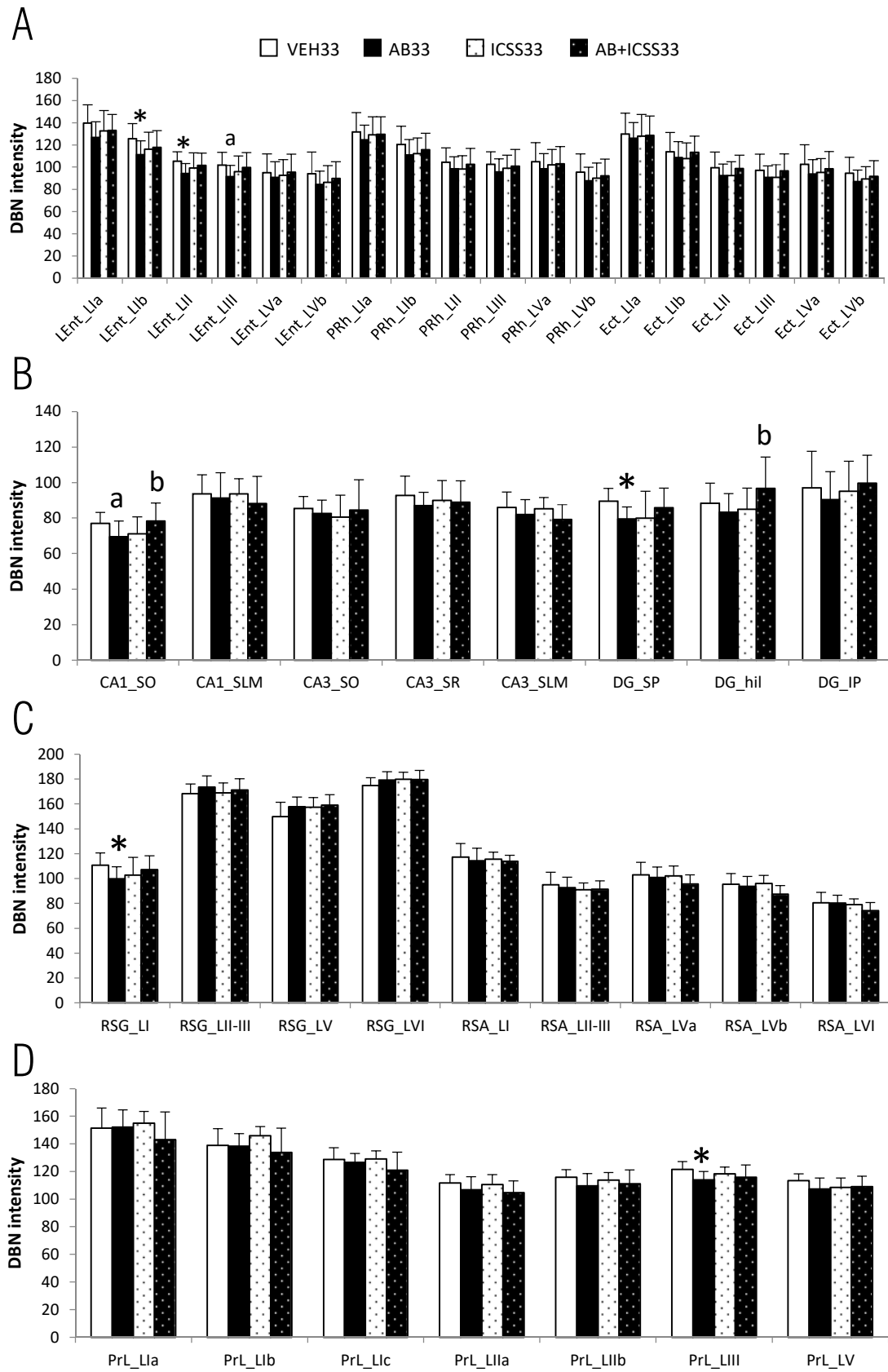


**Fig. 52 | Effects of A $\beta$  injection and ICSS treatment on DBN levels at day 33** (see figure on the previous page). DBN levels in **A.** rhinal cortices, **B.** hippocampus, **C.** retrosplenial cortex and **D.** prelimbic cortex, for VEH33, AB33, ICSS33 and AB+ICSS33 groups, sacrificed 33 days after A $\beta$  injection, resulting from labelling intensity quantification after DBN immunohistochemistry. Data are presented as mean $\pm$ SD; n=8, 10, 7 and 9 rats/group (VEH33, AB33, ICSS33 and AB+ICSS33, respectively). \*p<.05 vs VEH33; **a** p $\leq$ .07 vs VEH33; **b** p $\leq$ .07 vs AB. Abbreviations: DG: dentate gyrus; Ect: ectorhinal cortex; hil: hilus; IP: infrapyramidale; L: layer; LEnt: lateral entorhinal cortex; PRh: perirhinal cortex; PrL: prelimbic cortex; RSA: retrosplenial agranular cortex; RSG: retrosplenial granular cortex; SLM: *stratum lacunosum moleculare*; SO: *stratum oriens*; SP: suprapyramidale; SR: *stratum radiatum*.

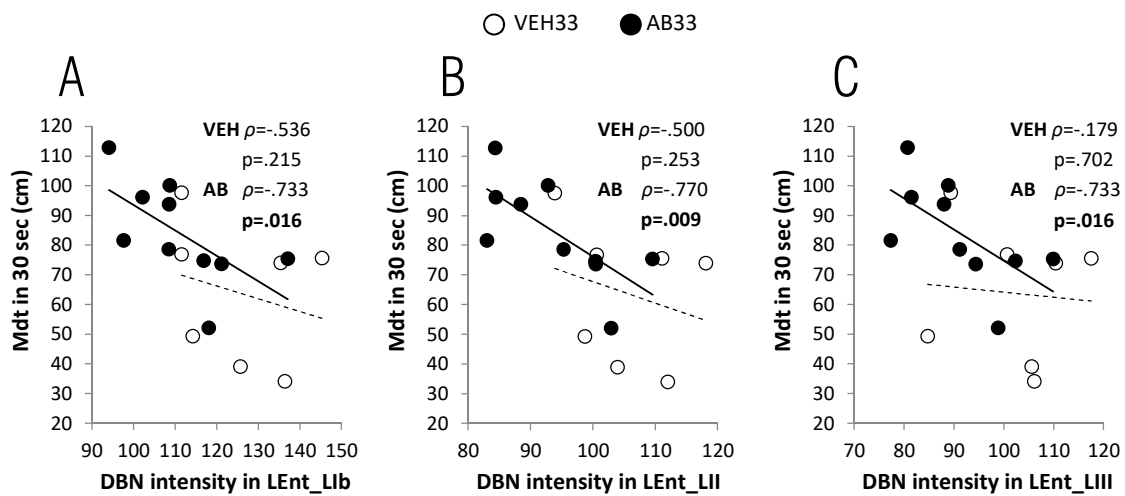


**Fig. 53 | Correlation between DBN levels in superficial layers of lateral entorhinal cortex and spatial memory, 33 days after A $\beta$  injection.** Scatter plot showing the relation between DBN immunolabelling intensity in **A.** layer Ib, **B.** layer II and **C.** layer III of lateral entorhinal cortex with mean distance to target area during the first 30 sec of probe test, in VEH33 and AB33 groups, sacrificed 33 days after A $\beta$  injection. Each dot represents a single rat. Spearman's correlation test was used to determine significance (p<.05).  $\rho$  = Spearman's correlation coefficient; n=7 and 10 rats/group (VEH33 and AB33, respectively). Abbreviations: L: layer; LEnt: lateral entorhinal cortex; Mdt: mean distance to target area.

### Alteration of ptau levels in A $\beta$ -injected rats

Twenty two (22) days after A $\beta$  injection, levels of phosphorylated tau were found significantly increased in specific hippocampal subregions (p=.037 and p=.014 vs VEH, for CA1\_3 and DG\_IP, respectively) (Fig. 54), positively correlating with neurodegeneration found in prelimbic cortex layers II-III (Fig. 55). Ptau levels were also increased in the prelimbic cortex layer III of AB22 rats (p=.029), and a tendency (p=.053) was also found in

layer V of prelimbic cortex (Fig. 54). Any significant difference was detected in ptau levels neither in rhinal cortices nor in retrosplenial cortex between AB22 and VEH22 groups (Fig. 54). However, strong positive correlations were found only in AB22 group between ptau levels in rhinal cortices (both layer II-III and global intensities) and DBN levels in superficial layers of prelimbic cortex, especially layer Ia (Fig. 56).

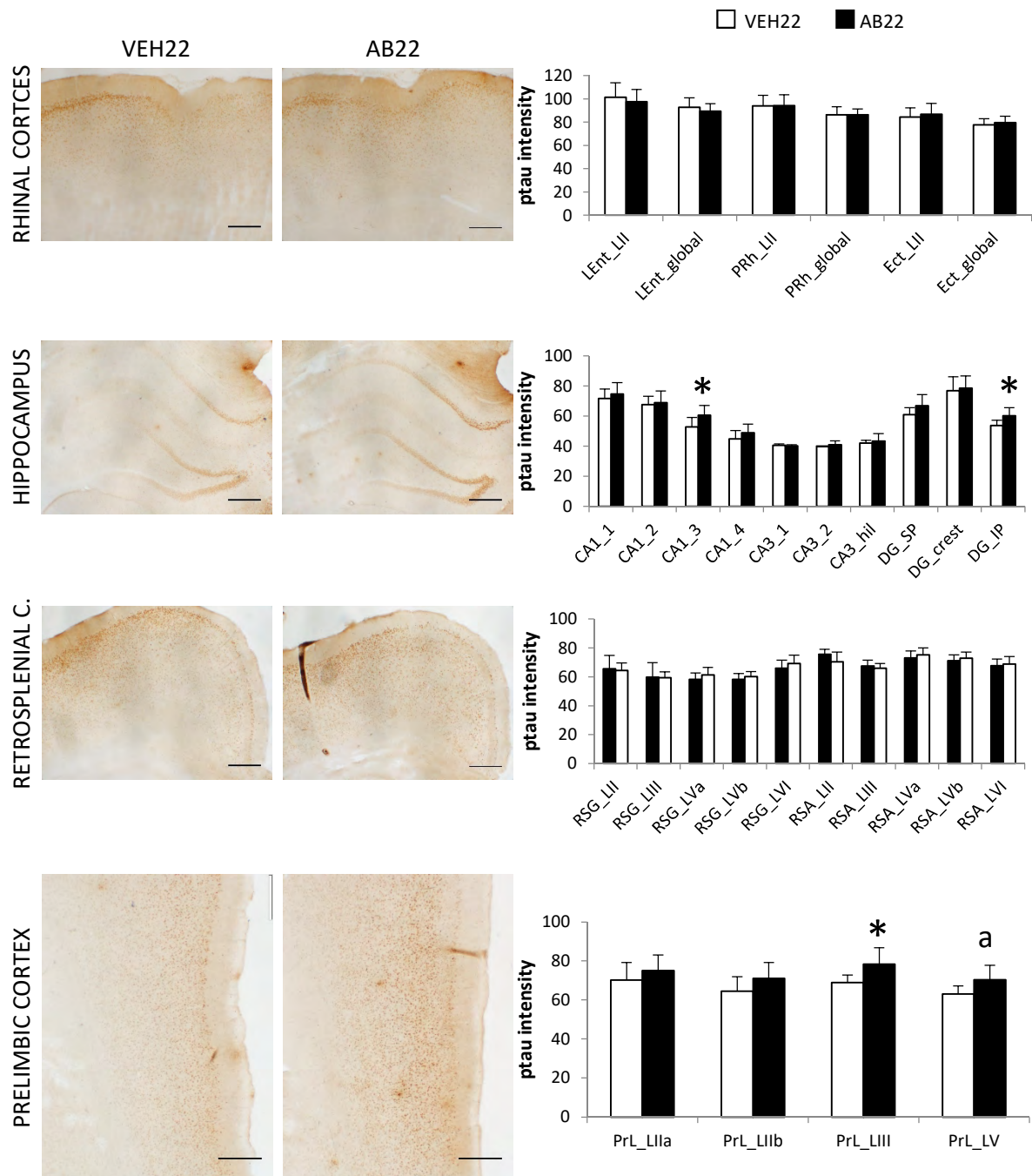


**Fig. 54 | Effects of A $\beta$  injection on ptau levels at day 22** (see figure on the previous page). Ptau levels in rhinal cortices, hippocampus, retrosplenial cortex and prelimbic cortex, in VEH22 and AB22 rats, sacrificed 22 days after A $\beta$  injection. In the left, representative photomicrographs showing ptau immunolabelling for each group in each region (scale bar=500  $\mu$ m). In the right, results of labelling intensity quantification. Data are presented as mean $\pm$ SD, n=8 and 7 rats/group (VEH22 and AB22, respectively). \*p<.05 vs VEH22; **a** p $\leq$ .07 vs VEH22. Abbreviations: DG: dentate gyrus; Ect: ectorhinal cortex; hil: hilus; IP: infrapyramidale; L: layer; LEnt: lateral entorhinal cortex; PRh: perirhinal cortex; PrL: prelimbic cortex; RSA: retrosplenial agranular cortex; RSG: retrosplenial granular cortex.

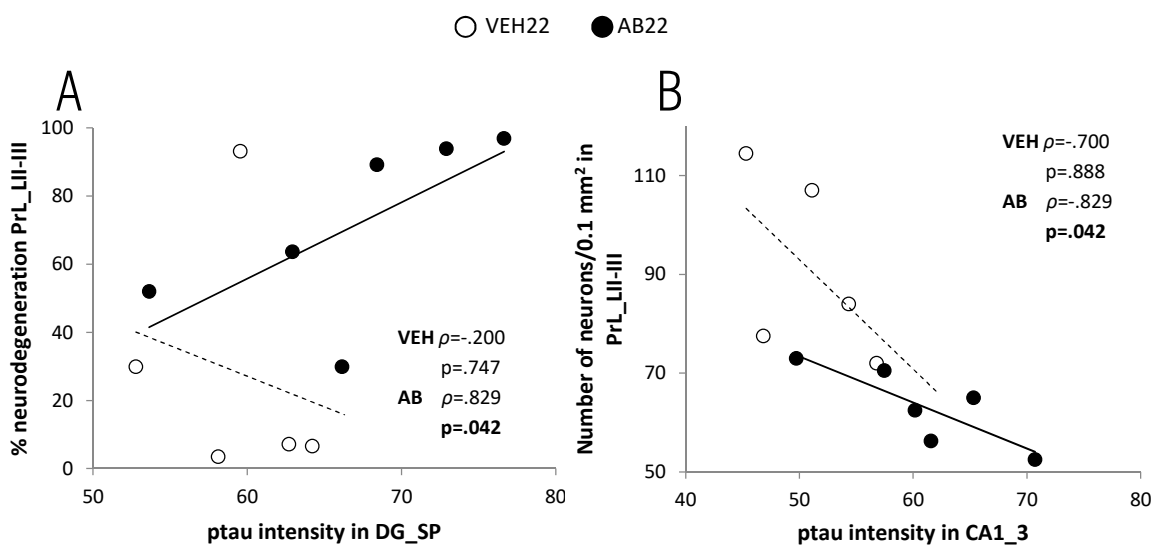


**Fig. 55 | Correlation between ptau levels in hippocampus and neurodegeneration in prelimbic cortex, 22 days after A $\beta$  injection.** Scatter plots showing **A.** the relation between ptau immunolabelling intensity in DG suprapyramidal layer (DG\_SP) and percentage of neurodegeneration in prelimbic cortex layer II-III and **B.** the relation between ptau immunolabelling intensity in CA1\_3 hippocampal region with total neuronal count in prelimbic cortex layer II-III, in VEH22 and AB22 groups, sacrificed 22 days after A $\beta$  injection. Each dot represents a single rat. Spearman's correlation test was used to determine significance ( $p < .05$ ).  $\rho$  = Spearman's correlation coefficient; n=5 and 6 rats/group (VEH22 and AB22, respectively).

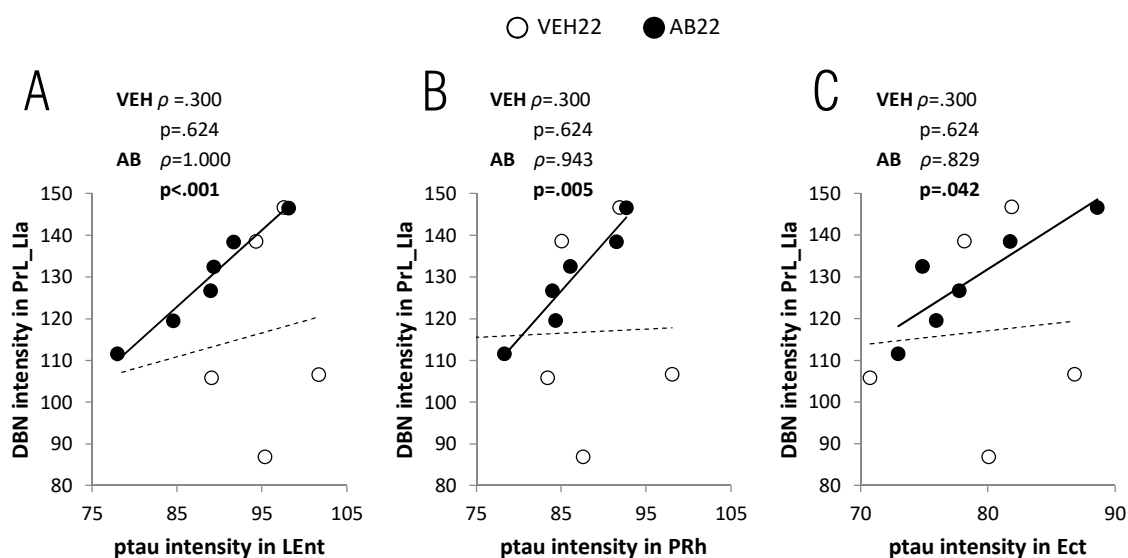


**Fig. 56 | Correlation between ptau levels in rhinal cortices and DBN levels in prelimbic cortex, 22 days after A $\beta$  injection.** Scatter plots showing the relation between DBN immunolabelling intensity in layer Ia of prelimbic cortex and ptau immunolabelling intensity in global **A.** lateral entorhinal cortex, **B.** perirhinal cortex and **C.** entorhinal cortex, in VEH22 and AB22 groups sacrificed 22 days after A $\beta$  injection. Each dot represents a single rat. Spearman's correlation test was used to determine significance ( $p < .05$ ).  $\rho$  = Spearman's correlation coefficient;  $n = 5$  and  $6$  rats/group (VEH22 and AB22, respectively). Abbreviations: Ect: entorhinal cortex; L: layer; LEnt: lateral entorhinal cortex; PRh: perirhinal cortex; PrL: prelimbic cortex.

At 33 days after A $\beta$  injection, ptau was found specifically increased in layer II of entorhinal cortex ( $p = .042$ ), but not in other rhinal cortices, hippocampus or prelimbic cortex. In retrosplenial cortex, a tendency ( $p = .053$ ) of increase was found in layer III of agranular part (see Fig. 57 and 58 minding to focus only on groups not receiving ICSS treatment; others will be reviewed in next section).

No significant correlations were found between ptau levels and impaired behavioural parameters, neither at 22 nor at 33 days after A $\beta$  injection.

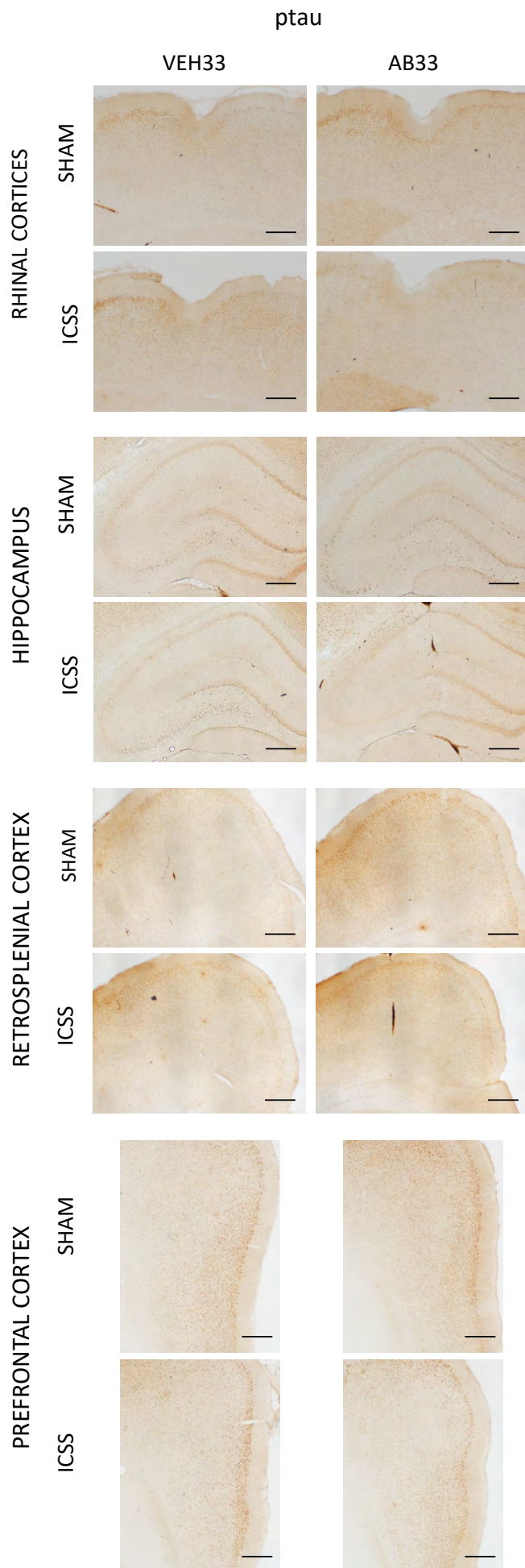


**Fig. 57 |** Effects of A $\beta$  injection and ICSS treatment on ptau levels at day 33. Representative photomicrographs of ptau immunolabelling in rhinal cortices, hippocampus, retrosplenial cortex and prefrontal cortex, for VEH33, AB33, ICSS33 and AB+ICSS33 rats, sacrificed 33 days after A $\beta$  injection (scale bar=500  $\mu$ m).

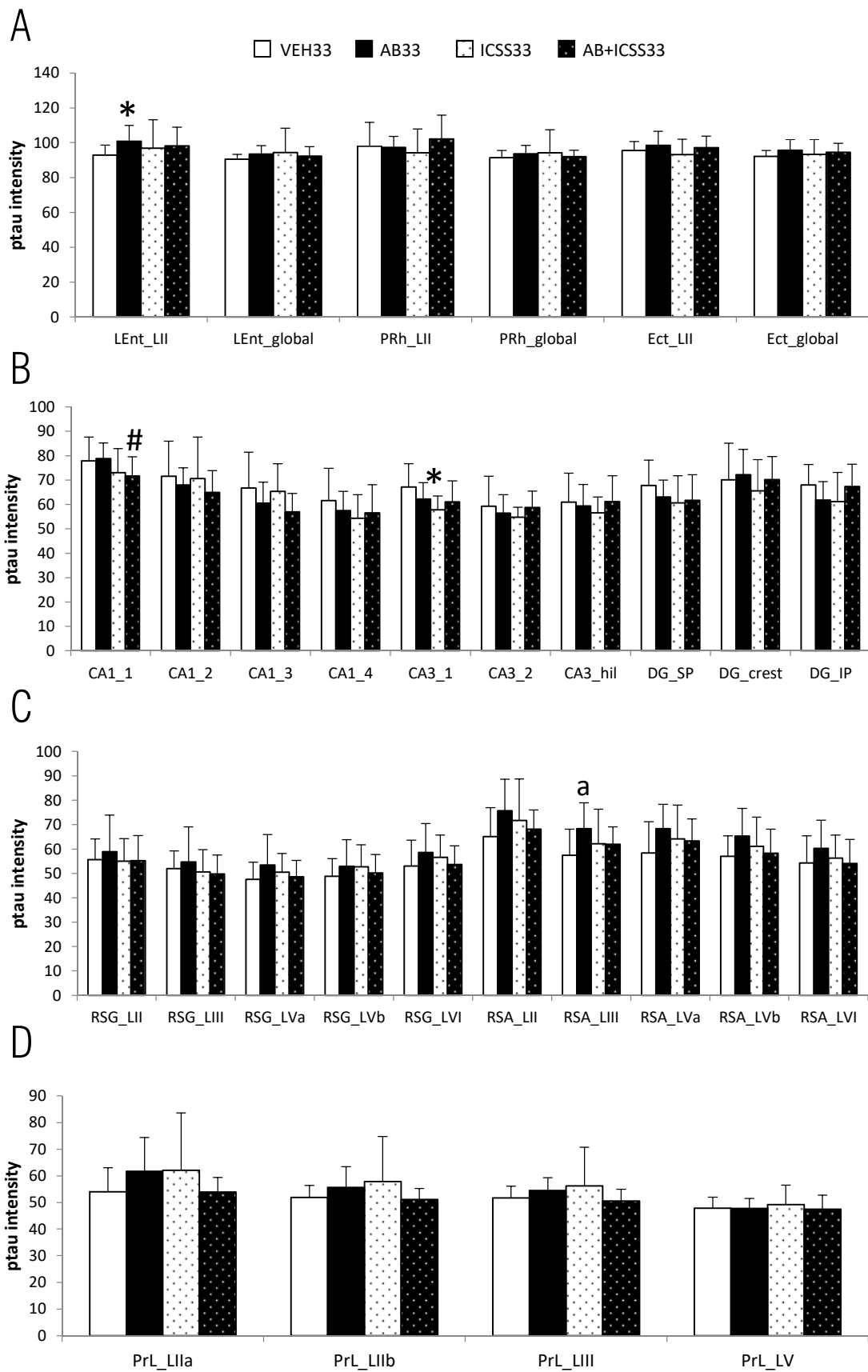




**Fig. 58 | Effects of A $\beta$  injection and ICSS treatment on ptau levels at day 33** (see figure on the previous page). Ptau levels in **A.** rhinal cortices, **B.** hippocampus, **C.** retrosplenial cortex and **D.** prelimbic cortex, for VEH33, AB33, ICSS33 and AB+ICSS33 groups, sacrificed 33 days after A $\beta$  injection, resulting from labelling intensity quantification after ptau immunohistochemistry. Data are presented as mean $\pm$ SD; n=8, 10, 7 and 9 rats/group (VEH33, AB33, ICSS33 and AB+ICSS33, respectively). \*p<.05 vs VEH33. #p<.05 vs AB; **a** p $\leq$ .07 vs VEH33. Abbreviations: DG: dentate gyrus; Ect: ectorhinal cortex; hil: hilus; IP: infrapyramidale; L: layer; LEnt: lateral entorhinal cortex; PRh: perirhinal cortex; PrL: prelimbic cortex; RSA: retrosplenial agranular cortex; RSG: retrosplenial granular cortex.

### 2.3. Effect of ICSS on early AD-like hallmarks in A $\beta$ -injected rats

Effect of ICSS treatment on early AD-like molecular hallmarks found in AB33 rats is presented in this section. In order to relate them to cognitive improvement, evidence of ICSS behavioural effect in A $\beta$ -injected rats is first presented.

#### Evidence of ICSS effects on behavioural affectations in A $\beta$ -injected rats

Administration of 5 post-training ICSS sessions were proved able to reverse spatial retention deficits in AB33 rats. In this sense, the mean distance to target area during the first 30 sec was significantly decreased in AB+ICSS33 group with respect to AB33 (p=.039), recovering VEH behaviour (Fig. 59B). Performance in acquisition phase, which was not affected in AB33 rats trained on days 26-30, was also not affected in AB+ICSS33 rats (Fig. 59A).

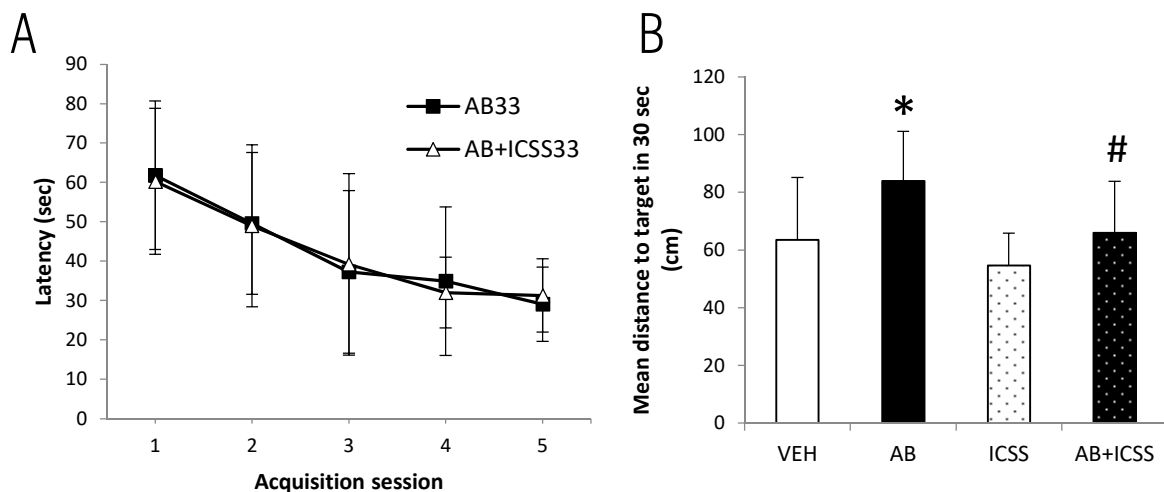


**Fig. 59 | Effects of ICSS treatment on spatial task acquisition and probe test in A $\beta$ -injected rats. A.** Mean escape latencies ( $\pm$ SD) for the five acquisition sessions in the MWM, for AB33 and AB+ICSS33 rats trained between days 26-30 after A $\beta$  injection. **B.** Mean distance to target area ( $\pm$ SD) during the first 30 seconds of probe test. n=8, 10, 7 and 9 rats/group (VEH33, AB33, ICSS33 and AB+ICSS33, respectively). \*p<.05 vs VEH; #p<.05 vs AB.

### Effect of ICSS on DBN levels in A $\beta$ -injected rats

AB+ICSS33 rats did not present any significant difference in DBN levels with respect to VEH33 in any of the studied regions, including those affected in AB33 group. In fact, a tendency of DBN increase was found in AB+ICSS33 rats with respect to AB33, in CA1 *stratum oriens* ( $p=.061$ ) and DG hilus region ( $p=.056$ ) (Fig. 51,52).

Additionally, correlations found in AB33 group between DBN levels in superficial layers of entorhinal cortex and behavioural affection (previously presented in Fig. 53), disappeared in AB+ICSS33 group, approximating to VEH33 dynamics (Fig. 60).

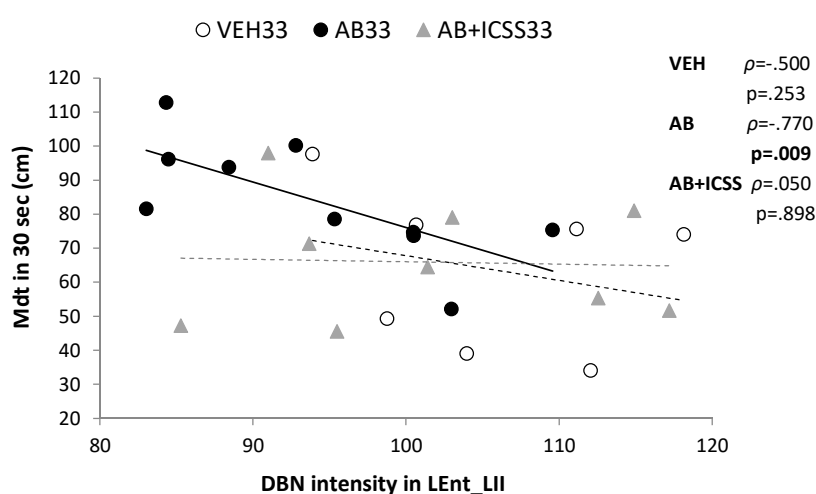


**Fig. 60** | Relation between DBN levels in superficial layers of lateral entorhinal cortex and spatial memory in ICSS-treated AB rats. Scatter plot showing the relation between DBN immunolabelling intensity in layer II of lateral entorhinal cortex with mean distance to target area during the first 30 sec of probe test, in VEH33, AB33 and AB+ICSS33 groups, showing loss of correlation in AB+ICSS33 group and approximation to VEH33 dynamics. Each dot represents a single rat. Spearman's correlation test was used to determine significance ( $p<.05$ ).  $\rho$  = Spearman's correlation coefficient;  $n=7, 10$  and  $9$  rats/group (VEH33, AB33 and AB+ICSS33, respectively). Abbreviations: L: layer; LEnt: lateral entorhinal cortex; Mdt: mean distance to target area.

### Effect of ICSS on ptau levels in A $\beta$ -injected rats

No significant differences between AB+ICSS33 and VEH33 groups were found in phosphorylated tau levels in any region, including those regions showing increase in AB33 (Fig. 57,58). ICSS effects on AB33 rats were evident in the most distal part of CA1, where a significant reduction was found ( $p=.028$ ) (Fig. 57,58).

## 2.4. Summary

Table 13 shows a summary of the main results of this study, regarding affectations displayed by A $\beta$  model in the “15-22 days” (AB22 group) and the “26-33 days” (AB33 group) time windows in relation to the studied AD hallmarks, as well as the effect of ICSS administered in AB33 rats.

**Table 13 | Summary of the main results in Study 2.** Table includes the effects of A $\beta$  injection, as well as of ICSS treatment on A $\beta$ -injected rats, on the studied behavioural and cell/molecular AD hallmarks.

	<b>A<math>\beta</math> EFFECT (15-22 DAYS)</b>		<b>A<math>\beta</math> EFFECT (26-33 DAYS)</b>		<b>ICSS EFFECT ON AB33 RATS</b>	
<b>Behaviour</b>	MWM acquisition: $\uparrow$ latencies sessions 4 and 5 MWM retention: $\downarrow$ time i target quadrant and annulus, $\uparrow$ distance to target MWM reversal: $\uparrow$ average latency		MWM acquisition: null effects MWM retention: $\uparrow$ distance to target in first 30 sec MWM reversal: $\uparrow$ 1 <sup>st</sup> trial latency		MWM acquisition: null effects MWM retention: $\downarrow$ distance to target in first 30 sec MWM reversal: null effects (data not shown)	
	<b>Temporal-parietal regions</b>	<b>Frontal regions</b>	<b>Temporal-parietal regions</b>	<b>Frontal regions</b>	<b>Temporal-parietal regions</b>	<b>Frontal regions</b>
<b>Neurodegen.</b>	No effect detected	$\downarrow$ number of neurons in PrL_LII-III	$\downarrow$ number of neurons in CA3	No effect detected	-	-
<b>DBN</b>	$\uparrow$ RSA_LVa	$\downarrow$ PrL_LIIb/III, $\uparrow$ PrL_LV	$\downarrow$ LEnt_LI-III, DG, CA1, RSG_LI	$\downarrow$ PrL_LIII	Recovers VEH levels. Tendency $\uparrow$ in DG and CA1	Recovers VEH levels
<b>ptau Ser202/Thr205</b>	$\uparrow$ CA1, DG	$\uparrow$ PrL_LIII/V	$\uparrow$ LEnt_LII, RSA_LIII	No effect detected	$\downarrow$ CA1 and recovers VEH levels in others	No effect detected

## 2.5. Discussion

Results from this study support the idea that a single amyloid- $\beta$  injection leads to a non-stable model of AD-like characteristics. While behavioural deficits are more evident when evaluated at the time window of 15-22 days after injection than at 26-33 days, suggesting a transiency on this model, molecular pathology of early AD is better emulated at the later time. At this moment, ICSS treatment consisting of 5 post-training sessions is able to ameliorate both remaining behavioural alterations and molecular pathology.

### Methodological considerations regarding A $\beta$ injection to model AD

Injection of amyloid- $\beta$  into the brain has been one of the most extended strategies to model sAD in rodents, sustained by the assumed role of A $\beta$  in triggering AD etiopathology. However, far from being a consistent procedure, a great variety of methodologies leading to different behavioural and neuropathological outcomes have been reported in a great deal of published works. A lower amount of studies had made an effort to assess crucial conditions for optimal model development (Giovannelli et al., 1995; Stine et al., 2011; Ueno et al., 2014; Kasza et al., 2017). Among them, Kasza et al. address the problem of the structural heterogeneity of oligomeric samples and present the development of a sAD rat model by icv injection of a low-dose but well-characterized oligomeric preparation, obtained by incubating A $\beta$  1-42 25  $\mu$ M for 168 h at 37°C. These conditions give rise to small oligomers of definite size and structure able to diffuse to brain parenchyma and cause the highest neurotoxicity (Kasza et al., 2017). Kasza's model showed spatial memory disturbances evaluated in the MWM, together with increased tau immunopositivity and decreased neuron viability in the hippocampus, seven days after A $\beta$  injection. On the basis of their results, the present study assessed the stability of this model over time, by characterizing spatial memory and neuropathology at 15-22 days and in a delayed term of 26-33 days, in order to evaluate its suitability for ICSS treatment testing.

Stability of the effects induced by an acute A $\beta$  exposure has been put into debate, as A $\beta$  is suggested to be eventually cleared from the brain parenchyma (Wong et al., 2016). It has been reported that a single injection of A $\beta$  oligomers resulted in transient behavioural deficits and histopathological effects, including A $\beta$  deposition and tau immunoreactivity (Sigurdsson et al., 1997; Cleary et al., 2005; Wong et al., 2016; Karthick et al., 2019). According to these results, the present study shows that injection of low-dose well-characterized aggregates resulted in transient spatial learning deficits, as well as non-stable histopathological effects.

### Behavioural and neurodegenerative AD-like affectations partially recover long after A $\beta$ injection

In the time window of 15-22 days after A $\beta$  injection, AB rats presented clear spatial learning and memory deficits, concerning both acquisition as well as retention at 72 hours. Cognitive flexibility, assessed in the reversal test, was also affected. These deficits develop along with a visible neurodegeneration in prelimbic cortex. Behavioural impairment was almost non-existent at a later time, evaluated 26-33 days after A $\beta$  injection. These results are in line with the findings by Karthick et al., who reported spatial learning and memory impairment 15 days after A $\beta$ -injection, which was not present on day 30 (Karthick et al., 2019). However, the present results suggest that rats trained at days 26-30 after A $\beta$  injection preserved a difficulty in spatial retention, revealed by differences in mean distance to target area in the probe test. While this variable has not historically been as popular as latencies to assess spatial memory impairment, it is considered a robust variable to assess spatial memory accuracy, especially in age-related impairment (Vorhees and Williams, 2006; Gallagher et al., 2015). Moreover, prelimbic neurodegeneration was also absent at day 33. Still, by then neuronal cell loss was perceived in CA3 hippocampal subfield. It was suggested that the fate of Nissl dark-stained neurons could differ depending on the regions of the brain, ending to survive in neocortex but dying in the hippocampus after traumatic brain injury (Ooigawa et al., 2006). Thus, while most behavioural and neurodegeneration signs seem to be transient in the present model, hypothetically cumulated neurodegeneration in hippocampus seem to be durable.

### Molecular AD-like affectation presents a particular progression after A $\beta$ injection

In the case of molecular hallmarks of AD synaptic damage (DBN levels) and tauopathy (ptau levels), disturbances in A $\beta$ -injected animals were found both at 22 and 33 days. However, a shift in regional distribution of molecular pathology is noticed.

On the one hand, a preference for prefrontal affectation was found at 22 days. Matching with neurodegeneration in layer II-III of prelimbic cortex, a significant decrease in DBN protein levels in layers II and III and an increase in ptau levels in layers III and V were found in this area. Direction of these changes corresponds to the expected alteration for AD described in the introduction part. Intriguingly, DBN levels were significantly increased in layer V of prelimbic cortex as well as in layer V of agranular retrosplenial cortex. This can be interpreted as an early and transient compensatory response to initial damage, which was already described and discussed for both AD patients as well as animal and *in vitro* AD models

(Merlo et al., 2019), aiming to tolerate A $\beta$  insult and delay the appearance of symptoms. In favour of this hypothesis are the findings of correlation analyses, showing association of a higher neurodegeneration percentage in the prelimbic cortex with increased DBN levels in different prefrontal and temporal-parietal regions, as well as association of higher ptau levels in rhinal cortices with higher DBN levels in prelimbic layers, both specific for AB group.

Additionally, increased DBN levels in rhinal cortices and layer V of prelimbic cortex were found associated with better behavioural performance. Although association between DBN levels and behavioural performance is also present in control rats, it is stronger and extended to more behavioural variables in AB group, with those less affected in cognition presenting more similar DBN levels to VEH rats. Thus, results suggest that behavioural impairment is somehow more associated with DBN alteration than with that of ptau, which holds no correlation with behavioural variables. This is in line with the idea that synaptic damage correlates more robustly with the degree of cognitive impairment than the number of amyloid plaques, tangles, and neuronal loss does (Ishizuka and Hanamura, 2017). Nonetheless, ptau levels do correlate with other neuropathological signs in the present study. In CA1 and DG hippocampal regions, the only temporal regions where ptau was found significantly increased in AB rats, and in rhinal cortices, ptau levels correlate with neurodegeneration and DBN levels of prelimbic cortex. These results demonstrate a clear interrelation of the different pathways and of the interconnected regions, suggesting once more a central part of prelimbic cortex in histopathological damage 22 days after A $\beta$  injection.

On the other hand, at 33 days, histopathological alteration in AB rats is mainly found in parietal-temporal regions, with a special relevance of lateral entorhinal cortex. In this sense, ptau levels were significantly increased only in layer II entorhinal cortex, and a tendency was found in layer III agranular retrosplenial cortex. DBN is found now decreased in layers I, II and III of lateral entorhinal cortex, correlating again with impaired mean distance to target area in behavioural test, and in layer I of granular retrosplenial cortex. Additionally, DBN is also decreased in hippocampal regions CA1 and DG and layer III prelimbic cortex, matching the regions with ptau pathology at 22 days, evidencing once more, at least, an interrelation of these molecular mechanisms, which was already suggested (Julien et al., 2008). Moreover, this out-of-phase concordance could insinuate a slightly downstream position of DBN decrease to tau pathology, in line with the idea that dysregulation of synaptic proteome is mediated by pathological tau (Jadhav et al., 2015).

Taken together, regional distribution of histopathological affectations at 33 days, concentrated in entorhinal cortex and hippocampus, resemble those typically described for early AD (Braak et al., 2006a; Khan et al., 2014), more than at 22 days, focused on prefrontal cortex. This progression from frontal cortex to temporal regions, which differs from the one described for AD (Braak et al., 2006a; Joy et al., 2018), together with the transiency of cognitive deficits, yields this single A $\beta$ -injection model not suitable for long-term treatment assessment. And what is more, attempts to optimize the model pursuing an enduring supply of A $\beta$  oligomers by implanted osmotic pumps or cannulas seemed to be incompatible with the proposed experimental design. In this sense, repeated infusion of oligomeric solution through a cannula resulted in failed ICSS behaviour establishment in our lab (data not shown), suggesting that injection of obstructive-prone amyloid solution propelled the electrode from the target site.

#### ICSS treatment partially alleviates long-lasting molecular AD hallmarks in the A $\beta$ -injected model


Nevertheless, this unsteadiness does not exclude the use of acute A $\beta$  injection as a model for assessing short-term effects of ICSS treatment in early-phase molecular hallmarks of AD, which are adequately emulated 33 days after injection. Present results show that ICSS amelioration of retention at 72 h goes along with subtle changes on DBN and ptau levels. In this sense, any of the molecular alterations found in AB rats were present in AB+ICSS group, neither related with differences in their levels nor in specific correlations, thus recovering a control-like pattern. Moreover, ICSS administered to AB rats causes a significant decrease in ptau levels in CA1, and some tendencies of increase in DBN levels were also found in CA1 and DG (at the hilus) hippocampal subfields, suggesting in accordance with Study 1 that ICSS mechanisms interfere with those of AD.

#### Conclusions

In conclusion, results from this study suggest that a single injection of low-dose well-characterized A $\beta$  oligomers generates a useful model to test the effect of short treatments on initial molecular hallmarks that occur in AD. In this sense, 5 post-training ICSS sessions were able to avoid ptau increase and DBN decrease in entorhinal cortex and hippocampus found in rats 33 days after A $\beta$  injection. Thus, these findings keep encouraging the research of ICSS administered to the MFB to fight sAD early molecular hallmarks. However, the observed transient behavioural impairment, together with instability and regressive regional migration of histopathological affectation, yields this model non suitable for long-term treatment

assessment. To this aim, other models that ideally present coexistence of behavioural and molecular pathology of early AD at a late time point after injection would be more appropriate.





### STUDY III. ICSS TREATMENT EFFECTS ON CELL AND MOLECULAR MARKERS OF EARLY ALZHEIMER'S DISEASE IN STZ-INJECTED MODEL

Results from Study 2 suggest that ICSS treatment is able to avoid molecular alterations related to early AD in a rat model generated by A $\beta$  icv injection. However, this model presented some limitations, especially regarding its transiency, that restrict its use in further studies. This section presents the results from Study 3, which according to the third aim of this thesis intended to assess the molecular effects of ICSS treatment in a sAD rat model obtained by STZ icv injection. Thus, effects of ICSS treatment administered in STZ model were assessed on the cell and molecular markers associated to early AD pathology, including neurodegeneration, DBN, tau and APP, as well as miRNAs and SIRT1, revealed in Study 1 to be potential treatment biomarkers in serum. Additional non-molecular affectations found in STZ-injected rats, including behavioural affection supporting AD resemblance, are also presented in first place as a general characterization upholding STZ model.

From the total of 38 animals intended for this study, seven subjects were excluded from the analysis. On the one hand, two STZ-injected rats died during the course of the study. Another two STZ rats did not display the characteristic body weight loss and increased reactivity, with further statistical analyses revealing these rats as outliers regarding behavioural affectations, and therefore were considered not to achieve the model. Thus, mortality index of 10.5% and model failure of 10.5% is reported for STZ injection in this study. On the other hand, one ICSS rat was euthanized because of convulsions derived from ICSS treatment. Finally, two VEH rats displayed poor performance in behavioural tests, and further statistical analyses revealed these rats as outliers. The final sample consisted of 31 subjects. Final sample size in each group is shown in Table 14, which summarizes the experimental conditions of the groups analysed in this study.

**Table 14** | Summary of the groups composing Study 3 is presented as a brief recap of the experimental design in Study 3, including final sample size for each group.

<i>Group</i>	<i>Icv injection</i>	<i>Treatment</i>	<i>MWM acquisition</i>	<i>Serum collection</i>	<i>MWM probe test</i>	<i>Sacrifice</i>	<i>Final sample size</i>
VEH	Vehicle	5 sham sessions on	On days 33-37	Day 37	Day 40	Day 40	11
STZ	STZ	days 33-37					10
ICSS	Vehicle	5 ICSS sessions					5
STZ+ICSS	STZ	on days 33-37					5

### 3.1. Physiological, histomorphological and behavioural affectations in STZ-injected model

General characterization of the non-molecular affectation in STZ model is presented in this section.

#### Physiological affectation in STZ-injected rats

A significant loss in body weight after the surgery was found in STZ-injected rats compared to VEH-injected rats ( $p=.020$ ,  $p=.021$ ,  $p=.021$ ,  $p=.011$ ,  $p=.001$  at days 1, 2, 3, 4 and 5 post-surgery) (Fig. 61A). Body weight was slowly regained after the post-surgery recovery period

and completely recovered before the start of the behavioural tasks, although significant differences with respect to VEH remain at the end of the study ( $p=.048$ )(Fig. 61A). Moreover, significant increased reactivity to manipulation assessed during the post-surgery recovery period was noticed in STZ rats ( $p<.001$  vs VEH)(Fig. 61B).

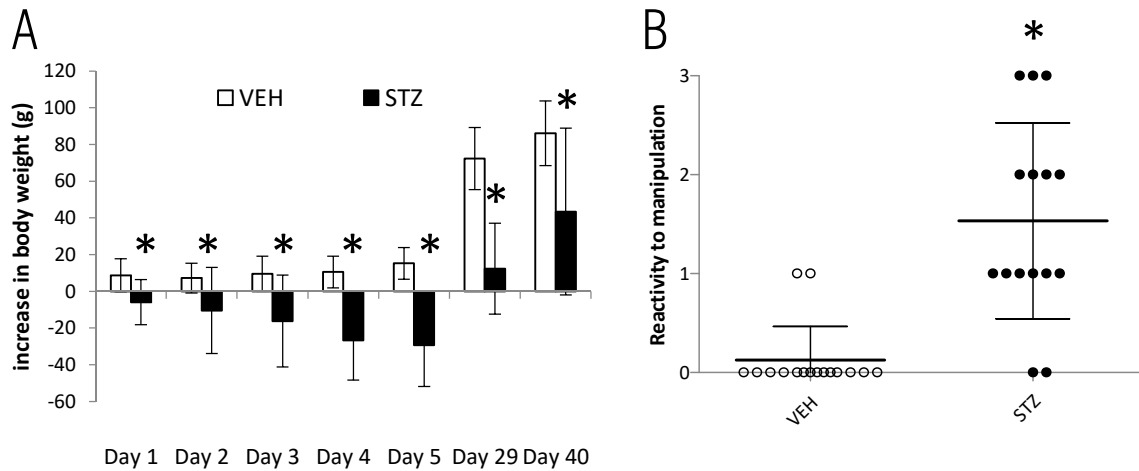


**Fig. 61 | Physiological affectations in STZ-injected rats. A.** Change in body weight compared to surgery day, at different time points in the post-surgery recovery period (days 1 to 5), before the initiation of behavioural tasks (day 29) and at the end of the study (day 40) for STZ and VEH animals. Data are presented as mean $\pm$ SD.  $n=8$  and 7 rats/group (VEH and STZ, respectively). \* $p<.05$  vs VEH. **B.** Reactivity to manipulation assessed in a 4-level scale during the post-surgery recovery period, for all STZ and VEH-injected animals, including those intended for later ICSS treatment. Each dot represents a single rat, and group mean $\pm$ SD is depicted;  $n=16$  and 15 rats/group (VEH-injected and STZ-injected, respectively). \* $p<.05$  vs VEH.

### Morphologic changes in the lateral ventricles and periventricular structures in STZ-injected rats

Morphologic alteration in the lateral ventricles and periventricular structures in STZ rats became evident during the tissue processing and histological analyses.  $\chi^2$  analysis revealed a significant greater incidence of lateral ventricle enlargement and presence of compressed hippocampus and decreased corpus callosum thickness in STZ rats (Fig. 62, Table 15). Two STZ rats displayed a degree of hippocampal compression so extreme that immunohistochemical analyses could not be performed in this area (Fig. 62B).

**Table 15 | Relationship between incidence of morphologic abnormalities and STZ administration.** Table shows the incidence (%) of ventricular and paraventricular morphologic abnormalities in VEH and STZ groups, together with p-values according to  $\chi^2$  analysis. n= 8 and 7 rats/group (VEH and STZ, respectively). Abbreviations: cc: corpus callosum; HP: hippocampus; LV: lateral ventricle.

	<i>LV enlargement</i>	<i>Compressed HP</i>	<i>Decreased cc thickness</i>
<i>VEH</i>	0%	12.5%	0%
<i>STZ</i>	57.1%	100%	100%
	<b>p=.013</b>	<b>p=.002</b>	<b>p=.001</b>

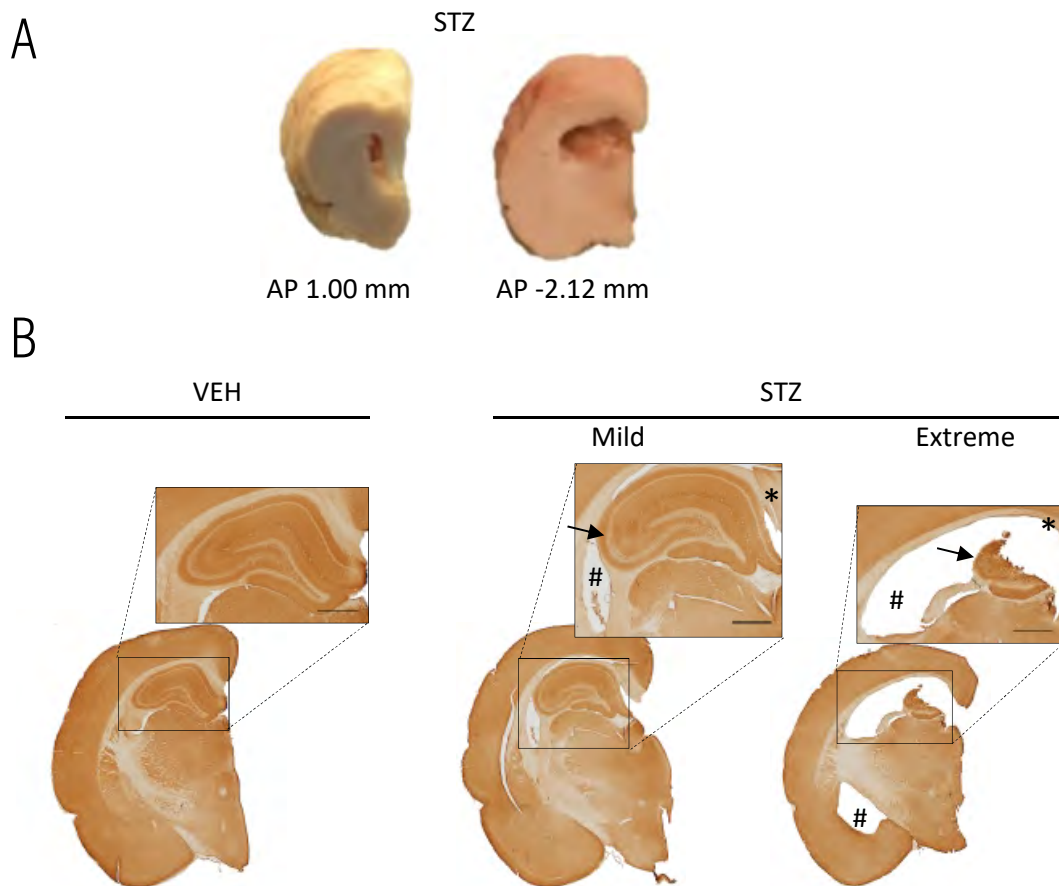


**Fig. 62 | Morphologic alterations in STZ-injected rat's brain.** **A.** Representative images of STZ left hemisphere coronal sections during cryotomy, showing ventricle enlargement and hippocampus compression at different antero-posterior distances from Bregma. **B.** Representative images of DBN stained coronal sections, for VEH and STZ rats, showing lateral ventricle enlargement (#) and hippocampus compression (arrow), together with corpus callosum shrinkage resulting in breakage (\*) in both mild cases (the most frequent type of cases) and extreme cases (only observed in two rats) (scale bar = 1 mm).

Behavioural affectation in STZ-injected rats

A  $2 \times 5$  ANOVA for repeated measures was conducted to study the acquisition phase performance of the MWM on days 33-37 after STZ injection. Analysis of the GROUP effect was statistically significant ( $F_{1,19}=15.443$ ,  $p=.001$ ), indicating a worse performance of the STZ group. Even though  $GROUP \times SESSION$  interaction did not reveal a significant difference ( $F_{4,76}=.904$ ,  $p=.466$ ), further simple effect analysis confirmed significant differences between groups in the 2<sup>nd</sup>, 3<sup>rd</sup> and 4<sup>th</sup> acquisition sessions according to their escape latencies ( $p=.003$ ,  $p=.013$  and  $p=.009$ , respectively) (Fig. 63A). In addition, the main effect of the SESSION was statistically significant ( $F_{4,76}=4.172$ ,  $p=.004$ ), showing learning in both experimental groups.

Moreover, an increased thigmotaxis was also perceived for STZ rats in the MWM acquisition phase, being statistically significant for the first 3 sessions, and presenting a tendency for sessions 4 and 5 ( $p=.007$ ,  $p=.010$ ,  $p=.042$ ,  $p=.061$  and  $p=.068$  for sessions 1 to 5, respectively) (Fig. 63B).

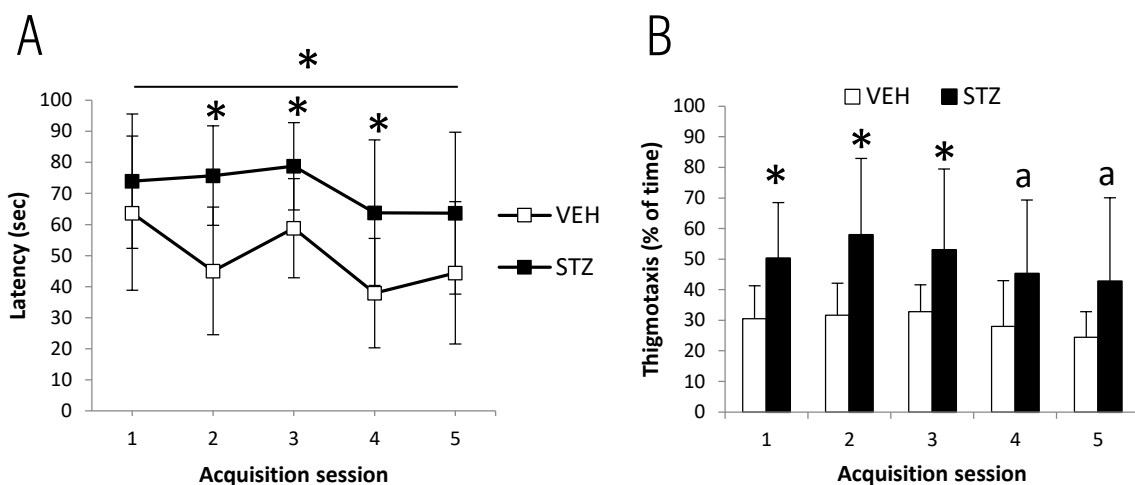


**Fig. 63 | Effects of STZ injection on spatial task acquisition. A.** Mean escape latencies ( $\pm$ SD) for the five acquisition sessions in the MWM, for STZ and VEH rats. **B.** Thigmotaxis or mean percentage of time spent in the walls ( $\pm$ SD) for the five acquisition sessions in the MWM, for STZ and VEH rats.  $n=11$  and  $10$  rats/group (VEH and STZ, respectively). \*  $p<.05$  vs VEH; **a**  $p\leq.07$  vs VEH.

Alteration in spatial retention was also revealed in STZ rats, which presented a significant decrease in percentage spent in the target quadrant ( $p=.023$ )(Fig. 64A) and in the annulus ( $p=.008$ )(Fig. 64B), together with an increase in the mean distance to target area ( $p=.013$ )(Fig. 64C) during the whole duration of the MWM probe test, compared to VEH.

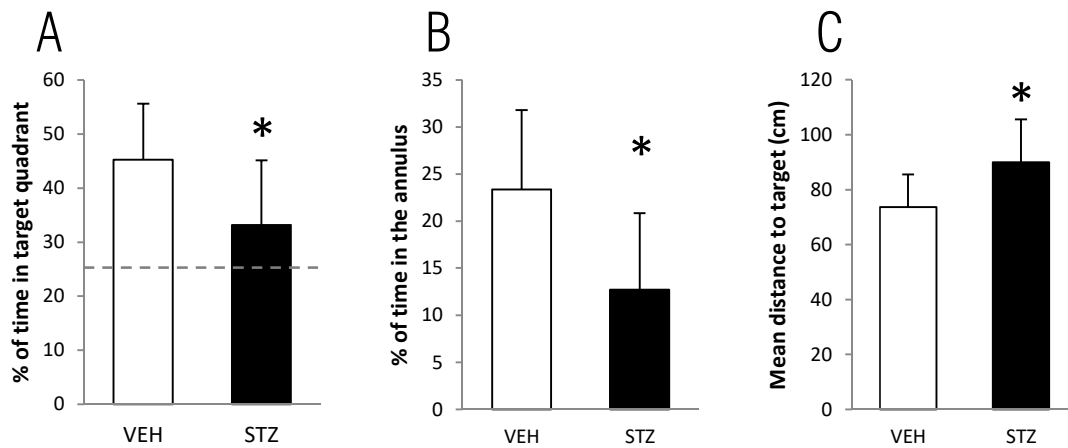


**Fig. 64 | Effects of STZ injection on spatial probe test.** Results of the MWM probe test for VEH and STZ rats. **A.** Percentage of time spent in target quadrant. The dashed line represents chance level. **B.** Percentage of time spent in the annulus area. **C.** Mean distance to target area during the whole test. Data are presented as mean±SD; n=11 and 10 rats/group (VEH and STZ, respectively). \* $p<.05$  vs VEH.

### 3.2. ICSS effects on AD hallmarks in STZ-injected rats

This section presents ICSS effects on cell and molecular AD hallmarks found in STZ-injected rats. Thus, for each hallmark, alterations displayed by STZ model are described and, after that, ICSS effects on these alterations are reported. In order to relate them with cognitive improvement, evidence of ICSS behavioural effect in STZ-injected rats is first presented.

#### Evidence of ICSS effect on behavioural affectations of STZ-injected rats

Some of the affected variables in STZ rats were improved after administration of 5 post-training sessions of ICSS. Latency in the third session of acquisition phase was reduced in the group receiving ICSS ( $p=.028$  vs STZ). Moreover, although no significant differences were found between STZ and STZ+ICSS groups in the probe test, differences found in the percentage of time spent in the target quadrant between STZ and VEH group disappeared in the STZ+ICSS group ( $p=.357$  vs VEH) (Fig. 65).

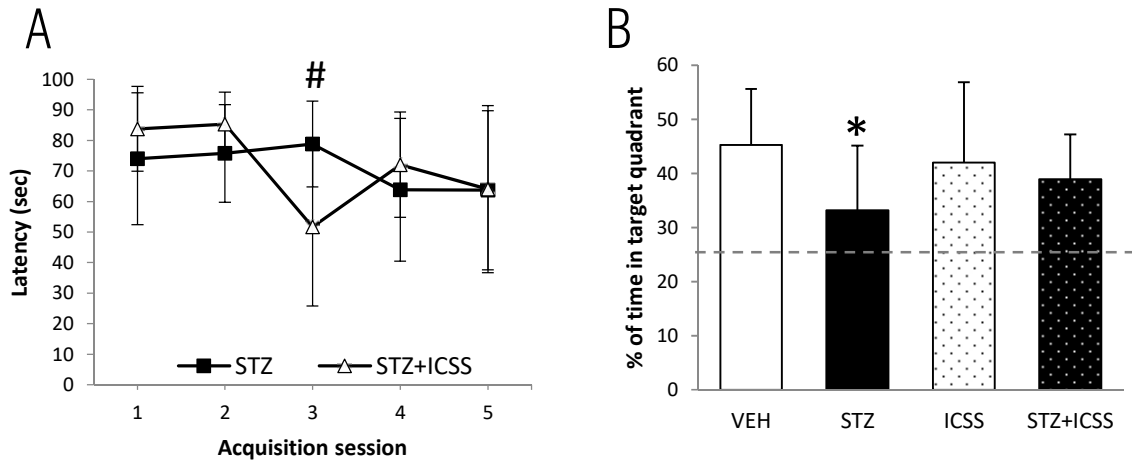


**Fig. 65 | Effects of ICSS treatment on STZ-induced disturbances on spatial learning and memory. A.** Mean escape latencies ( $\pm$ SD) for the five acquisition sessions in the MWM, for STZ and STZ+ICSS rats. **B.** Mean percentage of time spent in target quadrant ( $\pm$ SD) in the MWM probe test. The dashed line represents chance level.  $n=10$  or  $5$  rats/group (STZ and STZ+ICSS groups, respectively). \* $p<.05$  vs VEH; # $p<.05$  vs STZ.

#### Effect of ICSS on neurodegeneration in STZ-injected rats

Analysis of Nissl-stained sections revealed a significant decrease in the total number of neurons in CA1 region ( $p=.027$  vs VEH), but not in CA3 or DG hippocampal subfields, for STZ rats (Fig. 66A,B). Moreover, compared to control, neurons in STZ rats seem to exhibit a more vacuolated and swallowed morphology (Fig. 66A), resulting in more sparse density in CA1 and DG regions ( $p=.001$  and  $p=.021$  vs VEH, respectively) (Fig. 66C).

While ICSS treatment alone did not trigger any significant change in hippocampus neuronal number or density, when administered to STZ rats it seems to reverse hippocampal neurodegeneration displayed by STZ model. Thus, STZ+ICSS group presented a significant increase in DG neuronal density ( $p=.029$ ), and a tendency in CA1 neuronal density ( $p=.056$ ) (Fig. 66B,C) compared to STZ group.

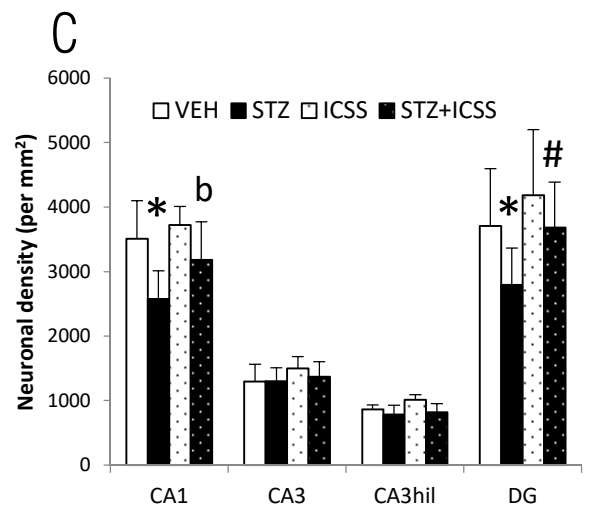
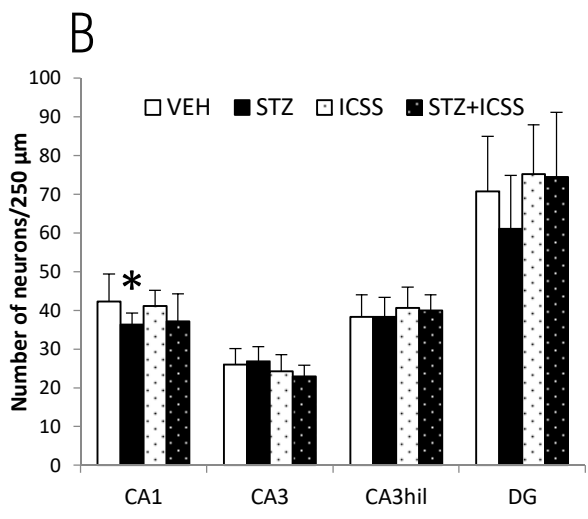
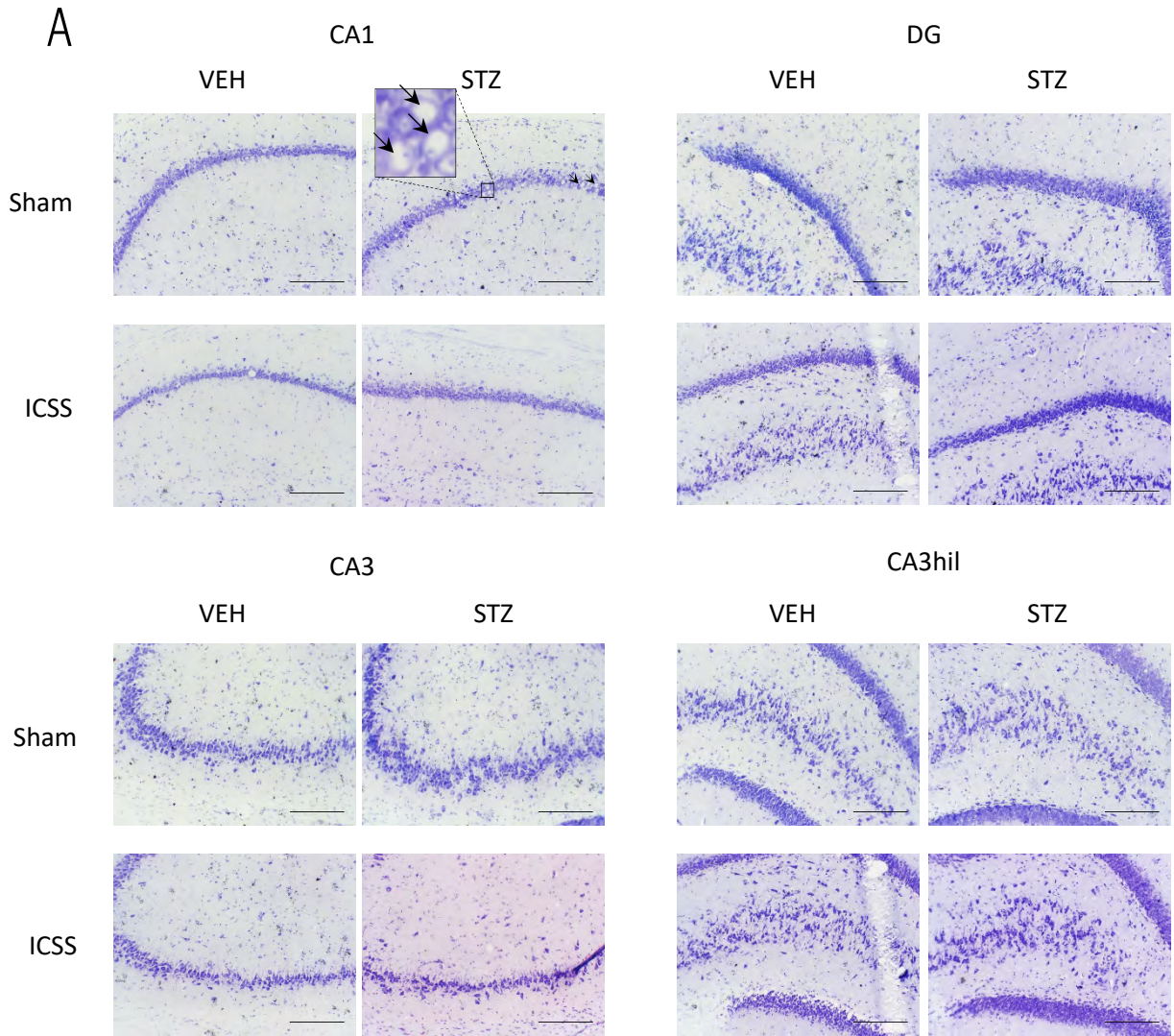




**Fig. 66 | Effects of STZ injection and ICSS treatment on hippocampal neurodegeneration** (see figure on the previous page). Results of Nissl staining analysis in hippocampal subregions, for VEH, STZ, ICSS and STZ+ICSS groups. **A.** Representative photomicrographs for Nissl staining in each hippocampal subregion for each group (scale bar=250  $\mu$ m). Examples of swallowed and vacuolated neurons found in STZ group are pointed with a black arrow, and shown magnified. **B-C.** Neuronal count in 250  $\mu$ m layer length (B) and neuronal density per mm<sup>2</sup> (C) in CA1, CA3 (distal part), CA3hil (proximal part, at the region of hilus) and dentate gyrus (DG) hippocampal subregions. Data are presented as mean $\pm$ SD; n=11, 8, 5 and 5 rats/group (VEH, STZ, ICSS and STZ+ICSS, respectively). \*p<.05 vs VEH; #p<.05 vs STZ; **b** p $\leq$ .07 vs STZ.

Regarding medial prefrontal cortex, no differences were found neither in the total nor in normal/degenerating number of neurons in prelimbic cortex layer II-III between STZ and VEH groups (Fig. 67A,B). However, important neurodegeneration was noticed in dorsal tectum (DTT) structure in STZ rats (Fig. 67C). Statistical analyses revealed significant differences between STZ and VEH groups in the number of DTT normal neurons (p=.017) and the percentage of neurodegeneration (p=.024), the last negatively correlating with neuronal density in hippocampal neurodegenerating areas for STZ group (Fig. 67D,E and Fig. 68). No differences were found in STZ+ICSS group with respect to STZ, but neither with respect to VEH (Fig. 67).

Neurodegenerative alteration in the hippocampus nor in DTT was not found to be significantly correlated with altered behavioural variables. Similarly, the recovery induced by ICSS is not significantly related with any improvement on behavioural performance.

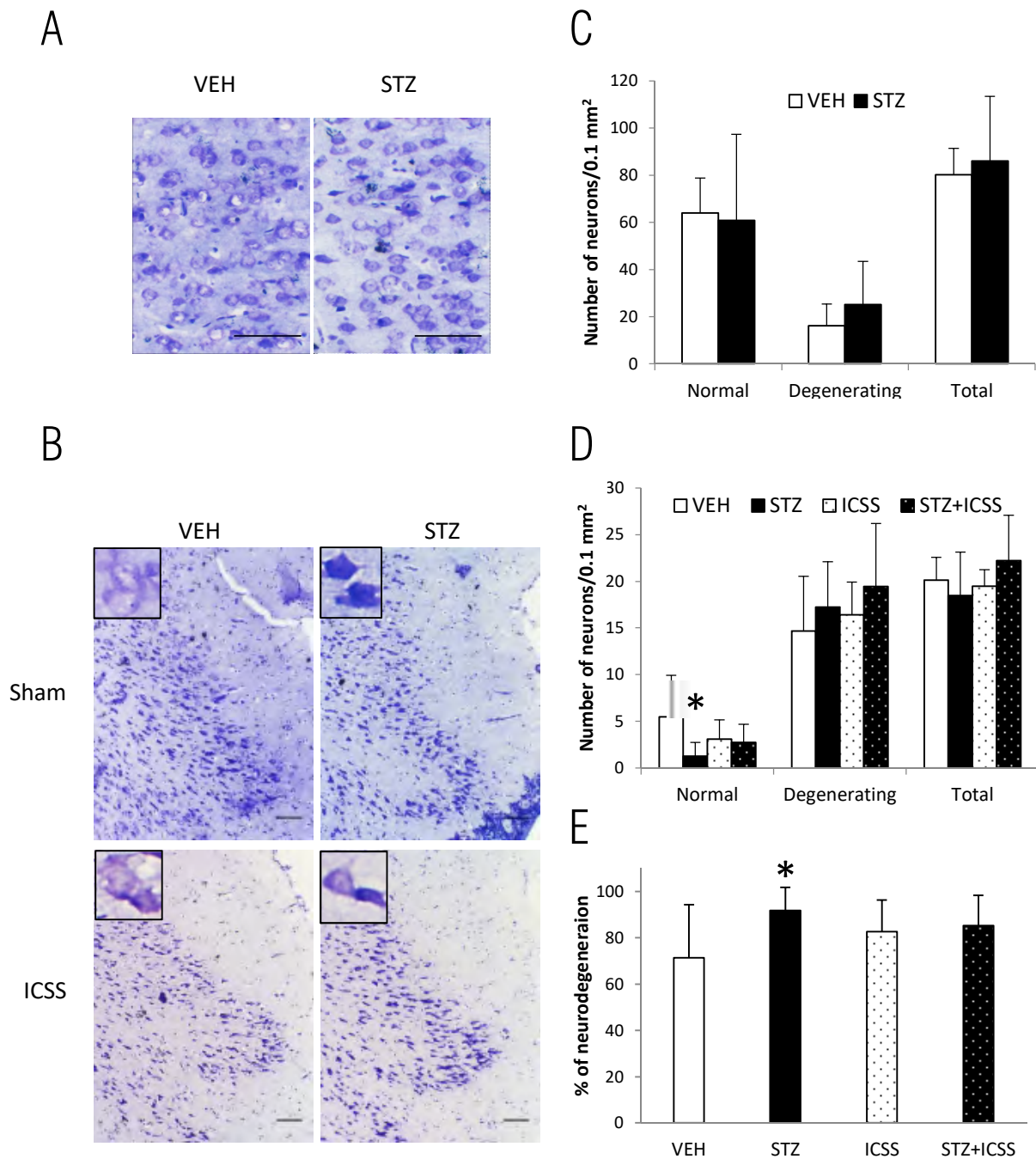


**Fig. 67 | Effects of STZ injection and ICSS treatment on medial prefrontal cortex neurodegeneration.** **A-B.** Representative photomicrographs for Nissl staining in layer II-III of prelimbic cortex (A) and DTT (B) for each group (scale bar=100  $\mu$ m). **C-E.** Neuronal count per 0.1 mm<sup>2</sup> (C-D) and percentage of neurodegeneration (E) in layer II-III of prelimbic cortex (C) and DTT (D-E). Data are presented as mean $\pm$ SD; n=10, 10, 4 and 5 rats/group (VEH, STZ, ICSS and STZ+ICSS, respectively). \*p<.05 vs VEH.

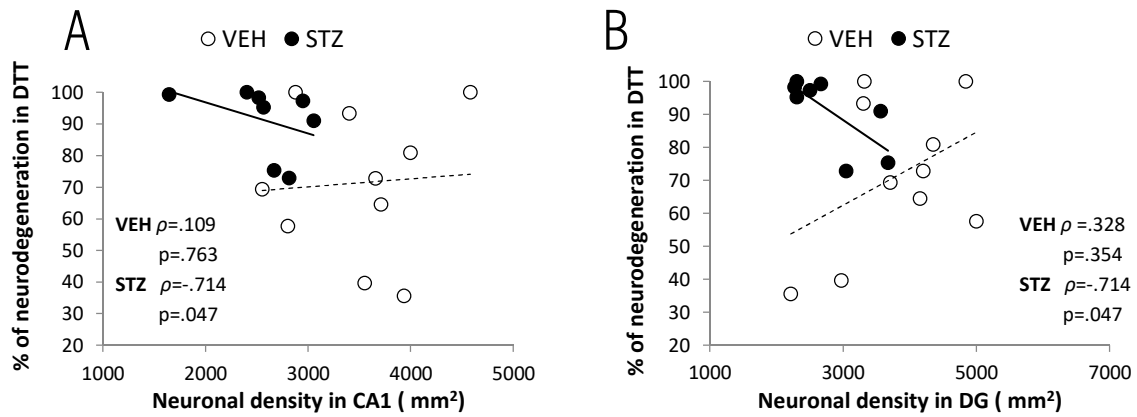


**Fig. 68 | Correlation between neurodegeneration in DTT and HP after STZ injection.** Scatter plot showing the relation between percentage of neurodegeneration in DTT and neuronal density (neurons per mm<sup>2</sup>) in CA1 and DG hippocampal subfields, according to Nissl staining analysis, in VEH and STZ groups. Each dot represents a single rat. Spearman's correlation test was used to determine significance ( $p < .05$ ).  $\rho$  = Spearman's correlation coefficient;  $n=10$  and  $8$  rats/group (VEH and STZ, respectively).

#### Effect of ICSS on DBN levels in STZ-injected rats

DBN levels were not altered in STZ-injected rats with respect to VEH in any of the regions analysed by immunohistochemistry, neither in temporal-parietal regions, including rhinal cortices, hippocampus and retrosplenial cortex, nor in frontal regions, including prelimbic cortex (Fig. 69,70). Similarly, results from Western blot did not identify any statistical difference between STZ and VEH in DBN levels, neither in medial prefrontal cortex nor in anterior DG extracts (Fig. 73,74). DBN levels were also not found to be correlated with the affected behavioural variables in STZ group.

ICSS treatment caused an increase in DBN levels, both in VEH and STZ rats, in different layers of rhinal cortices. In VEH rats, ICSS effect is more extended, involving layer I of lateral entorhinal cortex ( $p=.053$  and  $p=.028$  for layers Ia and Ib, respectively), layers I and II of perirhinal cortex ( $p=.009$ ,  $p=.013$  and  $p=.036$ , for layers Ia, Ib and II respectively) and layers I to V of entorhinal cortex ( $p=.003$ ,  $p=.023$ ,  $p=.053$ ,  $p=.028$ ,  $p=.055$  for layers Ia, Ib, II, III and Va respectively). Still, ICSS administered to STZ rats is able to increase levels of DBN in layer Ia of lateral entorhinal cortex ( $p=.028$ ), and layer V of entorhinal cortex ( $p=.045$ ) (Fig. 69,70A). In the other analysed regions, including hippocampus, retrosplenial cortex and prelimbic cortex, no significant increase of DBN levels because of ICSS treatment were found, according both immunohistochemistry and Western blot results (Fig. 69, 70B-D and 73).

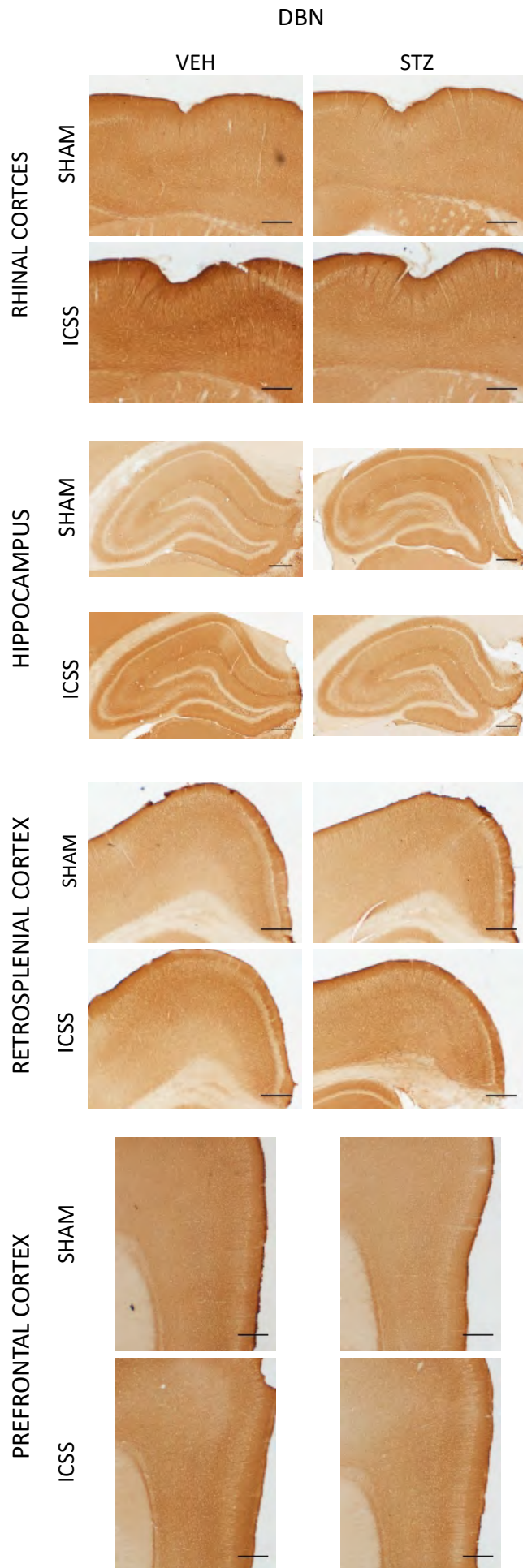


**Fig. 69** | Effects of STZ injection and ICSS treatment on DBN levels. Representative photomicrographs of DBN immunolabelling in rhinal cortices, hippocampus, retrosplenial cortex and prefrontal cortex, for VEH, STZ, ICSS and STZ+ICSS groups (scale bar=500  $\mu\text{m}$ ).

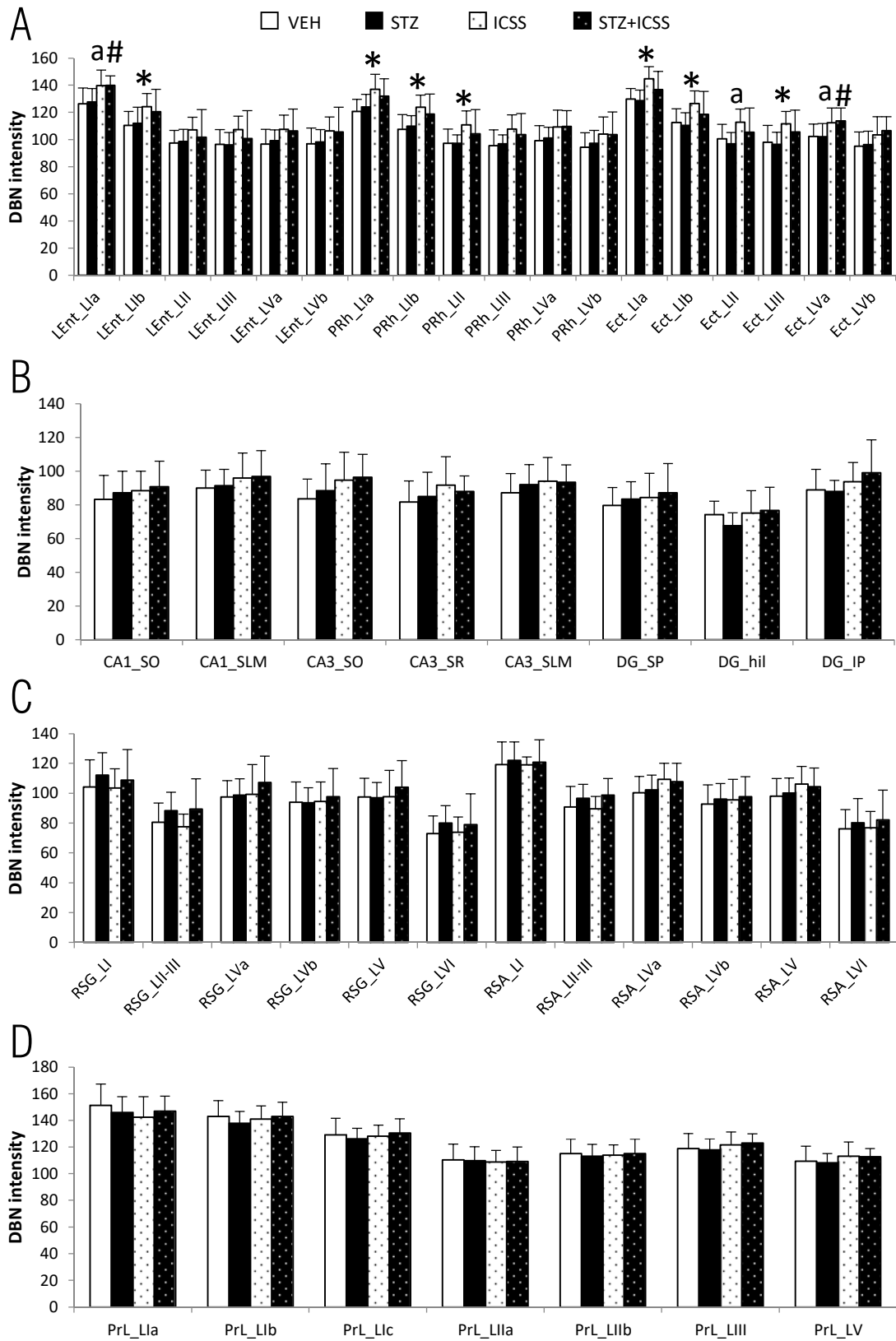


**Fig. 70 | Effects of STZ injection and ICSS treatment on DBN levels** (see figure on the previous page). DBN levels in **A.** rhinal cortices, **B.** hippocampus, **C.** retrosplenial cortex and **D.** prelimbic cortex, for VEH, STZ, ICSS and STZ+ICSS groups, resulting from labelling intensity quantification after DBN immunohistochemistry. Data are presented as mean $\pm$ SD; n=11, 10, 5 and 5 rats/group (VEH, STZ, ICSS and STZ+ICSS, respectively). \* $p < .05$  vs VEH; # $p < .05$  vs STZ; **a**  $p \leq .07$  vs VEH. Abbreviations: DG: dentate gyrus; Ect: ectorhinal cortex; hil: hilus; IP: infrapyramidale; L: layer; LEnt: lateral entorhinal cortex; PRh: perirhinal cortex; PrL: prelimbic cortex; RSA: retrosplenial agranular cortex; RSG: retrosplenial granular cortex; SLM: *stratum lacunosum moleculare*; SO: *stratum oriens*; SP: suprapyramidale; SR: *stratum radiatum*.

### Effect of ICSS on tau and ptau levels in STZ-injected rats

According to immunohistochemistry analysis, levels of tau protein phosphorylated at Ser202/ Thr205 sites were found significantly increased in STZ with respect to VEH group in CA3 hippocampal subregion, both at more distal parts and proximal parts ( $p = .027$ ,  $p = .002$  and  $p = .033$  for CA3\_1, CA3\_2 and CA3\_hilus, respectively), and presented a tendency in proximal CA1 ( $p = .07$  for CA1\_4). In retrosplenial cortex, a significant increase in ptau was found in agranular part layer V ( $p = .049$  and  $p = .067$  for layer Va and Vb, respectively) (Fig. 71, 72). Moreover, levels of ptau in different hippocampal subfields positively correlate with altered latencies in second acquisition session for STZ group (Table 16). Regarding frontal lobe, ptau Ser202/Thr205 alteration in STZ group seem to go in the opposite direction in prelimbic cortex, showing a significant decrease in ptau ( $p = .045$ ) in layer III, according to immunohistochemical analyses (Fig. 71, 72).

Generally speaking, levels of ptau Ser202/Thr205 seemed to be reduced because of ICSS treatment, both in VEH and STZ rats. On the one hand, ICSS treatment administered to VEH rats tended to reduce ptau levels in layer II-III prelimbic cortex ( $p = .006$ ,  $p = .060$ ,  $p = .056$  for layer IIa, IIb and III, respectively) and layer II granular retrosplenial cortex ( $p = .066$ ). On the other hand, STZ+ICSS presented significant decreased levels of ptau Ser202/Thr205 in perirhinal cortex ( $p = .055$  and  $p = .045$  for layer II and global, respectively) and a tendency in layer IIb of prelimbic cortex ( $p = .064$ ), with respect to STZ. Moreover, in CA3, where ptau was found increased in STZ rats, STZ+ICSS presented no differences from VEH group (Fig. 71, 72).

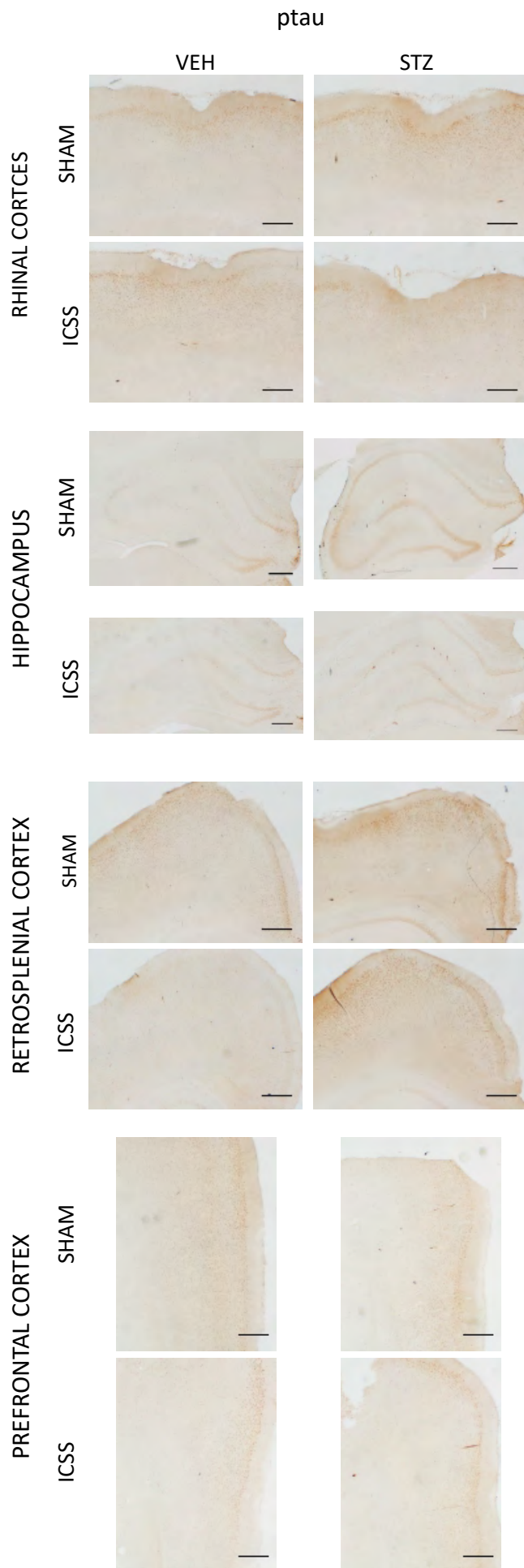


**Fig. 71** | Effects of STZ injection and ICSS treatment on ptau levels. Representative photomicrographs of ptau immunolabelling in rhinal cortices, hippocampus, retrosplenial cortex and prefrontal cortex, for VEH, STZ, ICSS and STZ+ICSS groups (scale bar=500  $\mu$ m).

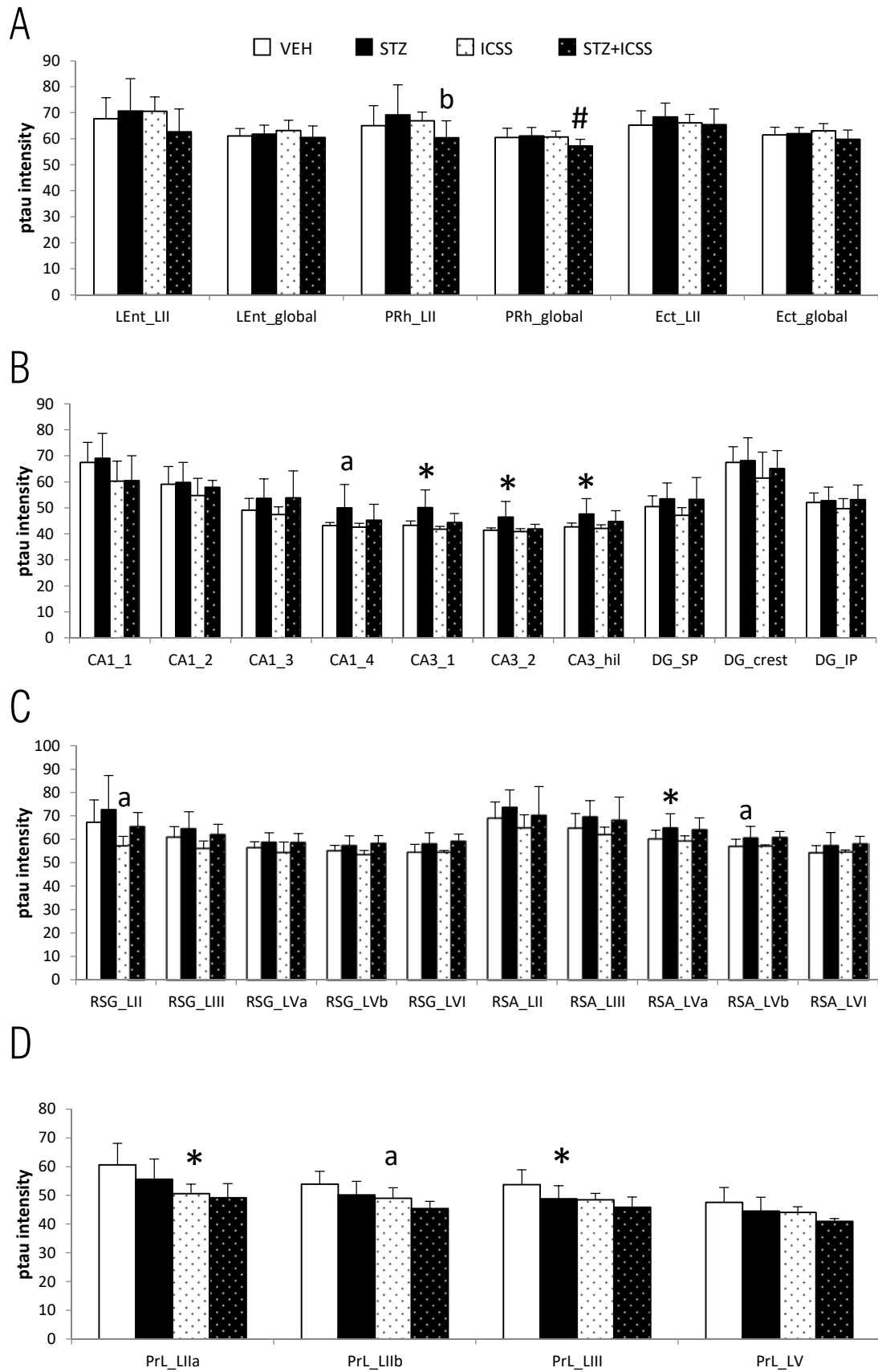




**Fig. 72 | Effects of STZ injection and ICSS treatment on ptau levels** (see figure on the previous page). Ptau levels in **A.** rhinal cortices, **B.** hippocampus, **C.** retrosplenial cortex and **D.** prelimbic cortex, for VEH, STZ, ICSS and STZ+ICSS groups, resulting from labelling intensity quantification after ptau Ser202/Thr205 immunohistochemistry. Data are presented as mean±SD; n=11, 10, 5 and 5 rats/group (VEH, STZ, ICSS and STZ+ICSS, respectively). \*p<.05 vs VEH; #p<.05 vs STZ; **a** p≤.07 vs VEH. Abbreviations: DG: dentate gyrus; Ect: ectorhinal cortex; hil: hilus; IP: infrapyramidale; L: layer; LEnt: lateral entorhinal cortex; PRh: perirhinal cortex; PrL: prelimbic cortex; RSA: retrosplenial agranular cortex; RSG: retrosplenial granular cortex.

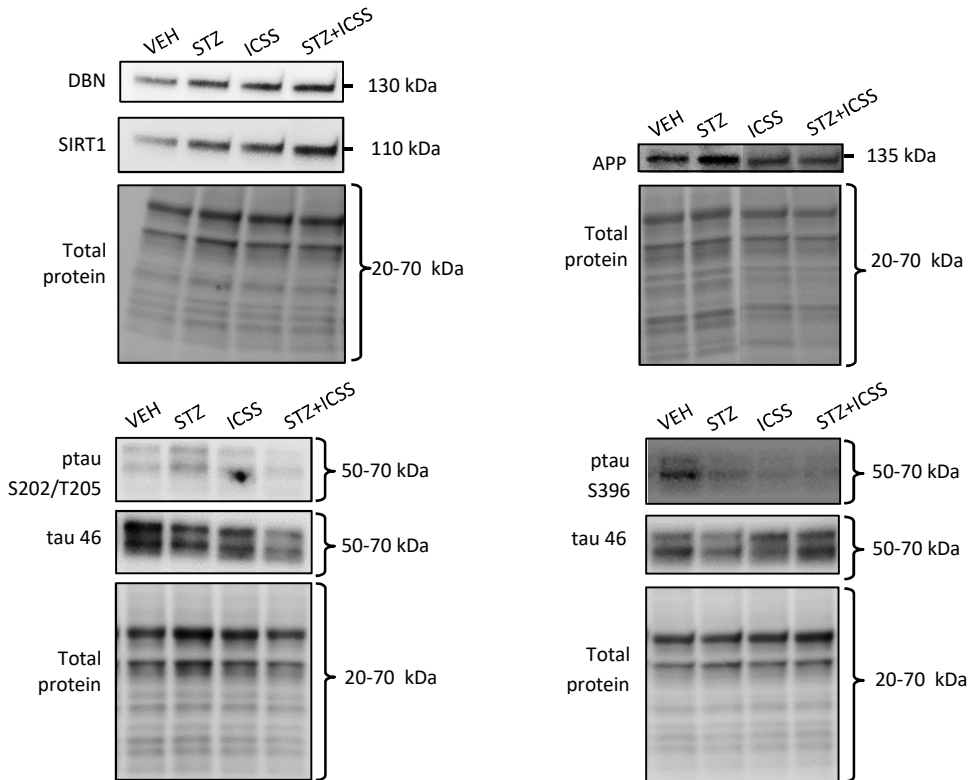
**Table 16 | Correlation analyses between ptau Ser202/Thr205 levels in hippocampal regions and latency in 2<sup>nd</sup> acquisition session in the MWM.** Table includes the correlations found significant for STZ group, according to Spearman's correlation test (p<.05, highlighted in the table).

		<i>Latency in 2<sup>nd</sup> acquisition session</i>			
		VEH	STZ	ICSS	STZ+ICSS
<i>ptau intensity levels</i>	CA1_3	$\rho=-.318$ p=.340	$\rho=.805$ <b>p=.016</b>	$\rho=.667$ p=.219	$\rho=.707$ p=.182
	CA1_4	$\rho=-.273$ p=.417	$\rho=.732$ <b>p=.039</b>	$\rho=.667$ p=.219	$\rho=.707$ p=.182
	CA3_1	$\rho=-.009$ p=.979	$\rho=.708$ <b>p=.050</b>	$\rho=.718$ p=.172	$\rho=.707$ p=.182
	DG_SP	$\rho=-.227$ p=.502	$\rho=.756$ <b>p=.030</b>	$\rho=.359$ p=.553	$\rho=.707$ p=.182
	DG_IP	$\rho=-.100$ p=.770	$\rho=.732$ <b>p=.039</b>	$\rho=.667$ p=.219	$\rho=.707$ p=.182

$\rho$  = Spearman's correlation coefficient; n = 11 and 8 rats/group (VEH and STZ, respectively).

Further Western blot analyses were performed to assess phosphorylation ratio relative to total tau levels, aiming to contrast immunohistochemistry results at Ser202/Thr205 site, and adding Ser396 site. A significant increase of tau phosphorylation ratio at Ser202/Thr205 (p=.014), accompanied by total tau decrease (p=.029), was detected in DG extracts of STZ rats with respect to VEH (Fig. 73). In STZ+ICSS group a tendency of reduction and recovery of VEH phosphorylation ratio at Ser202/Thr205 was noted (p=.076 vs STZ). In contrast, alteration of phosphorylation at Ser396 site was not perceived in DG of STZ rats (Fig. 73), although this site was affected by ICSS treatment alone (p=.011 ICSS vs VEH). In medial prefrontal cortex extracts, no significant difference in tau phosphorylation ratio between STZ and VEH groups was detected, neither in Ser202/Thr205 nor in Ser396 site (Fig. 74).

A



B

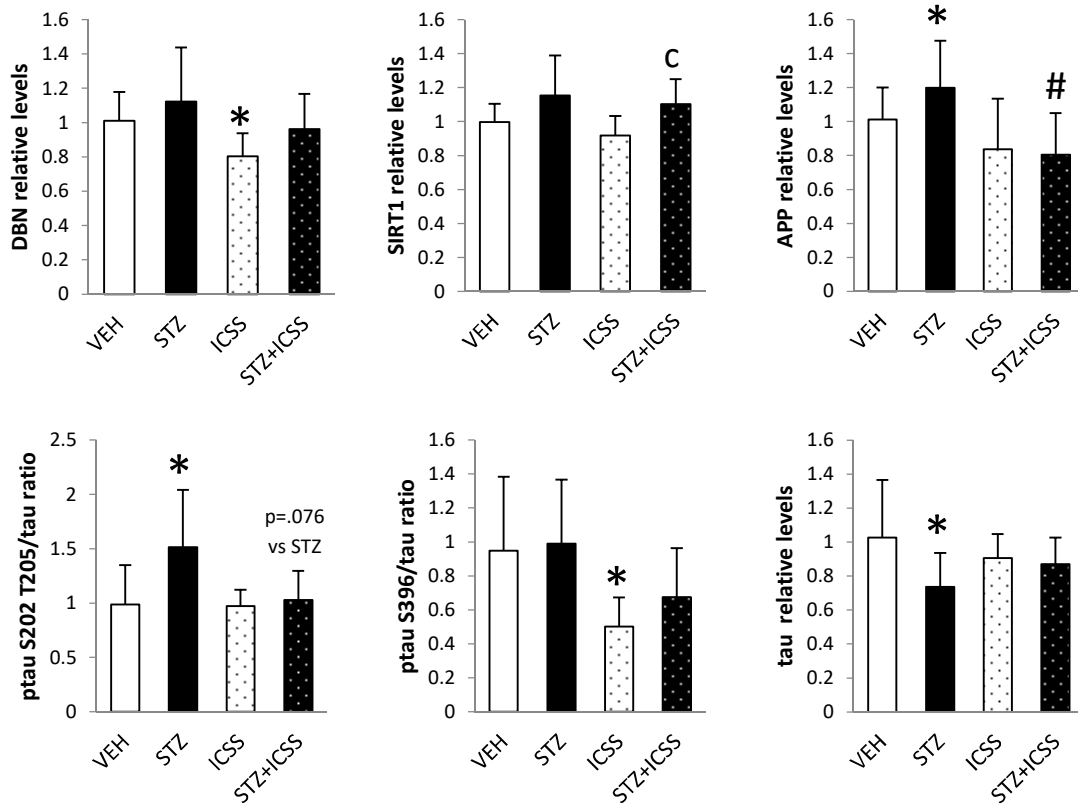


**Fig. 73** | Effects of STZ injection and ICSS treatment on DBN, SIRT1, APP, ptau and tau levels in DG extracts (see figure on the previous page). **A.** Representative Western blots for DBN, SIRT1, APP, ptau S202/T205, ptau S396 and tau proteins, together with total protein band patterns, in VEH, STZ, ICSS and STZ+ICSS groups. **B.** Resulting relative protein quantification using total protein as endogenous normalizer, and VEH group as reference, in VEH, STZ, ICSS and STZ+ICSS groups. Data are presented as mean±SD; n=11, 10, 5 and 5 rats/group (VEH, STZ, ICSS and STZ+ICSS, respectively). \*p<.05 vs VEH; #p<.05 vs STZ; c p≤.07 vs ICSS.

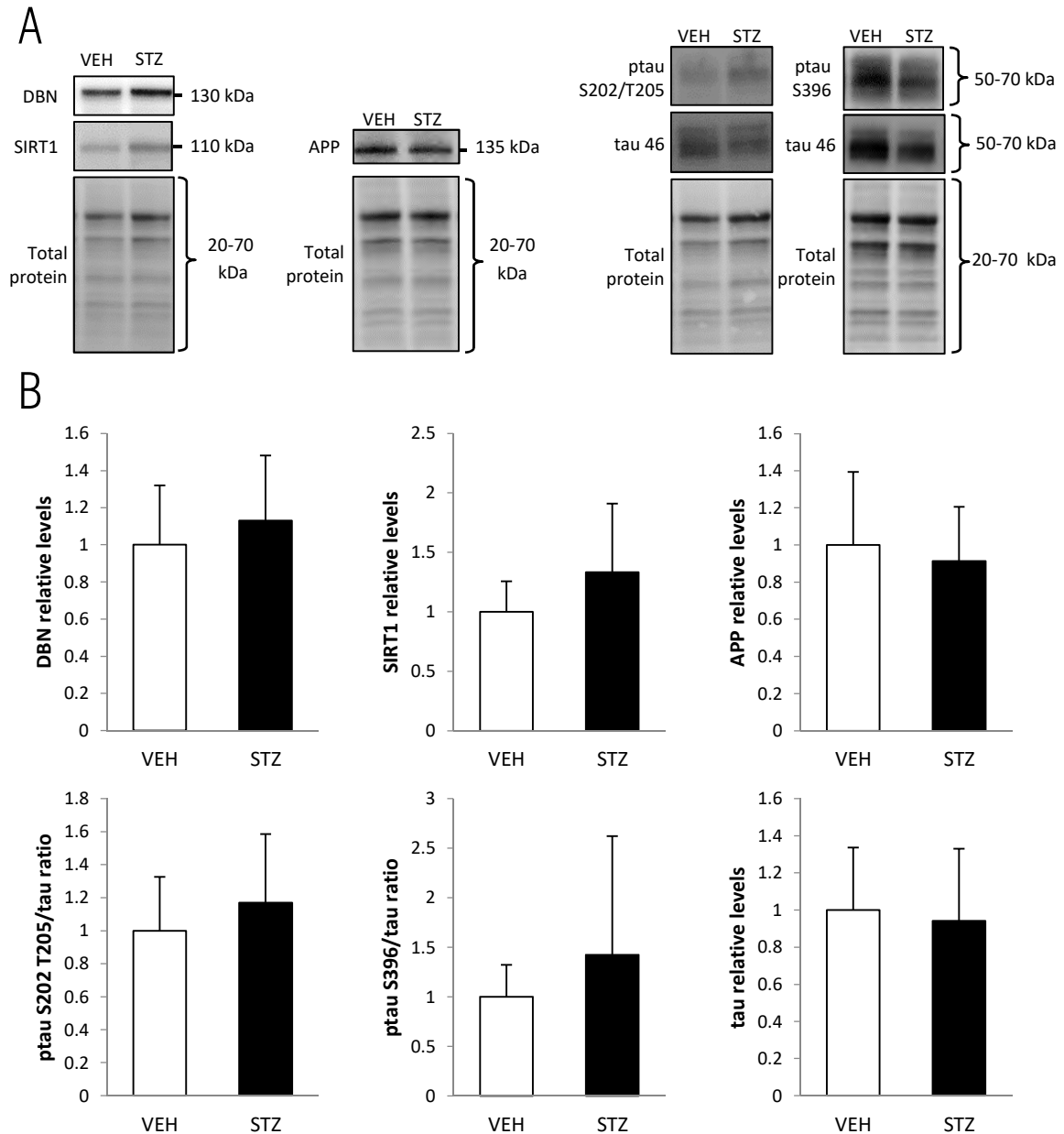


**Fig. 74** | Effects of STZ injection on DBN, SIRT1, APP, ptau and tau levels in mPFC extracts. **A.** Representative Western blots for DBN, SIRT1, APP, ptau S202/T205, ptau S396 and tau proteins, together with total protein band patterns, in VEH and STZ groups. **B.** Resulting relative protein quantification using total protein as endogenous normalizer, and VEH group as reference, in VEH and STZ groups. Data are presented as mean±SD; n=8 and 6 rats/group (VEH and STZ, respectively). No statistical significant differences were found between groups.

### Effect of ICSS on APP levels in STZ-injected rats

Results from Western blot analyses revealed that, while no differences in full-length APP levels between STZ and VEH-injected animals were found in mPFC extracts, a significant increase was found in DG extracts of STZ rats ( $p=.016$ ) (Fig. 73, 74). Moreover, altered levels of APP in DG were found to be significantly correlated with altered behavioural variables, including latencies in 2<sup>nd</sup> and 4<sup>th</sup> acquisition sessions and both time spent in the target quadrant and mean distance to target area during the probe test (Fig. 75). In VEH group, although relations between these variables do not reach statistical significance, tendencies of correlation showed inverse relation with respect to STZ (Fig. 75).

ICSS treatment administered to STZ rats caused a decrease in full-length APP levels ( $p=.029$  STZ+ICSS vs STZ), recovering normal levels, which is not detected when ICSS is administered to VEH rats (Fig. 73).

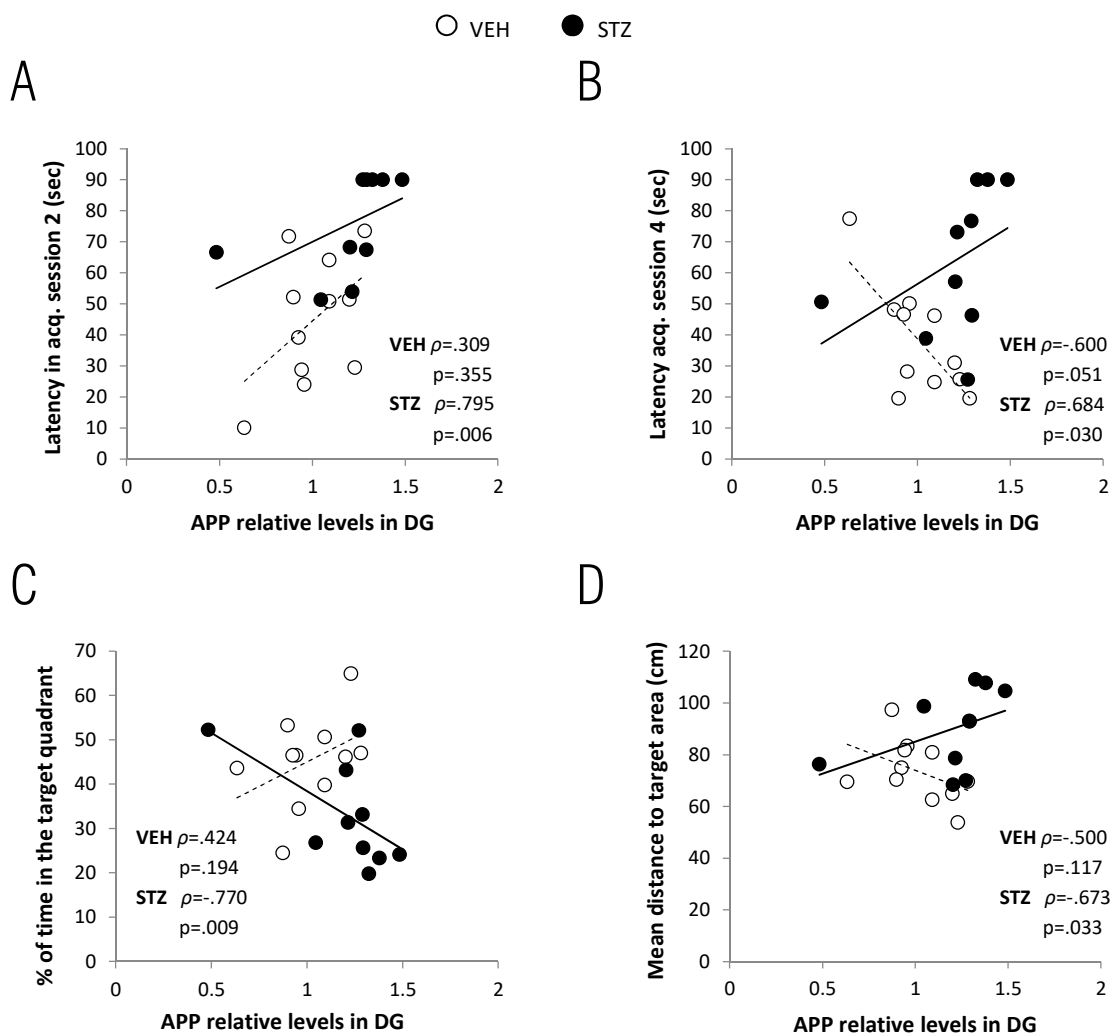


**Fig. 75 | Correlation between APP levels in DG and behavioural variables, after STZ injection** (see figure on the previous page). **A-D.** Scatter plots showing the relation between APP levels according to Western blot analysis and altered behavioural variables, including latencies in 2<sup>nd</sup> (A) and 4<sup>th</sup> (B) acquisition sessions, percentage of time spent in the target quadrant (C) and mean distance to target area (D) during the probe test, for VEH and STZ groups. Each dot represents a single rat. Spearman’s correlation test was used to determine significance ( $p < .05$ ).  $\rho$  = Spearman’s correlation coefficient;  $n=11$  and  $10$  rats/group (VEH and STZ, respectively).

### 3.3. STZ and ICSS effect on molecular regulators of AD hallmarks in DG hippocampal subfield and in serum

#### miRNA endogenous normalizers in DG and serum after STZ injection and ICSS treatment

Stability values for the bibliographic-based selected endogenous normalizer candidates, including miR-16, miR-124, let-7a and let-7b, are shown in Table 17 and 18, for DG and serum samples from STZ, VEH, ICSS and STZ+ICSS groups. miR-124 was not included in the serum analysis as it was not detected in most of the serum samples. Stability ranking order was maintained both in DG and serum if only STZ and VEH samples were included in the analyses (data not shown). Thus, according to both NormFinder and GeNorm algorithm, miR-16 and let-7a were confirmed to be the most stable miRNAs in DG subfield and serum, respectively, both regarding AD model condition and ICSS condition.

**Table 17 | Stability values for miRNA endogenous candidates in DG after STZ and ICSS.** Samples from VEH, STZ, ICSS and STZ+ICSS rats were used in the analysis ( $n=5-13$  samples/group).

	<i>NormFinder stability value</i>	<i>GeNorm score</i>
<i>miR-16-5p</i>	0.066	1.196
<i>let-7a-5p</i>	0.085	1.319
<i>let-7b-5p</i>	0.120	2.113
<i>miR-124-3p</i>	0.146	2.041

**Table 18 | Stability values for miRNA endogenous candidates in serum after STZ and ICSS.** Samples from VEH, STZ, ICSS and STZ+ICSS rats ( $n=5-13$  samples/group).

	<i>NormFinder stability value</i>	<i>GeNorm score</i>
<i>let-7a-5p</i>	0.068	0.679
<i>let-7b-5p</i>	0.110	0.733
<i>miR-16-5p</i>	0.307	1.16

### miRNA changes in DG after STZ injection and ICSS treatment

Six ICSS-regulated miRNA candidates selected from Study 1 results, including miR-196a, miR-495, miR-132, miR-134, miR-146a and miR-181c, were analysed in both VEH and STZ-injected rats, receiving ICSS or sham treatment. No significant differences were found in any of the analysed candidate miRNAs between STZ and VEH group in DG subfield. However, STZ+ICSS and ICSS groups, which were subjected to lower variability, present some detectable differences that revealed an underlying STZ effect. miR-495 is significantly lower expressed ( $p=.018$ ), while miR-146a presents a tendency to be overexpressed ( $p=.064$ ) in STZ+ICSS group with respect to ICSS group (Fig. 76).

Regarding ICSS effect, miR-146a also displayed a statistical tendency of reduction in STZ+ICSS group in relation to STZ ( $p=.068$ ), which seem to be similar in VEH group, although far from significance (Fig. 76).

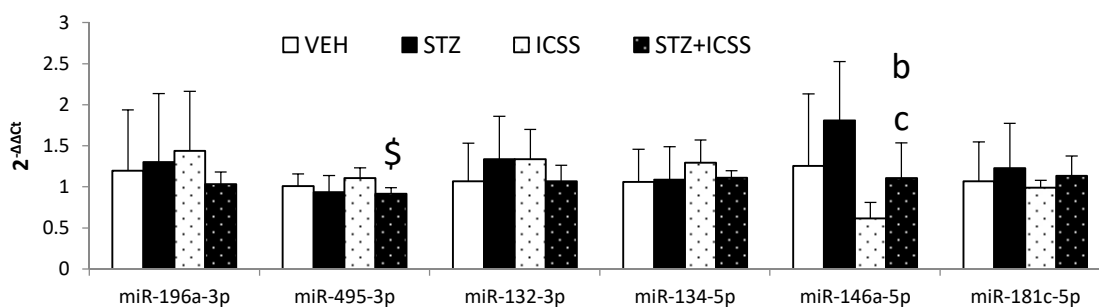


**Fig. 76 | Effects of STZ injection and ICSS treatment on miRNAs in DG.** Relative expression of miRNA candidates detected by qRT-PCR in DG, for VEH, STZ, ICSS and STZ+ICSS groups, calculated as  $2^{-\Delta\Delta C_t}$ , using miR-16 as endogenous normalizer, and VEH group mean as the reference sample. Data are presented as mean  $\pm$  SD,  $n=5-11$  rats/group. \$ $p < .05$  vs ICSS; **b**  $p \leq .07$  vs STZ; **c**  $p \leq .07$  vs ICSS.

### miRNA changes in serum after STZ injection and ICSS treatment

In serum, although levels of miR-134 were under the detection limit for more than 75% of the samples belonging to indistinct groups, miR-196a, miR-495, miR-132, miR-181c and miR-146a were detected in more than 80% of serum samples (Table 19). For these miRNAs, analysis using detected samples revealed no significant differences or tendencies regarding STZ or ICSS effect in any of the analysed candidate miRNAs (Fig. 77).

**Table 19 | Detection frequencies of candidate miRNAs in serum samples.** Percentage of samples which presented a detectable Ct is shown for each target miRNA in each group (VEH, STZ, ICSS and STZ+ICSS) and in the whole sample set.

	<i>miR-196a-3p</i>	<i>miR-495-3p</i>	<i>miR-132-3p</i>	<i>miR-134-5p</i>	<i>miR-146a-5p</i>	<i>miR-181c-5p</i>
VEH	100	81.82	100	18.18	100	100
STZ	100	70.00	100	20.00	100	100
ICSS	100	100	100	60.00	100	80.00
STZ+ICSS	100	100	80.00	0	100	100
<b>TOGETHER</b>	<b>100</b>	<b>83.87</b>	<b>96.77</b>	<b>22.58</b>	<b>100</b>	<b>96.77</b>

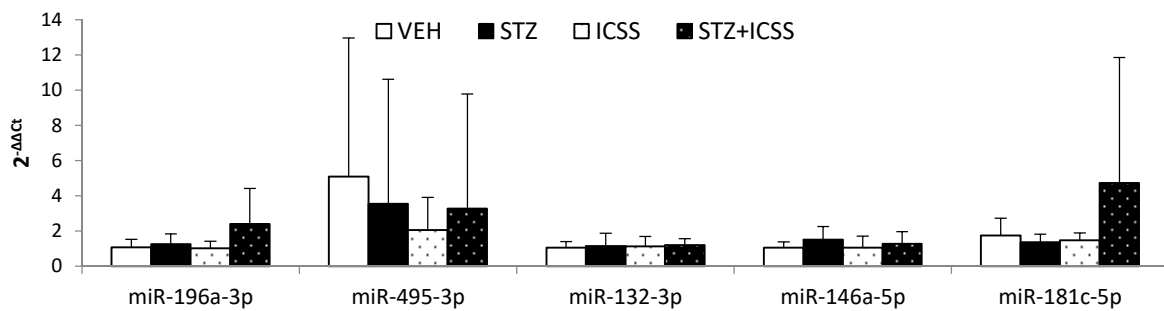


**Fig. 77 | Effects of STZ injection and ICSS treatment on miRNAs in serum.** Relative expression of miRNA candidates detected by qRT-PCR in DG, for VEH, STZ, ICSS and STZ+ICSS groups, calculated as  $2^{-\Delta\Delta C_t}$ , using let-7a as endogenous normalizer, and VEH group mean as the reference sample. Data are presented as mean  $\pm$  SD, n=5-11 rats/group. No statistical significant differences or tendencies were found between groups.

### SIRT1 levels in DG and serum after STZ injection and ICSS treatment

SIRT1 levels in DG extracts seem to be increased because of STZ injection ( $p=.078$  STZ vs VEH and  $p=.058$  STZ+ICSS vs ICSS) (Fig. 73), while any significant change was observed in mPFC extracts (Fig. 74). SIRT1 levels in tissue were not found to be significantly correlated with any behavioural variable.

In serum, SIRT1 levels were found significantly reduced in STZ rats ( $p=.045$ ) (Fig. 78). ICSS treatment caused a significant increase, both when administered to VEH rats ( $p=.017$  ICSS vs VEH) and also to STZ rats ( $p=.001$  STZ+ICSS vs STZ), which not only recovered normal levels but increased with respect to VEH group ( $p=.005$  STZ+ICSS vs VEH). Moreover, SIRT1 levels in serum were found positively correlated with DG neuronal density in STZ-injected rats, with those receiving ICSS treatment occupying the zone in the top of the

correlation (Fig. 79). In STZ group, but not in others, SIRT1 serum levels also correlate with other histopathological hallmarks, such as DBN and ptau levels in different regions, especially involving DG and retrosplenial granular cortex (Table 20).

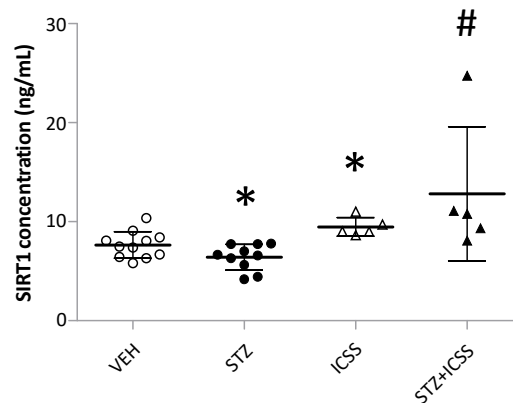


**Fig. 78** | Effects of STZ injection and ICSS treatment on SIRT1 levels in serum. Each single dot represents a single rat from groups VEH, STZ, ICSS and STZ+ICSS groups, respectively. Each dot represents a single rat, and group mean  $\pm$  SD is depicted; n=11, 10, 5 and 5 rats/group (VEH, STZ, ICSS and STZ+ICSS, respectively). \* $p < .05$  vs VEH; # $p < .05$  vs STZ.

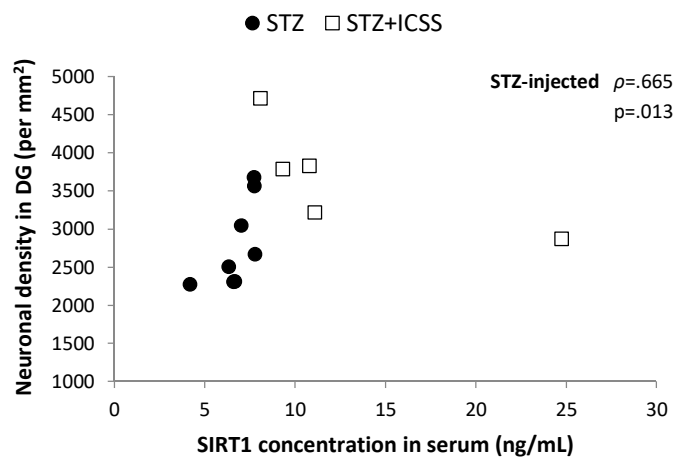


**Fig. 79** | Correlation between SIRT1 concentration in serum and neuronal density in DG after STZ injection. Spearman's correlation test was used to determine significance ( $p < .05$ ). Each dot represents a single rat.  $\rho$  = Spearman's correlation coefficient; n=10 and 5 rats/group (STZ and STZ+ICSS, respectively).



**Table 20 | Correlation analyses between SIRT1 serum levels and histopathological hallmarks.** Table includes all the correlations found significant for STZ group, according to Spearman's correlation test ( $p < .05$ , highlighted in the table).

	<i>SIRT1 levels in serum</i>			
	VEH	STZ	ICSS	STZ+ICSS
<i>DBN</i>	$\rho = .236$	$\rho = -.762$	$\rho = .600$	$\rho = .300$
<i>DG_IP</i>	$p = .511$	<b><math>p = .028</math></b>	$p = .285$	$p = .624$
<i>DBN</i>	$\rho = -.176$	$\rho = -.745$	$\rho = .100$	$\rho = .900$
<i>RSG_LI</i>	$p = .627$	<b><math>p = .013</math></b>	$p = .873$	<b><math>p = .037</math></b>
<i>DBN</i>	$\rho = .006$	$\rho = -.770$	$\rho = .800$	$\rho = .700$
<i>RSG_LII-IV</i>	$p = .987$	<b><math>p = .009</math></b>	$p = .104$	$p = .188$
<i>DBN</i>	$\rho = .036$	$\rho = -.770$	$\rho = .600$	$\rho = .600$
<i>RSG_LVI</i>	$p = .915$	<b><math>p = .009</math></b>	$p = .285$	$p = .285$
<i>DBN</i>	$\rho = .286$	$\rho = -.786$	$\rho = .200$	$\rho = .300$
<i>PRL_LIb</i>	$p = .535$	<b><math>p = .021</math></b>	$p = .800$	$p = .624$
<i>DBN</i>	$\rho = -.309$	$\rho = -.745$	$\rho = -.300$	$\rho = .400$
<i>DG extract</i>	$p = .355$	<b><math>p = .013</math></b>	$p = .624$	$p = .505$
<i>ptau S202/T205</i>	$\rho = -.073$	$\rho = -.857$	$\rho = .600$	$\rho = .100$
<i>DG_CREST</i>	$p = .832$	<b><math>p = .007</math></b>	$p = .285$	$p = .873$
<i>ptau S202/T205</i>	$\rho = .282$	$\rho = -.810$	$\rho = .600$	$\rho = .300$
<i>DG_IP</i>	$p = .401$	<b><math>p = .015</math></b>	$p = .285$	$p = .624$
<i>ptau S202/T205</i>	$\rho = -.430$	$\rho = -.721$	$\rho = .800$	$\rho = .300$
<i>RSG_LII</i>	$p = .214$	<b><math>p = .019</math></b>	$p = .200$	$p = .624$
<i>ptau S202/T205</i>	$\rho = -.152$	$\rho = -.648$	$\rho = .800$	$\rho = .400$
<i>RSG_LIII</i>	$p = .676$	<b><math>p = .043</math></b>	$p = .200$	$p = .505$
<i>ptau S202/T205</i>	$\rho = -.164$	$\rho = -.685$	$\rho = .800$	$\rho = .300$
<i>RSG_LVa</i>	$p = .651$	<b><math>p = .029</math></b>	$p = .200$	$p = .624$
<i>ptau S202/T205</i>	$\rho = .143$	$\rho = -.683$	$\rho = .200$	$\rho = .300$
<i>PRL_LIIa</i>	$p = .760$	<b><math>p = .042</math></b>	$p = .800$	$p = .624$
<i>ptau S396</i>	$\rho = -.455$	$\rho = -.782$	$\rho = .200$	$\rho = .100$
<i>DG extract</i>	$p = .160$	<b><math>p = .008</math></b>	$p = .747$	$p = .873$

$\rho$  = Spearman's correlation coefficient; n=11, 10, 5 and 5 rats/group (VEH, STZ, ICSS and STZ+ICSS, respectively). Abbreviations: DG: dentate gyrus; IP: infrapyramidal; L: layer; PrL: prelimbic cortex; RSG: retrosplenial granular cortex.

### 3.4. Summary

Table 21 shows a summary of the main results of this study, regarding both affectations displayed by STZ model in relation to the studied AD hallmarks, as well as the effect of ICSS administered in this condition.

**Table 21 | Summary of the main results in Study 3.** Table includes the effects of STZ injection, as well as of ICSS treatment on STZ-injected rats, on the studied behavioural and cell/molecular AD hallmarks.

	<b>STZ EFFECT</b>		<b>ICSS EFFECT ON STZ RATS</b>	
<b>Behaviour</b>	MWM acquisition: ↑ latencies sessions 2, 3 and 4 MWM retention: ↓ time in target quadrant and annulus, ↑ distance to target		MWM acquisition: ↓ latency session 3 MWM retention: disappear differences in time in target quadrant	
	<b>Temporal-parietal regions</b>	<b>Frontal regions</b>	<b>Temporal-parietal regions</b>	<b>Frontal regions</b>
<b>Neurodegeneration</b>	↓ neuronal density in CA1 and DG	↑ % neurodegeneration DTT	↑ neuronal density in CA1 and DG	No effect detected
<b>DBN</b>	No effect detected	No effect detected	↑ LEnt_LI, Ect_LV	No effect detected
<b>ptau Ser202/Thr205</b>	↑ HP subregions, RSA_LV	↓ PrL_LIII	↓ PRh, tendency to recover in HP subfields	No effect detected
<b>ptau Ser396</b>	No effect detected	No effect detected	No effect detected	-
<b>APP</b>	↑ DG	No effect detected	↓ DG	-
	<b>brain tissue</b>	<b>serum</b>	<b>brain tissue</b>	<b>serum</b>
<b>miRNAs</b>	↓ miR-495, tendency ↑ miR-146a in DG (when comparing groups receiving ICSS)	No effect detected	tendency ↓ miR-146a in DG	No effect detected
<b>SIRT1</b>	No effect detected	↓	No effect detected	↑

### 3.5. Discussion

This study confirms that icv injection of STZ is able to recapitulate extensive behavioural and neuropathological distinctive features of AD 40 days after, including overexpression of phosphorylated tau and APP in hippocampal formation. In this sense, icv injection of STZ is proposed as a suitable model to study effects of ICSS treatment. Although with some limitations, this study is the first to report ICSS effects in rescuing histopathological alteration in a sAD model, while also providing an insight into its molecular mechanisms including miRNAs and SIRT1.

#### Methodological considerations regarding STZ injection to model AD

Based on the hypothesis that glucose hypometabolism is an upstream cause in the AD cascade, icv-administration of the diabetogenic toxin STZ is being increasingly used to mimic sporadic AD in rats, administering a typical dose of 3 mg/kg (Grieb, 2016) solved in saline or citrate buffer.

Different methodological concerns were optimised for the development of this study. On the one hand, citrate buffer at a controlled pH of 4.4-4.5 was determined to be preferred in front of saline, as the latest resulted in an impracticable effervescent solution. This phenomenon, already reported by others (Wang-Fischer and Garyantes, 2018), could be due to pH instability in commercial saline solution (Reddi, 2013), leading to more rapid decomposition of STZ, resulting in nitric oxide release.

On the other hand, initial pilot experiment using 3 mg/kg resulted in 75% mortality and severe irritability in surviving animals (data not shown). Reduction of the dosage to 2 mg/kg, accompanied with attentive post-surgical cares, led to mortality reduction (to 10.5%) and easy-going manipulation of animals. A possible explanation to the high mortality experimented in our lab could be that, when using heavy animals (around 400 g), 3 mg/kg could result in an excessive amount of STZ to tolerate at once. Thus, it is insinuated that linear dosage scaling in relation to body weight, which seems to come from historical intraperitoneal administration of STZ to cause systemic diabetes, could be put into debate. Moreira-Silva et al. also used 2 mg/kg in similar weighted Wistar rats (Moreira-Silva et al., 2018), and sustained that this is the most optimum dose to model sporadic AD (Moreira-Silva et al., 2019). While lower doses ( $\leq 1$  mg/kg) resulted in a very slow neurodegenerative process (Kraska et al., 2012), which some report to be reversible (Mehla et al., 2013), higher

doses ( $\geq 3$  mg/kg) produce aggressive neurotoxicity (Kraska et al., 2012) accompanied by alteration in locomotor activity (Dehghan-Shasaltaneh et al., 2016), differing from the neurodegenerative process observed in sAD.

In the present study, injection of 2 mg/kg resulted in a complete model integrating both behavioural and histopathological hallmarks of sAD, which appeared accompanied by physiological alterations including body weight loss and increased reactivity. Based on its consistency, this study suggest that presence of these physiological affectations can be used as a marker of STZ-injection success. Body weight loss after icv STZ injection has been coherently reported. It is hypothetically attributed to STZ effect when reaching the hypothalamus from the third ventricle (Shoham et al., 2003; Poddar et al., 2020), disturbing its role in controlling feeding behaviour, thermoregulation and glucose homeostasis in peripheral organs (Elizondo Vega et al., 2015; Thorens, 2015). Poddar et al. also suggested that loss of body weight is an important indicator to distinguish vulnerability to STZ, in this case in relation to mitochondrial dysfunction (Poddar et al., 2020). Reactivity could be associated with septohippocampal cholinergic alteration (Morris et al., 1982; Smith, 1988), a sign also found in the model (data not shown). Moreover, reactivity detection in the model matches the association between cognitive dysfunction and agitation/hyperactivity in AD patients (Asada et al., 2000). Thus, presence of these physiological effects are signs of correct STZ circulation in the ventricular system and expected effect in vulnerable areas, upholding the model. According to the presence of this signs, success of model generation was estimated to be 89.5%.

#### Long-lasting behavioural, histomorphological and molecular AD-like characteristics uphold the use of STZ-injected model for long-term treatment assessment in early AD

Behavioural characterization of this model, assessed from day 33 to day 40 after STZ injection, included both impaired spatial learning and memory as well as signs of emotional deficit. In this sense, increased latencies in acquisition phase of the MWM and altered mean distance to target area and time spent in the target quadrant in the probe test are reported. An anxiety marker such as thigmotaxis in the MWM (Treit and Fundytus, 1988) was also found altered in the model, agreeing with symptoms reported for AD patients (Ferretti et al., 2001).

Morphologically, STZ brains were distinguished by tissue softening together with evident enlarging of brain ventricles and atrophy of paraventricular structures, such as corpus

callosum and hippocampus. These signs, already reported by other authors after icv injection of STZ (Shoham et al., 2003; Kraska et al., 2012; Knezovic et al., 2015; Voronkov et al., 2019), are also characteristic of human AD brains (Luxenberg et al., 1987; Smith, 2002; DeTure and Dickson, 2019). Loss of neural tissue was also noticed in Nissl staining analysis, which revealed decreased neuronal density in CA1 and DG hippocampal subfields. Particular affection of neuronal loss in CA1 against CA3 match results from AD patients (Padurariu et al., 2012). At a level of frontal lobe, no neuronal loss was found in superficial layers of prefrontal cortex, but notable neurodegeneration was distinguished in dorsal tenia tecta structure, correlating with neuronal density in affected hippocampal subfields. This structure is considered both part of the hippocampal continuation with a role in associative learning and attention (Maddux and Holland, 2011), as well as part of the olfactory cortex, receiving inputs from both the prefrontal cortex and the olfactory bulb. Thus, this observation, which was not reported before, is especially interesting taking into account that early stages of AD disease are characterized by olfactory deficits, being the central olfactory system one of the first subcortical areas to present neurofibrillary tangles (Zou et al., 2016).

At a molecular level, the model was characterized by alteration of the defining hallmarks of AD, including APP and ptau, in the hippocampus, correlating with altered performance in spatial learning.

Specifically, expression of APP is found increased in DG extracts, negatively correlating with both acquisition and retention performance, but not in medial prefrontal cortex extracts.

Regarding taupathology, the present work agrees with other studies describing increased phosphorylation in Ser202/Thr205 after 1 month of STZ injection at 3 mg/kg (Knezovic et al., 2015), and demonstrates that the lower dose of 2 mg/kg was sufficient to trigger this hallmark. Moreover, this study presents the first accurate characterization of regional affection of phosphorylated tau at site Ser202/Thr205 in STZ-injected model. By targeting the same epitope as Braak et al. in their studies in AD human brains, this screening enables to infer the hypothetical Braak stage in the model. Although no alteration was distinguished in entorhinal cortex, increased ptau levels localized in the hippocampus, especially in CA1 and CA3 subfields, and in layer V in retrosplenial cortex, but not in frontal areas resemble distribution found in AD Braak stages II-III (Braak et al., 2006a).

Tau phosphorylation alteration was further contrasted by Western blot. This methodology, although does not allow sublayer discrimination, enables to obtain the phosphorylation ratio

by normalization by total tau levels. This methodological distinction could explain discrepancies between Western blot and immunohistochemical results. In this sense, Western blot results showed that STZ rats presented increased phosphorylation of tau at site Ser202/Thr205 together with a reduction in total tau levels in DG subfield extracts, where no significant alteration was perceived in immunohistochemistry results. Although reduction in total tau levels is not a characteristic feature described for AD, it was already reported long after STZ injection (Osmanovic Barilar et al., 2015), and seem to be present also after 24h exposition to STZ in SH-SY5Y human neuroblastoma cell line (data from starting preliminary experiments in our lab, not shown in this thesis). Anyhow, Western blot results confirm the presence of tau pathology in the hippocampus, but not in the mPFC.

Moreover, Western blot also allowed a rapid screening of other phosphorylation sites. Regional and temporal profile throughout AD pathology of different tau phosphorylation sites seem to be similar to that of Ser202/Thr205 in human brains (Neddens et al., 2018). However, Ser396 has been described to show only weak and late phosphorylation and minor progression (Su et al., 1994; Neddens et al., 2018). Despite the fact that STZ rat model was reported to present increased tau phosphorylation in Ser396 one month after STZ injection at 3 mg/kg (Xu et al., 2014; Huang et al., 2018), in our study, DG extracts of STZ rats showed no alteration in this site. Thus, present results, in accordance with Moreira-Silva et al. results using 2 mg/kg (Moreira-Silva et al., 2018), suggest that alteration in Ser396 site could be dosage dependent, as already noticed by Zappa Villar et al. (Zappa Villar et al., 2018). In this sense, a dose of 2 mg/kg seems again to mimic a more realistic model of early AD.

Altogether, regional distribution of molecular alteration focused in the hippocampus, together with behavioural and histological abnormalities after STZ injection seem to converge to model early sporadic AD condition. Moreover, these effects are proved to be durable at least 40 days after STZ injection. Salkovic-Petrisic group, one of the greatest experts in the use of STZ model, define a biphasic response pattern after STZ injection (3 mg/kg), especially regarding the insulin receptor signalling cascade but correlating also with cognitive deficits: an acute phase ( $\leq 1$  month) is followed by partial attenuation of some hallmarks (1 to 3-6 months), which decline again in a phase ending to be chronic (from 6 months on) (Osmanovic Barilar et al., 2015). Although the extent and dynamics of affectation following icv-STZ injection is known to depend on the amount of toxin injected (Kraska et al., 2012), pilot experiments in our lab indicate that behavioural and morphological alterations are sustained at least 8 months after STZ injection at 2 mg/kg (data not shown).

Alteration of molecular pathology, including the levels of the postsynaptic marker DBN which was not perceived in the present study, lacks to be assessed at this later time point. Anyhow, STZ injection in the reported conditions seems to be a suitable strategy to inspect both immediate as well as long-term effects of ICSS treatment on a sAD model.

#### ICSS treatment affects AD-like molecular hallmarks in STZ-injected model

Slight differences in the behavioural variables affected by STZ were perceived in rats receiving ICSS treatment, suggesting that ICSS would be exerting a memory improving effect also in AD-like pathological conditions. Based on this suggestion and according to the main aim of this study, this work approaches for the first time the effect of a DBS therapy on the early AD-like cell and molecular alterations found in a sAD model, obtained by icv-STZ.

Five post-training sessions of ICSS were found capable to induce an increase in neuronal density in the hippocampus of STZ-injected rats, but not in control rats. Specifically, a tendency was found in CA1 and a significant increase was detected in DG of STZ rats subjected to ICSS treatment. These results are in line with the findings of Leplus et al., who found reduced neuronal death in the DG of AD transgenic rats (TgF344-AD) after 5 weeks of fornical DBS, but not in wild type rats (Leplus et al., 2019). They suggested that this neuroprotective effect could be linked with reduced microglia activation and neuroinflammation (Leplus et al., 2019). However, it could be also related with neurogenesis-related pathways reported after ICSS in DG (Huguet et al., 2009, 2020; Takahashi et al., 2009), which could be strengthened in pathological condition. In this regard, Mann et al. demonstrated increased neurogenesis in the DG of AD triple transgenic mice (mutated transgenes for APP and tau on a PS1 knock-in background) after 25 days of bilateral entorhinal cortex high frequency DBS (Mann et al., 2018).

ICSS treatment also reduced the levels of full-length APP in DG extracts of STZ rats, demonstrating again similar effects to longer treatments of fornical or entorhinal cortex DBS in transgenic AD animals, which reported a reduction of APP and/or amyloid burden in the hippocampus (Mann et al., 2018; Leplus et al., 2019). Moreover, ICSS treatment also caused a tendency of reduction in ptau Ser202/Thr205 levels in DG extracts of STZ-injected rats, which, to our knowledge, has not been reported before in AD transgenic models. Tau phosphorylated at Ser396, instead, is only reduced in control rats receiving ICSS, but not in STZ-injected ones, evidencing once more the different dynamics of the two phosphorylation sites.

Nevertheless, no consistent correlations were found between the molecular changes and behavioural performance of STZ rats subjected to ICSS treatment, hindered by a limited dispersion in the values and a small sample size. In this sense, both tendencies in molecular hallmarks as well as behavioural effects should be further assessed with an increased sample size. Still, DBN levels in rhinal cortices, which were revealed significantly increased after ICSS treatment in the contralateral hemisphere in immunohistochemical analysis, positively correlate with mean distance to target area in the probe test in STZ+ICSS group. Thus, while DBN did not seem to be affected by STZ at the studied time point, it seems to have a role in neural plasticity enhancement that would support memory improvements found after ICSS.

ICSS treatment affects molecular regulators of AD pathology in STZ-injected model: SIRT1 emerges as a promising serum biomarker for both AD-like pathology and ICSS treatment in STZ rat model

Finally, this work also addresses for the first time the implication of gene expression regulatory molecules, including miRNAs and SIRT1, in both AD-like STZ effects and recovery effects of 5 post-training ICSS sessions evaluated 72 hours after the last session.

Regarding miRNA analysis, miR-16 and let-7a suitability as endogenous normalizers for tissue and serum samples, respectively, suggested in Study 1, was confirmed in STZ conditions. Moreover, STZ and ICSS effects on different ICSS-regulated miRNA candidates selected according to Study 1 results, including miR-196a, miR-495, miR-132, miR-134, miR-181c and miR-146a, were assessed in both DG and serum, with only slight changes observed in DG. On the one hand, miR-495 expression was found to be reduced in STZ+ICSS group with respect to ICSS, indicating an underlying effect of STZ unable to be compensated by ICSS. As discussed in Study 1, where it was reported to be increased 90 minutes after ICSS session, miR-495 has been reported to be downregulated in AD (Wang et al., 2011) and seems to be related with activity-dependent remodelling of synaptic plasticity (Wang et al., 2012). Thus, although miR-495 is not a well-known miRNA, results from these studies encourage its study in the context of sAD. On the other hand, miR-146a emerged as a modulated miRNA candidate in this condition. Although an increase in this miRNA could not be statistically proven in STZ rats, because of a high variability in this group, a tendency of decrease in miR-146a was perceived in the STZ+ICSS group respect to the untreated STZ. miR-146a is broadly reported to be selectively upregulated in AD affected regions and to have a role in mediating neuroinflammatory response in AD, through a NF- $\kappa$ B and complement factor H-dependent pathway (Lukiw et al., 2008; Tan et al., 2013; Samson et al.,



2017). In transgenic AD models, miR-146a is found to correlate with senile plaque density and synaptic pathology (Yang et al., 2015). Altogether, present results points that miR-146a could be an interesting target to be further studied to unravel mechanisms mediating ICSS neuroprotective effects, especially regarding results from Leplus et al., who reported decreased neuroinflammation in TgF344-AD rats after forniceal DBS (Leplus et al., 2019).

Regarding SIRT1 levels, although no significant alteration was perceived in tissue, interesting changes were found in serum. A decrease in SIRT1 levels was reported for the first time in STZ-injected rats' serum, accurately resembling results described for AD patients where it has been described as a biomarker of early AD pathology (Kumar et al., 2013b). In STZ group, SIRT1 serum levels were found significantly associated with both DBN and ptau Ser202/Thr205 levels in different areas, especially in DG hippocampal subfield and granular retrosplenial cortex, as well as with DG neuronal density. Interestingly, ICSS treatment caused a significant increase in SIRT1 serum levels in STZ rats, not only recovering but overcoming control levels, motivating the use of SIRT1 also as a treatment biomarker.

### Conclusions

Overall, although limited by a small sample size, the present study shows for the first time the effects of 5 post-training ICSS sessions in an integrated and durable sporadic AD rat model, obtained by icv injection of intermediate-dose STZ. In summary, ICSS treatment is able to recover neurodegeneration deficits, APP and ptau alterations, and provide improved plasticity conditions evidenced by increased DBN levels in temporal-parietal regions associated with memory function. Although significant changes cannot be detected in miRNAs, slight tendencies in DG levels, highlighting miR-146a, suggest that these regulatory molecules are modulated by ICSS treatment in a pathological AD-like context and, thus, they could have a role in mediating ICSS recovery effects on AD deficits triggered by STZ. Thus, it is worth to persist on further studying the potential role of serum levels of some of these miRNAs as treatment biomarkers in AD condition. However, in this regard, the most meaningful contribution of this work is the assertiveness of SIRT1 as a promising ICSS treatment biomarker, in addition to the already suggested use as AD pathology biomarker, in the STZ-injected model.

## GENERAL DISCUSSION

Development of drugs to treat Alzheimer's disease is defined by a devastating long story of clinical trial failures, which ends in no available current therapies to prevent, arrest, or cure this disease. In this scenario, neuromodulatory approaches, including electrical stimulation of deep brain areas, have growth in interest as novel therapeutic options for AD. Although the underlying molecular mechanisms are not clearly understood, DBS aimed at different brain regions has been suggested to alleviate AD cognitive symptoms.

To this aim, the election of the brain target is still in debate. Clinical trials targeting either the fornix or the nucleus basalis of Meynert together with preclinical studies exploring DBS of different areas sustaining or modulating memory circuits have shown promising early data for memory improvement in AD (Laxton and Lozano, 2013; Aldehri et al., 2018). However, it remains uncertain which of these targets is most effective and if their therapeutic mechanisms are similar or unique for each target.

Our group has a long tradition studying the effects of MFB stimulation by means of ICSS in rodents, showing that it is able to physiologically activate both cognitive-related areas as well as systems related to emotional domain (Huguet et al., 2009; Kádár et al., 2011, 2013, 2016, 2018). Its memory improving effects are extensively reported in physiological conditions both in young (Segura-Torres et al., 1988; Redolar-Ripoll et al., 2002; Hermer-Vazquez et al., 2005; Soriano-Mas et al., 2005; Ruiz-Medina et al., 2008; Aldavert-Vera et al., 2013; Chamorro-López et al., 2015; García-Brito et al., 2017) and aged rats (Aldavert-Vera et al., 1997), and also in rats with specific brain lesions (Redolar-Ripoll et al., 2003; Segura-Torres et al., 2009; Kádár et al., 2014). These behavioural improvements, together with molecular plasticity events triggered by ICSS (Huguet et al., 2009, 2020; Kádár et al., 2011, 2013, 2016, 2018; Aldavert-Vera et al., 2013; Chamorro-López et al., 2015), suggest that MFB stimulation could be also effective in AD context. However, its effects had never been assessed in AD context nor in relation to molecular correlates of AD pathology. This thesis approaches for

the first time this situation, aiming to assess the potential use of rewarding stimulation at the MFB as a treatment for AD in a preclinical rodent model, focusing on its molecular effects.

## About the suitability of animal AD models to study ICSS treatment effect

In order not to be led to false conclusions, the election of the model for the specific purpose and the accurate knowledge of the displayed pathology in relation with human AD is essential (Drummond and Wisniewski, 2016). To be used in this work, three requirements are demanded for an AD rat model. First, a sporadic model is preferred over transgenic-engineered models, in order to ensure the highest transnationality to the prevailing type of AD (Zhang et al., 2019). Second, the model needs to mimic the main neuropathological hallmarks of early AD pathology, which will be interrogated for ICSS effects, and concurring behavioural deficits. Third, AD-like alterations are required to be durable along time in order to reliably use this model in future inspection of long-term ICSS treatment effects. In this way, further studies could address the limitation of the lack of works evaluating sustained effects long after a DBS procedure.

Attending to the requirements, two different models obtained by single bilateral icv injection of A $\beta$  peptide or STZ toxin were evaluated in Study 2 and Study 3, respectively. Both chemicals were suggested to trigger AD-like neuropathological hallmarks by interceding at different levels of AD hypothetical pathological cascade (Hoyer et al., 1994; Selkoe, 2008; Grieb, 2016), and are being extensively used as sporadic AD models in preclinical research.

In this work, characterization of AD-like pathology in the models was mainly based on the study of a. neurodegeneration, b. hyperphosphorylated tau pathology at Ser202/Thr205, as used to define AD Braak stages in human brain (Braak et al., 2006a), c. synaptic deficits evidenced by altered DBN levels reported in early AD (Counts et al., 2006, 2012), as synapse loss was suggested to be more correlated with cognitive impairment than plaques and tangles (Terry et al., 1991), and d. spatial learning and memory alteration, as sign of episodic memory deficit symbolic of early AD. Presence of amyloid plaques was not assessed in these models as rodent amyloid- $\beta$  is not able to aggregate in plaques (Marksteiner and Humpel, 2008; Ueno et al., 2014). Neuropathology was assessed in parietal-temporal regions, including entorhinal cortex, hippocampus, where AD pathology is first initiated, and retrosplenial cortex, as well as in frontal medial regions, including prelimbic cortex, where it is thought to progress

according to the disconnection hypothesis (Braak and Braak, 1991a; Reid and Evans, 2013; Migliaccio et al., 2015).

Neuropathology accompanied with memory deficits was displayed in both models. However, distinctions related to similarity to AD pathology stage and progression can be made. In A $\beta$  model, two stages of distinct neuropathology were inspected. In a first stage, assessed 15-22 days after A $\beta$  injection, memory affectation was evident and neuropathological affectation found at sacrifice is mainly concentrated in frontal regions. Although phosphorylated tau pathology was also present in the hippocampus, regional preference for frontal neurodegeneration did not match any expected stage in early AD. In a later stage at 33 days after A $\beta$  injection, temporal affectation is preferred, with tau pathology restricted to superficial layers of entorhinal cortex, highly resembling initial stages described for AD Braak stage I-II (Braak et al., 2006a), but only marginal memory deficits were found when evaluated at 26-33 days. Thus, although molecular affectation at this stage resembles very early AD, general evolution for this model inverted the posterior-to-anterior progression expected for sAD pathology (Migliaccio et al., 2015). Moreover, and in accordance to other reported results (Sigurdsson et al., 1997; Cleary et al., 2005; Wong et al., 2016; Karthick et al., 2019), A $\beta$  model displayed signs of transiency. Altogether, under the conditions used in this study, A $\beta$  model failed in featuring AD progression and thus, the use of this model was discontinued for the impossibility to assess long-term effects of ICSS treatment.

In STZ model, both neurodegeneration and tau pathology were selectively affected in the parietal-temporal lobe, especially hippocampus, resembling Braak stages II-III (Braak et al., 2006a). Moreover, concurring extensive behavioural deficits, including both memory-related and emotional deficits, were presented. However, DBN levels, which seemed to be strongly related with behavioural characterization in A $\beta$  model, was not found affected in STZ model 40 days after injection, although other synaptic proteins such as synaptophysin or syntaxin have been reported altered in this model (Moreira-Silva et al., 2018). Additional extensive affectations resembling early AD were found in STZ model, including morphological alterations in lateral ventricles and periventricular structures, APP increased levels in hippocampus and decreased SIRT1 serum levels. Furthermore, in favour of the use of STZ model, both pilot studies in our group together with other studies suggest that this model presents sustained long-term progression (Osmanovic Barilar et al., 2015).

Altogether, both A $\beta$  and STZ models here reported have been found to mimic different aspects of early AD molecular pathology, if used at 33 and 40 days after injection,

respectively. However, STZ model, presenting enduring regional-selective alteration related to the main AD hallmarks (APP and tau phosphorylation) accompanied with behavioural affectation, presents the advantageous possibility of testing long-term treatment effects over the transient A $\beta$  model.

### About the ability of ICSS to fight cell and molecular AD hallmarks

The main evidence supporting the use of DBS for AD treatment is based on cognitive improving effects suggested in both clinical studies with AD patients (Laxton et al., 2010; Smith et al., 2012; Fontaine et al., 2013; Sankar et al., 2015; Kuhn et al., 2015; Lozano et al., 2016; Hardenacke et al., 2016) and preclinical studies using transgenic rodent AD models (Xia et al., 2017; Koulousakis et al., 2020). Although the present work also contributes to this bulk by presenting evidence of behavioural improvement after rewarding DBS aimed at the MFB in a sAD rodent model, the main focus was set on the cell and molecular effects. In this sense, until so far, only few studies have intended to understand the underlying biological cell/molecular effects of DBS in rodent AD models (Mann et al., 2018; Leplus et al., 2019). To our knowledge, the present work is the first of this type aiming to do so in a sporadic AD model and, of course, the first targeting the MFB.

Present results suggest that post-training administration of five MFB-ICSS sessions were enough to avoid the appearance of neuropathological signs underlying behavioural deficits, in both A $\beta$  and STZ-injected rats. Focusing on the STZ-induced model, ICSS treatment is able to increase neuronal density and decrease APP and ptau levels in the hippocampus, recovering control levels, according to results from Study 3. These effects were not evidenced when DBS was administered in physiological conditions, as reported in Study 1 and studies performed by other authors (Gondard et al., 2015). However, they resemble those described after longer DBS treatments targeting fornix or entorhinal cortex in transgenic AD models (Mann et al., 2018; Leplus et al., 2019).

Overall, these results suggest that molecular mechanisms underlying ICSS are able to intercede at the level of altered AD neuropathological hallmarks when administered in AD-like pathological conditions.

## About the implication of AD-related gene expression regulators in ICSS facilitating effect: emergence of potential non-invasive treatment biomarkers

In the way to shed more light upon the mechanisms underlying DBS effects in alleviating AD, this study reports for the first time the implication of gene expression key regulators, like microRNAs and SIRT1, in the demonstrated ICSS facilitating effect, both in physiological and AD pathological conditions. These findings not only contribute to comprehend the bases of treatment efficacy and be able to optimize it, but also to uncover novel therapeutic and diagnostic molecular targets that can serve as potential treatment biomarkers.

In addition to come up with a list of ICSS-regulated miRNA candidates accessible to be further studied, results from Study 1 demonstrated the upregulation of miR-132, miR-181c and miR-495, as well as SIRT1 protein in hippocampal subfields short after ICSS session administration. However, among them, only miR-495 seem to retain an increasing tendency when evaluated in pathological conditions in Study 3 seventy-two hours after ICSS in a five-days regimen, when miR-146a also emerges as another ICSS-regulated miRNA. In this regard, whether ICSS effect on these molecules is stable or instead it is part of an acute transient action mediating plasticity events through the already discussed mechanisms is put into debate. Indeed, it was already suggested that transient overexpression of miR-132 is induced with activity and mediates memory formation (Wang et al., 2013), while permanent excessive transgenic overexpression result in damaged cognition and spatial memory in healthy mice (Hansen et al., 2010, 2013). However, variations between individual miRNAs could respond, in part, to reported differential regulation of their stability (Bail et al., 2010; Gantier et al., 2011). Thus, further investigations are needed, but the present results suggest that, even with distinct time and condition-dependent dynamics, different miRNAs and SIRT1 could be implied in triggering changes in plasticity and AD-related protein expression reported after ICSS effects both physiological and AD-like pathological conditions.

Caution needs to be taken when extrapolating these results, as it is unclear if the processes enabled by DBS are similar or unique for each brain target. However, involvement of these AD-related molecular regulators on DBS mechanism opens new lines of investigation regarding its applicability in AD treatment, such as the use of these molecules as DBS treatment biomarkers. On this subject, this work especially highlights the study of miR-132 and SIRT1 to this purpose, being already proposed as AD treatment biomarkers (Kumar et

al., 2013b; Xie et al., 2018) While miR-132 serum levels seem to mirror the acute increase found in tissue, SIRT1 is insinuated to hold a more prolonged rise which relates to neuropathological signs in AD-like condition. Anyhow, both molecules have been proved to be detectable in rat serum and susceptible to ICSS treatment.

## Concluding remarks and future directions

According to the main aim of this work, molecular effects reported after ICSS sustain the promising potential of rewarding stimulation of the MFB for the treatment of AD. In essence, ICSS treatment has been proven able to intercede the neuropathological signs of AD in a well-characterized sporadic AD model, contributing to the behavioural improvement in this pathological context. Key regulators of AD neuropathology like specific miRNAs and the deacetylase SIRT1 have been demonstrated to take part in the underlying molecular mechanisms. Moreover, evidences for the use of these molecules as promising treatment biomarkers in serum have been presented.

All things considered, an evident field of investigation is suggested intending to reach the evaluation of MFB as a DBS target in AD patients. Moreover, ICSS success sets interest in novel treatments for AD with rewarding approaches. In this sense, over other DBS targets, reward-upholding brain areas, and especially the MFB, emerge as promising potential targets of DBS for integrative treatment of AD cognitive and neuropsychiatric symptoms.

In addition, the results presented in this thesis set some cues that open the door to multiple research lines. In this sense, the characterization of sporadic AD models could serve as the basis for their use in similar preclinical research, including evaluation of long-term treatment effects. Moreover, the presentation of ICSS-regulated miRNA candidates can develop into further interesting experimental studies, both questioning their unknown cellular role as well as their ignored alteration in AD. Similarly, evaluation of the suggested biomarkers in the context of approved DBS treatments could be also considered.

## CONCLUSIONS

In relation to the first aim of this thesis, regarding the effects of intracranial self-stimulation to the medial forebrain bundle (ICSS) administered in physiological conditions on molecular markers of Alzheimer's disease (AD) pathology:

1. **ICSS administered in physiological conditions presents overlapping regulatory mechanisms with AD.** Specifically, ICSS treatment upregulates miR-132, miR-181c, miR-495 and SIRT1 protein, all of them related to synaptic plasticity and altered in AD, in specific hippocampal subfields. In contrast, ICSS treatment in these conditions do not seem to importantly affect DG levels of other proteins related to main AD hallmarks, including APP, ptau/tau and DBN.
2. **MiR-132 and SIRT1 protein are suggested as potential DBS treatment biomarkers in serum.** Particularly, serum miR-132 is upregulated after ICSS treatment, negatively correlating with its levels in DG. Serum SIRT1, despite not being directly affected by ICSS, positively correlates with miR-132 serum levels.
3. **At a methodological level, miR-16 and let-7a emerge as suitable endogenous normalizers** to test miRNA changes in hippocampal tissue and serum, respectively, after ICSS treatment.

In relation to the second aim of this thesis, regarding the molecular effects of ICSS treatment on early AD neuropathological hallmarks in a sporadic AD rat model obtained by A $\beta$  icv injection:

4. **A $\beta$  model displays signs of early pathology but fails in reproducing AD progression.** At 15-22 days time window after A $\beta$  injection, spatial memory disturbances are evident, but neurodegeneration, decreased DBN levels and increased ptau levels are focused on prelimbic cortex. Instead, at 26-33 days time window memory alterations are marginal, but neurodegeneration and altered DBN and ptau levels are concentrated on temporal-parietal structures. Thus, acute bilateral icv injection of low-dose well-characterized A $\beta$ 1-42 aggregates results in transient



AD-like memory deficits and inverted anterior-to-posterior transition of regional neuropathological signs.

5. **ICSS treatment alleviates early AD hallmarks in A $\beta$  model.** In detail, five post-training ICSS sessions administered on days 26-30 after A $\beta$  injection were able to avoid ptau increase and DBN decrease in entorhinal cortex and hippocampus found at day 33 and rescues the slight memory alterations.

In relation to the third aim of this thesis, regarding the molecular effects of ICSS treatment on early AD neuropathological hallmarks in a sporadic AD rat model obtained by STZ icv injection:

6. **STZ model displays long-lasting coexistence of behavioural and neuropathological affectation.** In particular, acute bilateral icv injection of medium dose STZ results in neurodegeneration, increased phosphorylated tau pathology and APP levels in the hippocampus evaluated after 40 days, together with spatial memory deficit and alteration of some emotional response evaluated at days 33-40.
7. **ICSS treatment recovers neuropathological hallmarks of AD in STZ model.** Notably, five post-training ICSS sessions administered on days 33-37 after STZ injection increased neuronal density and reduced the levels of APP and ptau in hippocampal subfields. Additionally, ICSS increases the levels of synaptic protein DBN in specific layers of rhinal cortices.
8. **SIRT1 is reaffirmed as a promising DBS treatment biomarker in serum in AD-like conditions.** ICSS treatment increases SIRT1 serum levels, which are reduced in STZ model correlating with AD hallmarks.



## REFERENCES

- Adeli S, Zahmatkesh M, Tavoosidana G, Karimian M and Hassanzadeh G. (2017). Simvastatin enhances the hippocampal klotho in a rat model of streptozotocin-induced cognitive decline. *Prog. Neuro-Psychopharmacology Biol. Psychiatry*, 72, 87–94.
- Aggleton JP and Brown MW. (1999). Episodic memory, amnesia, and the hippocampal-anterior thalamic axis. *Behav. Brain Sci.*, 22(3), 425–444.
- Aggleton JP, Pralus A, Nelson AJD and Hornberger M. (2016). Thalamic pathology and memory loss in early Alzheimer's disease: moving the focus from the medial temporal lobe to Papez circuit. *Brain*, 139, 1877–1890.
- Akbarnejad Z, Esmailpour K, Shabani M, Asadi-Shekaari M, Saeedi goraghani M and Ahmadi-Zeidabadi M. (2017). Spatial memory recovery in Alzheimer's rat model by electromagnetic field exposure. *Int. J. Neurosci.*, 7454.
- Aksoy-Aksel A, Zampa F and Schratt G. (2014). MicroRNAs and synaptic plasticity—a mutual relationship. *Philos. Trans. R. Soc. B Biol. Sci.*, 369(1652).
- Albani D, Polito L, Batelli S, De Mauro S, Fracasso C, Martelli G, Colombo L, Manzoni C, Salmona M, Caccia S, Negro A and Forloni G. (2009). The SIRT1 activator resveratrol protects SK-N-BE cells from oxidative stress and against toxicity caused by  $\alpha$ -synuclein or amyloid- $\beta$  (1-42) peptide. *J. Neurochem.*, 110(5), 1445–1456.
- Aldavert-Vera L, Costa-Miserachs D, Massané S-Rotger E, Soriano-Mas C, Segura-Torres P and Morgado-Bernal I. (1997). Facilitation of a Distributed Shuttle-Box Conditioning with Posttraining Intracranial Self-Stimulation in Old Rats. *Neurobiol. Learn. Mem.*, 67, 254–258.
- Aldavert-Vera L, Huguet G, Costa-miserachs D, Pena S, Ortiz D, Kádár E, Morgado-bernal I and Segura-torres P. (2013). Intracranial self-stimulation facilitates active-avoidance retention and induces expression of c-Fos and Nurr1 in rat brain memory systems. *Behav. Brain Res.*, 250, 46–57.
- Aldehri M, Temel Y, Alnaami I, Jahanshahi A and Heschem S. (2018). Deep brain stimulation for Alzheimer's Disease: An update. *Surg. Neurol. Int.*, 9(58).
- Aldridge GM, Podrebarac DM, Greenough WT and Weiler IJ. (2008). The use of total protein stains as loading controls: an alternative to high-abundance single protein controls in semi-quantitative immunoblotting. *J. Neurosci. Methods*, 172(2), 250–254.
- Allen G, Barnard H, McColl R, Hester AL, Fields JA, Weiner MF, Ringe WK, Lipton AM, Brooker M, McDonald E, Rubin CD and Cullum CM. (2007). Reduced hippocampal functional connectivity in Alzheimer disease. *Arch. Neurol.*, 64(10), 1482–1487.
- Altuna-Azkargorta M and Mendioroz-Iriarte M. (2020). Blood biomarkers in Alzheimer's disease. *Neurol. English Ed.*
- Alzheimer's Association. (2019). *FDA-approved treatments for Alzheimer's*.

- Amakiri N, Kubosumi A, Tran J and Reddy PH. (2019). Amyloid Beta and MicroRNAs in Alzheimer's Disease. *Front. Neurosci.*, 13(430).
- Amani M, Zolghadrasab M and Salari AA. (2019). NMDA receptor in the hippocampus alters neurobehavioral phenotypes through inflammatory cytokines in rats with sporadic Alzheimer-like disease. *Physiol. Behav.*, 202, 52–61.
- Andersen CL, Jensen JL and Ørntoft TF. (2004). Normalization of real-time quantitative reverse transcription-PCR data: A model-based variance estimation approach to identify genes suited for normalization, applied to bladder and colon cancer data sets. *Cancer Res.*, 64(15), 5245–5250.
- Angyán L. (1975). Autonomic effects of hypothalamic self-stimulation in the cat. *Physiol. Behav.*, 15(5), 495–498.
- Aronoff JM, Gonnerman LM, Almor A, Arunachalam S, Kempler D and Andersen ES. (2006). Information content versus relational knowledge: Semantic deficits in patients with Alzheimer's disease. *Neuropsychologia*, 44(1), 21–35.
- Asada T, Kinoshita T and Kakuma T. (2000). Analysis of behavioral disturbances among community-dwelling elderly with Alzheimer disease. *Alzheimer Dis. Assoc. Disord.*, 14(3), 160–167.
- Asadbegi M, Yaghmaei P, Salehi I, Komaki A and Ebrahim-Habibi A. (2017). Investigation of thymol effect on learning and memory impairment induced by intrahippocampal injection of amyloid beta peptide in high fat diet- fed rats. *Metab. Brain Dis.*, 32(3), 827–839.
- Avery MC and Krichmar JL. (2017). Neuromodulatory systems and their interactions: A review of models, theories, and experiments. *Front. Neural Circuits*, 11(108).
- Bachurin SO, Bovina E V. and Ustyugov AA. (2017). Drugs in Clinical Trials for Alzheimer's Disease: The Major Trends. *Med. Res. Rev.*, 37(5), 1186–1225.
- Bail S, Swerdel M, Liu H, Jiao X, Goff LA, Hart RP and Kiledjian M. (2010). Differential regulation of microRNA stability. *RNA*, 16(5), 1032–1039.
- Bakker R, Tiesinga P and Kötter R. (2015). The Scalable Brain Atlas: Instant Web-Based Access to Public Brain Atlases and Related Content. *Neuroinformatics*, 13(3), 353–366.
- Baldermann JC, Hardenacke K, Hu X, Köster P, Horn A, Freund H-J, Zilles K, Sturm V, Visser-Vandewalle V, Jessen F, Maintz D and Kuhn J. (2018). Neuroanatomical Characteristics Associated With Response to Deep Brain Stimulation of the Nucleus Basalis of Meynert for Alzheimer's Disease. *Neuromodulation Technol. Neural Interface*, 21(2), 184–190.
- Balietti M, Giuli C and Conti F. (2018). Peripheral Blood Brain-Derived Neurotrophic Factor as a Biomarker of Alzheimer's Disease: Are There Methodological Biases? *Mol. Neurobiol.*, 55(8), 6661–6672.
- Bao J, Mahaman YAR, Liu R, Wang J-Z, Zhang Z, Zhang B and Wang X. (2017). Sex Differences in the Cognitive and Hippocampal Effects of Streptozotocin in an Animal Model of Sporadic AD. *Front. Aging Neurosci.*, 9(347).
- Bariselli S, Glangetas C, Tzanoulinou S and Bellone C. (2016). Ventral tegmental area subcircuits process

- rewarding and aversive experiences. *J. Neurochem.*, 139(6), 1071–1080.
- Barnes J, Bartlett JW, van de Pol LA, Loy CT, Scahill RI, Frost C, Thompson P and Fox NC. (2009). A meta-analysis of hippocampal atrophy rates in Alzheimer's disease. *Neurobiol. Aging*, 30(11), 1711–1723.
- Bartolotti N, Bennett DA and Lazarov O. (2016). Reduced pCREB in Alzheimer's disease prefrontal cortex is reflected in peripheral blood mononuclear cells. *Mol. Psychiatry*, 21(9), 1158–1166.
- Bastle RM, Oliver RJ, Gardiner AS, Pentkowski NS, Bolognani F, Allan AM, Chaudhury T, St. Peter M, Galles N, Smith C, Neisewander JL and Perrone-Bizzozero NI. (2018). In silico identification and in vivo validation of miR-495 as a novel regulator of motivation for cocaine that targets multiple addiction-related networks in the nucleus accumbens. *Mol. Psychiatry*, 23(2), 434–443.
- Basu J and Siegelbaum SA. (2015). The corticohippocampal circuit, synaptic plasticity, and memory. *Cold Spring Harb. Perspect. Biol.*, 7(11).
- Bauernfeind AL, Barks SK, Duka T, Grossman LI, Hof PR and Sherwood CC. (2014). Aerobic glycolysis in the primate brain: Reconsidering the implications for growth and maintenance. *Brain Struct. Funct.*, 219(4), 1149–1167.
- Bayles KA. (1982). Language function in senile dementia. *Brain Lang.*, 16(2), 265–280.
- Becker JT and Overman AA. (2002). The semantic memory deficit in Alzheimer's disease. *Rev. Neurol.*, 35(8), 777–783.
- Benabid AL, Pollak P, Louveau A, Henry S and De Rougemont J. (1987). Combined (thalamotomy and stimulation) stereotactic surgery of the vim thalamic nucleus for bilateral parkinson disease. *Stereotact. Funct. Neurosurg.*, 50(1–6), 344–346.
- Benedikz E, Kloskowska E and Winblad B. (2009). The rat as an animal model of Alzheimer's disease. *J. Cell. Mol. Med.*, 13(6), 1034–1042.
- Bhatnagar S, Chertkow H, Schipper HM, Yuan Z, Shetty V, Jenkins S, Jones T and Wang E. (2014). Increased microRNA-34c abundance in Alzheimer's disease circulating blood plasma. *Front. Mol. Neurosci.*, 7(2).
- Bick SKB and Eskandar EN. (2016). Neuromodulation for restoring memory. *Neurosurg. Focus*, 40(5).
- Bicks LK, Koike H, Akbarian S and Morishita H. (2015). Prefrontal cortex and social cognition in mouse and man. *Front. Psychol.*, 6(1805).
- Bird CM, Chan D, Hartley T, Pijnenburg YA, Rossor MN and Burgess N. (2010). Topographical short-term memory differentiates Alzheimer's disease from frontotemporal lobar degeneration. *Hippocampus*, 20(10), 1154–1169.
- Bishop MP, Thomas Elder S and Heath RG. (1963). Intracranial self-stimulation in man. *Science*, 140(3565), 394–396.
- Blennow K, Wallin A, Ågren H, Spenger C, Siegfried J and Vanmechelen E. (1995). Tau protein in cerebrospinal fluid - A biochemical marker for axonal degeneration in Alzheimer disease? *Mol. Chem. Neuropathol.*, 26(3), 231–245.
- Blennow K, de Leon MJ and Zetterberg H. (2006). Alzheimer's disease. *Lancet*, 368(9533), 387–403.

- Boix-Trelis N, Vale-Martínez A, Guillazo-Blanch G, Costa-Miserachs D and Martí-Nicolovius M. (2006). Effects of nucleus basalis magnocellularis stimulation on a socially transmitted food preference and c-Fos expression. *Learn. Mem.*, 13(6), 783–793.
- Bonda DJ, Lee H gon, Camins A, Pallàs M, Casadesus G, Smith MA and Zhu X. (2011). The sirtuin pathway in ageing and Alzheimer disease: Mechanistic and therapeutic considerations. *Lancet Neurol.*, 10(3), 275–279.
- Boyd ES and Gardner LC. (1962). Positive and negative reinforcement from intracranial stimulation of a teleost. *Science*, 136(3516), 648–649.
- Braak H and Braak E. (1991a). Neuropathological staging of Alzheimer-related changes. *Acta Neuropathol.*, 82(4), 239–259.
- Braak H and Braak E. (1991b). Alzheimer's disease affects limbic nuclei of the thalamus. *Acta Neuropathol.*, 81(3), 261–268.
- Braak H, Alafuzoff I, Arzberger T, Kretschmar H and Tredici K. (2006a). Staging of Alzheimer disease-associated neurofibrillary pathology using paraffin sections and immunocytochemistry. *Acta Neuropathol.*, 112(4), 389–404.
- Braak H, Rüb U, Schultz C and Del Tredici K. (2006b). Vulnerability of cortical neurons to Alzheimer's and Parkinson's diseases. *J. Alzheimer's Dis.*, 9, 35–44.
- Brem A-K, Ran K and Pascual-Leone A. (2013). Learning and memory. *Handb. Clin. Neurol.*, 116, 693–737.
- Brodsky H and Donkin M. (2009). Family caregivers of people with dementia. *Dialogues Clin. Neurosci.*, 11(2), 217–228.
- Brunet A, Sweeney LB, Sturgill JF, Chua KF, Greer PL, Lin Y, Tran H, Ross SE, Mostoslavsky R, Cohen HY, Hu LS, Cheng HL, Jedrychowski MP, Gygi SP, Sinclair DA, Alt FW and Greenberg ME. (2004). Stress-Dependent Regulation of FOXO Transcription Factors by the SIRT1 Deacetylase. *Science*, 303(5666), 2011–2015.
- Bubb EJ, Kinnavane L and Aggleton JP. (2017). Hippocampal–diencephalic–cingulate networks for memory and emotion: An anatomical guide. *Brain Neurosci. Adv.*, 20, 1–20.
- Buckner RL, Andrews-Hanna JR and Schacter DL. (2008). The brain's default network: Anatomy, function, and relevance to disease. *Ann. N. Y. Acad. Sci.*, 1124, 1–38.
- Buerger K, Ewers M, Pirttilä T, Zynkowski R, Alafuzoff I, Teipel SJ, DeBernardis J, Kerkman D, McCulloch C, Soininen H and Hampel H. (2006). CSF phosphorylated tau protein correlates with neocortical neurofibrillary pathology in Alzheimer's disease. *Brain*, 129, 3035–3041.
- Burgos K, Malenica I, Metpally R, Courtright A and Rakela B. (2014). Profiles of Extracellular miRNA in Cerebrospinal Fluid and Serum from Patients with Alzheimer's and Parkinson's Diseases Correlate with Disease Status and Features of Pathology Profiles of Extracellular miRNA in Cerebrospinal Fluid and Serum from Patients. *PLoS One*, 9(5), e94839.
- Carlisle HJ and Snyder E. (1970). The interaction of hypothalamic self-stimulation and temperature regulation.

*Experientia*, 26(10), 1092–1093.

- Cazala P, Cazals Y and Cardo B. (1974). Hypothalamic self-stimulation in three inbred strains of mice. *Brain Res.*, 81(1), 159–167.
- Cha J, Carlson JM, DeDora DJ, Greenberg T, Proudfit GH and Mujica-Parodi LR. (2014). Hyper-reactive human ventral tegmental area and aberrant mesocorticolimbic connectivity in overgeneralization of fear in generalized anxiety disorder. *J. Neurosci.*, 34(17), 5855–5860.
- Chamorro-López J, Miguéns M, Morgado-Bernal I, Kastanauskaite A, Selvas A, Cabané-Cucurella A, Aldavert-Vera L, DeFelipe J and Segura-Torres P. (2015). Structural plasticity in hippocampal cells related to the facilitative effect of intracranial self-stimulation on a spatial memory task. *Behav. Neurosci.*, 129(6), 720–730.
- Chen Y, Liang Z, Blanchard J, Dai CL, Sun S, Lee MH, Grundke-Iqbal I, Iqbal K, Liu F and Gong CX. (2013). A non-transgenic mouse model (icv-STZ mouse) of Alzheimer's disease: similarities to and differences from the transgenic model (3xTg-AD mouse). *Mol. Neurobiol.*, 47(2), 711–725.
- Chen GF, Xu TH, Yan Y, Zhou YR, Jiang Y, Melcher K and Xu HE. (2017). Amyloid beta: Structure, biology and structure-based therapeutic development. *Acta Pharmacol. Sin.*, 38(9), 1205–1235.
- Chen Y, Fu AKY and Ip NY. (2019). Synaptic dysfunction in Alzheimer's disease: Mechanisms and therapeutic strategies. *Pharmacol. Ther.*, 195, 186–198.
- Chen Z and Zhong C. (2013). Decoding Alzheimer's disease from perturbed cerebral glucose metabolism: Implications for diagnostic and therapeutic strategies. *Prog. Neurobiol.*, 108, 21–43.
- Clark CM, Xie S, Chittams J, Ewbank D, Peskind E, Galasko D, Morris JC, McKeel DW, Farlow M, Weitlauf SL, Quinn J, Kaye J, Knopman D, Arai H, Doody RS, DeCarli C, Leight S, Lee VM-Y and Trojanowski JW. (2003). Cerebrospinal Fluid Tau and  $\beta$ -Amyloid: How Well Do These Biomarkers Reflect Autopsy-Confirmed Dementia Diagnoses? *Arch. Neurol.*, 60, 1696–1702.
- Cleary JP, Walsh DM, Hofmeister JJ, Shankar GM, Kuskowski MA, Selkoe DJ and Ashe KH. (2005). Natural oligomers of the amyloid- $\beta$  protein specifically disrupt cognitive function. *Nat. Neurosci.*, 8(1), 79–84.
- Codocedo JF, Allard C, Godoy JA, Varela-Nallar L and Inestrosa NC. (2012). SIRT1 Regulates Dendritic Development in Hippocampal Neurons. *PLoS One*, 7(10), 1–14.
- Coenen VA, Schumacher LV, Kaller C, Schlaepfer TE, Reinacher PC, Egger K, Urbach H and Reisert M. (2018). The anatomy of the human medial forebrain bundle: Ventral tegmental area connections to reward-associated subcortical and frontal lobe regions. *NeuroImage Clin.*, 18, 770–783.
- Coenen VA, Bewernick BH, Kayser S, Kilian H, Boström J, Greschus S, Hurlemann R, Klein ME, Spanier S, Sajonz B, Urbach H and Schlaepfer TE. (2019). Superolateral medial forebrain bundle deep brain stimulation in major depression: a gateway trial. *Neuropsychopharmacology*, 44(7), 1224–1232.
- Cogswell JP, Ward J, Taylor IA, Waters M, Shi Y, Cannon B, Kelnar K, Kempainen J, Brown D, Chen C, Prinjha RK, Richardson JC, Saunders AM, Roses AD and Richards CA. (2008). Identification of miRNA Changes in Alzheimer's Disease Brain and CSF Yields Putative Biomarkers and Insights into Disease Pathways. *J. Alzheimer's Dis.*, 14(1), 27–41.

- Cohen RS. (2013). Cell biology of the synapse. In *Neuroscience in the 21st Century: From Basic to Clinical* (pp. 309–349). Springer New York.
- Cohen JE, Lee PR, Chen S, Li W, Fields RD and Greenberg ME. (2011). MicroRNA regulation of homeostatic synaptic plasticity. *108*(28).
- Cordella A, Krashia P, Nobili A, Pignataro A, La Barbera L, Viscomi MT, Valzania A, Keller F, Ammassari-Teule M, Mercuri NB, Berretta N and D’Amelio M. (2018). Dopamine loss alters the hippocampus-nucleus accumbens synaptic transmission in the Tg2576 mouse model of Alzheimer’s disease. *Neurobiol. Dis.*, *116*, 142–154.
- Costantini LC, Barr LJ, Vogel JL and Henderson ST. (2008). Hypometabolism as a therapeutic target in Alzheimer’s disease. *BMC Neurosci.*, *9*(Supl2).
- Counts SE, Nadeem M, Lad SP, Wu J and Mufson EJ. (2006). Differential Expression of Synaptic Proteins in the Frontal and Temporal Cortex of Elderly Subjects With Mild Cognitive Impairment. *J Neuropathol Exp Neurol*, *65*(6), 592–601.
- Counts SE, He B, Nadeem M, Wu J, Scheff SW and Mufson EJ. (2012). Hippocampal Drebrin Loss in Mild Cognitive Impairment. *Neurodegener. Dis.*, *10*, 216–219.
- D’Hooge R and De Deyn PP. (2001). Applications of the Morris water maze in the study of learning and memory. *Brain Res. Rev.*, *36*(1), 60–90.
- Dandekar MP, Fenoy AJ, Carvalho AF, Soares JC and Quevedo J. (2018). Deep brain stimulation for treatment-resistant depression: An integrative review of preclinical and clinical findings and translational implications. *Mol. Psychiatry*, *23*(5), 1094–1112.
- De-Paula VJ, Radanovic M, Diniz BS and Forlenza O V. (2012). Alzheimer’s Disease. *Subcell. Biochem.*, *65*, 329–352.
- De la Monte SM. (2014). Type 3 diabetes is sporadic Alzheimer’s disease: mini-review. *Eur. Neuropsychopharmacol.*, *24*(12), 1954–1960.
- De La Monte SM, Tong M, Schiano I and Didsbury J. (2017). Improved Brain Insulin/IGF Signaling and Reduced Neuroinflammation with T3D-959 in an Experimental Model of Sporadic Alzheimer’s Disease. *J Alzheimers Dis*, *55*(2), 849–864.
- De Leon MJ, Ferris SH, George AE, Christman DR, Fowler JS, Gentes C, Reisberg B, Gee B, Emmerich M, Yonekura Y, Brodie J, Kricheft II and Wolf AP. (1983). Positron Emission Tomographic Studies of Aging and Alzheimer Disease. *Am. J. Neuroradiol.*, *4*(3), 568–571.
- De Marco M and Venneri A. (2018). Volume and connectivity of the ventral tegmental area are linked to neurocognitive signatures of Alzheimer’s disease in humans. *J. Alzheimer’s Dis.*, *63*(1), 167–180.
- De Souza LC, Chupin M, Lamari F, Jardel C, Leclercq D, Colliot O, Lehericy S, Dubois B and Sarazin M. (2012). CSF tau markers are correlated with hippocampal volume in Alzheimer’s disease. *Neurobiol. Aging*, *33*(7), 1253–1257.
- Dehghan-Shasaltaneh M, Naghdi N, Choopani S, Alizadeh L, Bolouri B, Masoudi-Nejad A and Riazi GH.



- (2016). Determination of the Best Concentration of Streptozotocin to Create a Diabetic Brain Using Histological Techniques. *J. Mol. Neurosci.*, 59(1), 24–35.
- DeIpoli AR, Rankin KP, Mucke L, Miller BL and Gorno-Tempini ML. (2007). Spatial cognition and the human navigation network in AD and MCI. *Neurology*, 69(10), 986–997.
- DeTure MA and Dickson DW. (2019). The neuropathological diagnosis of Alzheimer’s disease. *Mol. Neurodegener.*, 14(32).
- Döbrössy MD, Ramanathan C, Ashouri Vajari D, Tong Y, Schlaepfer T and Coenen VA. (2020). Neuromodulation in Psychiatric disorders: Experimental and Clinical evidence for reward and motivation network Deep Brain Stimulation: Focus on the medial forebrain bundle. *Eur. J. Neurosci.*, July, 1–25.
- Dos Santos Picanço LC, Ozela PF, Brito M de F de B, Pinheiro AA, Padilha EC, Braga FS, Silva CHT de P da, Santos CBR dos, Rosa JMC and Hage-Melim LI da S. (2018). Alzheimer’s Disease: A Review from the Pathophysiology to Diagnosis, New Perspectives for Pharmacological Treatment. *Curr. Med. Chem.*, 25, 3141–3159.
- Drummond E and Wisniewski T. (2016). Alzheimer’s Disease: Experimental Models and Reality. *Acta Neuropathol*, 133, 155–175.
- Du X, Wang X and Geng M. (2018). Alzheimer’s disease hypothesis and related therapies. *Transl. Neurodegener.*, 7(2).
- Dubois B, Feldman HH, Jacova C, DeKosky ST, Barberger-Gateau P, Cummings J, Delacourte A, Galasko D, Gauthier S, Jicha G, Meguro K, O’Brien J, Pasquier F, Robert P, Rossor M, Salloway S, Stern Y, Visser PJ and Scheltens P. (2007). Research criteria for the diagnosis of Alzheimer’s disease: revising the NINCDS-ADRDA criteria. *Lancet Neurol.*, 6(8), 734–746.
- Earls LR, Westmoreland JJ and Zakharenko SS. (2014). Non-coding RNA regulation of synaptic plasticity and memory: Implications for aging. *Ageing Res. Rev.*, 17, 34–42.
- Elizondo-Vega R, Cortes-Campos C, Barahona MJ, Oyarce KA, Carril CA and García-Robles MA. (2015). The role of tanycytes in hypothalamic glucosensing. *J. Cell. Mol. Med.*, 19(7), 1471–1482.
- Eriksson J, Vogel EK, Lansner A, Bergström F and Nyberg L. (2015). Neurocognitive Architecture of Working Memory. *Neuron*, 88(1), 33–46.
- Fagan AM, Mintun MA, Mach RH, Lee SY, Dence CS, Shah AR, LaRossa GN, Spinner ML, Klunk WE, Mathis CA, DeKosky ST, Morris JC and Holtzman DM. (2006). Inverse relation between in vivo amyloid imaging load and cerebrospinal fluid Abeta42 in humans. *Ann. Neurol.*, 59(3), 512–519.
- Falk JL. (1961). Septal stimulation as a reinforcer of and an alternative to consumatory behavior. *J. Exp. Anal. Behav.*, 4(3), 213–217.
- Fama R and Sullivan E V. (2015). Thalamic structures and associated cognitive functions: Relations with age and aging. *Neurosci Biobehav Rev.*, 54, 29–37.
- Fang C, Li Q, Min G, Liu M, Cui J, Sun J and Li L. (2016). MicroRNA-181c Ameliorates Cognitive Impairment Induced by Chronic Cerebral Hypoperfusion in Rats. *Mol Neurobiol*, 54, 8370–8385.

- Farbood Y, Shabani S, Sarkaki A, Mard SA, Ahangarpour A and Khorsandi L. (2017). Peripheral and central administration of T3 improved the histological changes, memory and the dentate gyrus electrophysiological activity in an animal model of Alzheimer's disease. *Metab. Brain Dis.*, 32(3), 693–701.
- Fatimy R El, Li S, Chen Z, Mushannen T, Gongala S, Wei Z, Balu DT, Rabinovsky R, Cantlon A, Elkhali A, Dennis JS, Sonntag KC, Walsh DM and Krichevsky AM. (2018). MicroRNA-132 provides neuroprotection for tauopathies via multiple signaling pathways. *Acta Neuropathol.*, 136, 537–555.
- Femminella GD, Ferrara N and Rengo G. (2015). The emerging role of microRNAs in Alzheimer's disease. *Front. Physiol.*, 6(40).
- Fenoy AJ, Schulz PE, Selvaraj S, Burrows CL, Zunta-Soares G, Durkin K, Zanotti-Fregonara P, Quevedo J and Soares JC. (2018). A longitudinal study on deep brain stimulation of the medial forebrain bundle for treatment-resistant depression. *Transl. Psychiatry*, 8(111).
- Ferguson MA, Lim C, Cooke D, Darby RR, Wu O, Rost NS, Corbetta M, Grafman J and Fox MD. (2019). A human memory circuit derived from brain lesions causing amnesia. *Nat. Commun.*, 10(3497).
- Ferreira-Vieira TH, Guimaraes IM, Silva FR and Ribeiro FM. (2016). Alzheimer's disease: Targeting the Cholinergic System. *Curr. Neuropharmacol.*, 14(1), 101–115.
- Ferretti L, Mccurry SM, Logsdon R, Gibbons L and Teri L. (2001). Anxiety and Alzheimer's disease. *J. Geriatr. Psychiatry Neurol.*, 14(1), 52–58.
- Fincha CE and Austad SN. (2015). Commentary: is Alzheimer's disease uniquely human? *Neurobiol. Aging*, 36(2), 535–555.
- Fletcher E, Carmichael O, Pasternak O, Maier-Hein KH and DeCarli C. (2014). Early brain loss in circuits affected by Alzheimer's disease is predicted by fornix microstructure but may be independent of gray matter. *Front. Aging Neurosci.*, 6(106).
- Fogel H, Frere S, Segev O, Bharill S, Shapira I, Gazit N, O'Malley T, Slomowitz E, Berdichevsky Y, Walsh DM, Isacoff EY, Hirsch JA and Slutsky I. (2014). APP Homodimers Transduce an Amyloid-b-Mediated Increase in Release Probability at Excitatory Synapses. *Cell Rep.*, 7, 1560–1576.
- Fontaine D, Deudon A, Lemaire JJ, Razzouk M, Viau P, Darcourt J and Robert P. (2013). Symptomatic treatment of memory decline in Alzheimer's disease by deep brain stimulation: A feasibility study. *J. Alzheimer's Dis.*, 34(1), 315–323.
- Fornier S, Baglietto-Vargas D, Martini AC, Trujillo-Estrada L and LaFerla FM. (2017). Synaptic Impairment in Alzheimer's Disease: A Dysregulated Symphony. *Trends Neurosci.*, 40(6), 347–357.
- Francis PT, Palmer AM, Snape M and Wilcock GK. (1999). The cholinergic hypothesis of Alzheimer's disease: a review of progress. *J Neurol Neurosurg Psychiatry*, 66, 137–147.
- Freund HJ, Kuhn J, Lenartz D, Mai JK, Schnell T, Klosterkoetter J and Sturm V. (2009). Cognitive functions in a patient with parkinson-dementia syndrome undergoing deep brain stimulation. *Arch. Neurol.*, 66(6), 781–785.
- Frisardi V, Solfrizzi V, Capurso C, Imbimbo BP, Vendemiale G, Seripa D, Pilotto A and Panza F. (2010). Is

- insulin resistant brain state a central feature of the metabolic-cognitive syndrome? *J. Alzheimer's Dis.*, 21(1), 57–63.
- Fu M-H, Li C-L, Lin H-L, Tsai S-J, Lai Y-Y, Chang Y-F, Cheng P-H, Chen C-M and Yang S-H. (2015). The Potential Regulatory Mechanisms of miR-196a in Huntington's Disease through Bioinformatic Analyses. *PLoS One*, 10(9), e0137637.
- Futch HS and Croft CL. (2018). SIRT1: A novel way to target Tau? *J. Neurosci.*, 38(36), 7755–7757.
- Gallagher M, Burwell RD and Burchinal M. (2015). Severity of Spatial Learning Impairment in Aging: Development of a Learning Index for Performance in the Morris Water Maze. *Behav. Neurosci.*, 129(4), 540–548.
- Gantier MP, McCoy CE, Rusinova I, Saulep D, Wang D, Xu D, Irving AT, Behlke MA, Hertzog PJ, MacKay F and Williams BRG. (2011). Analysis of microRNA turnover in mammalian cells following Dicer1 ablation. *Nucleic Acids Res.*, 39(13), 5692–5703.
- Gao J, Wang W-Y, Mao Y-W, Gräff J, Guan J-S, Pan L, Mak G, Kim D, Su SC and Tsai L-H. (2010). A novel pathway regulates memory and plasticity via SIRT1 and miR-134. *Nature*, 466(7310), 1105–1109.
- García-Brito S, Morgado-Bernal I, Biosca-Simon N and Segura-Torres P. (2017). Intracranial self-stimulation also facilitates learning in a visual discrimination task in the Morris water maze in rats. *Behav. Brain Res.*, 317, 360–366.
- García-Brito S, Aldavert-Vera L, Huguet G, Kádár E and Segura-Torres P. (2020). Orexin-1 receptor blockade differentially affects spatial and visual discrimination memory facilitation by intracranial self-stimulation. *Neurobiol. Learn. Mem.*, 169(107188).
- Garre-Olmo J. (2018). Epidemiology of Alzheimer's disease and other dementias. *Rev Neurol*, 66(1), 377–386.
- Geekiyange H and Chan C. (2011). MicroRNA-137/181c Regulates Serine Palmitoyltransferase and In Turn Amyloid , Novel Targets in Sporadic Alzheimer's Disease. *J. Neurosci.*, 31(41), 14820–14830.
- Geekiyange H, Jicha GA, Nelson PT and Chan C. (2012). Blood serum miRNA: Non-invasive biomarkers for Alzheimer's disease. *Exp. Neurol.*, 235(2), 491–496.
- Gezen-Ak D, Dursun E, Hanağasi H, Bilgiç B, Lohman E, Araz ÖS, Atasoy IL, Alaylioğlu M, Önal B, Gürvit H and Yilmazer S. (2013). BDNF, TNF $\alpha$ , HSP90, CFH, and IL-10 serum levels in patients with early or late onset Alzheimer's disease or mild cognitive impairment. *J. Alzheimer's Dis.*, 37(1), 185–195.
- Gibb WRG, Mountjoy CQ, Mann DMA and Lees AJ. (1989). The substantia nigra and ventral tegmental area in Alzheimer's disease and Down's syndrome. *J. Neurol. Neurosurg. Psychiatry*, 52(2), 193–200.
- Giovannelli L, Casamenti F, Scali C, Bartolini L and Pepeu G. (1995). Differential effects of amyloid peptides  $\beta$ -(1-40) and  $\beta$ -(25-35) injections into the rat nucleus basalis. *Neuroscience*, 66(4), 781–792.
- Glenner GG and Wong CW. (1984). Alzheimer's disease: Initial report of the purification and characterization of a novel cerebrovascular amyloid protein. *Biochem. Biophys. Res. Commun.*, 120(3), 885–890.
- Gold CA and Budson AE. (2009). Memory loss in Alzheimer's disease: implications for development of therapeutics. *Expert Rev Neurother*, 8(12), 1879–1891.

- Gómez-Isla T, Price JL, McKeel DW, Morris JC, Growdon JH and Hyman BT. (1996). Profound loss of layer II entorhinal cortex neurons occurs in very mild Alzheimer's disease. *J. Neurosci.*, 16(14), 4491–4500.
- Gondard E, Chau HN, Mann A, Tierney TS, Hamani C, Kalia SK and Lozano AM. (2015). Rapid modulation of protein expression in the rat hippocampus following deep brain stimulation of the fornix. *Brain Stimul.*, 8(6), 1058–1064.
- Goodman IJ and Brown JL. (1966). Stimulation of positively and negatively reinforcing sites in the avian brain. *Life Sci.*, 5(8), 693–704.
- Grady CL, Haxby J V., Schlageter NL, Berg G and Rapoport SI. (1986). Stability of metabolic and neuropsychological asymmetries in dementia of the alzheimer type. *Neurology*, 36(10), 1390–1392.
- Grady CL, Furey ML, Pietrini P, Horwitz B and Rapoport SI. (2001). Altered brain functional connectivity and impaired short-term memory in Alzheimer's disease. *Brain*, 124(4), 739–756.
- Gratwicke J, Zrinzo L, Kahan J, Peters A, Beigi M, Akram H, Hyam J, Oswal A, Day B, Mancini L, Thornton J, Yousry T, Limousin P, Hariz M, Jahanshahi M and Foltynie T. (2018). Bilateral deep brain stimulation of the nucleus basalis of meynert for Parkinson disease dementia a randomized clinical trial. *JAMA Neurol.*, 75(2), 169–178.
- Greicius MD, Srivastava G, Reiss AL and Menon V. (2004). Default-mode network activity distinguishes Alzheimer's disease from healthy aging: Evidence from functional MRI. *Proc. Natl. Acad. Sci. U. S. A.*, 101(13), 4637–4642.
- Grieb P. (2016). Intracerebroventricular Streptozotocin Injections as a Model of Alzheimer's Disease: in Search of a Relevant Mechanism. *Mol Neurobiol*, 53, 1741–1752.
- Grimmer T, Riemenschneider M, Förstl H, Henriksen G, Klunk WE, Mathis CA, Shiga T, Wester HJ, Kurz A and Drzezga A. (2009). Beta Amyloid in Alzheimer's Disease: Increased Deposition in Brain Is Reflected in Reduced Concentration in Cerebrospinal Fluid. *Biol. Psychiatry*, 65(11), 927–934.
- Groiss SJ, Wojtecki L, Sudmeyer M and Schnitzler A. (2009). Deep brain stimulation in Parkinson's disease. *Ther. Adv. Neurol. Disord.*, 2(6), 379–391.
- Grundke-Iqbal I, Iqbal K, Tung Y-C, Quinlan M, Wisniewski HM and Lester I Binder. (1986a). Abnormal phosphorylation of the microtubule-associated protein tau (tau) in Alzheimer cytoskeletal pathology. *Proc. Natl. Acad. Sci. U. S. A.*, 83(13), 4913–4917.
- Grundke-Iqbal I, Iqbal K, Quinlan M, Tung Y-C, Zaidi MS and Wisniewski HM. (1986b). Microtubule-associated Protein Tau: A component of Alzheimer paired helical filaments. *J. Biol. Chem.*, 261(13), 6084–6089.
- Guedes JR, Santana I, Cunha C, Duro D, Almeida MR, Cardoso AM, de Lima MCP and Cardoso AL. (2016). MicroRNA deregulation and chemotaxis and phagocytosis impairment in Alzheimer's disease. *Alzheimer's Dement. Diagnosis, Assess. Dis. Monit.*, 3, 7–17.
- Guo T, Noble W and Hanger DP. (2017). Roles of tau protein in health and disease. *Acta Neuropathol.*, 133(5), 665–704.

- Gupta A, Singh MP and Sisodia SS. (2018). A Review on Learning and Memory. *J. Drug Deliv. Ther.*, 8(2), 153–157.
- Hadar A, Milanesi E, Walczak M, Puzianowska-Kuźnicka M, Kuźnicki J, Squassina A, Niola P, Chillotti C, Attems J, Gozes I and Gurwitz D. (2018). SIRT1, miR-132 and miR-212 link human longevity to Alzheimer's Disease. *Sci. Rep.*, 8(1), 8465.
- Hamani C, McAndrews MP, Cohn M, Oh M, Zumsteg D, Shapiro CM, Wennberg RA and Lozano AM. (2008). Memory enhancement induced by hypothalamic/fornix deep brain stimulation. *Ann. Neurol.*, 63(1), 119–123.
- Hampel H, Teipel SJ, Fuchsberger T, Andreasen N, Wiltfang J, Otto M, Shen Y, Dodel R, Du Y, Farlow M, Möller HJ, Blennow K and Buerger K. (2004). Value of CSF  $\beta$ -amyloid1-42 and tau as predictors of Alzheimer's disease in patients with mild cognitive impairment. *Mol. Psychiatry*, 9(7), 705–710.
- Hansen KF, Sakamoto K, Wayman GA, Impey S and Obrietan K. (2010). Transgenic miR132 alters neuronal spine density and impairs novel object recognition memory. *PLoS One*, 5(11).
- Hansen KF, Karelina K, Sakamoto K, Wayman GA, Impey S and Obrietan K. (2013). MiRNA-132: a dynamic regulator of cognitive capacity. *Brain Struct. Funct.*, 218(3), 817–831.
- Hardenacke K, Hashemiyoon R, Visser-Vandewalle V, Zapf A, Freund HJ, Sturm V, Hellmich M and Kuhn J. (2016). Deep Brain Stimulation of the Nucleus Basalis of Meynert in Alzheimer's Dementia: Potential Predictors of Cognitive Change and Results of a Long-Term Follow-Up in Eight Patients. *Brain Stimul.*, 9(5), 799–800.
- Hardy J and Allsop D. (1991). Amyloid deposition as the central event in the aetiology of Alzheimer's disease. *Trends Pharmacol. Sci.*, 12(10), 383–388.
- Hardy JA and Higgins GA. (1992). Alzheimer's disease: The amyloid cascade hypothesis. *Science*, 256(5054), 184–185.
- Hardy J and Selkoe DJ. (2002). The amyloid hypothesis of Alzheimer's disease: Progress and problems on the road to therapeutics. *Science*, 297(5580), 353–356.
- Harigaya Y, Shoji M, Shirao T and Hirai S. (1996). Disappearance of actin-binding protein, drebrin, from hippocampal synapses in Alzheimer's disease. *J. Neurosci. Res.*, 43(1), 87–92.
- Harris RA, Tindale L and Cumming RC. (2014). Age-dependent metabolic dysregulation in cancer and Alzheimer's disease. *Biogerontology*, 15(6), 559–577.
- Heath RG. (1963). Electrical Self-Stimulation of the Brain in Man. *Am. J. Psychiatry*, 120, 571–577.
- Hébert SS, Horré K, Nicolai L, Papadopoulou AS, Mandemakers W, Silahatoglu AN, Kauppinen S, Delacourte A and De Strooper B. (2008). Loss of microRNA cluster miR-29a/b-1 in sporadic Alzheimer's disease correlates with increased BACE1/beta-secretase expression. *Proc. Natl. Acad. Sci. U. S. A.*, 105(17), 6415–6420.
- Her LS, Mao SH, Chang CY, Cheng PH, Chang YF, Yang HI, Chen CM and Yang SH. (2017). miR-196a enhances neuronal morphology through suppressing RANBP10 to provide neuroprotection in

- Huntington's disease. *Theranostics*, 7(9), 2452–2462.
- Hermer-Vazquez L, Hermer-Vazquez R, Rybinnik I, Greebel G, Keller R, Xu S and Chapin JK. (2005). Rapid learning and flexible memory in “habit” tasks in rats trained with brain stimulation reward. *Physiol. Behav.*, 84(5), 753–759.
- Hernandez-Rapp J, Rainone S, Goupil C, Dorval V, Smith PY, Saint-Pierre M, Vallée M, Planel E, Droit A, Calon F, Cicchetti F and Hébert SS. (2016). microRNA-132/212 deficiency enhances A $\beta$  production and senile plaque deposition in Alzheimer's disease triple transgenic mice. *Sci. Rep.*, 6(30953).
- Herskovits AZ and Guarente L. (2014). SIRT1 in neurodevelopment and brain senescence. *Neuron*, 81(3), 471–483.
- Hescham S, Lim LW, Jahanshahi A, Steinbusch HWM, Prickaerts J, Blokland A and Temel Y. (2013). Deep brain stimulation of the fornix area enhances memory functions in experimental dementia: The role of stimulation parameters. *Brain Stimul.*, 6(1), 72–77.
- Hescham S, Jahanshahi A, Schweimer J V., Mitchell SN, Carter G, Blokland A, Sharp T and Temel Y. (2016). Fornix deep brain stimulation enhances acetylcholine levels in the hippocampus. *Brain Struct. Funct.*, 221(8), 4281–4286.
- Hescham S, Temel Y, Schipper S, Lagiere M, Schönfeld LM, Blokland A and Jahanshahi A. (2017). Fornix deep brain stimulation induced long-term spatial memory independent of hippocampal neurogenesis. *Brain Struct. Funct.*, 222(2), 1069–1075.
- Hippius H and Neundörfer G. (2003). The discovery of Alzheimer's disease. *Dialogues Clin. Neurosci.*, 5(1), 101–108.
- Hooper MW and Vogel FS. (1976). The limbic system in Alzheimer's disease. A neuropathologic investigation. *Am. J. Pathol.*, 85(1), 1–20.
- Hotta H, Kagitani F, Kondo M and Uchida S. (2009). Basal forebrain stimulation induces NGF secretion in ipsilateral parietal cortex via nicotinic receptor activation in adult, but not aged rats. *Neurosci. Res.*, 63(2), 122–128.
- Hoyer S. (2002). The brain insulin signal transduction system and sporadic (type II) Alzheimer disease: an update. *J Neural Transm.*, 109, 341–360.
- Hoyer S, Muller D and Plaschke K. (1994). Desensitization of brain insulin receptor. Effect on glucose/energy and related metabolism. *J. Neural Transm. Suppl.*, 44(44), 259–268.
- Huang X-B, Chen Y-J, Chen W-Q, Wang N-Q, Wu X-L and Liu Y. (2018). Neuroprotective effects of tenuigenin on neurobehavior, oxidative stress, and tau hyperphosphorylation induced by intracerebroventricular streptozotocin in rats. *Brain Circ.*, 4(1), 24–32.
- Huang C, Chu H, Ma Y, Zhou Z, Dai C, Huang X, Fang L, Ao Q and Huang D. (2019). The neuroprotective effect of deep brain stimulation at nucleus basalis of Meynert in transgenic mice with Alzheimer's disease. *Brain Stimul.*, 12(1), 161–174.
- Hugon J, Mouton-Liger F, Cognat E, Dumurgier J and Paquet C. (2018). Blood-Based Kinase Assessments in

- Alzheimer's Disease. *Front. Aging Neurosci.*, 10(338).
- Huguet G, Aldavert-Vera L, Kádár E, Peña De Ortiz S, Morgado-Bernal I and Segura-Torres P. (2009). Intracranial self-stimulation to the lateral hypothalamus, a memory improving treatment, results in hippocampal changes in gene expression. *Neuroscience*, 162, 359–374.
- Huguet G, Kádár E, Serrano N, Tapias-Espinosa C, García-Brito S, Morgado-Bernal I, Aldavert-Vera L and Segura-Torres P. (2020). Rewarding deep brain stimulation at the medial forebrain bundle favours avoidance conditioned response in a remote memory test, hinders extinction and increases neurogenesis. *Behav. Brain Res.*, 378(112308).
- Hui S, Yang Y, Peng W, Sheng C, Gong W, Chen S, Xu P and Wang Z. (2017). Protective effects of Bushen Tiansui decoction on hippocampal synapses in a rat model of Alzheimer's disease. *Neural Regen Res*, 12(10), 1680–1686.
- Hussain RJ and Carpenter DO. (2005). A Comparison of the Roles of Protein Kinase C in Long-Term Potentiation in Rat Hippocampal Areas CA1 and CA3. *Cell. Mol. Neurobiol.*, 25(3/4), 649–661.
- Huston JP, Mueller CC and Mondadori C. (1977). Memory facilitation by posttrial hypothalamic stimulation and other reinforcers: A central theory of reinforcement. *Biobehav. Rev.*, 1(3), 143–150.
- Huston JP and Mueller CC. (1978). Enhanced passive avoidance learning and appetitive T-maze learning with post-trial rewarding hypothalamic stimulation. *Brain Res. Bull.*, 3(3), 265–270.
- Im HI and Kenny PJ. (2012). MicroRNAs in neuronal function and dysfunction. *Trends Neurosci.*, 35(5), 325–334.
- Impey S, Davare M, Lesiak A, Lasiek A, Fortin D, Ando H, Varlamova O, Obrietan K, Soderling TR, Goodman RH and Wayman GA. (2010). An activity-induced microRNA controls dendritic spine formation by regulating Rac1-PAK signaling. *Mol. Cell. Neurosci.*, 43(1), 146–156.
- Ishizuka Y and Hanamura K. (2017). Drebrin in Alzheimer's disease. In S. Y. Shirao T. (Ed.), *Drebrin. Advances in Experimental Medicine and Biology* (Vol. 1006, pp. 203–223).
- Jackson J, Jambrina E, Li J, Marston H, Menzies F, Phillips K and Gilmour G. (2019). Targeting the Synapse in Alzheimer's Disease. *Front. Neurosci.*, 13(735).
- Jadhav S, Cubinhova V, Zimova I, Brezovakova V, Madari A, Cigankova V and Zilka N. (2015). Tau-Mediated Synaptic Damage in Alzheimer's Disease. *Transl. Neurosci.*, 6, 214–226.
- Jahn H. (2013). Memory loss in alzheimer's disease. *Dialogues Clin. Neurosci.*, 15(4), 445–454.
- Janel N, Sarazin M, Corlier F, Corne H, De Souza LC, Hamelin L, Aka A, Lagarde J, Blehaut H, Hindié V, Rain JC, Arbones ML, Dubois B, Potier MC, Bottlaender M and Delabar JM. (2011). Plasma DYRK1A as a novel risk factor for Alzheimer's disease. *Transl. Psychiatry*, 4(8), 425.
- Jankowsky JL, Slunt HH, Gonzales V, Savonenko A V., Wen JC, Jenkins NA, Copeland NG, Younkin LH, Lester HA, Younkin SG and Borchelt DR. (2005). Persistent amyloidosis following suppression of A $\beta$  production in a transgenic model of Alzheimer disease. *PLoS Med.*, 2(12), 1318–1333.
- Jankowski MM, Ronnqvist KC, Tsanov M, Vann SD, Wright NF, Erichsen JT, Aggleton JP and O'Mara SM.

- (2013). The anterior thalamus provides a subcortical circuit supporting memory and spatial navigation. *Front. Syst. Neurosci.*, 7(45).
- Jęško H, Wencel P, Strosznajder RP and Strosznajder JB. (2017). Sirtuins and Their Roles in Brain Aging and Neurodegenerative Disorders. *Neurochem. Res.*, 42(3), 876.
- Jiang X, Chen LL, Lan Z, Xiong F, Xu X, Yin YY, Li P and Wang P. (2019). Icaritin Ameliorates Amyloid Pathologies by Maintaining Homeostasis of Autophagic Systems in A $\beta$ 1–42-Injected Rats. *Neurochem. Res.*, 44(12), 2708–2722.
- Jin J, Maren S, Adhikari A, Wotjak CT and Gómez-Lagunas F. (2015). Prefrontal-Hippocampal Interactions in Memory and Emotion. *Front. Syst. Neurosci.*, 9, 170.
- Joy T, Rao M and Madhyastha S. (2018). N-Acetyl Cysteine Supplement Minimize Tau Expression and Neuronal Loss in Animal Model of Alzheimer’s Disease. *Brain Sci.*, 8(10), 185.
- Julien C, Tremblay C, Bendjelloul F, Phivilay A, Coulombe MA, Émond V and Calon F. (2008). Decreased drebrin mRNA expression in Alzheimer disease: Correlation with tau pathology. *J. Neurosci. Res.*, 86(10), 2292–2302.
- Julien C, Tremblay C, Émond V, Lebbadi M, Jr NS, Bennett D a and Calon F. (2009). SIRT1 Decrease Parallels the Accumulation of tau in Alzheimer Disease. *J Neuropathol Exp Neurol*, 68(1), 48–74.
- Junod A, Lambert AE, Stauffacher W and Renold AE. (1969). Diabetogenic action of streptozotocin: relationship of dose to metabolic response. *J. Clin. Invest.*, 48(11), 2129–2139.
- Jurcovicova J. (2014). Glucose transport in brain-effect of inflammation. *Endocr. Regul.*, 48, 35–48.
- Kaboodvand N, Bäckman L, Nyberg L and Salami A. (2018). The retrosplenial cortex: A memory gateway between the cortical default mode network and the medial temporal lobe. *Hum. Brain Mapp.*, 39(5), 2020–2034.
- Kádár E, Aldavert-Vera L, Huguet G, Costa-Miserachs D, Morgado-Bernal I and Segura-Torres P. (2011). Intracranial self-stimulation induces expression of learning and memory-related genes in rat amygdala. *Genes, Brain Behav.*, 10, 69–77.
- Kádár E, Huguet G, Aldavert-Vera L, Morgado-Bernal I and Segura-Torres P. (2013). Intracranial self stimulation upregulates the expression of synaptic plasticity related genes and Arc protein expression in rat hippocampus. *Genes, Brain Behav.*, 12, 771–779.
- Kádár E, Ramoneda M, Aldavert-Vera L, Huguet G, Morgado-bernal I and Segura-torres P. (2014). Rewarding brain stimulation reverses the disruptive effect of amygdala damage on emotional learning. *Behav. Brain Res.*, 274, 43–52.
- Kádár E, Vico-Varela E, Aldavert-Vera L, Huguet G, Morgado-Bernal I and Segura-Torres P. (2016). Increase in c-Fos and Arc protein in retrosplenial cortex after memory-improving lateral hypothalamic electrical stimulation treatment. *Neurobiol. Learn. Mem.*, 128, 117–124.
- Kádár E, Vico-Varela E, Aldavert-Vera L, Huguet G, Morgado-Bernal I and Segura-Torres P. (2018). Arc protein expression after unilateral intracranial self-stimulation of the medial forebrain bundle is



upregulated in specific nuclei of memory-related areas. *BMC Neurosci.*, 19(48).

- Kalová E, Vlček K, Jarolímová E and Bureš J. (2005). Allothetic orientation and sequential ordering of places is impaired in early stages of Alzheimer's disease: corresponding results in real space tests and computer tests. *Behav. Brain Res.*, 159(2), 175–186.
- Kalra J, Kumar P, Majeed ABA and Prakash A. (2016). Modulation of LOX and COX pathways via inhibition of amyloidogenesis contributes to mitoprotection against  $\beta$ -amyloid oligomer-induced toxicity in an animal model of Alzheimer's disease in rats. *Pharmacol. Biochem. Behav.*, 146–147, 1–12.
- Kamat PK. (2015). Streptozotocin induced Alzheimer's disease like changes and the underlying neural degeneration and regeneration mechanism. *Neural Regen. Res.*, 10(7), 1050–1052.
- Kandimalla R and Reddy PH. (2017). Therapeutics of Neurotransmitters in Alzheimer's Disease. *J. Alzheimer's Dis.*, 57(4), 1049–1069.
- Karthick C, Nithyanandan S, Essa MM, Guillemin GJ, Jayachandran SK and Anusuyadevi M. (2019). Time-dependent effect of oligomeric amyloid- $\beta$  (1–42)-induced hippocampal neurodegeneration in rat model of Alzheimer's disease. *Neurol. Res.*, 41(2), 139–150.
- Kasza Á, Penke B, Frank Z, Bozsó Z, Szegedi V, Hunya Á, Németh K, Kozma G and Fülöp L. (2017). Studies for improving a rat model of Alzheimer's disease: ICV administration of well-characterized  $\beta$ -amyloid 1-42 oligomers induce dysfunction in spatial memory. *Molecules*, 22(11).
- Katche C, Dorman G, Slipczuk L, Cammarota M and Medina JH. (2013). Functional integrity of the retrosplenial cortex is essential for rapid consolidation and recall of fear memory. *Learn. Mem.*, 20(4), 170–173.
- Kealy J and Commins S. (2011). The rat perirhinal cortex: A review of anatomy, physiology, plasticity, and function. *Prog. Neurobiol.*, 93(4), 522–548.
- Kendzioriski C, Irizarry RA, Chen K-S, Haag JD and Gould MN. (2005). On the utility of pooling biological samples in microarray experiments. *102(12)*, 4252–4257.
- Kessels RPC, Rijken S, Joosten-Weyn Banningh LWA, Schuylenborgh-Van Es N Van and Olde Rikkert MGM. (2010). Categorical spatial memory in patients with mild cognitive impairment and Alzheimer dementia: Positional versus object-location recall. *J. Int. Neuropsychol. Soc.*, 16(1), 200–204.
- Khan UA, Liu L, Provenzano FA, Berman DE, Profaci CP, Sloan R, Mayeux R, Duff KE and Small SA. (2014). Molecular drivers and cortical spread of lateral entorhinal cortex dysfunction in preclinical Alzheimer's disease. *Nat. Neurosci.*, 17(2), 304–311.
- Khan IS, D'Agostino EN, Calnan DR, Lee JE and Aronson JP. (2019). Deep Brain Stimulation for Memory Modulation: A New Frontier. *World Neurosurg.*, 126, 638–646.
- Kilgard MP and Merzenich MM. (1998). Cortical map reorganization enabled by nucleus basalis activity. *Science*, 279(5357), 1714–1718.
- Kim D, Nguyen MD, Dobbin MM, Fischer A, Sananbenesi F, Rodgers JT, Delalle I, Baur JA, Sui G, Armour SM, Puigserver P, Sinclair DA and Tsai LH. (2007). SIRT1 deacetylase protects against

- neurodegeneration in models for Alzheimer's disease and amyotrophic lateral sclerosis. *EMBO J.*, 26(13), 3169–3179.
- Kinney JW, Bemiller SM, Murtishaw AS, Leisgang AM, Salazar AM and Lamb BT. (2018). Inflammation as a central mechanism in Alzheimer's disease. *Alzheimer's Dement. Transl. Res. Clin. Interv.*, 4, 575–590.
- Klinkenberg I, Sambeth A and Blokland A. (2011). Acetylcholine and attention. *Behav. Brain Res.*, 221(2), 430–442.
- Klunk WE, Engler H, Nordberg A, Wang Y, Blomqvist G, Holt DP, Bergström M, Savitcheva I, Huang GF, Estrada S, Ausén B, Debnath ML, Barletta J, Price JC, Sandell J, Lopresti BJ, Wall A, Koivisto P, Antoni G,... Långström B. (2004). Imaging Brain Amyloid in Alzheimer's Disease with Pittsburgh Compound-B. *Ann. Neurol.*, 55(3), 306–319.
- Knezovic A, Osmanovic-Barilar J, Curlin M, Hof PR, Simic G, Riederer P and Salkovic-Petrisic M. (2015). Staging of cognitive deficits and neuropathological and ultrastructural changes in streptozotocin-induced rat model of Alzheimer's disease. *J. Neural Transm.*, 122(4), 577–592.
- Koepsell H. (2020). Glucose transporters in brain in health and disease. *Pflugers Arch. Eur. J. Physiol.*, 472(9), 1299–1343.
- Kojima N and Shirao T. (2007). Synaptic dysfunction and disruption of postsynaptic drebrin-actin complex: A study of neurological disorders accompanied by cognitive deficits. *Neurosci. Res.*, 58(1), 1–5.
- Kos A, Olde Loohuis N, Meinhardt J, van Bokhoven H, Kaplan BB, Martens GJ and Aschrafi A. (2016). MicroRNA-181 promotes synaptogenesis and attenuates axonal outgrowth in cortical neurons. *Cell. Mol. Life Sci.*, 73(18), 3555–3567.
- Kosik KS and Krichevsky AM. (2005). The elegance of the microRNAs: A neuronal perspective. *Neuron*, 47(6), 779–782.
- Koulousakis P, Hove D van den, Visser-Vandewalle V and Sesia T. (2020). Cognitive Improvements after Intermittent Deep Brain Stimulation of the Nucleus Basalis of Meynert in a Transgenic Rat Model for Alzheimer's disease; a Preliminary Approach. *J Alzheimers Dis*, 73(2), 461–466.
- Krashia P, Nobili A and D'amelio M. (2019). Unifying hypothesis of dopamine neuron loss in neurodegenerative diseases: Focusing on alzheimer's disease. *Front. Mol. Neurosci.*, 12, 123.
- Kraska A, Santin MD, Dorieux O, Joseph-Mathurin N, Bourrin E, Petit F, Jan C, Chaigneau M, Hantraye P, Lestage P and Dhenain M. (2012). In vivo cross-sectional characterization of cerebral alterations induced by intracerebroventricular administration of streptozotocin. *PLoS One*, 7(9), e46196.
- Kroh EM, Parkin RK, Mitchell PS and Tewari M. (2010). Analysis of circulating microRNA biomarkers in plasma and serum using quantitative reverse transcription-PCR (qRT-PCR). *Methods*, 50(4), 298–301.
- Kuhn J, Hardenacke K, Lenartz D, Gruendler T, Ullsperger M, Bartsch C, Mai JK, Zilles K, Bauer A, Matusch A, Schulz RJ, Noreik M, Bührle CP, Maintz D, Woopen C, Häussermann P, Hellmich M, Klosterkötter J, Wiltfang J,... Sturm V. (2015). Deep brain stimulation of the nucleus basalis of Meynert in Alzheimer's dementia. *Mol. Psychiatry*, 20(3), 353–360.

- Kumar P, Dezso Z, MacKenzie C, Oestreicher J, AgoulNIK S, Byrne M, Bernier F, Yanagimachi M, Aoshima K and Oda Y. (2013a). Circulating miRNA Biomarkers for Alzheimer's Disease. *PLoS One*, 8(7).
- Kumar R, Chaterjee P, Sharma PK, Singh AK, Gupta A, Gill K, Tripathi M, Dey AB and Dey S. (2013b). Sirtuin1: a promising serum protein marker for early detection of Alzheimer's disease. *PLoS One*, 8(4), e61560.
- Kumar S and Reddy PH. (2016). Are circulating microRNAs peripheral biomarkers for Alzheimer's disease? *Biochim. Biophys. Acta - Mol. Basis Dis.*, 1862(9), 1617–1627.
- Kuss AW and Chen W. (2008). MicroRNAs in Brain Function and Disease. *Curr. Neurol. Neurosci. Rep.*, 8, 190–197.
- Lalla R and Donmez G. (2013). The role of sirtuins in Alzheimer's disease. *Front. Aging Neurosci.*, 5(16).
- Langley E, Pearson M, Faretta M, Bauer UM, Frye RA, Minucci S, Pelicci PG and Kouzarides T. (2002). Human SIR2 deacetylates p53 and antagonizes PML/p53-induced cellular senescence. *EMBO J.*, 21(10), 2383–2396.
- Lannert H and Hoyer S. (1998). Intracerebroventricular administration of streptozotocin causes long-term diminutions in learning and memory abilities and in cerebral energy metabolism in adult rats. *Behav. Neurosci.*, 112(5), 1199–1208.
- Latham GJ. (2010). Normalization of MicroRNA Quantitative RT-PCR Data in Reduced Scale Experimental Designs. *Methods Mol. Biol.*, 667, 19–31.
- Lau P, Bossers K, Janky R, Salta E, Frigerio CS, Barbash S, Rothman R, Sierksma ASR, Thathiah A, Greenberg D, Papadopoulou AS, Achsel T, Ayoubi T, Soreq H, Verhaagen J, Swaab DF, Aerts S and De Strooper B. (2013). Alteration of the microRNA network during the progression of Alzheimer's disease. *EMBO Mol. Med.*, 5(10), 1613–1634.
- Laxton AW, Tang-Wai DF, McAndrews MP, Zumsteg D, Wennberg R, Keren R, Wherrett J, Naglie G, Hamani C, Smith GS and Lozano AM. (2010). A phase I trial of deep brain stimulation of memory circuits in Alzheimer's disease. *Ann. Neurol.*, 68(4), 521–534.
- Laxton AW and Lozano AM. (2013). Deep Brain Stimulation for the Treatment of Alzheimer Disease and Dementias. *World Neurosurg.*, 80(3/4).
- Lecanu L and Papadopoulos V. (2013). Modeling Alzheimer's disease with non-transgenic rat models. *Alzheimers. Res. Ther.*, 5(3), 17.
- Lee JE, Jeong DU, Lee J, Chang WS and Chang JW. (2016). The effect of nucleus basalis magnocellularis deep brain stimulation on memory function in a rat model of dementia. *BMC Neurol.*, 16(6).
- Lee JC, Kim SJ, Hong S and Kim YS. (2019). Diagnosis of Alzheimer's disease utilizing amyloid and tau as fluid biomarkers. *Exp. Mol. Med.*, 51(53).
- Lein ES. (2004). Defining a Molecular Atlas of the Hippocampus Using DNA Microarrays and High-Throughput In Situ Hybridization. *J. Neurosci.*, 24(15), 3879–3889.
- Lein ES, Hawrylycz MJ, Ao N, Ayres M, Bensinger A, Bernard A, Boe AF, Boguski MS, Brockway KS, Byrnes

- EJ, Chen L, Chen L, Chen T-M, Chin MC, Chong J, Crook BE, Czaplinska A, Dang CN, Datta S, ... Jones AR. (2007). Genome-wide atlas of gene expression in the adult mouse brain. *Nature*, *445*(7124), 168–176.
- Lenzen S. (2008). The mechanisms of alloxan- and streptozotocin-induced diabetes. *Diabetologia*, *51*(2), 216–226.
- Lepus A, Lauritzen I, Melon C, Kerkerian-Le Goff L, Fontaine D and Checler F. (2019). Chronic fornix deep brain stimulation in a transgenic Alzheimer's rat model reduces amyloid burden, inflammation, and neuronal loss. *Brain Struct. Funct.*, *224*(1), 363–372.
- Lewczuk P, Esselmann H, Otto M, Maler JM, Henkel AW, Henkel MK, Eikenberg O, Antz C, Krause WR, Reulbach U, Kornhuber J and Wiltfang J. (2004). Neurochemical diagnosis of Alzheimer's dementia by CSF A $\beta$ 42, A $\beta$ 42/A $\beta$ 40 ratio and total tau. *Neurobiol. Aging*, *25*(3), 273–281.
- Li XH, Chen C, Tu Y, Sun HT, Zhao ML, Cheng SX, Qu Y and Zhang S. (2013). Sirt1 promotes axonogenesis by deacetylation of akt and inactivation of GSK3. *Mol. Neurobiol.*, *48*(3), 490–499.
- Ling X, Martins RN, Racchi M, Craft S and Helmerhorst E. (2002). Amyloid beta antagonizes insulin promoted secretion of the amyloid beta protein precursor. *J. Alzheimer's Dis.*, *4*(5), 369–374.
- Liang F, Kume S and Koya D. (2009). SIRT1 and insulin resistance. *Nat. Rev. Endocrinol.*, *5*, 367–373.
- Lisman JE and Grace AA. (2005). The hippocampal-VTA loop: Controlling the entry of information into long-term memory. *Neuron*, *46*(5), 703–713.
- Liu S zhi, Cheng W, Shao J wei, Gu Y fan, Zhu Y yi, Dong Q jing, Bai S yu, Wang P and Lin L. (2019). Notoginseng Saponin Rg1 Prevents Cognitive Impairment through Modulating APP Processing in A $\beta$  1–42 -injected Rats. *Curr. Med. Sci.*, *39*(2), 196–203.
- Llorens-Martín M, Blazquez-Llorca L, Benavides-Piccione R, Rabano A, Hernandez F, Avila J and DeFelipe J. (2014). Selective alterations of neurons and circuits related to early memory loss in Alzheimer's disease. *Front. Neuroanat.*, *8*(38).
- Lorent K, Overbergh L, Moechars D, de Strooper B, van Leuven F and van den Berghe H. (1995). Expression in mouse embryos and in adult mouse brain of three members of the amyloid precursor protein family, of the alpha-2-macroglobulin receptor/low density lipoprotein receptor-related protein and of its ligands apolipoprotein E, lipoprotein lipase, . *Neuroscience*, *65*(4), 1009–1025.
- Lozano AM, Fosdick L, Chakravarty MM, Leoutsakos J-M, Munro C, Oh E, Drake KE, Lyman CH, Rosenberg PB, Anderson WS, Tang-Wai DF, Pendergrass JC, Salloway S, Asaad WF, Ponce FA, Burke A, Sabbagh M, Wolk DA, Baltuch G, ... St B. (2016). A Phase II Study of Fornix Deep Brain Stimulation in Mild Alzheimer's Disease. *J. Alzheimer's Dis.*, *54*, 777–787.
- Ludewig S and Korte M. (2017). Novel insights into the physiological function of the APP (gene) family and its proteolytic fragments in synaptic plasticity. *Front. Mol. Neurosci.*, *9*(161).
- Luikart BW, Bensen ASL, Washburn EK, Perederiy J V., Su KG, Li Y, Kernie SG, Parada LF and Westbrook GL. (2011). MiR-132 mediates the integration of newborn neurons into the adult dentate gyrus. *PLoS One*, *6*(5).

- Lukiw WJ, Zhao Y and Jian GC. (2008). An NF- $\kappa$ B-sensitive micro RNA-146a-mediated inflammatory circuit in alzheimer disease and in stressed human brain cells. *J. Biol. Chem.*, 283(46), 31315–31322.
- Luxenberg JS, Haxby J V., Creasey H, Sundaram M and Rapoport SI. (1987). Rate of ventricular enlargement in dementia of the Alzheimer type correlates with rate of neuropsychological deterioration. *Neurology*, 37(7), 1135–1140.
- Lv Q, Du A, Wei W, Li Y, Liu G and Wang XP. (2018). Deep Brain Stimulation: A Potential Treatment for Dementia in Alzheimer's Disease (AD) and Parkinson's Disease Dementia (PDD). *Front. Neurosci.*, 12(360).
- Lyketsos CG, Carrillo MC, Ryan JM, Khachaturian AS, Trzepacz P, Amatnick J, Cedarbaum J, Brashear R and Miller DS. (2011). Neuropsychiatric symptoms in Alzheimer's disease. *Alzheimer's Dement.*, 7(5), 532–539.
- Lyons MK. (2011). Deep brain stimulation: Current and future clinical applications. *Mayo Clin. Proc.*, 86(7), 662–672.
- Ma C-Y, Yao M-J, Zhai Q-W, Jiao J-W, Yuan X-B and Poo M-M. (2014). SIRT1 suppresses self-renewal of adult hippocampal neural stem cells. *141*, 4698–4709.
- Maddux JM and Holland PC. (2011). Effects of dorsal or ventral medial prefrontal cortical lesions on five-choice serial reaction time performance in rats. *Behav. Brain Res.*, 221(1), 63–74.
- Makin S. (2018). The amyloid hypotesis on trial. *Nature*, 559(7715), S4–S7.
- Malekzadeh S, Edalatmanesh MA, Mehrabani D and Shariati M. (2017). Drugs Induced Alzheimer's Disease in Animal Model. *Galen Med. J.*, 6(3), 185–196.
- Mann A, Gondard E, Tampellini D, Milsted JAT, Marillac D, Hamani C, Kalia SK and Lozano AM. (2018). Chronic deep brain stimulation in an Alzheimer's disease mouse model enhances memory and reduces pathological hallmarks. *Brain Stimul.*, 11(2), 435–444.
- Mao Q, Zhang L, Guo Y, Sun L, Liu S, He P, Huang R, Sun L, Chen S, Zhang H and Xie P. (2016). Identification of suitable reference genes for BDV-infected primary rat hippocampal neurons. *Mol. Med. Rep.*, 14(6), 5587–5594.
- Marksteiner J and Humpel C. (2008). Beta-amyloid expression, release and extracellular deposition in aged rat brain slices. *Mol. Psychiatry*, 13(10), 939–952.
- Martin A and Fedio P. (1983). Word production and comprehension in Alzheimer's disease: The breakdown of semantic knowledge. *Brain Lang.*, 19(1), 124–141.
- Martínez-Nicolás I, Carro J, Llorente TE and Meilán JJG. (2019). The Deterioration of Semantic Networks in Alzheimer's Disease. In T. Wisniewski (Ed.), *Alzheimer's Disease* (pp. 179–191). Codon Publications.
- Martínez-Redondo P and Vaquero A. (2013). The Diversity of Histone Versus Nonhistone Sirtuin Substrates. *Genes & Cancer*, 4(3–4), 148–163.
- Martorana A and Koch G. (2014). Is dopamine involved in Alzheimer's disease? *Front. Aging Neurosci.*, 6(252).
- McBain CJ. (2008). New directions in synaptic and network plasticity—a move away from NMDA receptor mediated plasticity. *J Physiol*, 586, 1473–1474.

- McKinnon C, Gros P, Lee DJ, Hamani C, Lozano AM, Kalia L V. and Kalia SK. (2019). Deep brain stimulation: potential for neuroprotection. *Ann. Clin. Transl. Neurol.*, 6(1), 174–185.
- McLin DE, Miasnikov AA and Weinberger NM. (2002). Induction of behavioral associative memory by stimulation of the nucleus basalis. *Proc. Natl. Acad. Sci. U. S. A.*, 99(6), 4002–4007.
- McMurray MS, Conway SM and Roitman JD. (2017). Brain Stimulation Reward Supports More Consistent and Accurate Rodent Decision-Making than Food Reward. *ENeuro*, 4(2), e0015.
- Mehla J, Pahuja M and Gupta YK. (2013). Streptozotocin-induced sporadic Alzheimer's Disease: Selection of appropriate dose. *J. Alzheimer's Dis.*, 33(1), 17–21.
- Merlo S, Spampinato SF and Sortino MA. (2019). Early compensatory responses against neuronal injury: A new therapeutic window of opportunity for Alzheimer's Disease. *CNS Neurosci. Ther.*, 25, 5–13.
- Mestdagh P, Van Vlierberghe P, De Weer A, Muth D, Westermann F, Speleman F and Vandesompele J. (2009). A novel and universal method for microRNA RT-qPCR data normalization. *Genome Biol.*, 10(R64).
- Mesulam M, Shaw P, Mash D and Weintraub S. (2004). Cholinergic nucleus basalis tauopathy emerges early in the aging-MCI-AD continuum. *Ann. Neurol.*, 55(6), 815–828.
- Metzler-Baddeley C, Hunt S, Jones DK, Leemans A, Aggleton JP and O'Sullivan MJ. (2012). Temporal association tracts and the breakdown of episodic memory in mild cognitive impairment. *Neurology*, 79(23), 2233–2240.
- Michán S, Li Y, Meng-Hsiu Chou M, Parrella E, Ge H, Long JM, Allard JS, Lewis K, Miller M, Xu W, Mervis RF, Chen J, Guerin KI, H Smith LE, McBurney MW, Sinclair DA, Baudry M, de Cabo R and Longo VD. (2010). SIRT1 is essential for normal cognitive function and synaptic plasticity. *J Neurosci*, 30(29), 9695–9707.
- Migliaccio R, Agosta F, Possin KL, Canu E, Filippi M, Rabinovici GD, Rosen HJ, Miller BL and Gorno-Tempini ML. (2015). Mapping the progression of atrophy in early- and late-onset alzheimer's disease. *J. Alzheimer's Dis.*, 46(2), 351–364.
- Miller BH and Wahlestedt C. (2010). MicroRNA dysregulation in psychiatric disease. *Brain Res.*, 1338, 89–99.
- Minoshima S, Giordani B, Berent S, Frey KA, Foster NL and Kuhl DE. (1997). Metabolic reduction in the posterior cingulate cortex in very early Alzheimer's disease. *Ann. Neurol.*, 42(1), 85–94.
- Mirzadeh Z, Bari A and Lozano AM. (2015). The rationale for deep brain stimulation in Alzheimer's disease. *J. Neural Transm.*, 123, 775–783.
- Mishra SK, Singh S, Shukla S and Shukla R. (2018). Intracerebroventricular streptozotocin impairs adult neurogenesis and cognitive functions via regulating neuroinflammation and insulin signaling in adult rats. *Neurochem. Int.*, 113, 56–68.
- Mitchell AS, Czajkowski R, Zhang N, Jeffery K and Nelson AJD. (2018). Retrosplenial cortex and its role in spatial cognition. *Brain Neurosci. Adv.*, 2, 1–13.
- Mondadori C, Ornstein K, Waser PG and Huston JP. (1976). Post-trial reinforcing hypothalamic stimulation

can facilitate avoidance learning. *Neurosci. Lett.*, 2(4), 183–187.

Montero-Pastor A, Vale-Martínez A, Guillazo-Blanch G and Martí-Nicolovius M. (2004). Effects of electrical stimulation of the nucleus basalis on two-way active avoidance acquisition, retention, and retrieval. *Behav. Brain Res.*, 154(1), 41–54.

Moonis M, Swearer JM, Dayaw MPE, St. George-Hyslop P, Rogaeva E, Kawarai T and Pollen DA. (2005). Familial Alzheimer disease: Decreases in CSF A $\beta$ 42 levels precede cognitive decline. *Neurology*, 65(2), 323–325.

Moradifard S, Hoseinbeyki M, Ganji SM and Minuchehr Z. (2018). Analysis of microRNA and Gene Expression Profiles in Alzheimer's Disease: A Meta-Analysis Approach. *Sci. Rep.*, 8(1), 1–18.

Morales M and Margolis EB. (2017). Ventral tegmental area: Cellular heterogeneity, connectivity and behaviour. *Nat. Rev. Neurosci.*, 18(2), 73–85.

Moreira-Silva D, Carrettiero DC, Oliveira ASA, Rodrigues S, Dos Santos-Lopes J, Canas PM, Cunha RA, Almeida MC and Ferreira TL. (2018). Anandamide Effects in a Streptozotocin-Induced Alzheimer's Disease-Like Sporadic Dementia in Rats. *Front. Neurosci.*, 12(653).

Moreira-Silva D, Vizin R, Martins T, Ferreira T, Almeida M and Carrettiero D. (2019). Intracerebral Injection of Streptozotocin to Model Alzheimer Disease in Rats. *Bio Protoc*, 9(20), e3397.

Morris R. (1984). Developments of a water-maze procedure for studying spatial learning in the rat. *J. Neurosci. Methods*, 11(1), 47–60.

Morris RGM, Garrud P, Rawlins JNP and O'Keefe J. (1982). Place navigation impaired in rats with hippocampal lesions. *Nature*, 297(5868), 681–683.

Mosconi L. (2013). Glucose metabolism in normal aging and Alzheimer's disease: Methodological and physiological considerations for PET studies. *Clin. Transl. Imaging*, 1(4), 217–233.

Mucke L and Selkoe DJ. (2012). Neurotoxicity of amyloid  $\beta$ -protein: Synaptic and network dysfunction. *Cold Spring Harb. Perspect. Med.*, 2(7), 1–17.

Muir JL, Dunnett SB, Robbins TW and Everitt BJ. (1992). Attentional functions of the forebrain cholinergic systems: effects of intraventricular hemicholinium, physostigmine, basal forebrain lesions and intracortical grafts on a multiple-choice serial reaction time task. *Exp. Brain Res.*, 89(3), 611–622.

Nakashiba T, Cushman JD, Pelkey KA, Renaudineau S, Buhl DL, McHugh TJ, Barrera VR, Chittajallu R, Iwamoto KS, McBain CJ, Fanselow MS and Tonegawa S. (2012). Young dentate granule cells mediate pattern separation, whereas old granule cells facilitate pattern completion. *Cell*, 149(1), 188–201.

Nakazawa K, Quirk MC, Chitwood RA, Watanabe M, Yeckel MF, Sun LD, Kato A, Carr CA, Johnston D, Wilson MA and Tonegawa S. (2002). Requirement for Hippocampal CA3 NMDA Receptors in Associative Memory Recall. *Science*, 297(5579), 211–218.

Neddens J, Temmel M, Flunkert S, Kerschbaumer B, Hoeller C, Loeffler T, Niederkofler V, Daum G, Attems J and Hutter-Paier B. (2018). Phosphorylation of different tau sites during progression of Alzheimer's disease. *Acta Neuropathol. Commun.*, 6(1), 52.

- Nelson PT and Wang WX. (2010). MiR-107 is reduced in Alzheimer's disease brain neocortex: Validation study. *J. Alzheimer's Dis.*, 21(1), 75–79.
- Nestor PJ, Fryer TD, Ikeda M and Hodges JR. (2003). Retrosplenial cortex (BA 29/30) hypometabolism in mild cognitive impairment (prodromal Alzheimer's disease). *Eur. J. Neurosci.*, 18(9), 2663–2667.
- Neth BJ and Craft S. (2017). Insulin resistance and Alzheimer's disease: Bioenergetic linkages. *Front. Aging Neurosci.*, 9(345).
- Ng F, Wijaya L and Tang BL. (2015). SIRT1 in the brain—connections with aging-associated disorders and lifespan. *Front. Cell. Neurosci.*, 9(64).
- Ng TKS, Ho CSH, Tam WWS, Kua EH and Ho RC-M. (2019). Decreased Serum Brain-Derived Neurotrophic Factor (BDNF) Levels in Patients with Alzheimer's Disease (AD): A Systematic Review and Meta-Analysis. *Int. J. Mol. Sci.*, 20(2), 257.
- Nobili A, Latagliata EC, Viscomi MT, Cavallucci V, Cutuli D, Giacobuzzo G, Krashia P, Rizzo FR, Marino R, Federici M, De Bartolo P, Aversa D, Dell'Acqua MC, Cordella A, Sancandi M, Keller F, Petrosini L, Puglisi-Allegra S, Mercuri NB,... D'Amelio M. (2017). Dopamine neuronal loss contributes to memory and reward dysfunction in a model of Alzheimer's disease. *Nat. Commun.*, 8(14727).
- Nudelman AS, Dirocco DP, Lambert TJ, Garelick MG, Nathanson NM and Storm DR. (2010). Neuronal Activity Rapidly Induces Transcription of the CREB- Regulated microRNA-132, in vivo. *Hippocampus*, 20(4), 492–498.
- Okada K, Nishizawa K, Kobayashi T, Sakata S and Kobayashi K. (2015). Distinct roles of basal forebrain cholinergic neurons in spatial and object recognition memory. *Sci. Rep.*, 5(13158).
- Olde Loohuis NFM, Kole K, Glennon JC, Karel P, Van der Borg G, Van Gemert Y, Van den Bosch D, Meinhardt J, Kos A, Shahabipour F, Tiesinga P, van Bokhoven H, Martens GJM, Kaplan BB, Homberg JR and Aschrafi A. (2015). Elevated microRNA-181c and microRNA-30d levels in the enlarged amygdala of the valproic acid rat model of autism. *Neurobiol. Dis.*, 80, 42–53.
- Olds J. (1958). Self-stimulation of the brain. *Science*, 127(3294), 315–324.
- Olds J and Milner P. (1954). Positive reinforcement produced by electrical stimulation of septal area and other regions of rat brain. *J. Comp. Physiol. Psychol.*, 47(6), 419–427.
- Ooigawa H, Nawashiro H, Fukui S, Otani N, Osumi A, Toyooka T and Shima K. (2006). The fate of Nissl-stained dark neurons following traumatic brain injury in rats: Difference between neocortex and hippocampus regarding survival rate. *Acta Neuropathol.*, 112(4), 471–481.
- Osmanovic Barilar J, Knezovic A, Grü E, Riederer P and Salkovic-Petrisic M. (2015). Nine-month follow-up of the insulin receptor signalling cascade in the brain of streptozotocin rat model of sporadic Alzheimer's disease. *J Neural Transm.*, 122, 565–576.
- Padurariu M, Ciobica A, Mavroudis I, Fotiou D and Baloyannis S. (2012). Hippocampal neuronal loss in the CA1 and CA3 areas of Alzheimer's disease patients. *Psychiatr. Danub.*, 24(2), 152–158.
- Pai B, Siripornmongkolchai T, Berentsen B, Pakzad A, Vieuille C, Pallesen S, Pajak M, Simpson TI, Armstrong



- JD, Wibrand K and Bramham CR. (2014). NMDA receptor-dependent regulation of miRNA expression and association with Argonaute during LTP in vivo. *Front. Cell. Neurosci.*, 7(285).
- Pan X, Kaminga AC, Wen SW, Wu X, Acheampong K and Liu A. (2019). Dopamine and dopamine receptors in Alzheimer's disease: A systematic review and network meta-analysis. *Front. Aging Neurosci.*, 11(175).
- Panther P, Kuehne M, Voges J, Nullmeier S, Kaufmann J, Hausmann J, Bittner D, Galazky I, Heinze H-J, Kupsch A and Zaehle T. (2019). Electric stimulation of the medial forebrain bundle influences sensorimotor gaiting in humans. *BMC Neurosci.*, 20(20).
- Park SJ, Kim YH, Nam GH, Choe SH, Lee SR, Kim SU, Kim JS, Sim BW, Song BS, Jeong KJ, Lee Y, Park Y II, Lee KM, Huh JW and Chang KT. (2015). Quantitative expression analysis of APP pathway and tau phosphorylation-related genes in the ICV STZ-induced non-human primate model of sporadic alzheimer's disease. *Int. J. Mol. Sci.*, 16(2), 2386–2402.
- Patnaik R, Sharma A, Skaper SD, Muresanu DF, Lafuente JV, Castellani RJ, Nozari A and Sharma HS. (2018). Histamine H3 Inverse Agonist BF 2649 or Antagonist with Partial H4 Agonist Activity Clobenpropit Reduces Amyloid Beta Peptide-Induced Brain Pathology in Alzheimer's Disease. *Mol. Neurobiol.*, 55(1), 312–321.
- Paxinos G and Watson C. (2006). *The Rat Brain in Stereotaxic Coordinates* (hard cover). Academic Press.
- Peltier HJ and Latham GJ. (2008). Normalization of microRNA expression levels in quantitative RT-PCR assays: Identification of suitable reference RNA targets in normal and cancerous human solid tissues. *RNA*, 14(5), 844–852.
- Persson J, Lind J, Larsson A, Ingvar M, Slegers K, Van Broeckhoven C, Adolfsson R, Nilsson LG and Nyberg L. (2008). Altered deactivation in individuals with genetic risk for Alzheimer's disease. *Neuropsychologia*, 46(6), 1679–1687.
- Petrella JR, Sheldon FC, Prince SE, Calhoun VD and Doraiswamy PM. (2011). Default mode network connectivity in stable vs progressive mild cognitive impairment. *Neurology*, 76(6), 511–517.
- Picciotto MR, Higley MJ and Mineur YS. (2012). Acetylcholine as a Neuromodulator: Cholinergic Signaling Shapes Nervous System Function and Behavior. *Neuron*, 76(1), 116–129.
- Pichler S, Gu W, Hartl D, Gasparoni G, Leidinger P, Keller A, Meese E, Mayhaus M, Hampel H and Riemenschneider M. (2017). The miRNome of Alzheimer's disease: consistent downregulation of the miR-132/212 cluster. *Neurobiol. Aging*, 50(167), 1–10.
- Pihlajamaki M, O'Keefe K, Bertram L, Tanzi RE, Dickerson BC, Blacker D, Albert MS and Sperling RA. (2010). Evidence of altered posteromedial cortical fMRI activity in subjects at risk for alzheimer disease. *Alzheimer Dis. Assoc. Disord.*, 24(1), 28–36.
- Pilipenko V, Narbutė K, Amara I, Trovato A, Scuto M, Pupure J, Jansone B, Poikans J, Bisenieks E, Klusa V and Calabrese V. (2019). GABA-containing compound gammapyrone protects against brain impairments in Alzheimer's disease model male rats and prevents mitochondrial dysfunction in cell culture. *J. Neurosci. Res.*, 97(6), 708–726.
- Poddar J, Singh S, Kumar P, Bali S, Gupta S and Chakrabarti S. (2020). Inhibition of complex I-III activity of

- brain mitochondria after intracerebroventricular administration of streptozotocin in rats is possibly related to loss of body weight. *Heliyon*, 6(7), e04490.
- Ponjoan A, Garre-Olmo J, Blanch J, Fages E, Alves-Cabreros L, Martí-Lluch R, Comas-Cufí M, Parramon D, Garcia-Gil M and Ramos R. (2019). Epidemiology of dementia: Prevalence and incidence estimates using validated electronic health records from primary care. *Clin. Epidemiol.*, 11, 217–228.
- Preston AR and Eichenbaum H. (2013). Interplay of hippocampus and prefrontal cortex in memory. *Curr. Biol.*, 23(17), 1–21.
- Prince M, Bryce R, Albanese E, Wimo A, Ribeiro W and Ferri CP. (2013). The global prevalence of dementia: A systematic review and metaanalysis. *Alzheimer's Dement.*, 9(1), 63-75.e2.
- Prince M, Wimo A, Guerchet M, Gemma-Claire Ali M, Wu Y-T, Prina M, Yee Chan K and Xia Z. (2015). *World Alzheimer Report 2015 The Global Impact of Dementia An Analysis of Prevalence, Incidence, Cost and Trends*.
- Prins SA, Przybycien-Szymanska MM, Rao YS and Pak TR. (2014). Long-term effects of peripubertal binge EtOH exposure on hippocampal microRNA expression in the rat. *PLoS One*, 9(1), e83166.
- Puzzo D, Privitera L, Leznik E, Fà M, Staniszewski A, Palmeri A and Arancio O. (2008). Picomolar amyloid- $\beta$  positively modulates synaptic plasticity and memory in hippocampus. *J. Neurosci.*, 28(53), 14537–14545.
- Qian Y, Song J, Ouyang Y, Han Q, Chen W, Zhao X, Xie Y, Chen Y, Yuan W and Fan C. (2017). Advances in roles of miR-132 in the nervous system. *Front. Pharmacol.*, 8(770).
- Qiu T, Liu Q, Chen YX, Zhao YF and Li YM. (2015). A $\beta$ 42 and A $\beta$ 40: similarities and differences. *J. Pept. Sci.*, 21(7), 522–529.
- Rakieten N, Rakieten ML and Nadkarni MR. (1963). Studies on the diabetogenic action of streptozotocin (NSC-37917). *Cancer Chemother. Rep.*, 29, 91–98.
- Ramkumar K, Srikumar BN, Shankaranarayana Rao BS and Raju TR. (2008). Self-stimulation rewarding experience restores stress-induced CA3 dendritic atrophy, spatial memory deficits and alterations in the levels of neurotransmitters in the hippocampus. *Neurochem. Res.*, 33(9), 1651–1662.
- Rao BS, Desiraju T and Raju TR. (1993). Neuronal plasticity induced by self-stimulation rewarding experience in rats - a study on alteration in dendritic branching in pyramidal neurons of hippocampus and motor cortex. *Brain Res.*, 627(2), 216–224.
- Rao BS, Desiraju T, Meti BL and Raju TR. (1994). Plasticity of hippocampal and motor cortical pyramidal neurons induced by self-stimulation experience. *Indian J Physiol Pharmacol*, 38(1).
- Rao BS, Raju TR and Meti BL. (1998). Self-Stimulation of Lateral Hypothalamus and Ventral Tegmentum Increases the Levels of Noradrenaline, Dopamine, Glutamate, and AChE Activity, But Not 5-Hydroxytryptamine and GABA Levels in Hippocampus and Motor Cortex. *Neurochem. Res.*, 23(8), 1053–1059.
- Rao BS, Raju TR and Meti BL. (1999a). Increased numerical density of synapses in CA3 region of hippocampus and molecular layer of motor cortex after self-stimulation rewarding experience. *Neuroscience*, 91(3), 799–803.

- Rao BS, Raju TR and Meti BL. (1999b). Self-stimulation rewarding experience induced alterations in dendritic spine density in CA3 hippocampal and layer V motor cortical pyramidal neurons. *Neuroscience*, 89(4), 1067–1077.
- Rasmusson DD, Clow K and Szerb JC. (1992). Frequency-dependent increase in cortical acetylcholine release evoked by stimulation of the nucleus basalis magnocellularis in the rat. *Brain Res.*, 594(1), 150–154.
- Reddi BA. (2013). Why Is Saline So Acidic (and Does It Really Matter?). *Int. J. Med. Sci.*, 10(6), 747–750.
- Reddy PH, Tonk S, Kumar S, Vijayan M, Kandimalla R, Kuruva CS and Reddy AP. (2017). A critical evaluation of neuroprotective and neurodegenerative MicroRNAs in Alzheimer's disease. *Biochem. Biophys. Res. Commun.*, 483(4), 1156–1165.
- Redolar-Ripoll D, Aldavert-Vera L, Soriano-Mas C, Segura-Torres P and Morgado-Bernal I. (2002). Intracranial self-stimulation facilitates memory consolidation, but not retrieval: its effects are more effective than increased training. *Behav. Brain Res.*, 129(1–2), 65–75.
- Redolar-Ripoll D, Soriano-Mas C, Guillazo-Blanch G, Aldavert-Vera L, Segura-Torres P and Morgado-Bernal I. (2003). Posttraining intracranial self-stimulation ameliorates the detrimental effects of parafascicular thalamic lesions on active avoidance in young and aged rats. *Behav. Neurosci.*, 117(2), 246–256.
- Reid AT and Evans AC. (2013). Structural networks in Alzheimer's disease. *Eur. Neuropsychopharmacol.*, 23(1), 63–77.
- Reiman EM, Caselli RJ, Yun LS, Chen K, Bandy D, Minoshima S, Thibodeau SN and Osborne D. (1996). Preclinical Evidence of Alzheimer's Disease in Persons Homozygous for the  $\epsilon 4$  Allele for Apolipoprotein E. *N. Engl. J. Med.*, 334(12), 752–758.
- Riemenschneider M, Lautenschlager N, Wagenpfeil S, Diehl J, Drzezga A and Kurz A. (2002). Cerebrospinal fluid tau and  $\beta$ -amyloid 42 proteins identify Alzheimer disease in subjects with mild cognitive impairment. *Arch. Neurol.*, 59(11), 1729–1734.
- Rissman RA. (2009). Stress-induced tau phosphorylation: Functional neuroplasticity or neuronal vulnerability? *J. Alzheimer's Dis.*, 18(2), 453–457.
- Robert PH, Berr C, Volteau M, Bertogliati C, Benoit M, Sarazin M, Legrain S and Dubois B. (2006). Apathy in patients with mild cognitive impairment and the risk of developing dementia of Alzheimer's disease. A one-year follow-up study. *Clin. Neurol. Neurosurg.*, 108(8), 733–736.
- Roberts WW. (1958). Both rewarding and punishing effects from stimulation of posterior hypothalamus of cat with same electrode at same intensity. *J. Comp. Physiol. Psychol.*, 51(4), 400–407.
- Rodríguez-Sánchez E, Mora-Simón S, Patino-Alonso MC, García-García R, Escribano-Hernández A, García-Ortiz L, Perea-Bartolomé MV and Gómez-Marcos MA. (2011). Prevalence of cognitive impairment in individuals aged over 65 in an urban area: DERIVA study. *BMC Neurol.*, 11(147).
- Rogers JL and Kesner RP. (2004). Cholinergic modulation of the hippocampus during encoding and retrieval of tone/shock-induced fear conditioning. *Learn. Mem.*, 11(1), 102–107.
- Rolls ET, Burton MJ and Mora F. (1980). Neurophysiological analysis of brain-stimulation reward in the

- monkey. *Brain Res.*, 194(2), 339–357.
- Routtenberg A. (1974). Intracranial self-stimulation pathways as substrate for memory consolidation. *Nebraska Symp. Motiv.*, 22, 161–182.
- Routtenberg A and Lindy J. (1965). Effects of the availability of rewarding septal and hypothalamic stimulation on bar pressing for food under conditions of deprivation. *J. Comp. Physiol. Psychol.*, 60(2), 158–161.
- Rüb U, Stratmann K, Heinsen H, Del Turco D, Seidel K, den Dunnen W and Korf H-W. (2016). The Brainstem Tau Cytoskeletal Pathology of Alzheimer’s Disease: A Brief Historical Overview and Description of its Anatomical Distribution Pattern, Evolutional Features, Pathogenetic and Clinical Relevance. *Curr. Alzheimer Res.*, 13(10), 1178–1197.
- Ruiz-Medina J, Morgado-Bernal I, Redolar-Ripoll D, Aldavert-Vera L and Segura-Torres P. (2008). Intracranial self-stimulation facilitates a spatial learning and memory task in the Morris water maze. *Neuroscience*, 154(2), 424–430.
- Sahay A, Scobie KN, Hill AS, O’Carroll CM, Kheirbek MA, Burghardt NS, Fenton AA, Dranovsky A and Hen R. (2011). Increasing adult hippocampal neurogenesis is sufficient to improve pattern separation. *Nature*, 472(7344), 466–470.
- Salkovic-Petrisic M, Osmanovic J, Grünblatt E, Riederer P and Hoyer S. (2009). Modeling sporadic Alzheimer’s disease: The insulin resistant brain state generates multiple long-term morphobiological abnormalities including hyperphosphorylated tau protein and amyloid- $\beta$ . *J. Alzheimer’s Dis.*, 18(4), 729–750.
- Salkovic-Petrisic M, Knezovic A, Hoyer S and Riederer P. (2013). What have we learned from the streptozotocin-induced animal model of sporadic Alzheimer’s disease, about the therapeutic strategies in Alzheimer’s research. *J Neural Transm*, 120, 233–252.
- Salkovic-Petrisic M, Hoyer S and Riederer P. (2014). Experimental Approach to Alzheimer Disease. In R. M. Kostrzewa (Ed.), *Handbook of Neurotoxicity* (pp. 2025–2045).
- Salta E, Lau P, Frigerio CS, Coolen M, Bally-Cuif L and De Strooper B. (2014). A Self-Organizing miR-132/Ctbp2 Circuit Regulates Bimodal Notch Signals and Glial Progenitor Fate Choice during Spinal Cord Maturation. *Dev. Cell*, 30, 423–436.
- Salta E, Sierksma A, Eynden E Vanden and De Strooper B. (2016). miR-132 loss de-represses ITPKB and aggravates amyloid and TAU pathology in Alzheimer’s brain. *EMBO Mol Med*, 8(9), 1005–1018.
- Salta E, Walgrave H, Balusu S, Eynden E Vanden and Snoeck S. (2020). Impaired adult hippocampal neurogenesis in Alzheimer’s disease is mediated by microRNA-132 deficiency and can be restored by microRNA-132 replacement. *BioRxiv*.
- Sampath D, Sathyanesan M and Newton SS. (2017). Cognitive dysfunction in major depression and Alzheimer’s disease is associated with hippocampal–prefrontal cortex dysconnectivity. *Neuropsychiatr. Dis. Treat.*, 13, 1509–1519.
- Samson M, Porter N, Orekoya O, Hebert JR, Adams SA, Bennett CL and Steck SE. (2017). Alterations in micro RNA-messenger RNA (miRNA-mRNA) Coupled Signaling Networks in Sporadic Alzheimer’s

- Disease (AD) Hippocampal CA1. *J Alzheimers Dis Park.*, 7(2).
- Sanabria-Castro A, Alvarado-Echeverría I and Monge-Bonilla C. (2017). Molecular pathogenesis of Alzheimer's disease: An update. *Ann. Neurosci.*, 24(1), 46–54.
- Sang-Won Min X, Dongmin Sohn P, Li Y, Devidze N, Johnson JR, Krogan XnJ, Masliah E, Sue-Ann Mok X, Gestwicki JE and Li Gan X. (2018). SIRT1 Deacetylates Tau and Reduces Pathogenic Tau Spread in a Mouse Model of Tauopathy. *Neurobiol. Dis.*, 38(15), 3680–3688.
- Sankar T, Chakravarty MM, Bescos A, Lara M, Obuchi T, Laxton AW, McAndrews MP, Tang-Wai DF, Workman CI, Smith GS and Lozano AM. (2015). Deep brain stimulation influences brain structure in Alzheimer's disease. *Brain Stimul.*, 8(3), 645–654.
- Santos T de O, Mazucanti CHY, Xavier GF and Torrão A da S. (2012). Early and late neurodegeneration and memory disruption after intracerebroventricular streptozotocin. *Physiol. Behav.*, 107(3), 401–413.
- Schnedl WJ, Ferber S, Johnson JH and Newgard CB. (1994). STZ Transport and Cytotoxicity: Specific Enhancement in GLUT2-Expressing Cells. *Diabetes*, 43(11), 1326–1333.
- Schonrock N, Ke YD, Humphreys D, Staufenbiel M, Ittner LM, Preiss T and Rgen Gö Tz J. (2010). Neuronal MicroRNA Deregulation in Response to Alzheimer's Disease Amyloid- $\beta$ . *PLoS One*, 5(6), e11070.
- Schonrock N, Humphreys DT, Preiss T and Götz J. (2012). Target Gene Repression Mediated by miRNAs miR-181c and miR-9 Both of Which Are Down-regulated by Amyloid- $\beta$ . *J Mol Neurosci*, 46, 324–335.
- Schwarzenbach H, Machado A, Silva D, Calin G and Pantel K. (2015). Data Normalization Strategies for MicroRNA Quantification. *Clin. Chem.*, 61(11).
- Schwarzenbach H, Machado da Silva A, Calin G and Pantel K. (2016). Which is the accurate data normalization strategy for microRNA quantification? *Clin Chem*, 61(11), 1333–1342.
- Segura-Torres P, Capdevila-Ortís L, Martí-Nicolovius M and Morgado-Bernal I. (1988). Improvement of shuttle-box learning with pre- and post-trial intracranial self-stimulation in rats. *Behav. Brain Res.*, 29(1–2), 111–117.
- Segura-Torres P, Aldavert-Vera L, Gatell-Segura A, Redolar-Ripoll D and Morgado-Bernal I. (2009). Intracranial self-stimulation recovers learning and memory capacity in basolateral amygdala-damaged rats. *Neurobiol. Learn. Mem.*, 93, 117–126.
- Selkoe DJ. (2002). Alzheimer's disease is a synaptic failure. *Science*, 298(5594), 789–791.
- Selkoe DJ. (2008). Soluble oligomers of the amyloid  $\beta$ -protein impair synaptic plasticity and behavior. *Behav. Brain Res.*, 192(1), 106–113.
- Serra L, D'Amelio M, Di Domenico C, Dipasquale O, Marra C, Mercuri NB, Caltagirone C, Cercignani M and Bozzali M. (2018). In vivo mapping of brainstem nuclei functional connectivity disruption in Alzheimer's disease. *Neurobiol. Aging*, 72, 72–82.
- Serrano-Pozo A, Frosch MP, Masliah E and Hyman BT. (2011). Neuropathological alterations in Alzheimer disease. *Cold Spring Harb. Perspect. Med.*, 1(1).
- Sethi P and Lukiw WJ. (2009). Micro-RNA abundance and stability in human brain: Specific alterations in

- Alzheimer's disease temporal lobe neocortex. *Neurosci. Lett.*, *459*(2), 100–104.
- Shahani N and Brandt R. (2002). Functions and malfunctions of the tau proteins. *Cell. Mol. Life Sci.*, *59*, 1668–1680.
- Shaik MM, Tamargo IA, Abubakar MB, Kamal MA, Greig NH and Gan SH. (2018). The role of microRNAs in Alzheimer's disease and their therapeutic potentials. *Genes (Basel)*, *9*(4).
- Sharma Y and Garabadu D. (2020). Ruthenium red, mitochondrial calcium uniporter inhibitor, attenuates cognitive deficits in STZ-ICV challenged experimental animals. *Brain Res. Bull.*, *164*, 121–135.
- Sheinerman KS, Tsvinsky VG, Crawford F, Mullan MJ, Abdullah L and Umansky SR. (2012). Plasma microRNA biomarkers for detection of mild cognitive impairment. *Aging*, *4*(9), 590–605.
- Sheline YI, Morris JC, Snyder AZ, Price JL, Yan Z, D'Angelo G, Liu C, Dixit S, Benzinger T, Fagan A, Goate A and Mintun MA. (2010). APOE4 allele disrupts resting state fMRI connectivity in the absence of amyloid plaques or decreased CSF A $\beta$ 42. *J. Neurosci.*, *30*(50), 17035–17040.
- Shi F, Liu B, Zhou Y, Yu C and Jiang T. (2009). Hippocampal volume and asymmetry in mild cognitive impairment and Alzheimer's disease: Meta-analyses of MRI studies. *Hippocampus*, *19*(11), 1055–1064.
- Shirao T, Hanamura K, Koganezawa N, Ishizuka Y, Yamazaki H and Sekino Y. (2017). The role of drebrin in neurons. *J. Neurochem.*, *141*(6), 819–834.
- Shoham S, Bejar C, Kovalev E and Weinstock M. (2003). Intracerebroventricular injection of streptozotocin causes neurotoxicity to myelin that contributes to spatial memory deficits in rats. *Exp. Neurol.*, *184*(2), 1043–1052.
- Siedlecki-Wullich D, Català-Solsona J, Fábregas C, Hernández I, Clarimon J, Lleó A, Boada M, Saura CA, Rodríguez-Álvarez J and Miñano-Molina AJ. (2019). Altered microRNAs related to synaptic function as potential plasma biomarkers for Alzheimer's disease. *Alzheimers. Res. Ther.*, *11*(46).
- Sigurdsson EM, Lee JM, Dong XW, Hejna MJ and Lorens SA. (1997). Bilateral injections of amyloid- $\beta$  25-35 into the amygdala of young Fischer rats: Behavioral, neurochemical, and time dependent histopathological effects. *Neurobiol. Aging*, *18*(6), 591–608.
- Small GW, Ercoli LM, Silverman DHS, Huang SC, Komo S, Bookheimer SY, Lavretsky H, Miller K, Siddarth P, Rasgon NL, Mazziotta JC, Saxena S, Wu HM, Mega MS, Cummings JL, Saunders AM, Pericak-Vance MA, Roses AD, Barrio JR and Phelps ME. (2000). Cerebral metabolic and cognitive decline in persons at genetic risk for Alzheimer's disease. *Proc. Natl. Acad. Sci. U. S. A.*, *97*(11), 6037–6042.
- Smith G. (1988). Animal models of Alzheimer's disease: experimental cholinergic denervation. *Brain Res. Rev.*, *13*(2), 103–118.
- Smith AD. (2002). Imaging the progression of Alzheimer pathology through the brain. *Proc. Natl. Acad. Sci. U. S. A.*, *99*(7), 4135–4137.
- Smith GS, Laxton AW, Tang-Wai DF, McAndrews MP, Diaconescu AO, Workman CI and Lozano AM. (2012). Increased Cerebral Metabolism After 1 Year of Deep Brain Stimulation in Alzheimer Disease. *Arch. Neurol.*, *69*(9), 1141–1148.

- Smith PY, Hernandez-Rapp J, Jolivette F, Lecours C, Bisht K, Goupil C, Dorval V, Parsi S, Morin F, Planel E, Bennett DA, Fernandez-Gomez F-J, Sergeant N, Buée L, Tremblay M-È, Calon F and Hébert SS. (2015). miR-132/212 deficiency impairs tau metabolism and promotes pathological aggregation in vivo. *Hum. Mol. Genet.*, 24(23), 6721–6735.
- Song J, Bai Z, Han W, Zhang J, Meng H, Bi J, Ma X, Han S and Zhang Z. (2012). Identification of suitable reference genes for qPCR analysis of serum microRNA in gastric cancer patients. *Dig. Dis. Sci.*, 57(4), 897–904.
- Sorg C, Riedl V, Mühlau M, Calhoun VD, Eichele T, Lässer L, Drzezga A, Förstl H, Kurz A, Zimmer C and Wohlschläger AM. (2007). Selective changes of resting-state networks in individuals at risk for Alzheimer's disease. *Proc. Natl. Acad. Sci. U. S. A.*, 104(47), 18760–18765.
- Soriano-Mas C, Redolar-Ripoll D, Aldavert-Vera L, Morgado-Bernal I and Segura-Torres P. (2005). Post-training intracranial self-stimulation facilitates a hippocampus-dependent task. *Behav. Brain Res.*, 160(1), 141–147.
- Sperling RA, Dickerson BC, Pihlajamaki M, Vannini P, LaViolette PS, Vitolo O V., Hedden T, Becker JA, Rentz DM, Selkoe DJ and Johnson KA. (2010). Functional Alterations in Memory Networks in Early Alzheimer's Disease. *NeuroMolecular Med.*, 12(1), 27–43.
- Sperling RA, Aisen PS, Beckett LA, Bennett DA, Craft S, Fagan AM, Iwatsubo T, Jack CR, Kaye J, Montine TJ, Park DC, Reiman EM, Rowe CC, Siemers E, Stern Y, Yaffe K, Carrillo MC, Thies B, Morrison-Bogorad M,... Phelps CH. (2011). Toward defining the preclinical stages of Alzheimer's disease: Recommendations from the National Institute on Aging-Alzheimer's Association workgroups on diagnostic guidelines for Alzheimer's disease. *Alzheimer's Dement.*, 7(3), 280–292.
- Squire LR. (2004). Memory systems of the brain: A brief history and current perspective. *Neurobiol. Learn. Mem.*, 82(3), 171–177.
- Squire LR, Genzel L, Wixted JT and Morris RG. (2015). Memory consolidation. *Cold Spring Harb. Perspect. Biol.*, 7(8).
- Squire LR and Zola SM. (1996). Structure and function of declarative and nondeclarative memory systems. *Proc. Natl. Acad. Sci. U. S. A.*, 93(24), 13515–13522.
- Stark P, Fazio G and Boyd ES. (1962). Monopolar and bipolar stimulation of the brain. *Am. J. Physiol.*, 203, 371–373.
- Stelzmann RA, Norman Schnitzlein H and Reed Murtagh F. (1995). An english translation of alzheimer's 1907 paper, "über eine eigenartige erkankung der hirnrinde." *Clin. Anat.*, 8(6), 429–431.
- Stine WB, Jungbauer L, Yu C and LaDu MJ. (2011). Preparing synthetic A $\beta$  in different aggregation states. *Methods Mol. Biol.*, 670, 13–32.
- Stoker AK and Markou A. (2011). The intracranial self-stimulation procedure provides quantitative measures of brain reward function. *Neuromethods*, 63, 307–331.
- Stoothoff WH and Johnson GVW. (2005). Tau phosphorylation: Physiological and pathological consequences. *Biochim. Biophys. Acta - Mol. Basis Dis.*, 1739(2), 280–297.

- Strozyk D, Blennow K, White LR and Launer LJ. (2003). CSF A $\beta$  42 levels correlate with amyloid-neuropathology in a population-based autopsy study. *Neurology*, 60(4), 652–656.
- Stuchlik A. (2014). Dynamic learning and memory, synaptic plasticity and neurogenesis: An update. *Front. Behav. Neurosci.*, 8(APR).
- Su JH, Cummings BJ and Cotman CW. (1994). Early phosphorylation of tau in alzheimer's disease occurs at ser-202 and is preferentially located within neurites. *Neuroreport*, 5(17), 2358–2362.
- Sunderland T, Linker G, Mirza N, Putnam KT, Friedman DL, Kimmel LH, Bergeson J, Manetti GJ, Zimmermann M, Tang B, Bartko JJ and Cohen RM. (2003). Decreased  $\beta$ -Amyloid1-42 and Increased Tau Levels in Cerebrospinal Fluid of Patients with Alzheimer Disease. *J. Am. Med. Assoc.*, 289(16), 2094–2103.
- Sweatt JD. (2010). Aging-Related Memory Disorders—Alzheimer's Disease. In *Mechanisms of Memory* (Second Edn). Elsevier Inc.
- Takahashi H, Sekino Y, Tanaka S, Mizui T, Kishi S and Shirao T. (2003). Drebrin-dependent actin clustering in dendritic filopodia governs synaptic targeting of postsynaptic density-95 and dendritic spine morphogenesis. *J. Neurosci.*, 23(16), 6586–6595.
- Takahashi H, Mizui T and Shirao T. (2006). Down-regulation of drebrin A expression suppresses synaptic targeting of NMDA receptors in developing hippocampal neurones. *J. Neurochem.*, 97, 110–115.
- Takahashi T, Zhu Y, Hata T, Shimizu-Okabe C, Suzuki K and Nakahara D. (2009). Intracranial self-stimulation enhances neurogenesis in hippocampus of adult mice and rats. *Neuroscience*, 158(2), 402–411.
- Takizawa C, Thompson PL, Van Walsem A, Faure C and Maier WC. (2014). Epidemiological and economic burden of Alzheimer's disease: A systematic literature review of data across Europe and the United States of America. *J. Alzheimer's Dis.*, 43(4), 1271–1284.
- Tan L, Yu J-T, Hu N and Tan L. (2013). Non-coding RNAs in Alzheimer's Disease. *Mol. Neurobiol.*, 47(1), 382–393.
- Tan L, Yu J-T, Tan M-S, Liu Q-Y, Wang H-F, Zhang W, Jiang T and Tan L. (2014a). Genome-Wide Serum microRNA Expression Profiling Identifies Serum Biomarkers for Alzheimer's Disease. *J. Alzheimers. Dis.*, 40(4), 1017–1027.
- Tan L, Yu J-T, Liu Q-Y, Tan M-S, Zhang W, Hu N, Wang Y-L, Sun L, Jiang T and Tan L. (2014b). Circulating miR-125b as a biomarker of Alzheimer's disease. *J. Neurol. Sci.*, 336(1–2), 52–56.
- Tapiola T, Alafuzoff I, Herukka S-K, Parkkinen L, Hartikainen P, Soininen H and Pirttilä T. (2009). Cerebrospinal Fluid  $\beta$ -Amyloid 42 and Tau Proteins as Biomarkers of Alzheimer-Type Pathologic Changes in the Brain. *Arch. Neurol.*, 66(3), 382–389.
- Taupin P and Gage FH. (2002). Adult neurogenesis and neural stem cells of the central nervous system in mammals. *J. Neurosci. Res.*, 69(6), 745–749.
- Terry RD. (2000). Cell death or synaptic loss in Alzheimer disease. *J. Neuropathol. Exp. Neurol.*, 59(12), 1118–1119.



- Terry RD, Masliah E, Salmon DP, Butters N, DeTeresa R, Hill R, Hansen LA and Katzman R. (1991). Physical basis of cognitive alterations in Alzheimer's disease: Synapse loss is the major correlate of cognitive impairment. *Ann. Neurol.*, 30(4), 572–580.
- Thorens B. (2015). GLUT2, glucose sensing and glucose homeostasis. *Diabetologia*, 58(2), 221–232.
- Tippmann F, Hundt J, Schneider A, Endres K and Fahrenholz F. (2009). Up-regulation of the  $\alpha$ -secretase ADAM10 by retinoic acid receptors and acitretin. *FASEB J.*, 23(6), 1643–1654.
- Todd TP, Bucci DJ and Medina JH. (2015). Retrosplenial Cortex and Long-Term Memory: Molecules to Behavior. *Neural Plast.*, 414173.
- Tola-Arribas MA, Yugueros MI, Garea MJ, Ortega-Valín F, Cerón-Fernández A, Fernández-Malvido B, San José-Gallegos A, González-Touya M, Botrán-Velicia A, Iglesias-Rodríguez V and Díaz-Gómez B. (2013). Prevalence of Dementia and Subtypes in Valladolid, Northwestern Spain: The DEMINVALL Study. *PLoS One*, 8(10), e77688.
- Toledano A, Álvarez MI, Carmona P, Toledano-Díaz A and Fernández-Verdecia CI. (2012). Alzheimer pathology in non-human primates and its pathophysiological implications. *Primates Classif. Evol. Behav.*, 27(6), 71–110.
- Tönnies E and Trushina E. (2017). Oxidative Stress, Synaptic Dysfunction, and Alzheimer's Disease. *J. Alzheimer's Dis.*, 57, 1105–1121.
- Treit D and Fundytus M. (1988). Thigmotaxis as a test for anxiolytic activity in rats. *Pharmacol. Biochem. Behav.*, 31(4), 959–962.
- Trillo L, Das D, Hsieh W, Medina B, Moghadam S, Lin B, Dang V, Sanchez MM, De Miguel Z, Ashford JW and Salehi A. (2013). Ascending monoaminergic systems alterations in Alzheimer's disease. Translating basic science into clinical care. *Neurosci. Biobehav. Rev.*, 37(8), 1363–1379.
- Tu S, Wong S, Hodges JR, Irish M, Piguet O and Hornberger M. (2015). Lost in spatial translation - A novel tool to objectively assess spatial disorientation in Alzheimer's disease and frontotemporal dementia. 67, 83–94.
- Turnbull IM, McGeer PL, Beattie L, Calne D and Pate B. (1985). Stimulation of the basal nucleus of Meynert in senile dementia of Alzheimer's type. *Appl. Neurophysiol.*, 48(1–6), 216–221.
- U. S. National Institutes of Health. (2021). *ClinicalTrials.gov*.
- Ueno H, Yamaguchi T, Fukunaga S, Okada Y, Yano Y, Hoshino M and Matsuzaki K. (2014). Comparison between the Aggregation of Human and Rodent Amyloid  $\beta$ -Proteins in GM1 Ganglioside Clusters. *Biochemistry*, 53, 7523–7530.
- Valenstein E, Bowers D, Verfaellie M, Heilman KM, Day A and Watson RT. (1987). Retrosplenial amnesia. *Brain*, 110(6), 1631–1646.
- Van Hoesen GW, Hyman BT and Damasio AR. (1991). Entorhinal cortex pathology in Alzheimer's disease. *Hippocampus*, 1(1), 1–8.
- Van Strien NM, Cappaert NLM and Witter MP. (2009). The anatomy of memory: An interactive overview of

- the parahippocampal- hippocampal network. *Nat. Rev. Neurosci.*, 10(4), 272–282.
- Vandesompele J, De Preter K, Pattyn F, Poppe B, Van Roy N, De Paepe A and Speleman F. (2002). Accurate normalization of real-time quantitative RT-PCR data by geometric averaging of multiple internal control genes. *Genome Biol.*, 3(7).
- Ventriglia M, Zanardini R, Bonomini C, Zanetti O, Volpe D, Pasqualetti P, Gennarelli M and Bocchio-Chiavetto L. (2013). Serum brain-derived neurotrophic factor levels in different neurological diseases. *Biomed Res. Int.*, 901082.
- Visani M, de Biase D, Marucci G, Taccioli C, Baruzzi A, Pession A, Baruzzi A, Albani F, Calbucci F, D'Alessandro R, Michelucci R, Brandes A, EusebiEusebi V, Ceruti S, Fainardi E, Tamarozzi R, Emiliani E, Cavallo M, Franceschi E,... Nobile C. (2013). Definition of miRNAs Expression Profile in Glioblastoma Samples: The Relevance of Non-Neoplastic Brain Reference. *PLoS One*, 8(1), 3–8.
- Vlassenko AG, Vaishnavi SN, Couture L, Sacco D, Shannon BJ, Mach RH, Morris JC, Raichle ME and Mintun MA. (2010). Spatial correlation between brain aerobic glycolysis and amyloid- $\beta$  (A $\beta$ ) deposition. *Proc. Natl. Acad. Sci. U. S. A.*, 107(41), 17763–17767.
- Vo N, Klein ME, Varlamova O, Keller DM, Yamamoto T, Goodman RH and Impy S. (2005). A cAMP-response element binding protein-induced microRNA regulates neuronal morphogenesis. *Proc. Natl. Acad. Sci. U. S. A.*, 102(45), 16426–16431.
- Vogels OJM, Renkawek K, Broere CAJ, ter Laak HJ and van Workum F. (1989). Galanin-like immunoreactivity within Ch2 neurons in the vertical limb of the diagonal band of Broca in aging and Alzheimer's disease. *Acta Neuropathol.*, 78(1), 90–95.
- Vorhees C V. and Williams MT. (2006). Morris water maze: Procedures for assessing spatial and related forms of learning and memory. *Nat. Protoc.*, 1(2), 848–858.
- Voronkov DN, Stavrovskaya A V, Stelmashook E V, Genrikhs EE and Isaev NK. (2019). Neurodegenerative Changes in Rat Brain in Streptozotocin Model of Alzheimer's Disease. *Bull. Exp. Biol. Med.*, 166(6), 762–766.
- Wang-Fischer Y and Garyantes T. (2018). Improving the Reliability and Utility of Streptozotocin-Induced Rat Diabetic Model. *J. Diabetes Res.*, 8054073.
- Wang J, Fivecoat H, Ho L, Pan Y, Ling E and Pasinetti GM. (2010). The role of Sirt1: At the crossroad between promotion of longevity and protection against Alzheimer's disease neuropathology. *Biochim. Biophys. Acta*, 1804, 1690–1694.
- Wang W-X, Huang Q, Hu Y, Stromberg AJ and Nelson PT. (2011). Patterns of microRNA expression in normal and early Alzheimer's disease human temporal cortex: white matter versus gray matter. *Acta Neuropathol.*, 121, 193–205.
- Wang W, Kwon EJ and Tsai L-H. (2012). MicroRNAs in learning, memory, and neurological diseases. *Learn. Mem.*, 19(9), 359–368.
- Wang RY, Phang RZ, Hsu PH, Wang WH, Huang HT and Liu IY. (2013). In vivo knockdown of hippocampal miR-132 expression impairs memory acquisition of trace fear conditioning. *Hippocampus*, 23(7), 625–633.

- Wang L, Liu W, Fan Y, Liu T and Yu C. (2017). Effect of rosiglitazone on amyloid precursor protein processing and A $\beta$  clearance in streptozotocin-induced rat model of Alzheimer's disease. *Iran J Basic Med Sci*, 20, 474–480.
- Waraczynski MA. (2006). The central extended amygdala network as a proposed circuit underlying reward valuation. *Neurosci. Biobehav. Rev.*, 30(4), 472–496.
- Weintraub S, Wicklund AH and Salmon DP. (2012). The neuropsychological profile of Alzheimer disease. *Cold Spring Harb. Perspect. Med.*, 2(4).
- West MJ, Coleman PD, Flood DG and Troncoso JC. (1994). Differences in the pattern of hippocampal neuronal loss in normal ageing and Alzheimer's disease. *Lancet*, 344(8925), 769–772.
- Whitehouse PJ, Price DL, Clark AW, Coyle JT and DeLong MR. (1981). Alzheimer disease: Evidence for selective loss of cholinergic neurons in the nucleus basalis. *Ann. Neurol.*, 10(2), 122–126.
- Whitehouse PJ, Price DL, Struble RG, Clark AW, Coyle JT and DeLong MR. (1982). Alzheimer's disease and senile dementia: Loss of neurons in the basal forebrain. *Science*, 215(4537), 1237–1239.
- Whitwell JL. (2010). Progression of atrophy in Alzheimer's disease and related disorders. *Neurotox. Res.*, 18(3–4), 339–346.
- Wibrand K, Pai B, Siripornmongkolchai T, Bittins M, Berentsen B, Ofte ML, Weigel A, Skaftnesmo KO and Bramham CR. (2012). MicroRNA Regulation of the Synaptic Plasticity-Related Gene Arc. *PLoS One*, 7(7), e41688.
- Witter MP, Naber PA, Van Haeften T, Machielsen WCM, Rombouts SARB, Barkhof F, Scheltens P and Lopes Da Silva FH. (2000). Cortico-hippocampal communication by way of parallel parahippocampal-subicular pathways. *Hippocampus*, 10(4), 398–410.
- Witter MP, Wouterlood FG, Naber PA and Van Haeften T. (2006). Anatomical Organization of the Parahippocampal-Hippocampal Network. *Ann. N. Y. Acad. Sci.*, 911(1), 1–24.
- Wong HKA, Veremeyko T, Patel N, Lemere CA, Walsh DM, Esau C, Vanderburg C and Krichevsky AM. (2013). De-repression of FOXO3a death axis by microRNA-132 and -212 causes neuronal apoptosis in Alzheimer's disease. *Hum. Mol. Genet.*, 22(15), 3077–3092.
- Wong RS, Cechetto DF and Whitehead SN. (2016). Assessing the Effects of Acute Amyloid  $\beta$  Oligomer Exposure in the Rat. *Int. J. Mol. Sci.*, 17(9).
- Wright JS and Panksepp J. (2012). An Evolutionary framework to understand foraging, wanting, and Desire: The Neuropsychology of the SEEKING system. *Neuropsychobanalysis*, 14(1), 5–39.
- Xia F, Yiu A, Stone SSD, Oh S, Lozano AM, Josselyn SA and Frankland PW. (2017). Entorhinal cortical deep brain stimulation rescues memory deficits in both young and old mice genetically engineered to model Alzheimer's disease. *Neuropsychopharmacology*, 42(13), 2493–2503.
- Xie L, Helmerhorst E, Taddei K, Plewright B, Van Bronswijk W and Martins R. (2002). Alzheimer's beta-amyloid peptides compete for insulin binding to the insulin receptor. *J. Neurosci.*, 22(10).
- Xie B, Zhou H, Zhang R, Song M, Yu L, Wang L, Liu Z, Zhang Q, Cui D, Wang X and Xu S. (2018). Serum

- miR-206 and miR-132 as Potential Circulating Biomarkers for Mild Cognitive Impairment. *J. Alzheimer's Dis.*, 45(3), 721–731.
- Xu Z-P, Li L, Bao J, Wang Z-H, Zeng J, Liu E-J, Li X-G, Huang R-X, Gao D, Li M-Z, Zhang Y, Liu G-P and Wang J-Z. (2014). Magnesium protects cognitive functions and synaptic plasticity in streptozotocin-induced sporadic Alzheimer's model. *PLoS One*, 9(9), e108645.
- Xu J, Jackson CW, Khoury N, Escobar I and Perez-Pinzon MA. (2018). Brain SIRT1 Mediates Metabolic Homeostasis and Neuroprotection. *Front. Endocrinol.*, 9, 702.
- Yamashita S, Hashimoto M, Haque AM, Nakagawa K, Kinoshita M, Shido O and Miyazawa T. (2017). Oral Administration of Ethanolamine Glycerophospholipid Containing a High Level of Plasmalogen Improves Memory Impairment in Amyloid  $\beta$ -Infused Rats. *Lipids*, 52(7), 575–585.
- Yang G, Sau C, Lai W, Cichon J and Li W. (2015). Increased expression of miRNA-146a in Alzheimer's disease transgenic mouse models. *Neurosci. Lett.*, 487(1), 94–98.
- Yeung F, Hoberg JE, Ramsey CS, Keller MD, Jones DR, Frye RA and Mayo MW. (2004). Modulation of NF- $\kappa$ B-dependent transcription and cell survival by the SIRT1 deacetylase. *EMBO J.*, 23(12), 2369–2380.
- Yu D, Yan H, Zhou J, Yang X, Lu Y and Han Y. (2019). A circuit view of deep brain stimulation in Alzheimer's disease and the possible mechanisms. *Mol. Neurodegener.*, 14(1), 1–12.
- Zappa Villar MF, Hanotte JL, Lockhart EF, Tripodi LS, Morel GR and Reggiani PC. (2018). Intracerebroventricular streptozotocin induces impaired Barnes maze spatial memory and reduces astrocyte branching in the CA1 and CA3 hippocampal regions. *J. Neural Transm.*, 125, 1787–1803.
- Zhang L, Fang Y, Lian Y, Chen Y, Wu T, Zheng Y, Zong H, Sun L, Zhang R, Wang Z and Xu Y. (2015a). Brain-Derived Neurotrophic Factor Ameliorates Learning Deficits in a Rat Model of Alzheimer's Disease Induced by A $\beta$ 1-42. *PLoS One*, 10(4).
- Zhang J-G, Zhang C, Hu W-H, Wu D-L and Zhang K. (2015b). Behavioral Effects of Deep Brain Stimulation of the Anterior Nucleus of Thalamus, Entorhinal Cortex and Fornix in a Rat Model of Alzheimer's Disease. *Chin. Med. J. (Engl.)*, 128(9), 1190.
- Zhang L, Chen C, Mak MSH, Lu J, Wu Z, Chen Q, Han Y, Li Y and Pi R. (2019). Advance of sporadic Alzheimer's disease animal models. *Med. Res. Rev.*, 40, 431–458.
- Zott B, Busche MA, Sperling RA and Konnerth A. (2018). What Happens with the Circuit in Alzheimer's Disease in Mice and Humans? *Annu Rev Neurosci*, 41, 277–297.
- Zou YM, Lu D, Liu LP, Zhang HH and Zhou YY. (2016). Olfactory dysfunction in Alzheimer's disease. *Neuropsychiatr. Dis. Treat.*, 12, 869–875.

